The Pennsylvania State University

The Graduate School

Materials Science and Engineering

DIELECTRIC AND PIEZOELECTRIC NONLINEARITIES IN ORIENTED $Pb(Yb_{1/2}Nb_{1/2})O_3$-$PbTiO_3$ THIN FILMS

A Thesis in

Materials Science and Engineering

by

Nazanin Bassiri Gharb

Submitted in Partial Fulfillment
of the Requirements
for the Degree of

Doctor of Philosophy

December 2005

The thesis of Nazanin Bassiri Gharb was reviewed and approved* by the following:

Susan Trolier-McKinstry
Professor of Ceramic Science and Engineering
Thesis Advisor
Chair of Committee

Clive A. Randall
Professor of Materials Science and Engineering

Thomas R. Shrout
Professor of Materials

Srinivas Tadigadapa
Associate Professor of Electrical Engineering

Dragan Damjanovic
Adjoint Scientifique, Ecole Polytechnique Fédérale de Lausanne

Gary L. Messing
Distinguished Professor of Ceramics Science and Engineering
Head of the Department of Materials Science and Engineering

*Signatures are on file in the Graduate School

ABSTRACT

This work provides a comprehensive study of the ac field amplitude dependence of the dielectric constant, quantifying the extrinsic contributions of the domain walls and phase boundaries in two different orientations of PYbN-PT thin films. From the Rayleigh parameters obtained it was determined that {100} films had a higher concentration of mobile interfaces. The Rayleigh parameters decreased logarithmically with frequency. Comparison of the irreversible Rayleigh parameters' dependence on frequency confirmed a higher concentration of mobile interfaces in {100} oriented PYbN-PT thin films. Frequency dependent Rayleigh parameters were used successfully to predict the dielectric permittivity of the films over a range of three orders of magnitude for frequency and one order of magnitude of field amplitude.

Biaxial strain fields were applied and the nonlinear behavior was measured. It was found that for both orientations of the films, 180° domain wall motion was the major source of dielectric nonlinearity. The temperature dependence of the nonlinear behavior showed a reduction of both Rayleigh parameters at decreasing temperatures, indicating a reduction of the mobility of the interfaces. As the temperature increased towards the Curie temperature, the Rayleigh parameters showed a net increase in the reversible Rayleigh parameters and a much smaller increase in the irreversible Rayleigh parameter, indicating higher reversible mobility of the interfaces.

The piezoelectric Rayleigh parameters also showed logarithmic dependence on frequency and a higher concentration of mobile interfaces in {100} oriented films.

Electric field dependent dielectric and piezoelectric nonlinearities showed comparable amounts of extrinsic contributions to the nonlinear response, under the same applied bias field levels. A normalized frequency dependence of the Rayleigh parameters showed comparable trends for ε_{init} and d_{init}, and α_{ε} and α_{d}, indicating similar phenomena are responsible for the dielectric and piezoelectric nonlinearities. In the literature, only ferroelastic non-180° domain walls are considered to contribute to the piezoelectric effect. However in many ferroelectric films, their mobility is considerably reduced. A dynamic poling model is proposed, allowing a *largely reversible 180° domain wall motion* contribution to the piezoelectric nonlinearity. This model predicts a Rayleigh-like behavior of the piezoelectric coefficient with electric field, accompanied by the creation of a second order harmonic of strain. Experimental measurements of the higher order harmonics of polarization and strain confirmed the model's predictions.

Measurement of the $e_{31,f}$ piezoelectric coefficients as a function of increasing ac strain levels didn't show piezoelectric nonlinearities. Ferroelectric 180° domain wall motion, in fact, can't be activated by application of homogeneous strain fields. The second order harmonic of the piezoelectric response proved to be at least one order of magnitude smaller than the first and third order harmonics. The observation of a Rayleigh behavior in $d_{33,f}$ along with a strong second harmonic in the strain response for electric field drive, coupled with the lack of the amplitude dependence for a strain excitation is consistent with the dynamic poling model.

It was therefore demonstrated that piezoelectric nonlinearity can appear in thin films even in cases where *only 180° domain wall motion* is operative. This mechanism

will be important in any ferroelectric with large-scale, nearly reversible motion of domain walls (tilted hysteresis loops).

TABLE OF CONTENTS

LIST OF FIGURES

LIST OF TABLES

ACKNOWLEDGEMENTS

I owe many thanks to many people for this work, foremost Prof. Susan Trolier-McKinstry. I could never have accomplished what I did over the last four years without her guidance and directions. I definitely will count her among the most influential people in my life beyond the scientific formation. Seldom I have known a person that could lead so much by example and I count myself lucky to have had such a role model for my future. I'm indebted to Susan with more than the "thank you" I am saying here, I owe partly to her the person I am today. A special thank you also goes to Dr. Dragan Damjanovic. If it wasn't for reading his publications on the subject and the ever enlightening discussions with him, I probably would have worked on a very different subject. To Susan and Dragan I owe my passion for ferroelectrics.

Due thanks also to Professors Clive Randall, Thomas Shrout, Srinivas Tadigadapa and last but not least, Eric Cross who never denied me the answer to a question, and usually added a new question to make me think further and beyond. It has been an honor working with all of you.

Very special thank you-s to Paul Moses: almost none of the electrical characterizations present in this work would have been possible without his help. The deposition of the films used in this work wouldn't have been possible without the help of Bill Drawl and Tim Klinger: thank you! By all three, I appreciate the smile with which they always answered my continuous naggings and crazy cries for help: they helped even when what I was asking was "quite" impossible.

Two other people I have to thank beyond the “technical” support: Barb Davies and Kathy Gummo, my adoptive moms in the New Land. The fact that I got to this point and receive a doctoral degree wouldn’t have been possible without you. So, “thanks moms”.

Nichole Wonderling, Maria Klimkewich are owed special thanks for the help and training for X-ray diffraction and scanning electrode microscopy, respectively. Beyond all this, I have to thank the whole staff and technical personnel at MRL. I enjoyed all the corridor talks, the short and long conversations on anything from the weather of the day to shopping and politics.

Last but not least, I have to thank the whole STM group, past and present and, why not, future at this point: people you are great. There are many of you and I hope I won’t forget anyone’s name: Azo, Bob, Dan, Eunki, Han, Ichiro, Ioanna, Jiangong, Juan, Junling, Mike B., Mike U., Mustafa, Paul K., Pum, Ravi, Raja, Song-won, Takeshi.

Chapter 1

Introduction

This chapter briefly introduces the background for the conducted research. It then traces the main objectives and plans for the different parts of this thesis, giving a basic guideline for the experiments conducted.

1.1 Introduction

Ferroelectric thin films are used in a wide range of applications including capacitors, non-volatile memories, microelectromechanical systems (MEMS), pyroelectric sensors, as well as wave-guides and modulators in optical devices. The dielectric and electromechanical responses of ferroelectric materials are in part intrinsic (the average crystallographic response of the ferroelectric material) and in part extrinsic, mainly due to the motion of the ferroelectric domain walls and phase boundaries.[1] These extrinsic contributions have been shown to constitute up to 60-70% of the response of the room temperature dielectric and piezoelectric response in ferroelectric bulk

ceramics.[2][3] It is of interest to develop materials with *inherently* higher dielectric and piezoelectric response. Perovskite solid solutions with $PbTiO_3$ on the rhombohedral side of morphotropic phase boundary (MPB), poled along the [001] crystallographic direction have been reported to exhibit particularly high dielectric and piezoelectric response.[4][5] Among these systems, $0.5Pb(Yb_{1/2}Nb_{1/2})O_3$-$0.5PbTiO_3$ (PYbN-PT) has been reported to have one of the highest transition temperatures, promising devices with higher temperature stability and wider temperature range of application. In this research, highly {111} and {100} oriented PYbN-PT thin films were deposited and characterized.

In many applications, there is a drive towards smaller ferroelectric film thickness [6], resulting in higher applied electric fields at a given voltage. At higher ac fields, extrinsic contributions become more prominent.[7] As a result, the behavior becomes "nonlinear", i.e. the relationship between dielectric displacement (or strain) and electric field is not linear (described by *constant* dielectric permittivity or piezoelectric coefficients), but instead depends on parameter(s) that are function of the amplitude of the ac applied field itself.[8] The aim of this work is first to find a set of parameters that would allow prediction and control of the behavior at higher fields of MEMS devices and capacitive components based on ferroelectric thin films; and second, to quantify the extrinsic contributions to the dielectric and piezoelectric properties. In analogy to ferromagnetic materials, Rayleigh analysis was used as the principal tool for the quantification of these contributions.

Lord Rayleigh [9] showed in 1887 for ferromagnetic materials that the relative magnetic permeability (μ) had a linear dependence on the applied magnetic field

amplitude (H_0) at intermediate fields. He also showed that the same parameters used to describe this linear relationship could describe the hysteretic dependence of the magnetic inductance (B) on magnetic field (H). These could be expressed as $B = (\mu_{init} + \alpha H_0)H \pm \frac{\alpha}{2}\left(H_0^2 - H^2\right)$ and $\mu = \mu_{init} + \alpha H_0$, where the applied magnetic field is $H = H_0 \sin(\omega t)$, μ_{init} is the reversible Rayleigh parameter due mainly to the reversible motion (vibration) of the domain walls and the intrinsic response of the material, and α is the irreversible Rayleigh parameter, which is due to the irreversible motion of the domain walls. The Rayleigh analysis was shown later by Neel [**10**][**11**] to describe, in general, the hysteretic effects of the motion of interfaces across a random and uniform distribution of potential energy barriers. More recently, Damjanovic et al.[**12**][**13**][**14**][**15**][**16**][**17**] and Hall et al. [**18**][**19**][**20**][**21**][**22**] used the Rayleigh approach to describe the dielectric and piezoelectric properties of ferroelectrics in terms of vibration and motion of *ferroelectric* and ferroelastic domain walls and phase boundaries. Using the Rayleigh Law, it is therefore possible to first quantify the role of the domain walls in controlling properties and second to predict the hysteretic behavior of the polarization or strain against the applied electric field.

1.2 Thesis Organization and Statement of Goals

Based on the above introduction, the organization of this thesis is as follows:

Literature review and experimental procedure (Chapter 1 and 2)

A review of the literature work is presented in order to introduce the concepts used in this thesis. The fundamental equations for study of the ferroelectric and piezoelectric phenomena are given. Different approaches to study and separate intrinsic and extrinsic contributions to the dielectric and piezoelectric phenomena are reviewed.

Preparation and characterization of highly {100} and {111} oriented PYbN-PT thin films (Chapters 3 and 4)

A chemical solution deposition route is developed for PYbN-PT. Processing times and temperatures are targeted to obtain a chemically homogeneous and stable solution. To increase the perovskite content and the {100} or {111} orientation, the amount of excess lead source, pyrolysis and crystallization temperatures, and finally the heating rates used for the crystallization step are optimized.

Dielectric nonlinearity in {100} and {111} oriented PYbN-PT thin films (Chapter 5)

The extrinsic contributions to the dielectric properties at high field of the PYbN-PT thin films are studied through the ac field amplitude dependence of the dielectric permittivity. The results are quantitatively compared, to study the relative concentration of the mobile interfaces in differently oriented thin films. To verify the applicability of the Rayleigh analysis, the results from the study of the real part of the dielectric permittivity are compared with the Rayleigh predictions for the imaginary part of the permittivity and the polarization-electric field hysteresis loops. The nonlinear studies are

then extended to the nonlinear behavior in a wider frequency range. After verification of the Rayleigh behavior at each frequency, the Rayleigh parameters' dependence on the frequency of the applied field is studied. A combined function of amplitude and frequency dependence of the dielectric permittivity is sought that could predict the dielectric permittivity values over an intermediate frequency and field range.

To separate the contributions to the dielectric nonlinearity due to the ferroelectric, or ferroelastic wall and phase boundaries motion, nonlinear measurements were also performed under applied biaxial strain. Strain fields can affect the motion of the ferroelastic domain walls and phase boundaries, but can't affect the motion of the ferroelectric 180° domain walls.

Many ferroelectric thin films have internal bias fields. The domain structure can become clamped under these bias fields, modifying the motion of the domain walls and therefore their contribution to the dielectric properties. The dielectric nonlinearities are therefore measured under applied positive and negative DC fields to study the effects of the bias fields on the domain wall mobility.

It is also goal of this work to study the temperature dependence of the motion of the domain walls and the effects of phase transformations on the Rayleigh parameters. The temperature dependence of the dielectric nonlinearities is important also in view of the technological applications of the ferroelectric films and the functional temperature range of the devices. No previous reports exists on the dielectric properties of PYbN-PT below room temperatures, therefore the temperature dependence of dielectric permittivity of the films was also studied down to cryogenic temperatures.

Piezoelectric nonlinearity in {100} and {111} oriented PYbN-PT thin films (Chapter 6)

The ac field amplitude dependence of the piezoelectric coefficient is analyzed for the {100} and {111} oriented films to study the ferroelastic domain wall mobility and their contribution to the piezoelectric effect in these films. To confirm the Rayleigh-like behavior of the piezoelectric nonlinearity, the higher harmonic response and hysteretic behavior of the strain as a function of the amplitude of the applied field are used. Due to their crystallographic orientation, the rhombohedral perovskite {100} oriented films should not exhibit any piezoelectric nonlinearity. A physical model is sought in order to explain the unexpected experimental results. AC strain dependence of the $e_{31,f}$ piezoelectric coefficient was studied to confirm the proposed model.

Dielectric nonlinearity in other ferroelectric thin films (Chapter 7)

The ac field amplitude dependence of the dielectric permittivity is analyzed for other ferroelectric thin film materials, in order to create a reference library for the extrinsic contributions to the dielectric properties of the different films. Different "hard" and "soft" systems are studied to examine different degrees of mobility of the domain walls, and the dielectric nonlinear behavior of the films. Due to the high T_C and high loss levels at around the transition temperature, it was impossible to verify the disappearance of the domain structure (and therefore nonlinear behavior) in PYbN-PT films at temperatures higher than T_C. Therefore, alternative ferroelectric thin films with lower transition temperatures and lower loss values are studied.

Conclusions and future work (Chapter 8)

Finally a summary of the performed work and basic achievements is reported. Suggestions are made for future work to expand the knowledge about the ferroelectric domain wall contributions to the dielectric and piezoelectric properties of thin films.

Chapter 2

Literature Review

This chapter contains a review of the literature relevant to the current investigation. A general background is given about piezoelectric and electromechanical properties, followed by a summary of ferroelectric phenomena. Creation of the domain structures in ferroelectric phases is discussed in view of the intrinsic and extrinsic contributions to the dielectric and piezoelectric response of the ferroelectric materials. The effects of the extrinsic contributions are shown in terms of the frequency and amplitude of the ac electrical field, temperature, and aging of the electric and electromechanical behavior of ferroelectrics. In particular, the dielectric and piezoelectric nonlinearities, especially the ac field dependence of the dielectric and piezoelectric coefficients are illustrated. The Rayleigh Law is detailed for discussion of these nonlinearities. The chapter concludes with an examination of literature reports on lead zirconate titanate, some complex oxide-lead titanate solid solutions and in particular, the $(1\text{-}x)Pb(Yb_{1/2}Nb_{1/2})O_3\text{-}xPbTiO_3$ system used in this investigation.

2.1 Piezoelectric Materials

Piezoelectric materials are materials that develop charge on the sample surfaces when exposed to applied stresses. Conversely, under applied electric field, they undergo a change in their dimensions according to:

$$D_i = d_{ijk}\sigma_{jk} \text{ (direct effect)} \qquad x_{ij} = d_{kij}E_k \text{ (converse effect)} \qquad \textbf{2.1}$$

In Equation **2.1** D_i is the dielectric displacement, σ_{jk} is the applied stress, d_{ijk} is the piezoelectric coefficient and x_{ij} is the strain produced by the applied electric field E_j. Here and in the following chapters of this thesis, the reduced matrix notation for tensor properties with the Einstein convention summation over repeated indices are used interchangeably. [23] Other piezoelectric coefficients used are e, g and h, defined as:

$$D_i = e_{ikl}x_{kl} \text{ (direct effect)} \qquad \sigma_{ij} = -e_{kij}E_k \text{ (converse effect)} \qquad \textbf{2.2}$$

$$E_i = -g_{ikl}\sigma_{kl} \text{ (direct effect)} \qquad x_{ij} = g_{kij}D_k \text{ (converse effect)} \qquad \textbf{2.3}$$

$$E_i = -h_{ikl}x_{kl} \text{ (direct effect)} \qquad \sigma_{ij} = -h_{kij}D_k \text{ (converse effect)} \qquad \textbf{2.4}$$

Conventionally for a polycrystalline sample, the poling axis for a ferroelectric material is referred to as axis "3". For an unconstrained ferroelectric, the proportionality constants for the direct and converse effects are identical in magnitude.

The above-mentioned definitions of the piezoelectric coefficients are based on the assumption that the polarization-stress and strain-field relations are linear. This treatment is sufficient for small signal excitations, but many times, for higher driving fields, non-

linear effects can take place, so that the piezoelectric coefficients are not constant. This will be described in detail in section **2.5**.

Of the 32 crystallographic systems, only 21 are noncentrosymmetric and among these all except the cubic 423 have non-zero components in their piezoelectric coefficient tensor and therefore can exhibit the piezoelectric effect. [**1**] The non-zero components and their relationship are reported in literature for each of the symmetry classes. [**23**] [**24**]

It should be mentioned that some[1] higher order electromechanical properties can appear in all crystals. One such property is electrostriction, which is a quadratic effect. [**23**] Electrostriction is a mechanical deformation of a material due to application of an electric field or an induced dielectric displacement at zero stress values. [**25**] The strain amount is proportional to the square of the electric stimuli, with the proportionality constant, M_{ijkl} or Q_{ijkl} being the electrostrictive coefficient tensor, as shown in equations **2.5** and **2.6** :

$$x_{ij} = M_{ijkl} E_k E_l \qquad \textbf{2.5}$$

$$x_{ij} = Q_{ijkl} D_k D_l \qquad \textbf{2.6}$$

The two above equations are related by equation **2.7**:

$$\frac{\partial D_i}{\partial E_j} = (1 + \chi_{ij})\varepsilon_0 = \varepsilon_r \varepsilon_0 \qquad \textbf{2.7}$$

[1] Higher order odd terms exist only in piezoelectric materials, while the even terms, the higher order electrostrictive effects, are present in all crystals.

where χ_{ij} is the dielectric susceptibility, ε_0 is the dielectric permittivity of free space and ε_r is the relative permittivity of the crystal. In a ferroelectric material (for details see section **2.2**), the total polarization is due to the spontaneous polarization (P_s) of the crystal plus the induced polarization (P_{ind}) due to the application of the electric field. For an electric field applied along the z direction, E_3, the strain created in the crystal can be written as [**26**]:

$$x_3 = Q_{33}(P_s + P_{ind})^2 = Q_{33}P_s^2 + 2Q_{33}P_sP_{ind} + Q_{33}P_{ind}^2$$
$$\cong Q_{33}P_s^2 + 2Q_{33}P_s\varepsilon_0\varepsilon_r E_3 + Q_{33}\varepsilon_0^2\varepsilon_r^2 E_3^2 \qquad \textbf{2.8}^{[2]}$$

Therefore,

$$d_{33} = 2Q_{33}P_s\varepsilon_0\varepsilon_r \qquad \textbf{2.9}$$

$$M_{33} = Q_{33}\varepsilon_0^2\varepsilon_r^2 \qquad \textbf{2.10}$$

In particular, Equation **2.9** shows that the piezoelectric coefficient of a ferroelectric crystal and its electrostrictive coefficients are connected by the spontaneous polarization P_s and the relative dielectric permittivity ε_r. Since Q_{ij} and P_s are nearly temperature independent (for temperatures well below T_C) [**27**][**28**], the piezoelectric strain coefficient and the relative dielectric permittivity are inter-related: a ferroelectric crystal with high piezoelectric coefficient, exhibits also high dielectric properties. It

[2] Note that in Equation 2.8 through 2.10 the reduced matrix notation has been used.

should be noted, however, that in many ferroelectrics, the dominant nonlinearity in the strain response is due to domain wall motion, rather than electrostriction. [1][12][17]

2.2 Ferroelectric Materials

A ferroelectric is a material that shows, over some temperature range, a spontaneous polarization P_s that is re-orientable between crystallographically defined states upon application of sufficiently high electric fields. [29]

Among the twenty crystal systems that exhibit piezoelectricity, ten are polar (including 1, 2, m, mm2, 4, 4mm, 3, 3m, 6, and 6mm). Polar crystals have a permanent dipole, and the polarization depends on the temperature (pyroelectricity). Some of these ten crystallographic classes exhibit ferroelectricity. In fact, the existence of a permanent dipole moment doesn't guarantee ferroelectricity, because the electric field necessary to reorient the polarization direction between the equilibrium directions can be higher than the breakdown field of the sample. Therefore all ferroelectrics are pyroelectric and all pyroelectrics are also piezoelectric, but not vice versa.

Randomly oriented ferroelectric ceramics have, in general, an ∞∞m symmetry due to the random distribution of polarization vectors in the ceramics after cooling through T_C, resulting in no net piezoelectric response of the ceramic. By applying a dc electric field for sufficient time and at an appropriate level, the polarization in each

domain can be aligned to the energetically favorable directions, resulting in a non-centrosymmetric ∞m piezoelectric ceramic. This process is referred to as poling.

Depending on the microscopic origin of P_s, two main categories of proper ferroelectrics can be defined [29]:

1. P_s is connected with small shifts in the positions or orientations of the ionic sublattices below T_C : *displacive transitions*.
2. P_s is connected with ordering of dipolar groups below T_C : *order-disorder transitions*.

Ferroelectric materials with displacive transitions show Curie-Weiss constants (θ) around 10^5 K, while the ferroelectrics with order-disorder transitions have $\theta \sim 10^2$-10^3K. [29] Furthermore, the frequency dependence of the dielectric permittivity in the paraelectric phase is resonant for the displacive ferroelectrics, while it shows a relaxation behavior for the materials with order-disorder transitions. [29]

Ferroelectric materials are used in a wide range of electronic applications. These can be subdivided into the following main categories:

1) Dielectric applications in capacitors (multi-layer, thick or thin film forms). These applications are primarily based on the very high dielectric permittivities over a wide frequency range. [30][31][32][33][34]

2) Piezoelectric and electrostrictive applications in sensors and actuators for converting electric signals into mechanical ones (piezoelectric direct effect end electrostriction) and vice versa (piezoelectric converse effect). [35][36][37][38][39][40][41][42][43] [44] [45] [46]

3) Non-volatile memory applications. These devices use the direction and switching of the spontaneous polarization in thin film ferroelectrics to store information for random access memories. [47][48][49][50][51][52]

4) Pyroelectric sensors and arrays for intruder alarms and night vision capabilities. [53] [54] [55][56]

5) Electro-optic devices such as modulators, switches and guided wave structures. [57][58][59]

Ferroelectricity usually disappears above a critical temperature, T_C (Curie temperature), where the material becomes paraelectric[3,4]. Below T_C, the material develops a re-orientable spontaneous polarization. In the case of many perovskite-structured compounds, this transition leads to a transformation from a nonpolar, centrosymmetric lattice to a polar non-centrosymmetric structure. Above T_C the susceptibility in the material follows a Curie-Weiss-like behavior:

$$\chi = \frac{C}{T - \theta} \qquad \textbf{2.11}$$

In Equation **2.11** χ is the dielectric susceptibility, C is the Curie-Weiss constant of the material, T is the temperature and θ is the Curie-Weiss temperature, which for a second order ferroelectric material is equal to T_C, and for a first order ferroelectric is lower than

[3] In some other-than-proper ferroelectrics, such as polyvinylidene difluoride, the material can melt or decompose chemically before reaching this phase transition. [1]

[4] For detailed specification of the ferroelectric behavior at temperatures higher than T_C, see sections 2.7 and 2.7.1.

T_C [5].[1] [26] Ferroelectric materials show a maximum in the dielectric permittivity and loss tangent at T_C. [60] The distortion of the unit cell at T_C is accompanied by the creation of the spontaneous polarization and an accompanying strain in the material. On cooling to temperatures lower than T_C, the material tends to reduce its total energy by creating domain structures. [1] The domains are volumes of material where the polarization direction is uniform (or at least nearly so). The boundary where two domains of different orientation meet is called a domain wall and is denoted by the angle formed between the two adjacent polarization directions. Ferroelectric domain structure will be discussed in further detail in section 2.7.

One signature feature of the ferroelectric nature of a material is the polarization - electric field (P-E) hysteresis loop. P-E loops describe the variation of the net polarization of the material under large AC voltage excitation. The area of the curve is related to the energy loss associated with moving domain walls through the material. [61]

The saturation polarization, P_{sat}, is the linear extrapolation at zero field of the high field polarization. The remanent polarization, P_r, is the actual value of polarization at zero field. In a single domain single crystal measured with the applied electric field parallel to the direction of the spontaneous polarization (P_s), the remanent polarization and the saturation polarization are identical (or nearly so) and the electric field necessary for

---

[5] A ferroelectric with a second order transition shows a continuous change of the order parameter at, and below, the transition temperature, while a first order transition has a discontinuity in the spontaneous order parameter value at the transition temperature. In the case of proper ferroelectrics, the spontaneous order parameter is the spontaneous polarization. Typical behavior for these transitions is described in detail in reference [26]. The following discussions in this chapter will refer to proper ferroelectrics unless otherwise specified.

polarization reversal is equal to E_c. In polycrystalline samples and less than ideal single crystals, the saturation polarization is higher than the remanent polarization, because back-switching is possible due to local elastic or electric fields. [62] All this is schematically shown in Figure 2.1.

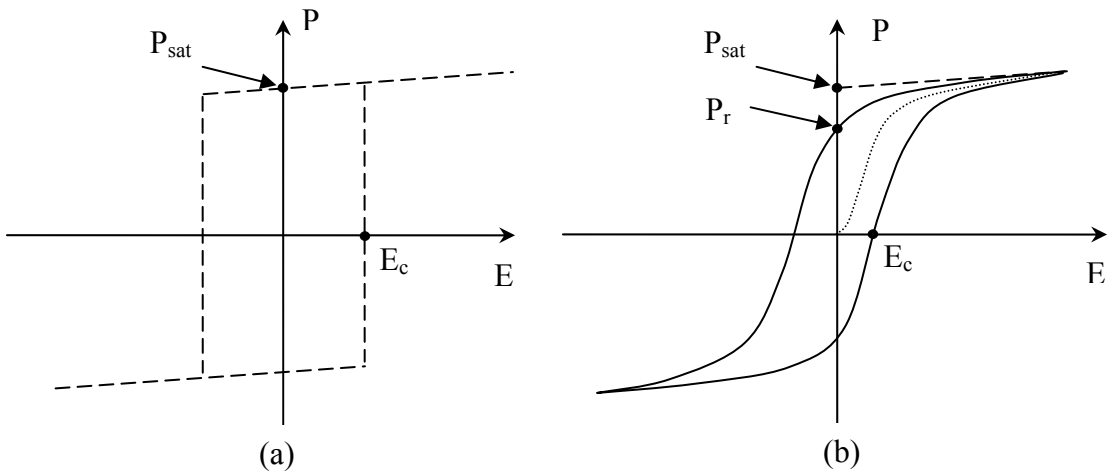

Figure 2.1: Typical bi-polar P-E hysteresis loops for (a) an ideal single crystal measured with the electric field parallel to P_s and (b) polycrystalline sample. For the polycrystalline sample, the process is shown from a depoled state (P=0) in the dotted line.

Figure 2.2 shows a schematic example of the domain configuration in an ideal ferroelectric crystal as it traverses a hysteresis loop. The perfectly poled, single domain crystal (point A) is taken to zero field (point B). As the field is first decreased then subsequently increased with the opposite polarity, small nuclei of domains with reverse polarization directions appear and grow as the negative field increases (point B through C). At field values $|E| > |E_c|$ large volumes of the sample begin to switch, as domains

with the reverse polarization direction continue to grow and merge (point D). The process continues until, ideally, at saturation, there is a single domain with reversed polarization direction (point E). As the electric field is increased, the material will again show nucleation of new domains (stage F) followed by similar processes until saturation is reached at the original single domain state.

The loop shape is frequency dependent and the area of the loop is related to the losses in the sample, for this reason the hysteresis measurement is usually performed at low frequencies.[63] Furthermore, some samples have more "square"-shaped loops: the more abrupt reversal of the polarization may be due to a very narrow distribution of the reversal energies required for the various domains present in the crystal. [64]

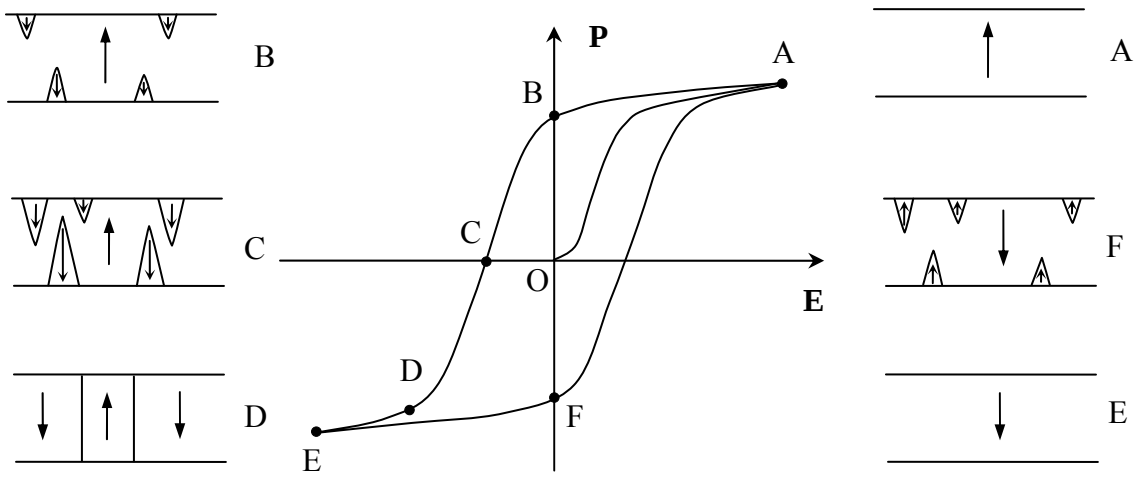

Figure 2.2: Schematic representation of the domain states in a uniaxial ferroelectric single crystal at different points of a P-E hysteresis loop. O: unpoled sample. A: perfectly poled sample would be in a single domain state. Between points B and C: nucleation and growth of domains with opposite polarization direction. D: mainly reverse oriented domains. E: the sample is ideally in a single domain state, with opposite polarization direction than case A. F: nucleation of reverse polarized domains, adapted from [29]

Although many different crystal structures can exhibit ferroelectricity, one of the most important in industrial applications is the perovskite structure. The perovskite structure, which has the high symmetry *m3m* point group for the prototype, is the stable form for many compounds with the ABO_3 chemical formula at elevated temperatures. This unit cell can be described by a cube, where the corner sites are occupied by the large A cations, the sites at the center of the faces are occupied by the oxygens and the site at the center of the cubic cell is occupied by the small B cation. An example of a material with the perovskite structure is $BaTiO_3$ in which the Ba atoms occupy the A sites and the smaller Ti atoms occupy the B sites.

When cooled through T_C, which for $BaTiO_3$ is ~130°C, the unit cell distorts by motion of the Ti atom along one of the <100> directions. [**26**] As this occurs, the unit cell elongates in the direction parallel to the Ti displacement, yielding a tetragonal distortion of the unit cell. Further cooling to ~5°C results in a transformation to an orthorhombic cell, with motion of the Ti atom along one of the <101> directions of the prototype cell. Finally, below ~ -90°C, the material undergoes a transition to a rhombohedral symmetry, with the Ti atom moving along one of the <111> directions of the cubic cell. [**65**] These transformations are schematically shown in Figure **2.3.**

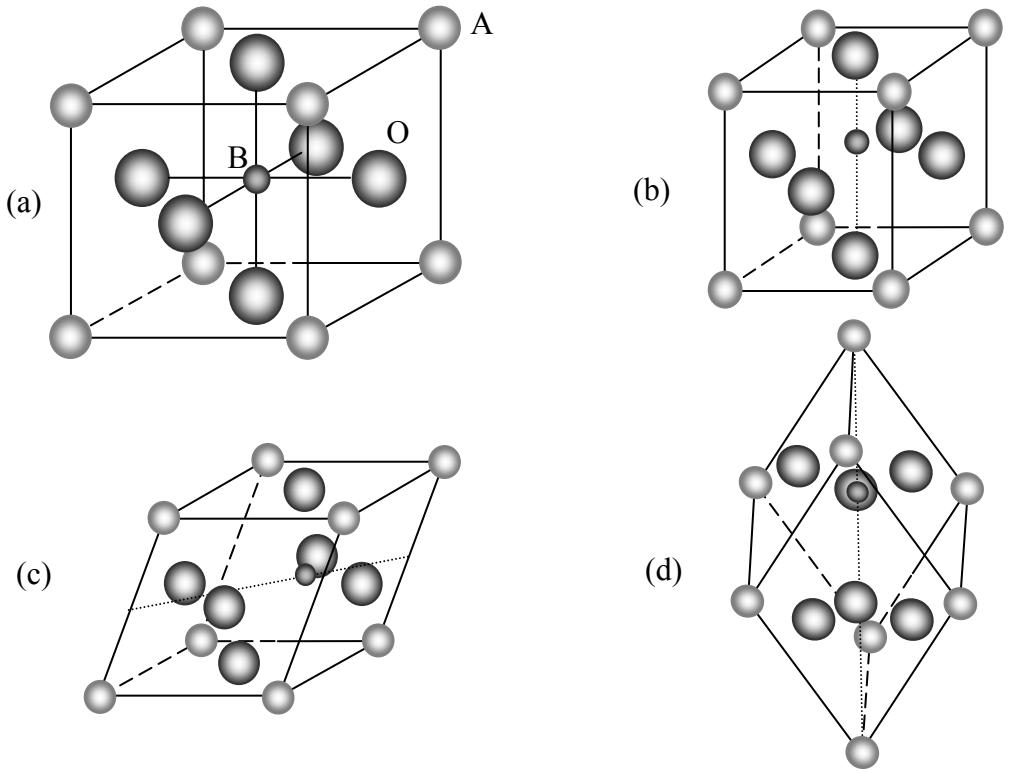

Figure 2.3: Schematic representation of the cubic perovskite structure (a) and its ferroelectric distortions (b-d). The distortions can be visualized in terms of the motion of the Ti atom towards one oxygen in the tetragonal cell (b), two oxygens in the orthorhombic cell (c) or three oxygens in the rhombohedral cell (d). Note that in all of the distorted versions, the displacement of ions as well as the resulting distortion in the shape of the unit cell are greatly exaggerated to facilitate visualization.

2.3 Ferroelectric Domain Structure

As mentioned in section 2.2, ferroelectric materials usually form smaller volumes (domains), each with uniform polarization direction, in an attempt to minimize the free energy of the system. Depending on the crystal structure of the ferroelectric, the number

of possible polarization directions and their avalaible orientations may vary. In a rhombohedral perovskite crystal, for example, the polarization in two adjacent domains can be 180, 109 or 71 degrees apart, as shown in Figure 2.4, giving rise to 180º, 109º or 71º domain walls. The two latter forms are usually referred to as non-180º domain walls. Similarly, in a tetragonal perovskite, the available domain walls can be 180º or 90º walls, where the latter are also referred to as non-180º domain walls. Figure 2.5 shows simplified schematics of ideal domain structures in ferroelectrics.

180º domain walls are purely ferroelectrically active: it means that they can be excited only by electrical fields and generally contribute only to the dielectric properties of the material. Non-180º domain walls are both ferroelectrically and ferroelastically[6] active and can be excited both by mechanical and electrical means, changing both the polarization and the strain. Therefore, they contribute to both the piezoelectric and the dielectric properties.[66][67] Consequently, only non-180º domain walls can potentially reduce the elastic energy of the ferroelectric.[29]

The following section analyzes the conditions for domain wall formation and their orientation.

---

[6] "If two or more domain states differ in their spontaneous deformation tensors and switchability is demonstrated, they constitute ferroelastic domain states." [29]

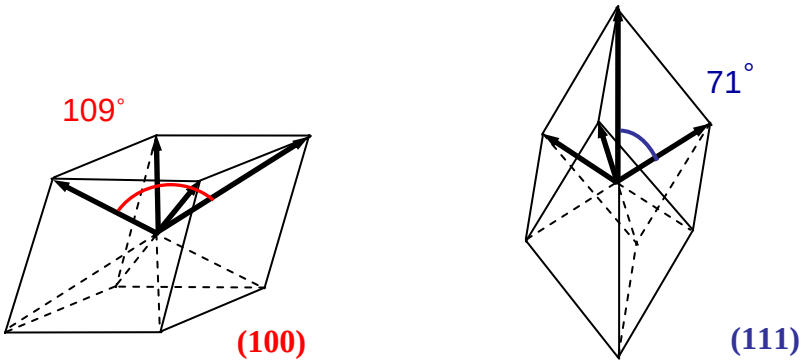

Figure **2.4**: Schematic representation of the available polarization directions in a rhombohedral cystal. For simplicity, two orientations of the crystal are shown and only upward polarization directions are indicated.

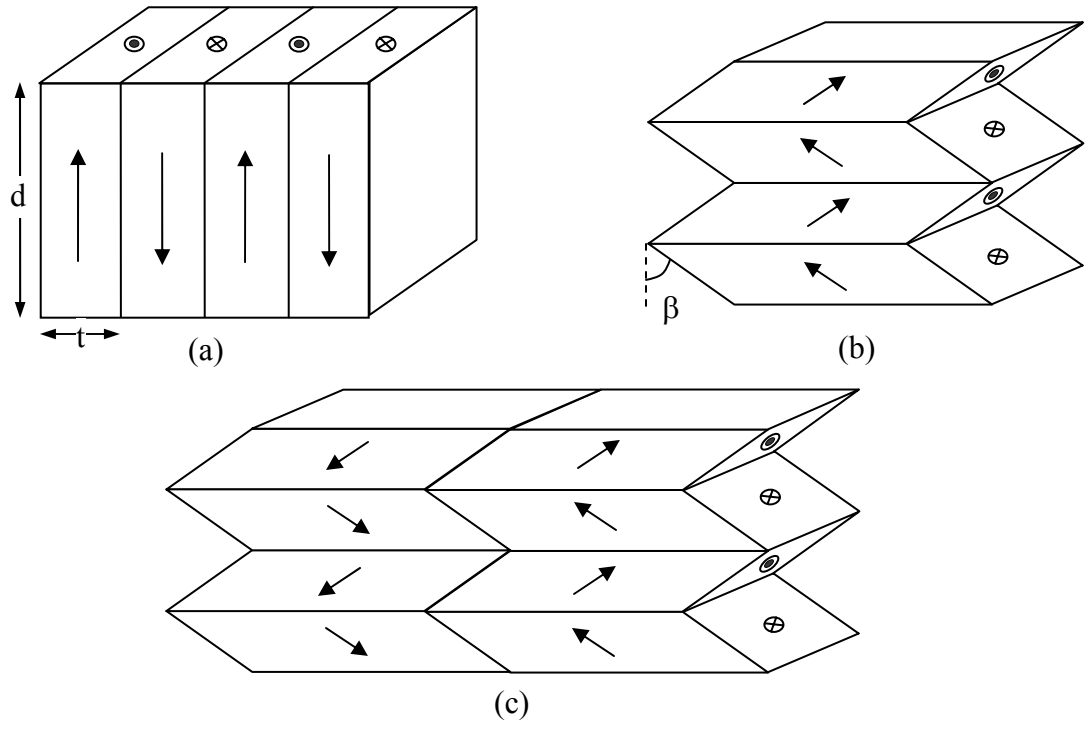

Figure **2.5**: Schematic representation of (a) 180º domain walls in a ferroelectric crystal after reference [**68**], (b) non-180º domain walls in a ferroelectric crystal after reference [**69**] and (c) a mixed domain structure after reference [**70**].

2.3.1 Ferroelectric Domain Formation

The occurrence of a spontaneous polarization in ferroelectric materials results in a change in lattice parameters and therefore is accompanied by the creation of a spontaneous strain[7] in the unit cell. [29] Due to the presence of surfaces, local imperfections and external boundary conditions, ferroelectric materials tend to lower their electrostatic and elastic energies by creating a domain structure. [1]

While in an ideal infinite ferroelectric the spontaneous polarization is uniform, due to the existence of surfaces and defects, in practice P_s is not uniform, leading to creation of depolarizing fields. The electrostatic energy associated with the depolarizing field is equal to, W_d [1]:

$$W_E = \frac{1}{2}\int_V D \bullet E \, dV \qquad \textbf{2.12}$$

In equation **2.12**, D is the dielectric displacement, E is the electric field and V is the volume of crystal. Free charge flow inside the crystal or in the surrounding medium can compensate for the depolarizing field, but in an insulating crystal and insulating medium this compensation can happen very slowly. To minimize W_E, different regions of the crystal polarize along different available spontaneous polarization directions. For a 180°

[7] Strain is defined in reference to the undistorted lattice.

domain structure such as in Figure 2.5a, the electrostatic energy becomes more complicated and can be written as [68][71]:

$$W_d = \frac{A_\varepsilon P_0^{\,2} V d}{t} \qquad \textbf{2.13}$$

In equation **2.13**, W_d is the depolarizing electrostatic energy, A_ε is a constant dependent on the dielectric permittivity of the material, t and V are the thickness and volume of the crystal respectively, P_0 is the polarization at the center of the domain and d is the domain width. It can be seen from equation **2.13** that this electrostatic energy decreases with a decrease in domain width. Therefore, a multi-domain crystal has a lower electrostatic energy than the single domain sample.

Creation of domains in ferroelectrics implies creation of domain walls, to which is also associated a free energy, W_w [1]:

$$W_w = \frac{\sigma}{d} V \qquad \textbf{2.14}$$

where σ is the energy per unit area of the domain wall. Therefore, to stabilize a 180° domain wall, the sum of both the depolarizing electrostatic energy and the domain wall energy is $W_d + W_w = 0$. This leads to the following relation [1]:

$$d \propto \sqrt{t} \qquad \textbf{2.15}$$

As can be seen in equation **2.15**, the domain size decreases with decreasing crystal size. Alternatively, in ceramics, the domain width decreases with the square root of the grain size. It should also be mentioned that in the presence of a large number of

free charges or if the charge mobility is high in the system at the ferroelectric phase transition (i.e. at T_c for proper ferroelectrics), the depolarizing field can be compensated, leading to the absence of a 180° domain structure. Good experimental examples of this include many $PbTiO_3$ and $K(Ta_{1-x}Nb_x)O_3$ single crystals. [72]

The elastic energy associated with the creation of the spontaneous strain in the ferroelectric can be reduced by creation of ferroelastic domain structures. The existence of external constraints (such as other grains or a substrate in the case of thin films) increases the amount of this elastic energy, promoting the creation of non-180° domain walls. Theoretical calculations performed for an array of twinned 90° domain walls (Figure 2.5c) in a clamped $BaTiO_3$ grain [70] [73] showed that:

$$d = \sqrt{\frac{\sigma_{90^\circ} g}{2kc\beta^2}} \qquad \textbf{2.16}$$

In equation **2.16**, obtained by minimization of the total energy of the system, d is the domain width, σ_{90° is the energy per unit area of the 90° domain walls, g is the grain size, k is a constant, c is the domain wall stiffness and β is the shear angle of the domains. Similar to the results for the 180° domain walls, the domain width decreases with the square root of the grain size. It has been confirmed experimentally [74][75] that the size of the domains decreases with decreasing grain size in barium titanate and lead zirconate titanate ceramics.

With decreasing grain size, the elastic energy reduction by creation of non-180º domain walls drops progressively. At a critical grain size, the elastic energy reduction can

become smaller than the energy associated with the formation of domain walls: a single ferroelastic domain state would be more stable than a twinned domain state in this case and therefore no non-180º domain walls would appear at grain sizes equal or below the critical grain size. The critical grain size has been reported to be around 8nm for $PbTiO_3$ [76] and around 40nm for $BaTiO_3$ [69].

It is important to emphasize that any two domains do not meet at arbitrary angles, in general. Fousek and Janovec [77] treated in detail the conditions for creation and the permissible orientations of domain walls in twinned ferroelectric crystals for which polarization is the order parameter for the phase transition. Permissible walls were defined as planes of material along which *"the spontaneous deformation of two neighboring domains fit each other."* [77] The spontaneous deformation was determined by the piezoelectric and electrostrictive tensors. The conditions for the presence of a domain wall between two domains with spontaneous polarization vectors along crystallographically equivalent directions (conjugate vectors) were then discussed. It was shown that in general two domains with conjugate polarization directions can:

a) Be separated by a wall with arbitrary orientation. These walls are non ferroelastic: W_∞.

b) Be separated by one of two perpendicular permissible walls, whose crystallographic indices are determined by the symmetry of the system: W_f walls.

c) Be separated by one of two mutually perpendicular planes determined either by only the crystallographic symmetry of the system, W_f wall, or

for the *S* wall, both by the symmetry and by the piezoelectric and electrostrictive properties of the material;

d) Be separated by two mutually perpendicular walls, whose directions are determined by the symmetry elements of the crystal and its piezoelectric and electrostrictive properties: *S* wall;

e) Not have permissible walls because the boundary conditions of equal deformation in the two domains can't be fulfilled: *R* case.

The non-existence of permissible walls does not mean that the two conjugated domains can't exist in the same sample. They could be separated either by irregular boundaries with high stresses or be each adjacent to an intermediate domain with whom permissible walls can be created. [77]

As a final note, the conditions for existence and determination of orientation of permissible walls were based on the hypothesis of infinite crystals. In practice, crystals being of finite dimensions and non-perfect, the directions of the walls may be slightly misoriented with respect to the Fousek - Janovec predictions.

To summarize, the particular configuration of the domain structure in a particular ferroelectric ceramic might depend on many factors among which the build-up of the domain walls themselves, the elastic stress fields, the presence of free charge carriers, the presence and distribution of local defects. [77] [78]

2.4 Intrinsic and Extrinsic Contributions to the Dielectric and Piezoelectric Response

The dielectric and piezoelectric response of ferroelectric ceramics are usually due to both intrinsic and extrinsic contributions. The intrinsic part is mainly due to the lattice, and is the average response of the single domains present in the ceramic. The extrinsic contribution is primarily associated with the motion of the domain walls and phase boundaries and displacement of defects. [79] Figure 2.6 shows schematically the intrinsic and domain wall contributions to the dielectric and piezoelectric properties.

In a perfect ferroelectric capacitor, the intrinsic and extrinsic parts both contribute to the real components (as defined in Equation 2.17) of the dielectric and piezoelectric

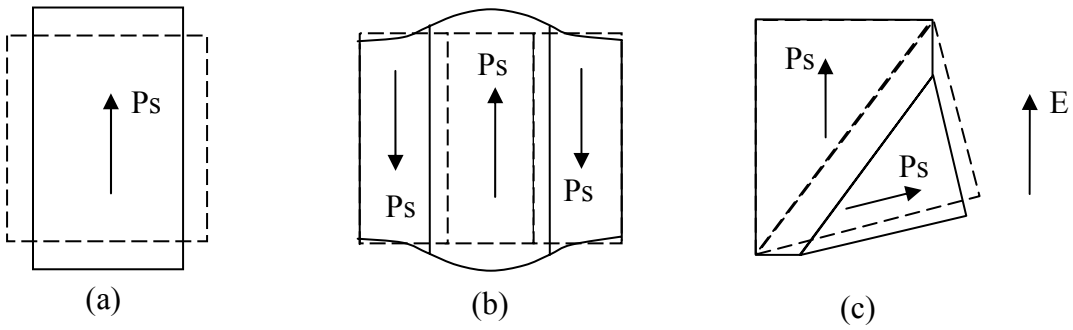

Figure 2.6: (a) Intrinsic contribution from a single domain under application an electric field E; (b) dielectric extrinsic contribution from the motion of a 180º domain wall; (c) dielectric and piezoelectric extrinsic contributions from the motion of a non-180º domain wall. The dashed lines represent the configurations before the application of the external electric field.

response, while the extrinsic component can also contribute to the loss mechanisms and therefore to the imaginary part of the response. [80]

$$\varepsilon^* = \varepsilon' - j\varepsilon'' \quad \text{and} \quad |\varepsilon^*| = \sqrt{(\varepsilon')^2 + (\varepsilon'')^2} = \varepsilon_r$$
$$d^* = d' - jd'' \quad \text{and} \quad |d^*| = \sqrt{(d')^2 + (d'')^2} = d \qquad \textbf{2.17}$$

In Equation 2.17, ε^* is the complex dielectric permittivity, ε_r is the absolute value of the dielectric permittivity, d^* is the complex piezoelectric coefficient and d is its absolute value[8]. ε', ε'', d' and d'' are the real and imaginary parts of the dielectric permittivity and the real and imaginary parts of the piezoelectric coefficient, respectively. Therefore, in a perfect ferroelectric ceramic with no resistive components, we can represent the real and imaginary parts of the dielectric and piezoelectric coefficients as in Equation 2.18:

$$\varepsilon' = \varepsilon'_{intrinsic} + \varepsilon'_{extrinsic} \quad \text{and} \quad \varepsilon'' = \varepsilon''_{extrinsic}$$
$$d' = d'_{intrinsic} + d'_{extrinsic} \quad \text{and} \quad d'' = d''_{extrinsic} \qquad \textbf{2.18}$$

To distinguish between the intrinsic and the extrinsic contributions to the properties of a ferroelectric, generally the variations of the property have been studied as a function of the ambient and excitation conditions. Investigations have been performed in terms of amplitude and frequency of the probing field, temperature and aging times. The amplitude of the field dependence will be discussed in detail in the following section, while the other methods are discussed below.

---

[8] Throughout this thesis,* denotes a complex entity, ' and " indicate respectively the real and imaginary parts of the same complex entity.

The frequency dispersion of the dielectric properties of ferroelectrics usually shows a step in the Gigahertz frequency range (see Figure 2.7). The origin of the step has been associated with the loss of contributions from domain wall vibrations and defect reorientation, although alternative mechanisms have also been suggested. [81][82][83][84][85][86] If indeed the fall in the dielectric permittivity is due to freezing of the domain wall contribution, then the dielectric permittivity at frequencies higher than this can be attributed to the ionic intrinsic response and the electronic displacement of atoms in the ferroelectric. The major drawback of this method is the fact that the measurement techniques present practical issues for the evaluation of the dielectric properties in the gigahertz range.

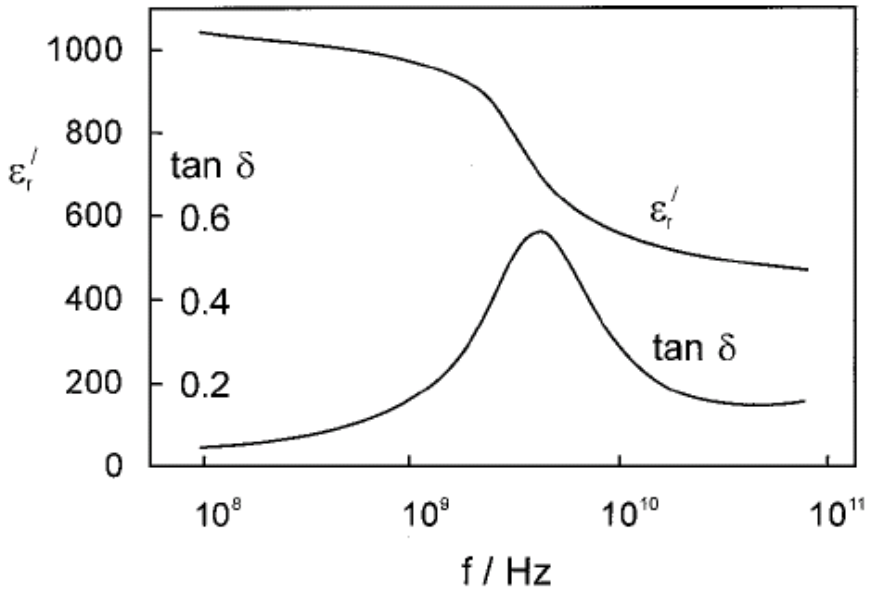

Figure 2.7: Frequency dependence of dielectric permittivity and loss of barium titanate ceramic, after reference [87].

The temperature dependence of the piezoelectric and dielectric properties has been used by several authors to separate the extrinsic and intrinsic contributions in ferroelectrics. [80][88][89][90][91][92] Because extrinsic contributions are based on thermally activated mechanisms, the reduction of temperature to values close to zero Kelvin should reduce the extrinsic contributions to almost null values. Using the remaining response and an approximation for the temperature dependence of the intrinsic properties, it is possible to derive the amount of intrinsic response at any other temperature. Figure 2.8 shows an example of the drop of the extrinsic contributions to the dielectric permittivity in a $Pb(Zr_{0.52}Ti_{0.48})O_3$ thin film. The authors in this case [93], assumed the low temperature (~12K) dielectric permittivity to be equivalent to the intrinsic contribution and almost invariant with temperature. Using a modified Landau–Ginzburg–Devonshire (LGD) theory which includes a polar cluster re-orientation term [94], the dc electric field dependence of the dielectric permittivity were studied. Extrinsic contribution was calculated as the reorientable polar cluster term.

Another method used to distinguish between the extrinsic and intrinsic contribution has been devised by Zhang et al. [2]. The authors assumed that the hydrostatic piezoelectric coefficient doesn't have extrinsic contributions due to the fact that domain wall motion doesn't involve volume changes. Extrinsic contributions to ε_{33}, d_{33} and d_{31} coefficients were derived (Figure 2.9) using constitutive relationships between the dielectric, piezoelectric and electromechanical properties, as in equations 2.19 to 2.21.

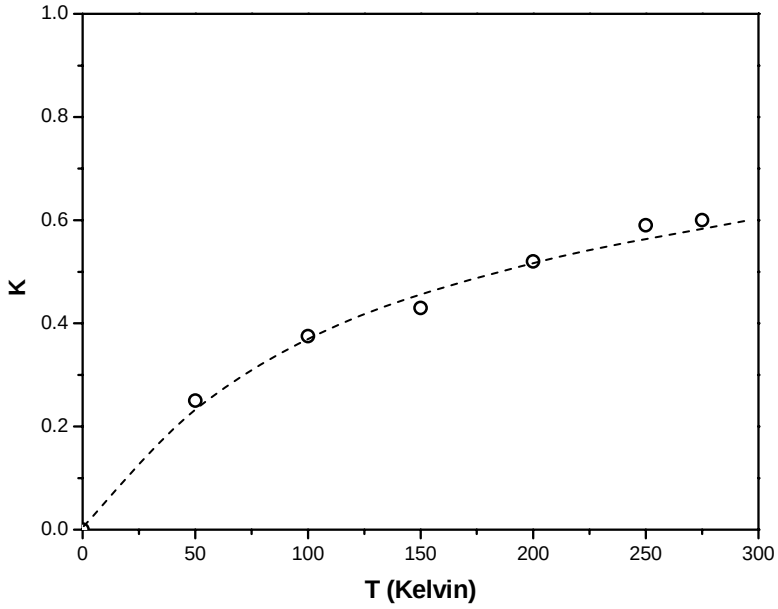

Figure **2.8**: Temperature dependence of the ratio $K = \frac{\varepsilon_{extrinsic}}{\varepsilon_{total}}$ of the extrinsic contribution relative ($\varepsilon_{extrinsic}$) to the whole dielectric permittivity (ε_{total}) in a $Pb(Zr_{0.52}Ti_{0.48})O_3$ thin film, after reference [**93**].

$$d_h = 2\varepsilon_{33}\varepsilon_0 Q_h P_r \qquad \textbf{2.19}$$

$$d_{33} = 2\varepsilon_{33}\varepsilon_0 Q_{11} P_r \qquad \textbf{2.20}$$

$$d_{13} = 2\varepsilon_{33}\varepsilon_0 Q_{12} P_r \qquad \textbf{2.21}$$

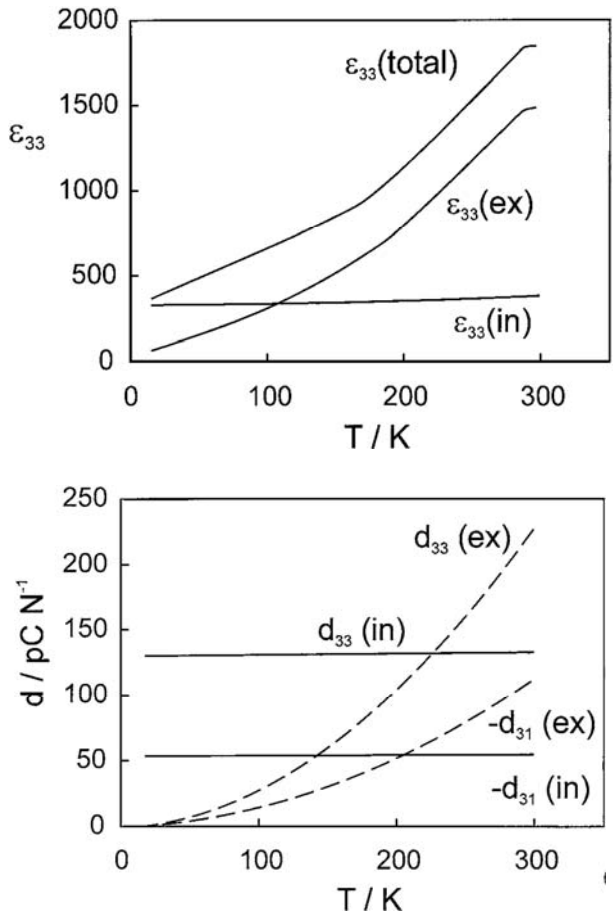

Figure **2.9**: Calculated temperature dependence of extrinsic contributions to dielectric (ε_{33}) and piezoelectric (d_{ij}) constants for soft PZT ceramics, after Zhang et al. [2]

From the temperature dependence of the hydrostatic piezoelectric coefficient d_h and remanent polarization P_r, the temperature dependence of the intrinsic dielectric permittivity $\varepsilon_{33(\text{int})}$ can be derived.[9] From this follows the temperature dependence of the intrinsic piezoelectric coefficients d_{33} and d_{31}. It should be noted, however, that the

[9] As mentioned in section 2.1, the electrostrictive coefficients Q_{ij} are nearly temperature independent.

derived values give the wrong temperature dependence of the intrinsic properties for some coefficients.

Arlt et al. [95][96] proposed a method based on the aging time of the dielectric and piezoelectric properties of the ferroelectrics with vibrating domain wall contributions. The intrinsic contributions are considered to be independent of the aging time and therefore the properties of the ferroelectric can be written as in Equation 2.22 :

$$\varepsilon'(t) = \varepsilon'_{intrinsic} + \varepsilon'_{extrinsic}(t) \text{ and } \varepsilon'' = \varepsilon''_{extrinsic}(t)$$
$$d'(t) = d'_{intrinsic} + d'_{extrinsic}(t) \text{ and } d'' = d''_{extrinsic}(t) \qquad \textbf{2.22}$$

The phenomenological model of the vibrating wall [96], as developed by Arlt et al., predicted also that the ratio of the imaginary to the real component of the dielectric coefficient should be constant and equal to the loss tangent of the domain wall motion, as shown in Equation 2.23 and reproduced in Figure 2.10.

$$\frac{\varepsilon''_{domain\ vibration}}{\varepsilon'_{domain\ vibration}} = \tan\delta_{domain\ vibration} \qquad \textbf{2.23}$$

Note that in general, a similar expression can be written also for the ratio of the imaginary and real piezoelectric coefficients, but because the theoretical evaluation has been shown only for 180° domain wall vibration, the loss tangent for the dielectric and piezoelectric properties is not necessarily the same.

Plotting the real vs. imaginary parts of either of these coefficients in terms of the aging time yields a line that has as its gradient the loss tangent. Extrapolation to zero loss

produces the intrinsic contribution to the property. Thus, the extrinsic contribution at any given aging time can be deduced.

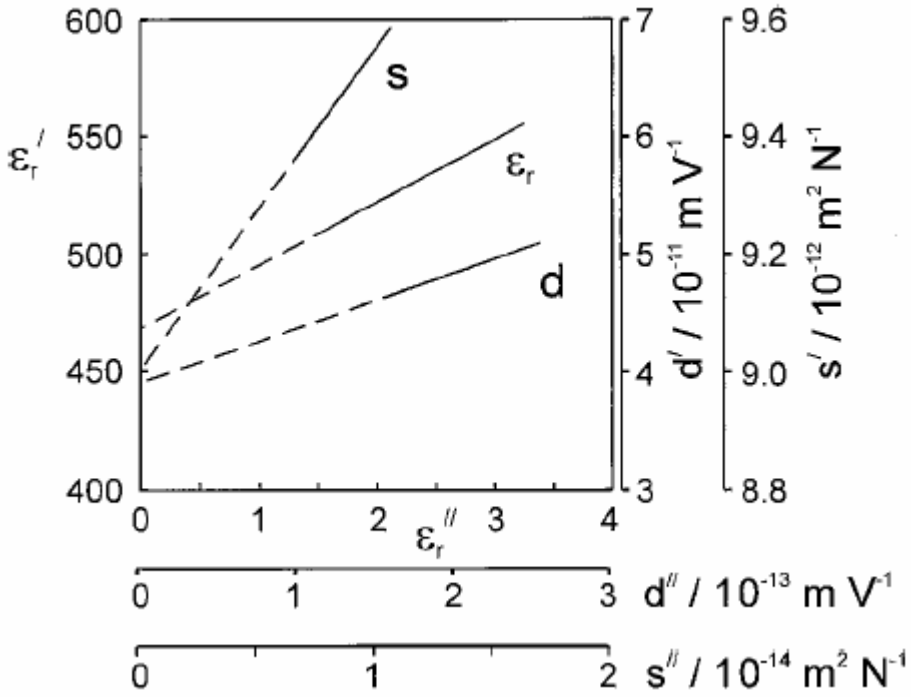

Figure **2.10**: Time dependent dielectric (ε_r), piezoelectric (d) and elastic coefficients (s) for hard PZT ceramic, after Herbiet et al.[**95**]

The above method can be applied only to those ferroelectric ceramics that exhibit relevant aging times. The aging method has been used successfully to study the clamping effects of the acceptor dopants on the motion of domain walls in hard ferroelectrics. [**95**] It was also experimentally applied by Eitel [**97**] to bismuth scandate-lead titanate ceramics, which showed a good adherence to Equation **2.23**.

2.5 AC Field Dependence of Dielectric and Piezoelectric Coefficients

Another method used to separate the extrinsic contributions to the dielectric and piezoelectric properties of ferroelectrics is the study of the amplitude dependence of the response. Conventionally, the linear relationship between dielectric displacement D and electric field E determines the relative dielectric permittivity, ε_r, while the linear relationship between the strain x and E determines the piezoelectric coefficient d, as in Equation **2.24:**

$$D = \varepsilon_0 \varepsilon_r E \qquad \text{and} \qquad x = dE \tag{2.24}$$

Dielectric and piezoelectric nonlinearity refer, respectively, to cases where ε_r and d are dependent on the driving field. Although the linear description is a valid approximation at lower field and stress levels, it becomes more and more inaccurate when higher external fields are applied. In piezoelectric actuators where the operating conditions are far from the linear behavior range, the real piezoelectric coefficient of soft PZT can vary from its low field value by ~100%. [**8**] Due to the application of piezoelectric thin films in MEMS, such nonlinearities may also be important. Similarly the thickness reduction of capacitive components has been accompanied with an increase in the applied electric fields. These fields are far beyond the onset of the nonlinear behavior. Thus, as in the ferroelectric capacitor field, the need for understanding, quantifying and modeling of these nonlinearities has increased. [**98**][**12**]

The nonlinear response has, in principle, both intrinsic and extrinsic components. In most cases, because the working conditions of the device are at field values below the

coercive field, the intrinsic nonlinearities are insignificant and therefore, the dominant nonlinearity in bulk ferroelectric perovskite ceramics is extrinsic in origin. [8]

It has been reported for different ferroelectric ceramics and thin films that a threshold field E_{th} exists, below which the dielectric and piezoelectric responses are independent of the ac field levels. [79][98][12][99] This value of E_{th} is often not easily set: in fact the increase in the properties can happen gradually and therefore an onset point is set relatively arbitrarily. A 5% rise with respect to the low field value has been proposed as the reference for E_{th} .[3] Because the nonlinearities have been associated with interface pinning, the threshold field is considered a measure of the degree of pinning in the material.[100][101]

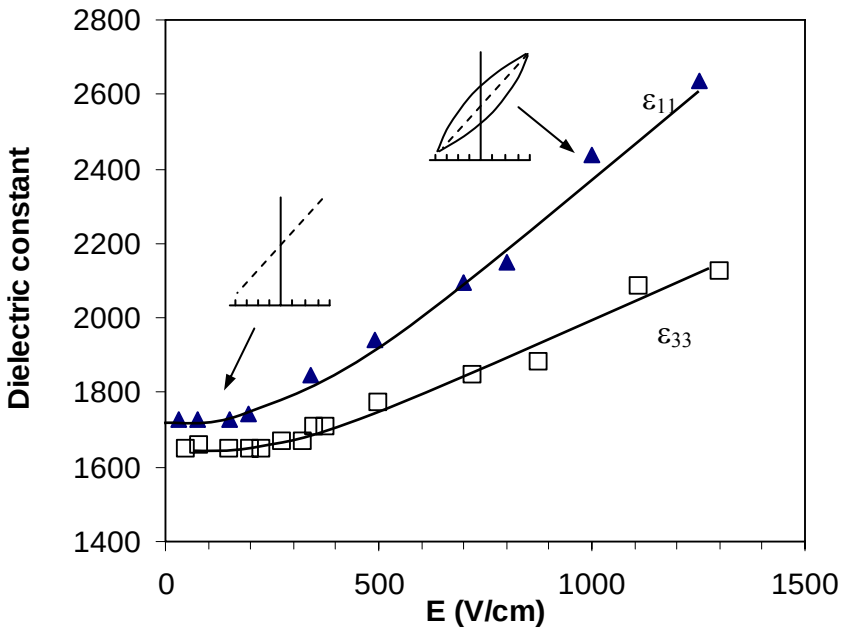

Figure 2.11: The nonlinear behavior of the dielectric permittivities ε_{11} and ε_{33} with the applied AC field in soft PZT ceramic, after Li et al.[3]

The behavior of the dielectric permittivity and piezoelectric coefficients for ac field amplitudes higher than E_{th} can be described by the Rayleigh Law.

2.6 Rayleigh Law

The Rayleigh Law was originally applied in 1887 by Lord Rayleigh to magnetization and magnetic permeability in ferromagnetic materials. It was shown that the magnetic permeability had a linear dependence on the amplitude of the applied magnetic field over an intermediate field range.[9] Although the Rayleigh Law was based on empirical observations, Néel demonstrated that the motion of a ferromagnetic wall in a randomly distributed energy profile created a magnetization could be described by the Rayleigh Law.[10][11] The mechanism involved the motion of a domain wall from one potential energy well to a new position under the application of a large enough drive field that would allow it to surpass an initial energy barrier. The pinning and unpinning of the domain walls from their original positions yields hysteretic behavior. Kronmüller later proposed correlations between the defect concentrations and the Rayleigh parameters, with defect concentration controlling the potential energies involved in the domain wall pinning and therefore their motion. [102]

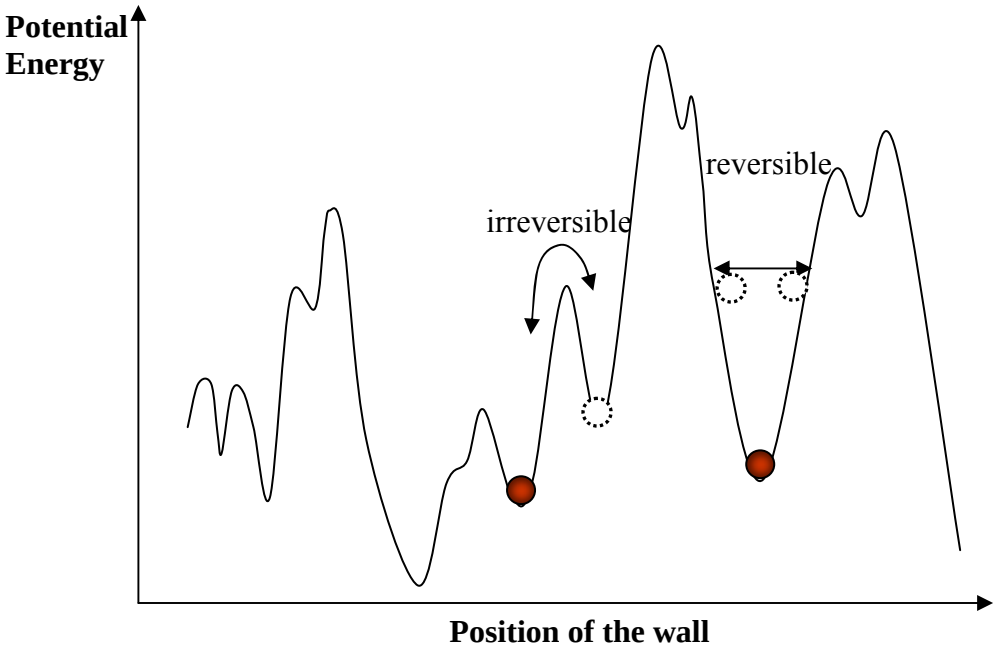

Figure 2.12: A schematic of the motion of interfaces (filled circles) in reversible or irreversible fashion in the available energy landscape. The position of the interface under applied field is indicated by the dotted circles. After reference [15]

In general, the Rayleigh relations describe the behavior of a material containing interfaces whose motion exhibit hysteresis and whose energy potentials/barriers for motion are uniformly distributed. In the case of ferroelectric materials, the interfaces have been associated with domain walls and phase boundaries moving across randomly distributed pinning centers. [10][11][14][103] In fact, the Rayleigh law has been demonstrated to successfully describe the nonlinear dielectric and piezoelectric behavior of ferroelectric bulk ceramics [13][14][15][97][104][105] and thin films [16][17][106]. The Rayleigh law, as given in Equations 2.25 through 2.30, can describe the ac electric field dependence of the permittivity and piezoelectric response of ferroelectric thin films

in sub-switching conditions, where the density and the structure of the domain walls remain unchanged with field cycling.

$$\varepsilon' = \varepsilon'_{init} + \alpha' E_0 \quad \text{(real dielectric permittivity)} \quad \textbf{2.25}$$

$$\varepsilon'' = \alpha'' E_0 = \frac{4}{3\pi}\alpha' E_0 \quad \text{(imaginary dielectric permittivity)} \quad \textbf{2.26}$$

$$P(E) = (\varepsilon'_{init} + \alpha' E_0)E \pm \frac{\alpha'}{2}(E^2 - E_0^2) \quad \text{(dielectric polarization)} \quad \textbf{2.27}$$

$$d' = d'_{init} + \alpha' E_0 \quad \text{(real piezoelectric coefficient)} \quad \textbf{2.28}$$

$$d'' = \alpha'' E_0 = \frac{4}{3\pi}\alpha' E_0 \quad \text{(imaginary piezoelectric coefficient)} \quad \textbf{2.29}$$

$$x(E) = (d'_{init} + \alpha' E_0)E \pm \frac{\alpha'}{2}(E^2 - E_0^2) \quad \text{(strain)} \quad \textbf{2.30}$$

E_0 is the amplitude of the driving field $E = \sin(\omega t)E_0$, P is the dielectric polarization, ε'_{init} and α' are the reversible and irreversible Rayleigh coefficients, respectively. α'' is the irreversible imaginary Rayleigh coefficient, which is equal to $\frac{4}{3\pi}\alpha'$. Separate Rayleigh parameters ($\varepsilon'_{init}, \alpha'$ and α'') and (d'_{init}, α' and α'') are determined for the dielectric and piezoelectric properties. ε'_{init} and d'_{init} are due to contributions from the intrinsic lattice and reversible boundary motion, while $\alpha' E_0$ is due to the irreversible domain wall or phase boundary displacement. A reversible motion involves the motion of the interface around its equilibrium position along the walls of the potential energy well. An irreversible motion of the interface (domain wall or phase boundary) refers to the

motion of the interface from one potential energy well to another, acquiring a new position as in Figure **2.12**.

The field dependence of the dielectric permittivity (or of the piezoelectric coefficient) can be separated into three main zones (Figure **2.13**):

1. an initial zone where the dielectric permittivity is independent of the applied field's amplitude: **low field region**;
2. **Rayleigh region**: at intermediate field values, the dielectric permittivity (or the piezoelectric coefficient) increases linearly with the applied electric field amplitude. This zone usually extends up to one third or one half the coercive field values;
3. at higher fields, the onset of switching (and depoling in the case of pre-poled samples) changes the energy landscape of the system. The Rayleigh Law no longer applies and the field dependence becomes sub or super linear. This zone is called the **high field region**.

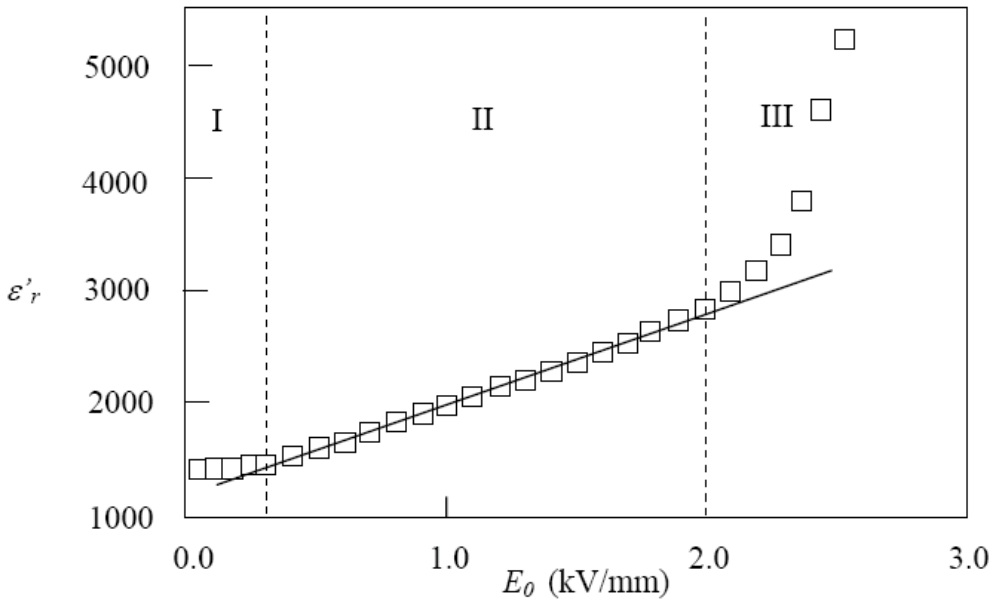

Figure **2.13**: Schematic of the ac field dependence of dielectric permittivity of hard PZT ceramic after reference [**18**]. The low field region (I), with constant dielectric permittivity, and the high field region (III) are separated by the Rayleigh region at intermediate fields (II) where the Rayleigh Law can be applied to the linear increase for dielectric permittivity with the amplitude of the applied ac field.

Considering that in many ferroelectrics the distribution of the energy barriers is not perfectly random and uniform, the experimentally observed behavior could show a smooth blending between the three regions, reducing the extent of the Rayleigh region. Robels et al. [**107**] showed this smooth blending of the regions with an almost complete elimination of the Rayleigh region, proposing a square field dependence of the dielectric permittivity for acceptor doped barium titanate and PZT ceramics that included the ac field dependence of the permittivity at low and intermediate high fields (Equation **2.31**).

$$\varepsilon_r(E_0) = \varepsilon_r(0) + aE_0^2 - bE_0^4 \qquad \textbf{2.31}$$

Equation **2.31** was showed to be valid both for the real and imaginary parts of the dielectric permittivity with positive a', a'' (or equivalently b' and b'' for piezoelectric properties) coefficients. The authors also reported that all the nonlinear coefficients decreased significantly with aging. Reduction of the nonlinear effect with aging was also reported by Hall and Ben-Omran [**20**] for cobalt-doped $BaTiO_3$ ceramics.

With a different approach, Mueller et al. [**108**][**109**] investigated the dielectric and piezoelectric nonlinearities in soft PZT ceramics and proposed a power law dependence of the coefficients on the ac field amplitude as in Equation **2.32**:

$$m(E_0) = m_0 + A\left(\frac{E_0 - E_t}{E_t}\right)^{\Phi} \qquad \textbf{2.32}$$

where m is either the dielectric or the piezoelectric coefficient, m_0 is the low field value, E_t is a threshold field and Φ is an exponent. The closer the Φ value to 1, the closer the material's behavior is to the Rayleigh predications. Indeed Φ was found to be close to 1 for soft lead zirconate titanate ceramics in measurements with the electric fields parallel to the polar axis (ε_{33} and d_{33}), while in shear-mode measurements (ε_{11} and d_{15}), Φ values were as high as ~1.2.

The Rayleigh Law has been applied not only to the ac electric field dependence of dielectric permittivity and piezoelectric coefficient but also to the ac stress dependence of the piezoelectric coefficient (d_{33} and d_{31}). The results have been shown to predict successfully the P-E hysteresis curves for different ferroelectric systems. It should be mentioned that at higher fields, the prediction became less accurate, probably due to intrinsic nonlinearity, causing an asymmetry in the shape of the hysteresis curves and

modification of the domain walls concentration and the energy profile of the system. [18][97][101] Both the dielectric permittivity and the piezoelectric coefficients have been shown to follow a logarithmic decay with frequency, which in analogy with the ferromagnetic domain walls, has been used to confirm the interface motion origin of the nonlinear phenomena. [13][15][16][19][110][111].

Boser [103] showed by theoretical calculations supported by the experimental observations by Hagemann [112] in $BaTiO_3$ ceramics doped with Fe, that in a ferroelectric material, the irreversible dielectric Rayleigh coefficient is inversely proportional to the concentration of pinning centers for the domain walls, as in Equation 2.33.

$$\alpha' \propto P_{sat}{}^{2} \frac{F_D}{L_3 N} \qquad \textbf{2.33}$$

P_{sat} is the saturation polarization, F_D is the area of the domain wall that moves as a whole, L_3 is the average distance between the domain walls and N is the number of pinning centers (Fe ions) per unit volume. The interaction between dopant and domain wall was considered to be elastic rather than electrostatic, which resulted in a higher interaction (pinning) with respect to a pure electrostatic consideration. [103][113]

In support of the domain wall motion origin of the dielectric nonlinearities, Hall et al. [21][22] also showed how Arlt et al.'s prediction [95][96] for contributions of domain walls' vibration at low field could be extended at higher fields in the Rayleigh region. The authors reported a linear relationship between the real and imaginary parts of the dielectric permittivity as a function of the ac field amplitude instead of aging time for

hard lead zirconate titanate ceramics. The dependence became sub-linear in the high field region, indicating the onset of the contribution from a lossier polarization mechanism, such as ferroelectric domain switching.

The Rayleigh Law also predicts creation of higher order harmonics. In fact, by developing with Fourier expansion Equations **2.27** and **2.30**, we obtain:

$$P(E) = (\varepsilon'_{init} + \alpha' E_0) E_0 \sin(\omega t) + \frac{4\alpha' E_0^2}{3\pi}\cos(\omega t) + \\ + \frac{4\alpha' E_0^2}{15\pi}\cos(3\omega t) - \frac{4\alpha' E_0^2}{105\pi}\cos(5\omega t) + \cdots \qquad \textbf{2.34}$$

$$x(E) = (d'_{init} + \alpha' E_0) E_0 \sin(\omega t) + \frac{4\alpha' E_0^2}{3\pi}\cos(\omega t) + \\ + \frac{4\alpha' E_0^2}{15\pi}\cos(3\omega t) - \frac{4\alpha' E_0^2}{105\pi}\cos(5\omega t) + \cdots \qquad \textbf{2.35}$$

It is seen that Rayleigh Law requires that the nonlinear effects be accompanied by creation of only odd order harmonics of strain and polarization. Phenomenological theory, on the other hand, is based on the polynomial expansion of a polynomial field dependence of polarization or strain. Equation **2.36** shows the field dependence of polarization (an equivalent equation can be written for the piezoelectric response):

$$P = P_0 + a_1 E + a_2 E^2 + a_3 E^3 + a_4 E^4 + \ldots \qquad \textbf{2.36}$$

A Fourier transform of Equation **2.36** yields:

$$
\begin{aligned}
P = P_0 + \frac{1}{2}a_2 E_m^2 + \frac{3}{8}a_4 E_m^4 + \ldots \\
+ \sin(\omega t)(\mathrm{a}_1 \mathrm{E}_\mathrm{m} + \frac{3}{4}\mathrm{a}_3 \mathrm{E}_\mathrm{m}^3 + \frac{5}{8}\mathrm{a}_5 \mathrm{E}_\mathrm{m}^5 + \ldots) + \\
+ \cos(2\omega t)(-a_2 E_m^2 - \frac{1}{2}a_4 E_m^4 - \frac{15}{32}a_6 E_m^6 + \ldots) + \\
+ \sin(3\omega t)(-\frac{1}{4}a_3 E_m^3 - \frac{5}{16}a_5 E_m^5 + \frac{21}{64}a_7 E_m^7 + \ldots) + \ldots
\end{aligned}
\qquad \textbf{2.37}
$$

As can be seen in Equation **2.37**, the phenomenological theory allows the presence of all the higher harmonics. Therefore, a study of the higher harmonic response of polarization and strain nonlinearity can also be used to distinguish between the intrinsic and extrinsic contributions to the dielectric and piezoelectric nonlinearities.[**17**] It is also important to note that the phenomenological theory based on a polynomial field dependence of the dielectric polarization shows no hysteretic behavior, while the Rayleigh approach predicts both a linear field dependence (in first approximation) of the dielectric permittivity (or piezoelectric coefficient) and a hysteretic behavior of the polarization (strain) with the ac field amplitude.

2.7 Ferroelectric Compositions

There are many different materials and compositions used for ferroelectric applications. But as mentioned in section **2.2**, oxide materials with the perovskite structure are one of the most widely used ferroelectric materials in industrial applications.

$BaTiO_3$ was the first ferroelectric perovskite to be discovered in the mid 1940's [114], and it became the subject for intensive studies [1] due to its higher ferroelectric properties and thermal and chemical stability with respect to other known ferroelectrics, the relatively simple structure, a ferroelectric transition temperature well above room temperature, and the ease of preparation in polycrystalline form [26]. Later in the 1950's, the $Pb(Zr,Ti)O_3$ (PZT) solid solution system was discovered, soon becoming the basis for most piezoelectric ceramics. The enormous success of the PZT system was due to superior piezoelectric properties and the possibility of higher operating temperatures. [63] [115] These were in part accredited to the existence of a morphtropic phase boundary (MPB) in the $xPbZrO_3$ - $(1-x)PbTiO_3$ system between rhombohedral and tetragonal phases at x~0.52. [63] [115] An MPB is a phase boundary that is nearly independent of temperature, but in practice, the MPB's exhibit some curvature with temperature. Later studies showed the presence of a monoclinic phase close to the MPB, attributing the increased properties of PZT at this composition to the existence of this lower symmetry structure. [116] Figure 2.14 shows the phase diagram of the PZT system with indication of the crystal symmetry of the different phases. At high temperatures, the material is in a cubic paraelectric state. The end member $PbZrO_3$ is an antiferroelectric[10]. Minor

[10] The concept of antiferroelectric was first introduced by Kittel [218] in analogy to antiferromagnetism. Antiferroelectrics show, similarly to ferroelectrics, high dielectric permittivity peaks at a transition temperature and above this temperature they show Curie-Weiss behavior. Antiferroelectrics have a net zero polarization and a center of symmetry, usually due to the opposite polarization in adjacent subcells of the crystal. Therefore, at low signal, there can't be any *P-E* hysteretic behavior. The free energy of the antiferroelectric crystals is usually very close to but below the free energy of a ferroelectric phase. Applying an electric field of appropriate strength can induce a transformation into this higher energy ferroelectric phase. A subsequent decrease in electric field returns the material to its original antiferroelectric phase. This is usually translated into a double *P-E* hysteresis loops. The dielectric properties of the material are different in the antiferroelectric and induced ferroelectric phases.[29]

additions of the other end member $PbTiO_3$ (a proper ferroelectric) are tolerated in the orthorhombic antiferroelectric state. Further additions of lead titanate transform the solid solution into a ferroelectric rhombohedral, ferroelectric monoclinic and finally a tetragonal ferroelectric phase.[1][116]

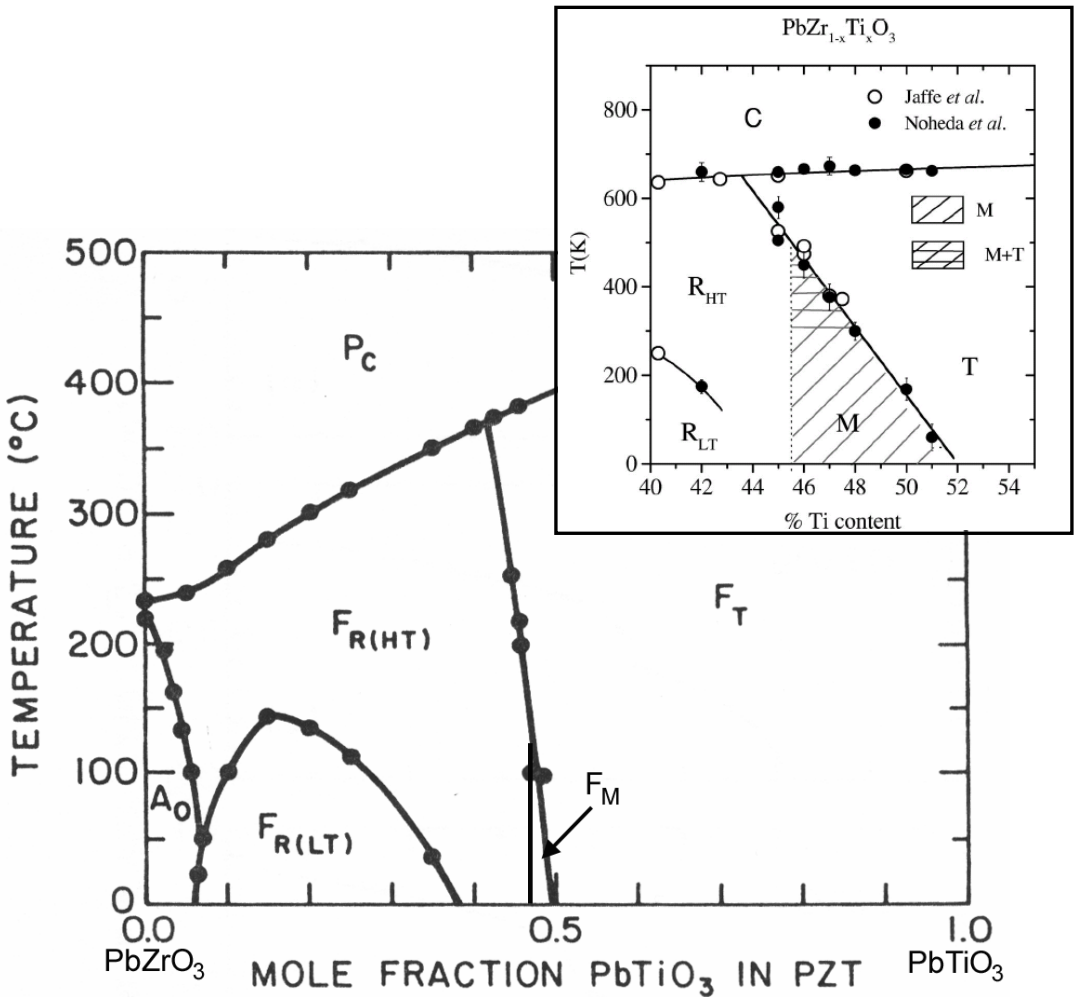

Figure 2.14: Phase diagram of the PZT system after references [63] and [116]. P_C is the paraelectric cubic phase, F indicates the ferroelectric phases, while the subscripts indicate the symmetry of the system. T is tetragonal, M is monoclinic, R(HT) and R(LT) are respectively the rhombohedral structures at high and low temperatures. A_O indicates an antiferroelectric orthorhombic phase. The inset shows details of the extension of the monoclinic phase as described by Noheda et al.[118]

The availability of multiple polarization directions from the crystal structures on both sides of the MPB, allows a better alignment of the ferroelectric dipoles during the poling process. The higher polarizability and degree of alignment leads to enhanced dielectric and piezoelectric properties of crystals close to the MPB composition.[63] Figure 2.15 shows the $PbTiO_3$ (PT) content dependence of the piezoelectric coefficients of PZT, as calculated by Haun et al. [119], with peaks corresponding to the MPB composition.

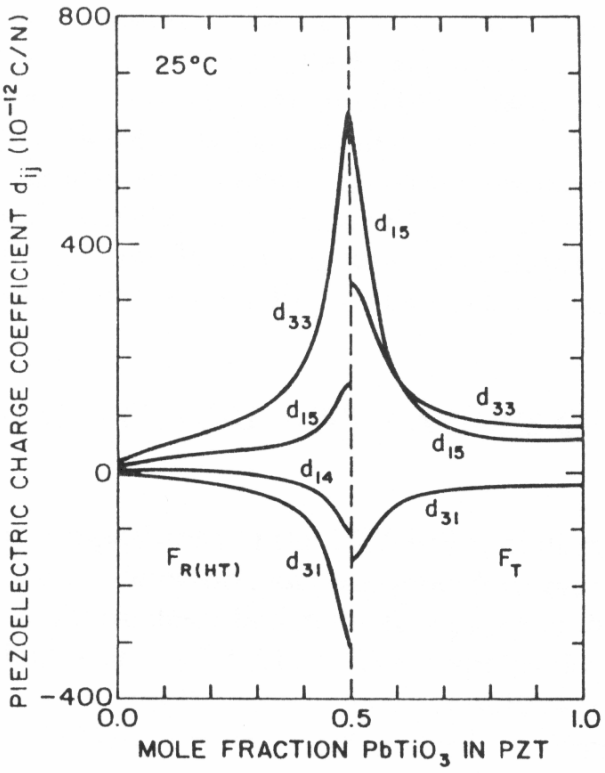

Figure 2.15: Calculated piezoelectric properties of PZT as a function of the $PbTiO_3$ content.[119]

The properties of PZT can be also be modified by addition of appropriate dopants, creating soft (lower T_C and higher dielectric and piezoelectric strain coefficients) or hard (higher T_C but lower dielectric and piezoelectric strain coefficients) PZT.

2.7.1 $Pb(B',B'')O_3$-$PbTiO_3$ Materials

Similarly to PZT, many other complex oxide solid solutions with the general formula $(1-x)A(B',B'')O_3$-$xPbTiO_3$ exhibit an MPB and have been studied for enhanced properties at MPB compositions. Although the perovskite *A* site can be occupied by different cations, some of the most studied compositions are the Pb-based complex oxide solid solutions with lead titanate (Pb^{2+} occupying the A site in the perovskite cell). The family of Pb-based MPB complex perovskites is usually referred to as *relaxor-ferroelectrics* because many of the end member $Pb(B',B'')O_3$ compositions showed relaxor dielectric behavior.

Relaxors are non-proper ferroelectrics, with a dielectric peak temperature T_m increasing with the measuring frequency. For temperatures well below T_m and high field strengths, the behavior of the material is distinctly ferroelectric with hysteretic $P-E$ behavior. Field cooling of a relaxor causes preservation of a spontaneous polarization at low temperatures and zero fields, which has a fast decay at subsequent increases in temperature, with depoling at temperature $T_F < T_m$. Furthermore, zero-field cooled relaxor

have a prototype symmetry that breaks only at microscopic level with the presence of micro-polar regions. More conventional macro-polar regions (domain-like) structures can be created by applying high field and decreasing the temperature. [29]

Table 2-1 reports a summary of properties of some of the perovskite MPB $Pb(B',B'')O_3$-$PbTiO_3$ piezoelectric ceramics.

Table 2-1: MPB perovskite $Pb(B',B'')O_3$-PT systems and their properties. Dielectric and piezoelectric properties refer to polycrystalline samples. *F* and *AF* refer to ferroelectric or antiferroelectric end members respectively. For comparison, data for undoped PZT ceramics are also shown.

End member $Pb(B',B'')O_3$	T_C of end member (°C)	*F* or *AF* end member	MPB composition (mol% PT)	T_C at MPB (°C)	ε_r at 1kHz	d_{33} (pC/N)	Ref.
$Pb(Mg_{1/3}Nb_{2/3})O_3$	-10	F	33	160	5000	690	[120]
$Pb(Zn_{1/3}Nb_{2/3})O_3$	140	F	9*	190	-	-	[121]
$Pb(Sc_{1/2}Nb_{1/2})O_3$	90	F	42	260	2200	450	[122]
$Pb(Sc_{1/2}Ta_{1/2})O_3$	26	F	45	205	4000	655	[123]
$Pb(Yb_{1/2}Nb_{1/2})O_3$	280	AF	50	360	1600	472	[124][125]
$PbZrO_3$	240	AF	48	360	800	220	[63][115]

* : value for single crystal sample

Many of these complex solid solutions have claimed higher dielectric and piezoelectric responses than undpoed PZT ceramics. Furthermore, many of these materials can also be produced in single crystal form, while no single crystal PZT of usable size could be produced.[27][126][127]

In single crystal form, $Pb(Mg_{1/3}Nb_{2/3})O_3$-$PbTiO_3$ (PMN-PT), $Pb(Zn_{1/3}Nb_{2/3})O_3$-$PbTiO_3$ (PZN-PT), $Pb(Sc_{1/2}Nb_{1/2})O_3$-$PbTiO_3$ (PSN-PT) and $Pb(Yb_{1/2}Nb_{1/2})O_3$-$PbTiO_3$ (PYbN-PT) have been shown to exhibit high piezoelectric, dielectric and

electromechanical coupling coefficients on the rhombohedral side of the MPB when measured along the [001] crystallographic direction, even though [111] is the polar direction. [4][5][128][129][130] This use of a different poling scheme to improve the properties of the material is referred to as "domain engineering"; because of the off-polarization direction poling (in this case, the [001] direction for a rhombohedral crystal), a multi-domain single crystal is created, which seems to indicate the central role of the domain structure for the enhancement of the properties of the crystal.

Park and Shrout [131] reported also large strains with reduced hysteresis for electric field dependence of strain in [001] oriented single crystals of PZN-8%PT poled along the <001> orientation. Crystals poled along the [111] crystallographic axis showed lower strain and piezoelectric coefficients. The authors suggested that the higher stability of the engineered domain configuration and reduced depoling in [001] poled samples were responsible for the observed effect.

Ozgul [132] showed also that the rhombohedral MPB PZN-PT and PYbN-PT crystals are not subject to fatigue when poled along the [001] direction at temperatures and fields lower than those required for rhombohedral-tetragonal phase transition. The same crystals underwent fatigue if poled along the [111] axis.

The domain engineered results are not valid only for relaxor-ferroelectrics: in fact single crystals of $BaTiO_3$ have also shown an increase in the piezoelectric properties due to poling along a crystallographic axis different from the polarization direction.[133] While the relaxor ferroelectrics have been probed for poling along [001] direction of the rhombohedral crystals, $BaTiO_3$ crystals that show a tetragonal structure at room temperature have been poled along the [111] direction. [133] The [111] poled $BaTiO_3$

single crystals showed twice larger piezoelectric coefficients with respect to [001] poled ones. It should be noted that this increase is much smaller than what has been reported for relaxor-ferroelectric system single crystals, but the authors attributed the difference to the different nature of relaxor and proper ferroelectric domain structures. [133]

The higher dielectric and piezoelectric responses in relaxor-ferroelectrics come usually at the expense of lower transition temperatures. Lower T_C is usually translated into a lower thermal stability of the properties of the material and lower stability of the polarization (P_r). At increasing temperatures, the energy barrier between different polarization directions in the material decreases, increasing the tendency of the dipoles to reorient, which results in a reduction of the net polarization in the material. [134] These factors greatly influence the thermal working range of the device, which is usually restricted to half the transition temperature.[135]

Among the above-mentioned systems, (1-x)Pb($Yb_{1/2}Nb_{1/2}$)O_3-x$PbTiO_3$ exhibits one of the highest Curie temperatures (≈360°C) near the morphotropic phase boundary (x≈0.5). [124][136] Therefore, piezoelectric properties with good temperature stability and a wide working temperature range can be expected.

2.7.2 (1-x)Pb($Yb_{1/2}Nb_{1/2}$)O_3-x$PbTiO_3$ (PYbN-PT) System

Antiferroelectricity in PYbN was first reported by Smolenskii et al. [137]. Later studies showed that PYbN had a monoclinically distorted perovskite structure [138][139] at temperatures lower than T_C (~300°C) [87][140]. Choo et al. [141] later on suggested

that at ~195°C PYbN undergoes an antiferroelectric to ferroelectric transition and therefore should be ferroelectric at room temperature. Kwon et al. [142] reported that PYbN's structure at room temperature is orthorhombic, with an ordering of the Yb^{3+} and Nb^{5+} ions in the octahedral sites of the perovskite cell and antiparallel displacements of Pb atoms.

Lead titanate was first reported to be ferroelectric in 1950.[143] It has a tetragonally distorted perovskite structure at room temperature and T_C ~490°C.[144] PT is typically modified to sinter bulk polycrystalline ceramics, which has the effect of reducing the Curie temperature.[145][146]

Addition of PT to PYbN entails substitution of Ti at the B-sites. (1-x)PYbN-xPT changes from antiferroelectric, to relaxor and then to normal ferroelectric behavior with increasing x, but the composition range of each of these zones is not uniformly agreed on in literature, as can be seen in the following review.

Yamamoto et. al [124] reported that the phases at room temperature change continuously from antiferroelectric $(x = 0)$ to ferroelectric $(x = 0.1 \text{ to } 0.15)$, relaxor $(x = 0.2 \text{ to } 0.49)$ and again ferroelectric $(x > 0.49)$. Lim et al. [136] reported phase changes from antiferroelectric $(0 \le x \le 0.1)$ to relaxor $(0.1 < x \le 0.25)$, and then ferroelectric for $x \ge 0.3$. In both cases, the samples were bulk ceramics and the authors agreed on the position of MPB at x~0.5 and corresponding T_C ~360°C. Their results are summarized in Figure 2.16. MPB PYbN-PT ceramics have also been produced by Duran et al. [125][147] with similar T_C values.

Zhang et al. [148] produced and characterized single crystals of PYbN-PT with compositions across the phase diagram ($0 \le x \le 0.9$). They reported a continuous change from relaxor to normal ferroelectric behavior in the range of $0.2 < x < 0.8$ and MPB at x~0.5. The Curie temperatures were slightly lower than the reported values for bulk ceramics due to addition of 1mol% Ba to the single crystal samples to increase perovskite stability.

Pulsed laser deposited PYbN-PT thin films have been reported by Bornand et al. [149][150][151], and Yoshimura et al. [152][153]; by reactive magnetron sputtering by Im et al.[154] and by chemical solution deposition by Zhang et al. [155] and Zhou et al. [156]. The hetero-epitaxial films by Bornand and Yoshimura showed higher Curie temperatures at the morphotropic phase boundary than either the single crystals or the polycrystalline samples of similar compositions by 10 to 20°C.

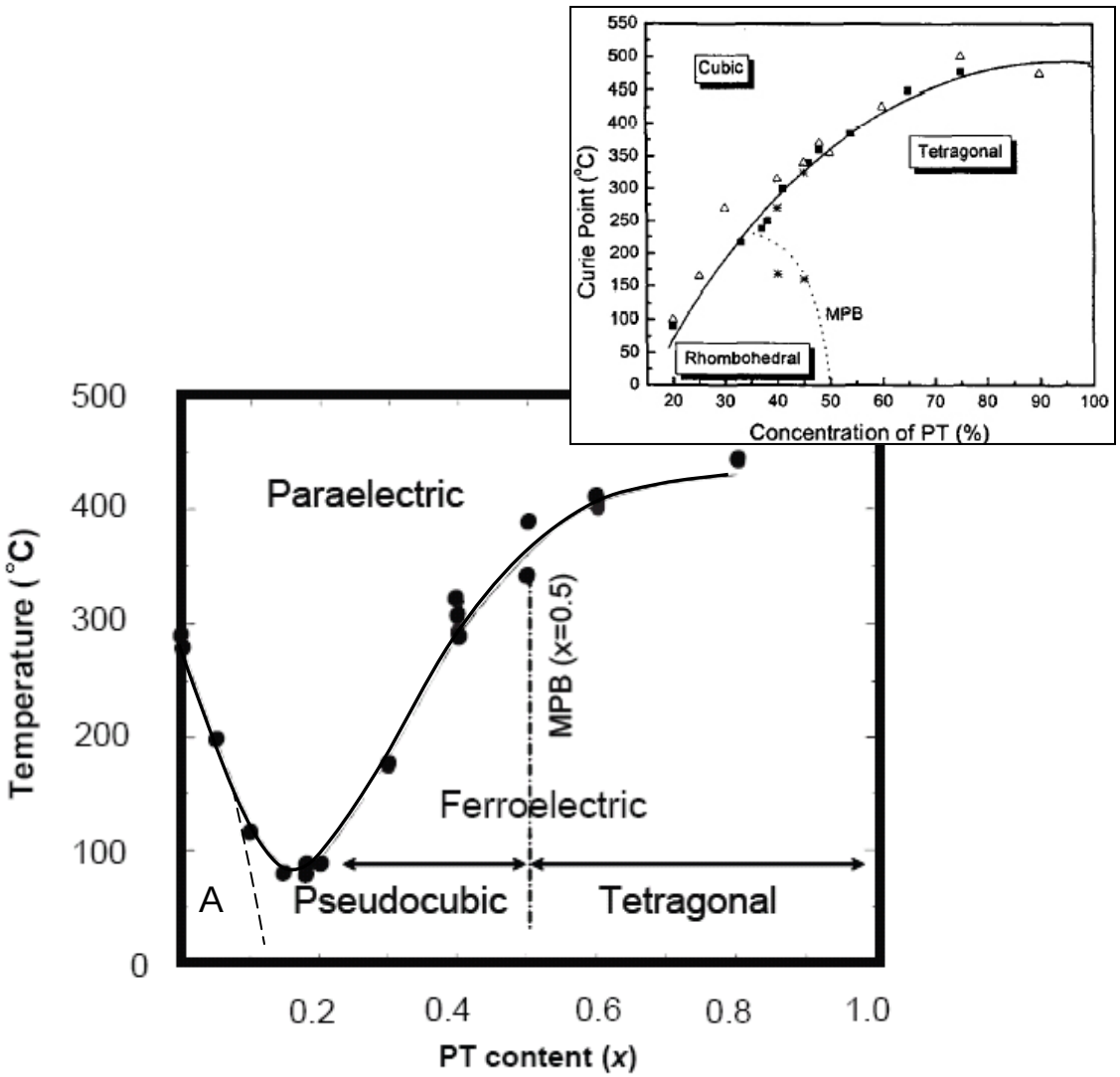

Figure **2.16**: Phase diagram of the (1-x)PYbN-xPT system after reference [**124**]. "A" indicates the extension of the antiferroelectric phase to room temperature after reference [**136**]. The inset shows the modification to the phase diagram for curvature of MPB by Zhang et al. [**157**].

As mentioned in section **2.7.1** single crystals (bulk and thin film) of PYbN-PT on the rhombohedral side of MPB have been reported to exhibit high piezoelectric, dielectric and electromechanical coefficients when poled along the [001] crystallographic

axis. A summary of the dielectric and piezoelectric properties of PYbN-PT bulk single crystals and epitaxial thin films is reported in Table 2-2.

Table 2-2: Dielectric and piezoelectric properties of (1-x) PYbN-PT bulk single crystals and epitaxial thin films.

	d_{33} (pC/N)			ε_{33} at $1kHz$		
	<100>	<110>	<111>	<100>	<110>	<111>
60PYbN-40PT single crystal [130]	1200	900	730	2100	2463	1628
	e_{31} (C/m^2)			ε_{33} at $1kHz$		
50PYbN-50PT epitaxial films on $SrTiO_3$ [152]	-12	-	-3.3	1300	-	1000
60PYbN-40PT epitaxial films on $SrTiO_3$ [152]	-9	-	-2.5	1300	-	1000

No indications were found in the literature regarding the amount of extrinsic and intrinsic contributions for the properties measured along different crystallographic orientations in this material.

Chapter 3

Experimental Procedure

This chapter details the procedures used to prepare lead ytterbium niobate – lead titanate ferroelectric thin films and to characterize their structure and microstructure. In addition, the procedures used to measure the electrical and electromechanical properties are discussed.

3.1 Chemical Solution Deposition Processing

Lead ytterbium niobate - lead titanate thin films prepared by a chemical solution deposition (CSD) method were used for the majority of the nonlinear dielectric and piezoelectric characterization in this work. The CSD method allows preparation of samples with good control of the chemistry and homogeneity.

A methoxyethanol-based route was chosen due to the good solubility of the precursors for many lead-based ferroelectrics. [158][159] Following the work of Zhou et al. on CSD PYbN-PT films [156], Yb-isopropoxide, $Yb[OCH(CH_3)_2]_3$ (Alfa Aesar, Ward

Hill, MA), and Nb-ethoxide, $Nb(OC_2H_5)_5$ (Chemat Technology Inc., Northridge, CA) were used as precursors. In a glove box, a stoichiometric amount of the Yb precursor was dissolved in 2-methoxyethanol, $CH_3OC_2H_4OH$ (Aldrich Chemical, Milwaukee, WI) by simple stirring at room temperature, before adding the Nb precursor. Unless otherwise specified, all the batching was performed by mass. The liquid was then mixed under flowing dry argon for 4 hours at 110º-120ºC in a rotary evaporator. Note that the temperatures listed through out this section refer to the temperatures of the oil bath in which the flask containing the solution was immersed. Titanium-IV isopropoxide, $Ti[OCH(CH_3)_2]_4$ (Aldrich Chemical, Milwaukee, WI) was then added in a glove box under dry atmosphere to the solution, followed by 8 hours of stirring under flowing dry argon at temperatures between 110º and 120ºC.

In a separate flask, lead acetate tri-hydrate, $(CH_3CO_2)_2Pb\bullet 3H_2O$ (Aldrich Chemical, Milwaukee, WI) was dissolved in 2-methoxyethanol and then vacuum distilled at 110ºC to obtain a white powder. In view of the volatilization of Pb at relatively low temperatures [**160**][**161**][**162**], the amount of Pb precursor used was 10 to 30% in excess of the stoichiometric requirements. The Yb-containing solution was then added to the dehydrated lead acetate and stirred for 4 additional hours under dry Ar flow at 110º-120ºC. The final solution was then vacuum distilled in an attempt to remove by-products [**163**] and adjusted by addition of more solvent to produce a total of 80ml of 0.17M solution. Figure **3.1** shows a schematic presentation of the different steps of the sol-gel preparation.

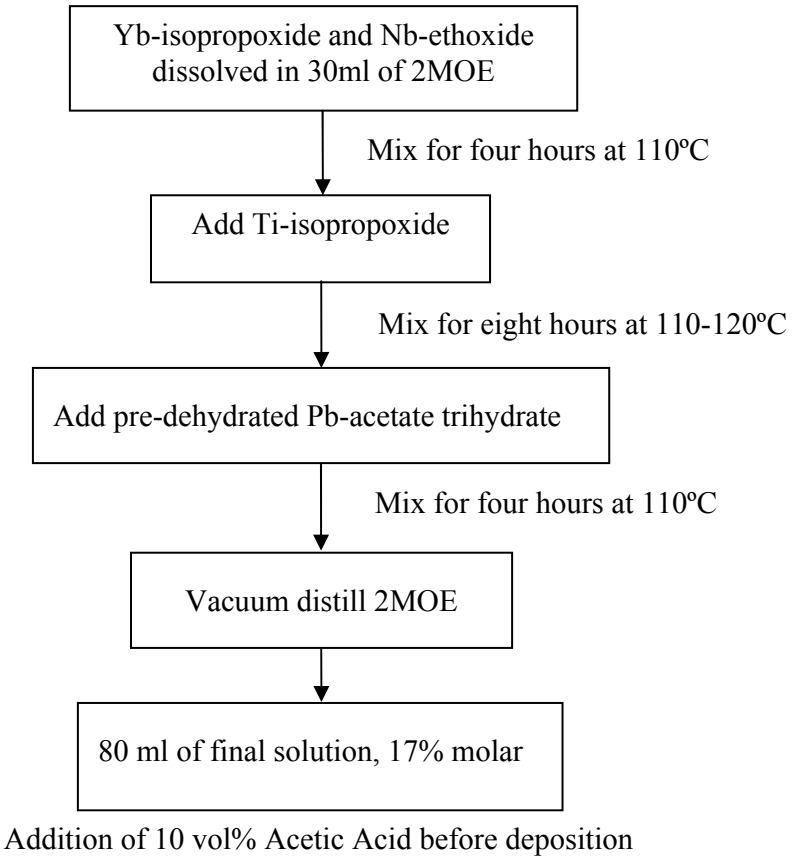

Figure **3.1**: Schematic flow-chart of the CSD preparation

The Yb^{3+} and Nb^{5+} ions located on the B-site of the perovskite structure have different charges. It has been reported for PYbN-PT thin films deposited by rf magnetron sputtering that any local compositional deviation from a 1:1 Yb:Nb ratio disturbs the charge valence at the B-sites. For less than 2% deviation, the perovskite phase is still achieved, probably by charge compensation due to creation of ionic defects.[**154**] In this work, the Nb and Yb sources were mixed in the first stage of the process in an attempt to obtain better mixing. The solution, because of the Yb and Ti precursors, is very sensitive

to the moisture level. It is imperative to avoid contact with humidity by working in controlled atmosphere with low humidity levels. This has been achieved by stirring the solution under a constant flow of dry argon. Addition of each component was performed in a glove box with humidity levels < 5% using Ar as the buffer gas. The temperature of the oil bath had to be kept higher than the boiling point for water, but lower than 120ºC. Higher temperatures induced partial loss of 2-methoxyethanol by evaporation (boiling point ~125°C). Consequently, changes in reflux temperatures and/or contact with ambient air had to be strictly avoided in order to prevent solution precipitation.

The obtained solutions were stable with a shelf life of up to many months. Before deposition, 10 vol% of acetic acid, CH_3COOH (J.T. Baker, Phillipsburg, NJ) was added to the solution and mixed for 5 minutes, in order to increase the stability of the solution to the ambient humidity for the spinning step. The shelf-time of this final solution was up to 24 hours.

3.2 Deposition and Crystallization of PYbN-PT Thin Films

To prepare films, the solution was spin coated on platinized (100) silicon substrates (Nova Electronics, Richardson, TX) at 3000 rpm. The silicon substrates had 1μm thick thermally grown silicon dioxide. This was sputter coated with 200 Å of Ti, used as adhesion layer, and 1500 Å of Pt. The platinum layer was crystallographically (111)-oriented. In addition to the above-mentioned substrates, similar wafers with a 10

nm thick {100}-oriented $PbTiO_3$ seed layer (courtesy of Dr. Paul Muralt, EPFL, Switzerland) [164][165] were used to obtain some of the {100} oriented PYbN-PT thin films.

Each deposition step was followed by a pyrolysis step at temperatures between 350ºC and 400ºC and a crystallization step. Crystallization was performed in a rapid thermal annealer (Heatpulse 210, AG Associates, San Jose, CA or RTP 600, Modular Process Techonology Corp., San Jose, CA) at temperatures between 550 and 750°C for 60 seconds. The pyrolysis temperature and hold time, as well as the crystallization temperature and ramp rates were varied in order to obtain {111} and {100} crystallographic orientations and decrease the amount of second phase. The deposition steps were repeated until the desired thickness was obtained. Final film thicknesses ranged between 100 and 680nm. Above this thickness, the preferential orientation of the films was reduced to less than 75%.

For electrical characterization, Pt top electrodes were sputtered through a shadow mask with circular openings (0.2 to 0.8mm in diameter). The electrodes were post-annealed at 500º-650ºC for 60 seconds. Figure 3.2 shows schematically the above mentioned steps.

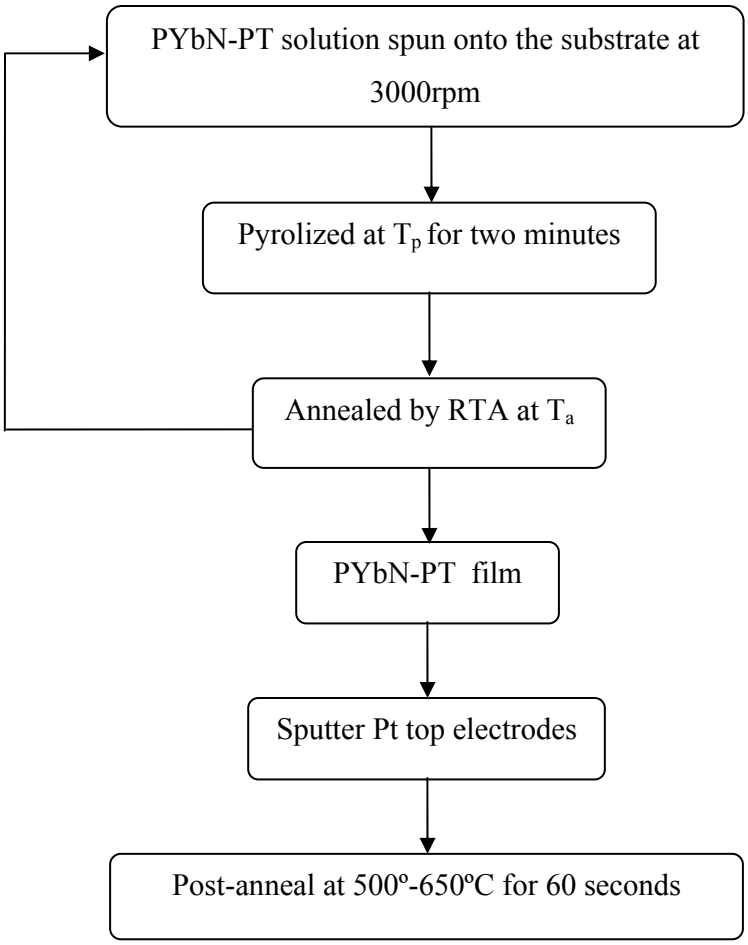

Figure 3.2: Schematic of the steps for preparation of PYbN-PT thin films.

3.3 Structural Characterization of the Films

The orientation of the films and the formation of the perovskite phase was studied by X-Ray diffraction (XRD). A Scintag Pad V X-ray Powder Diffractometer (Scintag Inc., Cupertino, CA) using Cu K_α radiation on a θ-2θ goniometer, equipped with a Ge

liquid nitrogen cooled solid-state detector, was used. Acquisition conditions were 35 kV and 30 mA. Scans were obtained typically from 20 to 60 degrees 2θ, with a step size of 0.02 degrees, a count time of 1.2 seconds and scan rates of 1.00 º/minute.

To study the formation of second phases close to the surface, X-Ray diffraction data in a grazing angle configuration were collected. A Scintag X2 (Scintag, Cupertino, CA) using Cu K_α radiation on a θ-θ goniometer equipped with a Si(Li) Peltier detector in grazing angle configuration was used. Data were collected for grazing angles from 0 to 15° were used.

3.4 Microstructural and Thickness Characterization

The surface morphology and film thickness were analyzed using a Scanning Electron Microscope, SEM (S-300H Hitachi, Hitachi Instruments, San Jose, CA). A thin gold film was sputtered on the top of the PYbN-PT films in order to increase the conductivity and reduce charging effects during the scans.

In order to measure the film thickness with a profilometer, a well-defined step must be created. However, it was found that wet-etching of the PYbN-PT films required long soaking times in strong acidic solutions (HF and HCl), which resulted in attack of adhesion layer between the Si and the Pt, therefore peeling the film from the underlying Si wafer (Figure 3.3 and Figure 3.4).

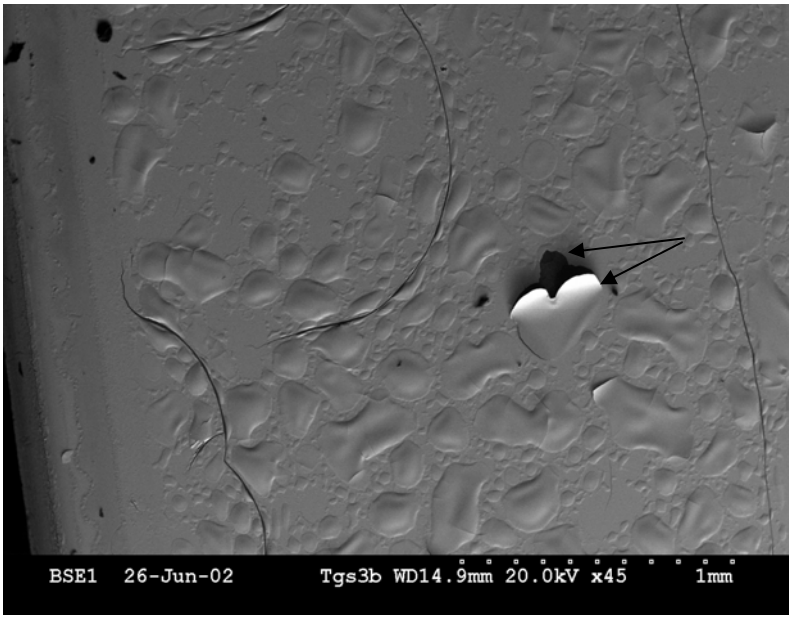

(1)

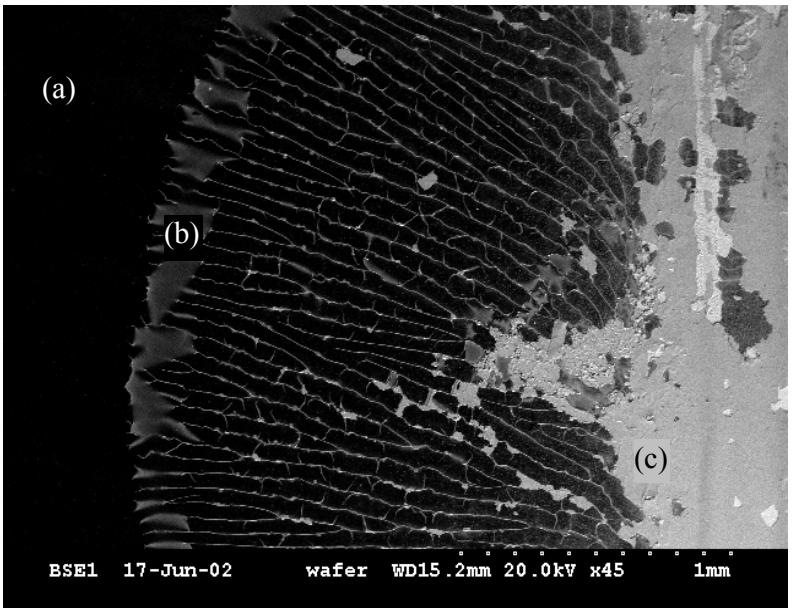

(2)

Figure **3.3**: Peeling of the film from the Si substrate in two different configurations.

(1) The sample's surface showed localized detachment of the film from the substrate. The round shape of the delamination spot has been associated before [**166**] to the attack of HF on TiO_x and SiO_2 from pinholes created by Ti diffusion through the Pt layer. The arrows indicate the actual peel off of part of the surface film (Pt and residual PYbN-PT oxide film) from the underlying Si substrates (in black contrast) as identified by EDS.

(2) A delamination pattern with almost complete removal of the oxide film, Pt and Ti adhesion layers. Underlying Si wafer in black contrast (a); Pt and Ti residues in metallic contrast, sunburst pattern (b); ferroelectric oxide film residues in light grey contrast (c).

Energy dispersion spectroscopy (EDS, IMIX, Princeton Gamma-Tech Inc., Princeton, NJ) was used to identify the chemical origin of the SEM contrast.

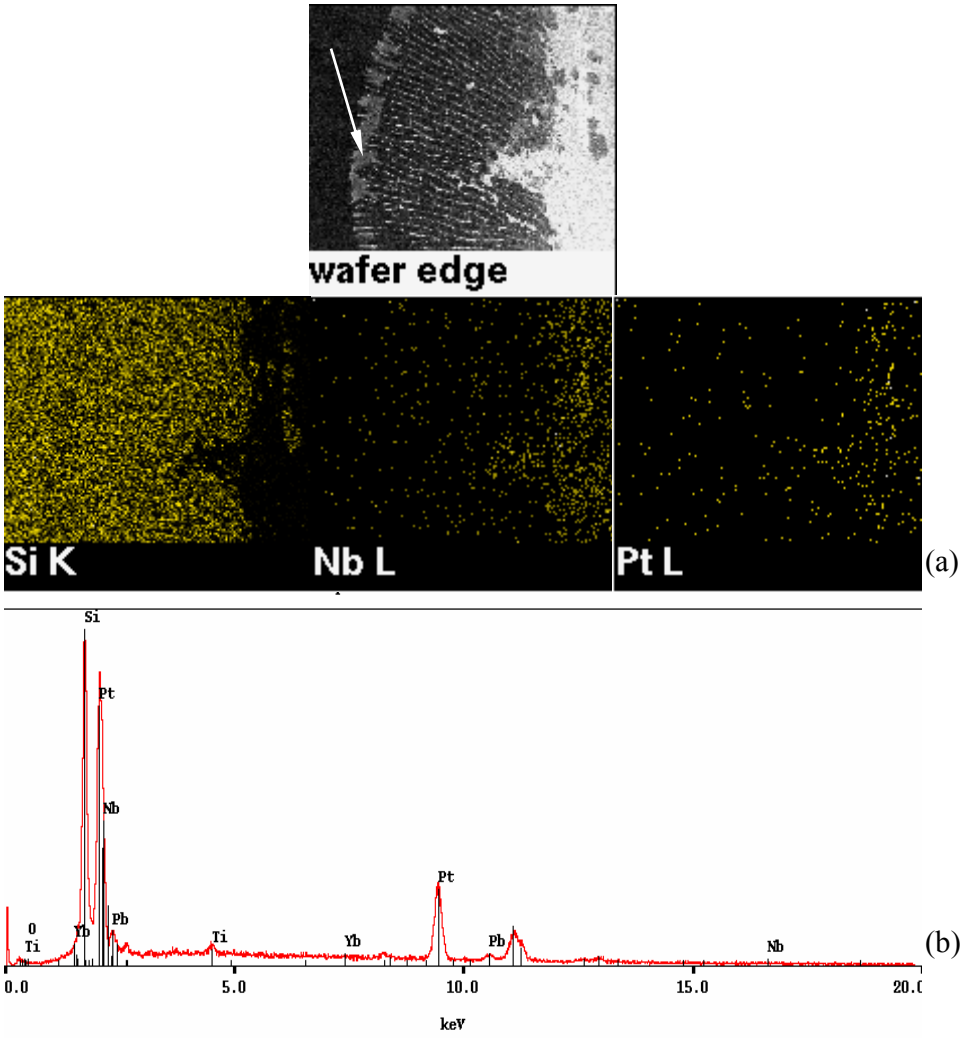

Figure **3.4**: EDS analysis of the sample shown in Figure **3.3**.(2). Figure (a) shows the chemical mapping of the sample shown in the SEM picture with Si (K line), Nb (L line) and Pt (L line). Figure (b) shows the EDS spectra for the point indicated by the arrow in part (a).

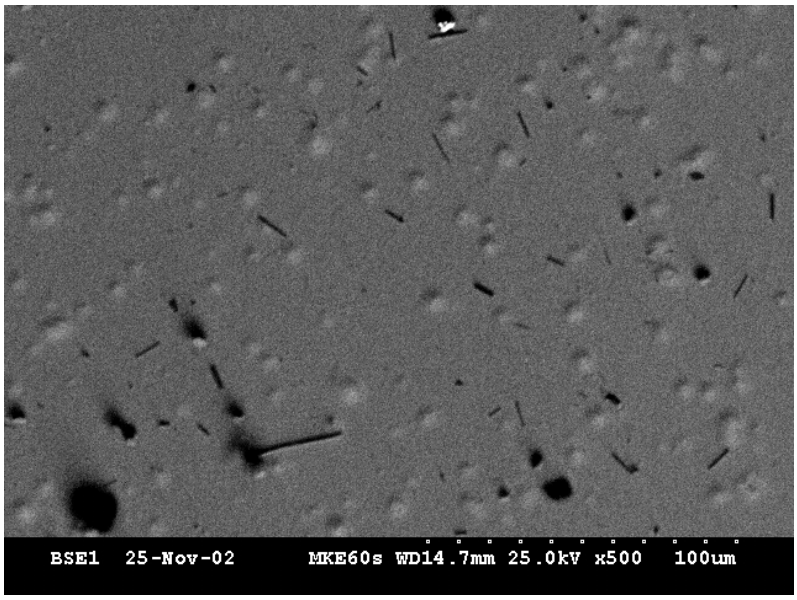

(a)

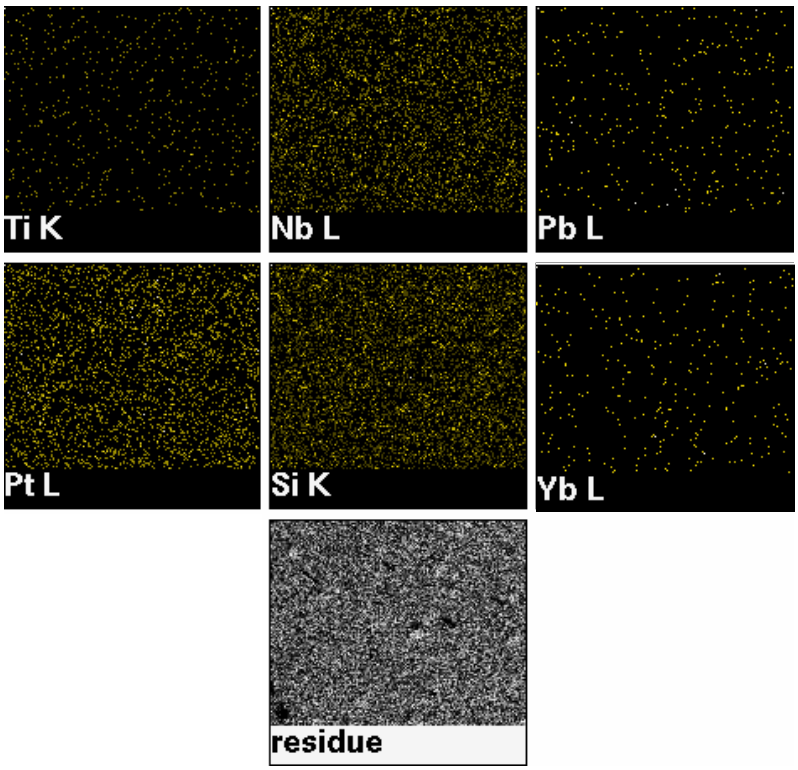

(b)

Figure **3.5**: SEM (a) and EDS chemical map (b) of sample surface after chemical etching with photoresist protection of sample. The hemispherical shapes in grey contrast are local delamination spots from the underlying Si wafer. The EDS spectra show prevalence of Nb in the film residues. The rod-like features were not big enough for a local EDS analysis.

Although covering the sides of the sample with protective coatings (photoresist) reduced this problem, film residues (Figure 3.5) and sloped step sidewalls were observed. As a result, it was not possible to create a clean step-edge for profilometry measurements in this way. Thus film thickness was measured by SEM using fracture cross-sections. The resulting thickness values were subject to approximately 5% error.

3.5 Characterization of the Surface Structure

An Atomic Force Microscope, AFM (Nanoscope III, Veeco Instruments, Chadds Ford, PA) was used in tapping mode to study the surface morphology and surface roughness of the PYbN-PT films. Silicon cantilevers, 160 μm long with a 300 kHz resonance frequency were used. For these measurements, the PYbN-PT samples were prepared by cutting smaller pieces (maximum dimension 10mm) that were then ultrasonically cleaned while immersed in acetone, de-ionized water, ethanol and de-ionized water, sequentially. The excess liquid was then dried off by N_2 airbrush.

3.6 X-Ray Photoemission Spectroscopy

The chemical composition of the films was studied with a Kratos Analytical (Chestnut Ridge, NY) Axis Ultra with a monochromatic Al K_α x-ray source. The samples

were wrapped in aluminum foil and mounted on conducting carbon tape. XPS quantification was performed by applying the appropriate relative sensitivity factors (RSFs) for the Kratos instrument to the integrated peak areas. These RSFs take into consideration the x-ray cross section and the transmission function of the spectrometer but do not take into consideration any preferential sputtering artifacts. The approximate sampling depth under these conditions was 25Å. The measurements were performed by Jeffrey Shallenberger at Penn State University.

3.7 Low Field Electrical Characterization

The capacitances and loss tangents of the PYbN-PT films were determined using a Hewlett-Packard (Agilent Technology, Palo Alto, CA) 4192A LF impedance analyzer. All the measurements, unless otherwise specified, were performed at 1 kHz with a 0.03 V oscillation voltage (rms). The frequency dependence of the low field capacitance and loss were measured using the same impedance analyzer. Point probes were used throughout this study for making contacts to the electrodes.

Given the difficulties in chemically etching the PYbN-PT films, an alternative system for contact to the bottom electrode has been used. Large pads ($\geq$ 30 mm^2) of Pt were deposited on the top the films resulting in a short-circuit to the bottom Pt electrode. These large pads of Pt were then regularly used as a means to contact the bottom electrodes and therefore will be referred to as bottom electrodes is this thesis.

3.8 High Field Electrical Characterization

Polarization-electric field hysteresis loops were obtained by use of an RT66A Standardized Ferroelectric Test System (Radiant Technology Inc., Albuquerque, NM). The values for coercive field, E_C and remanent polarization, P_r were extracted from the same measurements. An external amplifier (AVC Instrumentation 790 Series Power Amplifier) was used to increase the output voltage of the system. Maximum applied fields were up to 1000kV/cm. The measurement frequency was 30 Hz.

The tunability (capacitance-voltage) curves were obtained by use of a HP 4192A LF impedance analyzer at 1kHz and 0.03V (rms, ac voltage). In this measurement a small signal oscillating voltage was superimposed over a slowly swept dc bias. The top electrode was used for application of high voltage. The samples were first gradually taken to $+V_{DC}$. Capacitance data were then registered for DC voltage sweep from $+V_{DC}$ to $-V_{DC}$ and back to $+V_{DC}$.

Alternatively, an Aixacct TF Analyzer 2000 (Germany) with an option for multiple frequency measurements has been used for both the frequency dependent hysteresis loops, and tunability measurements.

3.9 Piezoelectric Measurements

The $d_{33,f}$ piezoelectric properties of the films were characterized by both double beam laser interferometry and scanning probe microscopy in the piezo-response mode (PFM). The former measurements were performed at the Ecole Polytechnique Federale de Lausanne, Switzerland by Dr. Susan Trolier-McKinstry, while the latter were made at University of Maryland by Dr. Florin Zavaliche and Jun Ouyang.

The piezoelectric $e_{31,f}$ coefficients were measured by modified wafer flexure method. Prior to any measurements the samples were first poled using an HP Harrison 6200B dc power supply (Agilent Technology, Palo Alto, CA).

It is important to underline that the piezoelectric coefficients measured in thin films differ from the equivalent values in bulk samples. This is due to the fact that thin films are usually clamped to a much thicker substrate and therefore the elastic behavior of the film is dominated in the plane by constraints from the substrate. Thus effective piezoelectric coefficients are measured for the thin films, $e_{31,f}$ and $d_{33,f}$ that are expressed by equations **3.1** and **3.2** [**167**][**168**]:

$$e_{31,f} = \frac{d_{31}}{s_{11}^E + s_{12}^E} \qquad \textbf{3.1}$$

$$d_{33,f} = d_{33} - \frac{s_{31}^E}{s_{11}^E - s_{12}^E} d_{31} \qquad \textbf{3.2}$$

where s_{ij}^{E} are the elastic moduli at constant electric field and d_{ij} are the piezoelectric coefficients for an unconstrained sample. The absolute value of $e_{31,f}$ is always larger than e_{31}, while $d_{33,f}$ is smaller than d_{33}.[169]

3.9.1 Double Beam Laser Interferometry

Double beam interferometry measures the AC displacements of the sample induced by an applied AC electric field. [117] The effective piezoelectric coefficient is then calculated by the ratio of the strain to the applied electric field.

The measurement set-up (see Figure 3.6) is based on the variation in the intensity of the interference fringes created by a reference beam and a second beam that has been reflected off both sides of the sample. The piezoelectric-coated substrate is aligned in the beam so that the laser strikes the front and back surfaces on either side of the same spot on the wafer. To improve the reflectivity, the back side of the sample was polished to a mirror finish with diamond paste. An alternating electric field is then applied via point probes, in order to drive the sample into oscillation. The use of the double beam configuration significantly reduces errors associated with piezoelectricaly-induced bending of the samples. [170][171]

The change in the intensity of the interference fringes is due to the variation of the path length of light (as in Equation **3.3**) by the strain created in the sample due to the piezoelectric effect (schematically shown in Figure **3.6** b).

$$I = \frac{1}{2}(I_{\max} + I_{\min}) + \frac{1}{2}(I_{\max} - I_{\min})\sin\left(\frac{4\pi\Delta L}{\lambda}\right) \qquad \textbf{3.3}$$

I is the light intensity, $I_{\max}$ and $I_{\min}$ are respectively the maximum and minimum light intensities in the interference fringes, ΔL is the optical path variation due to the piezoelectric strain created in the sample and λ is the wavelength of the laser beam.

The intensity change is detected by a photo-detector and converted into voltage changes as in equation **3.4**:

$$V_{out}(t) = V_{dc} + \frac{2\pi}{\lambda} V_{pp} \Delta L(t) \qquad \textbf{3.4}$$

where V_{dc} is any dc offset used, V_{pp} is the peak-to-peak voltage corresponding to the change of intensity from $I_{\max}$ to $I_{\min}$ and V_{out} is the voltage output from the pre-amplifier collected by an SR 830 lock-in amplifier (Stanford Research Systems, Sunnyvale, CA). From equation **3.4** and the knowledge of the wavelength of the laser beam, the change in the optical path due to the displacement of the sample is found.

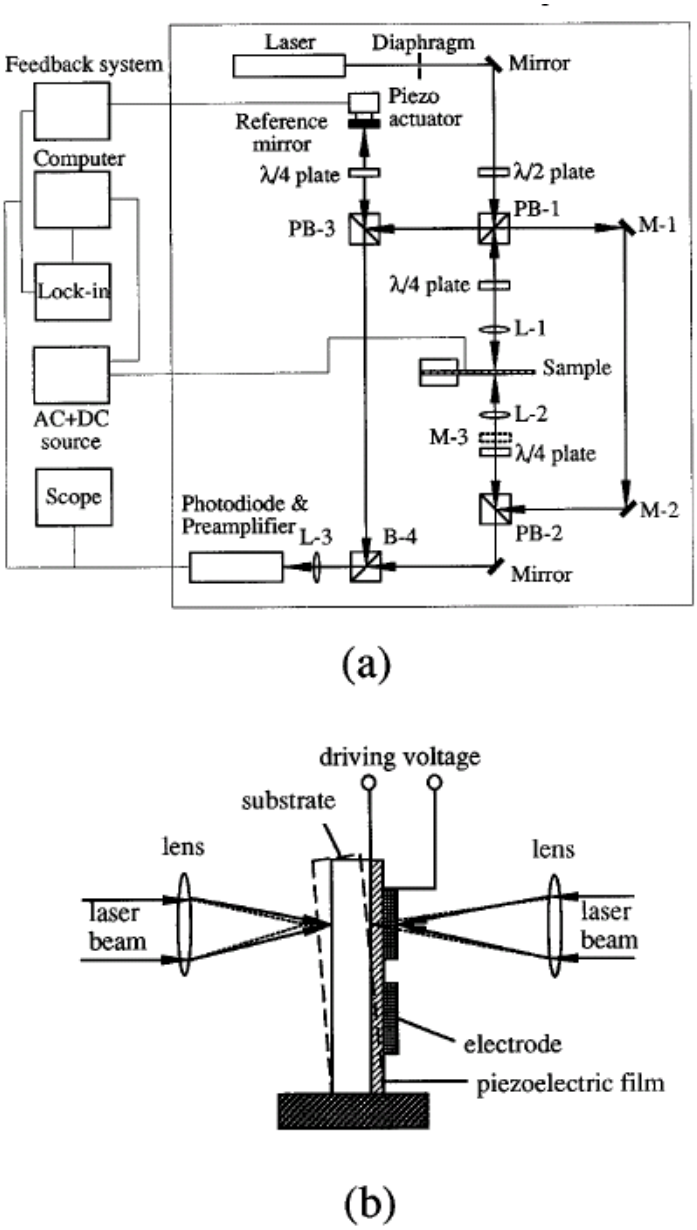

Figure **3.6**: Schematic of the (Mach-Zehnder) Double-Beam Laser Interferometer (a) and close-up of the sample (b) after [**117**]

The double beam interferometry measurements were performed for frequencies between 20 and 20000 Hz, with 0 to ± 6V dc voltages applied. Due to the nature of the

measurement itself, the experiments are extremely sensitive to presence of external noise and any vibrations associated with components of the system. These translated into the presence of various resonance peaks and an increased background noise for measurements at certain frequencies. Particular attention was paid to avoid these frequency ranges. At the higher end of the analyzed frequency range, a small continuous decrease in phase angle and piezoelectric constant was observed, probably due to the presence of a large resonance peak at even higher frequencies. Frequencies with phase angles differing from ideal by ≥10° were not used for final data analysis.

The same set-up was also used for the piezoelectric nonlinear measurements (principal and higher harmonics analysis). The nonlinear measurements were performed at frequencies far from resonances (as described in the previous paragraph) for AC sweeps typically from 0 to 2V (rms values). Simple nonlinear measurements were mostly performed under applied bias voltage (0 to $\pm$ 6V) in order to stabilize the polarization and the response of the samples. The higher harmonics analysis were made without DC bias.

3.9.2 Wafer Flexure Method

In order to measure the $e_{31,f}$ coefficients, a small chip of the sample (1 cm x 1 cm) was glued (by super glue) to the center of a 10 mils thick, 3" diameter Si wafer. The Si wafer was then clamped on the top of a cavity, by use of two polished Al rings fitted to

grooves as shown in Figure 3.7. The pressure in the cavity is cyclically changed at 4Hz by connection to a second cavity, on which an audio speaker was fixed. The motion of the audio speaker with the specific frequency modulated the pressure inside this second cavity and consequently the wafer fixed on the cavity is bent with the same frequency. The charge created by the sample was measured through an SR 830 lock-in amplifier (Stanford Research Systems, Sunnyvale, CA). The strain created by the cyclic pressure was measured by gluing a strain gage (Omega pre-wired strain gauge, KFG-1N, for which the gauge factor was 2.11 and the gauge resistance was 120 Ω, Omega Engineering, Stamford, CT) on the top electrode during a second set of measurements. The strain gauge was connected to a quarter bridge assembly (Figure 3.8), powered at +4V, read by the lock-in amplifier.

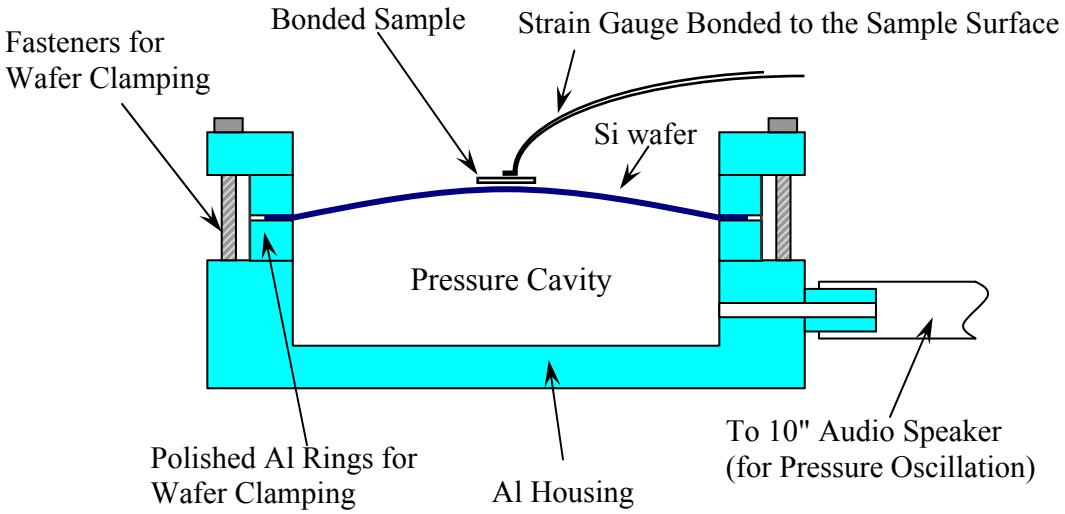

Figure 3.7: Schematic drawing of the experimental set-up for Wafer Flexure Method, after reference [172] and [173].

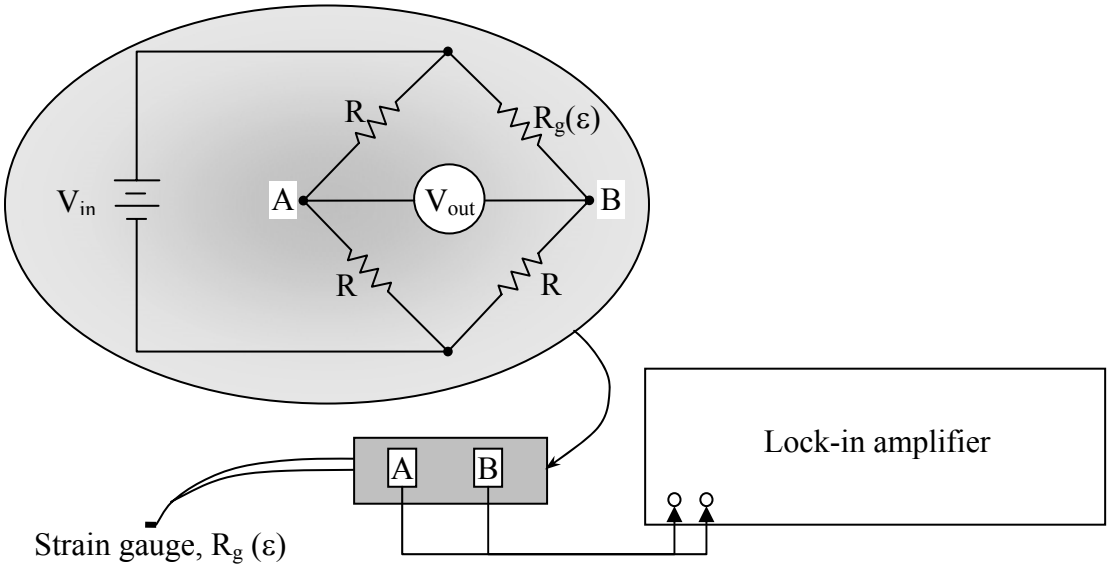

Figure **3.8**: Schematic of the quarter-bridge assembly used for strain measurement. V_{in} is the +4V input voltage, R are the resistances used in the quarter bridge circuit, equal to 120Ω, $R_g(\varepsilon)$ is the resistance of the strain gauge dependent on the strain. The output of this quarter bridge, V_{out}, is read through the connection to the lock-in amplifier.

The effective piezoelectric coefficient is then calculated as:

$$e_{31,f} = \frac{Q_3 / A}{x_1 + x_2} \qquad \textbf{3.5}$$

In Equation **3.5**, Q_3 is the collected charge, A is the electrode area and x_1 and x_2 are the strains measured along two mutually perpendicular directions on the top electrode. Further details of the set-up are reported elsewhere. [**174**]

Special attention is paid to seating of the wafer in the pressure rig: an imperfect clamping of the Si wafer can cause deviations of up to 26% with respect to the theoretical predictions, indicating wafer flexure in some mixed mode.[**174**] Previous characterization

[174] also found that the calculated $e_{31,f}$ are subject to standard deviation of ≤10% as a function of the position of the measured electrode in relation to the Si wafer and the pressure chamber. To increase the reproducibility of the results, the wafers, the removable clamps and the top part of the chamber were always mounted in the same orientation with respect to the bottom of the chamber.

3.9.3 Scanning Force Microscopy Piezo-response Mode (PFM)

Scanning Force Microscopy (SFM) in piezo-response mode (PFM) was used to verify the piezoelectric behavior and switching in the PYbN-PT thin films.[175][176][177][178] A modified Nanoscope III atomic force microscope was used. The SFM piezo-response measurements were performed in the vertical direction either on the oxide surface directly or on 50μm diameter top electrodes. The top electrodes were sputter deposited 80nm thick platinum that were patterned by a lift-off process.

Application of an external signal, through the contact SFM tip, generates a piezoelectric response in the ferroelectric film, with consequent vertical expansion or contraction, depending on the polarization state of the material. The read-out signal amplitude provides information about the magnitude of the piezoelectric coefficient (because it is proportional to the variation in thickness at any instant). The phase gives

information about the polarization state because it depends on the sign of the piezoelectric coefficient. Regions with opposite polarization orientations under applied AC signal, vibrate out of phase with each other, showing opposite contrast in the piezo-response image. [**179**] This piezo-response imaging mode can be used directly on the surface of the oxide layer. [**175**]

To check the poling quality of the films, a super-imposed dc bias can be applied through the scanning tip to the top electrode (write); the polarization configuration is consequently checked in piezo-response mode (read). [**180**] The reversibility of the domains can be mapped by reversing the applied DC voltage on the same electrode and the piezo-response image of the sample re-taken. Volumes of material with no domain switching will exhibit constant contrast for both voltage directions. [**175**]

As mentioned earlier, the piezoelectric coefficient of the material ($d_{33,f}$) can also be determined by using electrode contacts and readout of the amplitude of the response through the contact tip. In this case the voltage is applied through the bottom electrode contact, while the top electrode is grounded. This arrangement is done to minimize electrostatic attraction between the cantilever tip and the sample.

3.10 Nonlinear Dielectric Measurements

The nonlinear dielectric measurements were performed using a 4248A precision LCR meter (Agilent Technology, Palo Alto, CA). Contacts were made to top and bottom electrode using micro-probes with W probe tips. Where not otherwise specified, the measurements have been performed at 1 kHz. The frequency range was later expanded to range from 20 Hz to 200 kHz. At each frequency, the capacitance and loss tangent of the sample were registered continuously while the ac voltage was swept from 0 to 6V (rms values). The nonlinear dielectric measurements were also performed under applied bias (0 to $\pm$ 16V). Here the capacitance and loss tangent were measured at 1kHz for each bias voltage while the ac signal was continuously swept from 0 to 6V (rms values).

The measurements at room temperature were performed using a Cascade (Cascade Microtech, Inc., Beaverton, OR) probe station micropositioners. The probes (American Probe & Technologies, Inc.) were coaxially shielded up to 150mm from the tip point in order to reduce noise. The inner conductors were made of tungsten, with gold plated copper shield. The tips had a radius of ~20μm.

The nonlinear dielectric measurements were also performed at high (room temperature to ~400°C) and low (room temperature to ~6K) temperatures. Elevated temperature measurements were performed using a home-built high temperature thin film stage, while cryogenic data were acquired using a Desert Cryogenic Probe Station (Lake Shore Cryotronics Inc, Westerville, OH). These are described in detail in section 3.11. The temperatures were set manually at the desired values and stabilized for 5 minutes so

that the temperature oscillations had been reduced to ±1K before the ac voltage sweeps were done.

The higher harmonic response of the dielectric nonlinearities was measured through an SR 830 lock-in amplifier (Stanford Research Systems, Sunnyvale, CA). Figure 3.9 represents schematically the set-up used for the measurement and the electric circuit utilized.

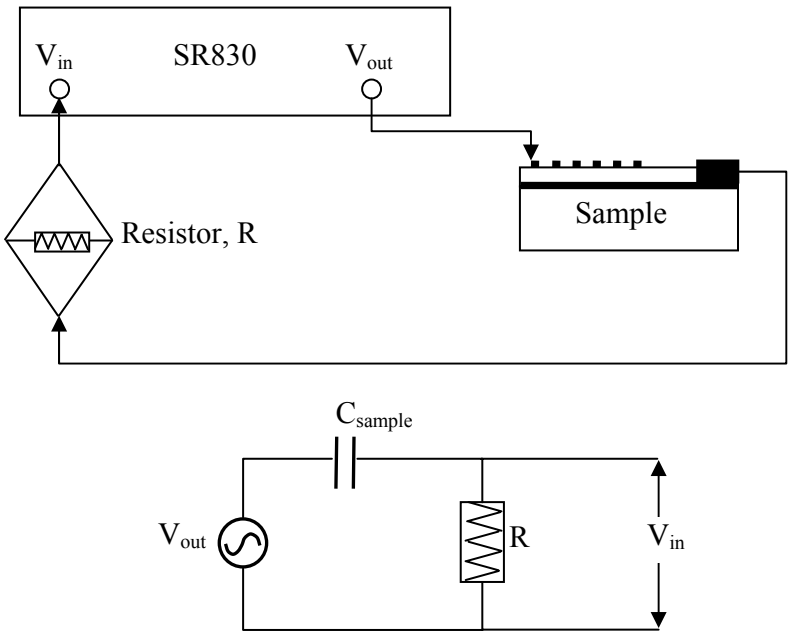

Figure 3.9: Schematic of the set-up used for the higher harmonics measurements and the equivalent electric circuit, as in Equation 3.6

The resistor was chosen so that the gain of the system, as defined by Equation **3.6**, is approximately equal to 100. This was found to be experimentally the optimum value in order to read with enough precision the first three harmonic responses from the sample. ω is the angular frequency at which the measurement is done, R is the resistance of the inserted resistor and C_{sample} is the capacitance of the sample.

$$Gain = \left| \frac{V_{out}}{V_{in}} \right| = \frac{1}{\omega R C_{sample}} \qquad \textbf{3.6}$$

The n[th] harmonic polarization $P_{n^{th}\ harmonic}$ is then obtained from the output voltage using equations **3.7** and **3.8** , where A is the area of the top electrode.

$$P'_{n^{th}\ harmonic} = \frac{V_{out, n^{th}\ harmonic}\sqrt{2}}{n\omega R A} \qquad \textbf{3.7}$$

$$P''_{n^{th}\ harmonic} = \tan(\delta).P'_{n^{th}\ harmonic} \qquad \textbf{3.8}$$

These measurements were performed in part at Penn State and in part at Ecole Polytechnique Federale de Lausanne for applied ac voltages from 0 to 2V (rms values) at frequencies between 20 and 20000 Hz.

3.11 High and Low Temperature Dielectric Measurements

The high temperature (room temperature to 400°C) dielectric measurements were performed using a thin film stage. The temperature on the top surface of the stage was computer controlled via resistance temperature interfaced detector (RTD) connected to an HP3478A multimeter (Agilent Technology, Palo Alto, CA). The RTD calibration range extended from room temperature up to 400°C. The accuracy of the temperature, measured as the difference between the temperature read by the RTD embedded on the top surface of the hot stage and the actual temperature on the top of the sample, was around 5%. The probe tips used for the measurement were Pt for top and W for bottom electrode contacts. Figure 3.10 shows a schematic representation in exploded view of the thin film hot stage.

Heating is performed by cartridge resistance heaters embedded in the heating chamber secured by a graphite shield. The graphite shield is used as the top surface for the heating chamber where the sample is placed. The sides of the chamber are covered in thermal insulation to reduce thermal loss to the ambient. The controller is directly connected to the cartridge heaters and the computer. The RTD, used for the temperature read-out and embedded in the graphite shield's top surface, is connected to the computer through a multimeter.

On the stage, the graphite surface is protected on the sides by the thermal insulating material. The probes enter the stage area through openings in these isolation walls (for simplicity, only one probe in Figure 3.10 is shown in the inserted position) and contacts are made by these to top and bottom electrodes. The probes are connected

through coaxial cables to the LCR meter that is read directly by the computer. A graphite cover is used to reduce air circulation to the top of the sample, and therefore reduce the cooling of the sample surface, and increase thermal uniformity. A schematic of the cable connections for the measurement between the different systems is shown in Figure **3.11**.

The measurements were performed on heating. The ramp rate between set temperatures was 2 °C/minute. Capacitance, loss tangent and temperature were automatically collected by a computer. Unless otherwise expressed, the measurements were performed at 0.03V, rms value. The frequency range extended from 20Hz to 200kHz. At each temperature step, a complete frequency sweep was performed and at each frequency, capacitance and dielectric loss values were monitored.

The nonlinear dielectric measurements were performed at fixed temperatures. As shown in Figures **3.10** and **3.11**, the temperature as read by the controller refers to the cartridge heaters beneath the hot stage. It was found experimentally that this temperature differed from the temperature on the top surface of the stage (as read by the RTD embedded on this surface) by ~5%. Therefore, the temperature controller was set at a temperature approximately 5% higher than the one desired. The final temperature of the stage was then controlled using the multimeter read-out of the top RTD and a temperature-resistance conversion chart. The accuracy of this temperature for the nonlinear sweep was approximately 5-6%°C.

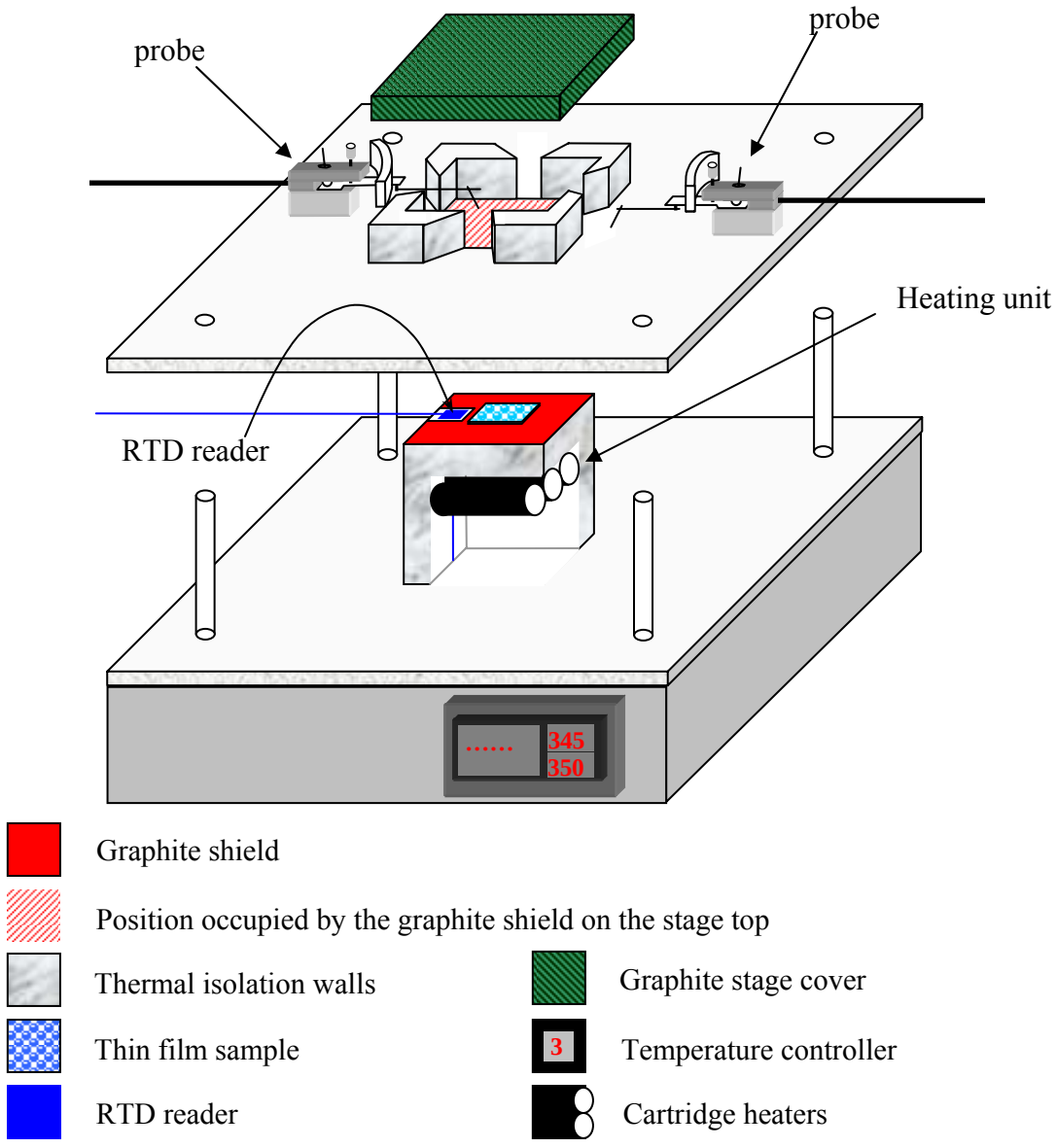

Figure **3.10**: Schematic of the high temperature thin film stage in an exploded view. The inside of the heating unit is also schematically shown. The controller is directly connected to the cartridge heaters and the computer. The RTD, used for the temperature read-out is connected to the computer through a multimeter. The probes enter the stage area through the openings in the isolation walls (for simplicity, only one probe is shown in the inserted position) and contacts are made by these to top and bottom electrodes.

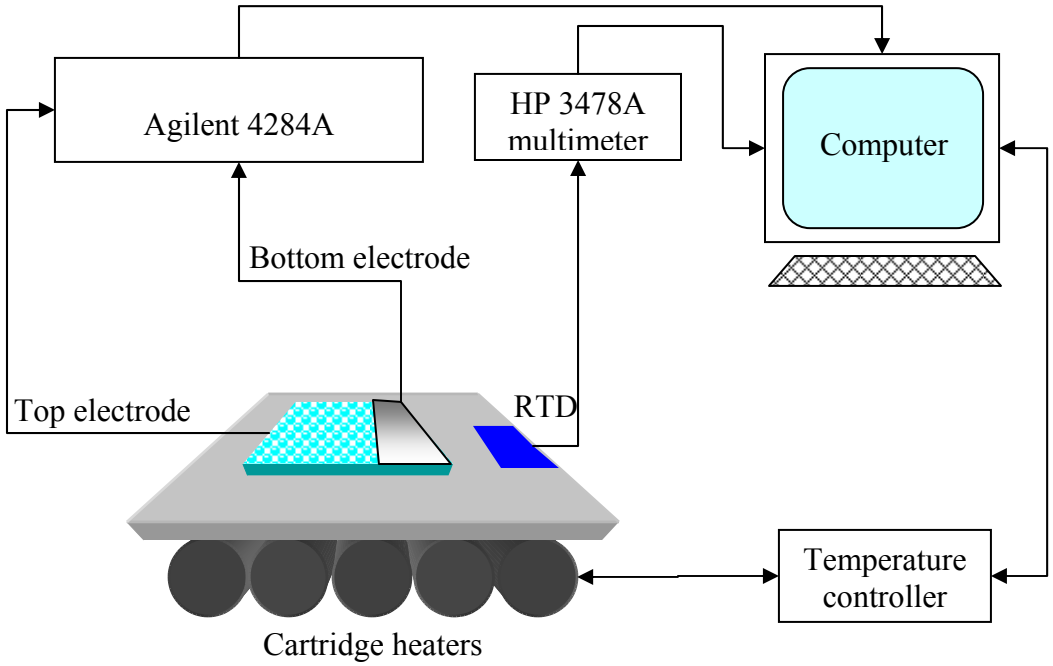

Figure **3.11**: Schematic of the electrical connections for high temperature dielectric measurements on the thin film stage.

The low temperature dielectric measurements (room temperature to 6K) were performed using a Desert Cryogenic Probe Station (Lake Shore Cryotronics Inc, Westerville, OH) with an automatic temperature controller at stage level and an intermediate temperature shield level. The probe tips used for the measurement were Be/Cu for top and W for bottom electrode contacts. Figure **3.13** shows a picture of the system and Figure **3.12** a schematic representation of the measurement chamber in exploded view.

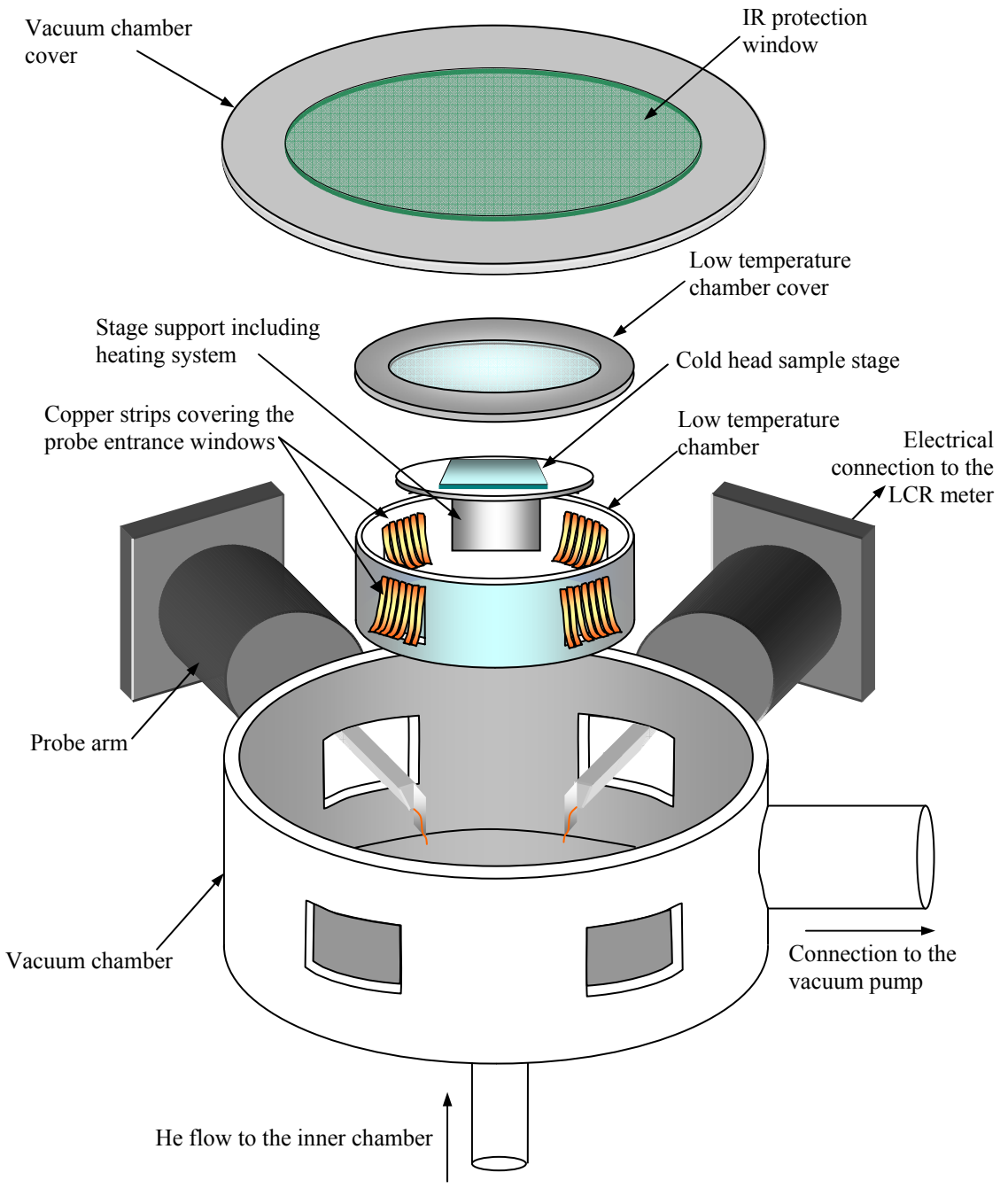

Figure **3.12**: Schematic representation of the Desert cryogenic probe station in exploded view. For simplicity only two probe arms are shown.

Figure **3.13**: A picture of the Desert cryogenic probe station used in this work.

The cryogenic probe station is composed of two chambers: the bigger one is connected directly to the vacuum pump while the smaller one, contained in the other, is where the refrigerating fluid flows into and contains the cold head. Each chamber has 4 openings (windows) on the sides for the entrance of the micropositioned probes, inserted into probe arms which are sealed to the windows of the outer chamber. The position of the probe tips inside the chamber is controlled from outside using manual positioners. The chamber windows are covered by copper foils fixed at one end. These are used to increase the thermal contact between the probes and the chamber walls. Both of the chambers' covers are secured by 12 bolts to the chambers themselves. While both covers are equipped with a glass window, the outer chamber also has an IR protection coating to reduce unwanted thermal exchange with the external ambient. The system is also

equipped with a video interfaced microscope that allows precise positioning of the probes.

The chambers are first taken to vacuum levels ~ 10^{-6} Torr and then cooled in continuous-transfer by liquid He. The cold head stage, inserted in the internal chamber (which works as a temperature shield), is equipped with a heater system that regulates the temperature to the set-point required by the user. The heater allows the stage to be heated to temperatures up to 475K. Final stage temperature is controlled through a LakeShore Model 331 controller (Lake Shore Cryotronics Inc, Westerville, OH).

The dielectric capacitance and loss tangent were measured as a function of temperature, from ~295K to ~6K, on cooling (ramp rate ~ - 2.0 K/min). An initial heating to temperatures ~150°C was performed before each measurement in order to reduce the presence of residual humidity that could be detrimental to the measurements at the very low temperatures. The dielectric nonlinearity measurements were performed at constant temperature for ac voltage sweeps from 0 to 6V for frequencies between 100Hz and 1MHz. The temperatures were set manually at the desired values and held for 5 minutes until the temperature oscillations had been reduced to ±1K before the ac voltage sweeps were done.

3.12 Biaxial Stress Measurements

The dielectric nonlinear properties of the PYbN-PT films were also studied while the sample was exposed to applied biaxial tensile stress. This was done in order to assess whether there was a significant contribution of non-180° domain wall motion to the dielectric response. In order to apply the biaxial stress, a small chip of the sample (~1cm^2) was glued using Epoxy 907 (Miller-Stephenson, Danbury, CN) to a 3" aluminum wafer. The wafer was then clamped on the top of a cylindrical aluminum cavity that was pressurized using a N_2 gas cylinder. The pressure inside the cavity was controlled by the tank regulator. The strain on the sample was measured by use of a strain gauge glued on the top of the electrode during a second run of the experiments. The dielectric nonlinearities were then measured as specified in section **3.10** under tensile bias stress.

3.13 Nonlinear $e_{31,f}$ Measurements

To confirm the results obtained by the double beam interferometer, the piezoelectric nonlinear measurements were also performed in direct mode, by implementing the e_{31} set-up to accommodate variable pressure levels and therefore, variable stress/strain levels on the substrate. Because of the higher pressure levels used, a

circular piece of spring steel, rather than a Si wafer, was used for mounting the wafer chip. Analogously to the e_{31} measurements, a small, approximately square-shaped piece of sample ($\leq$ 1 cm^2) was attached on the center top of the substrate by super glue. The substrate was then clamped on the top of the cylindrical cavity as in the usual $e_{31,f}$-measurement set-up.

To control the level of the strain in the sample, the inside cavity was connected to a gas cylinder through a manifold connected to two gas solenoids. A controller circuit periodically opened the first solenoid "a" connecting the chamber to the gas cylinder. In the second half of the period, the solenoid valve "a" was closed and the solenoid valve "b" opened, allowing the pressurized gas in the chamber to be discharged to the atmosphere. The lock-in amplifiers, using synchronized source signals, were connected respectively to the controller circuit for the solenoid valves and a pressure gauge monitoring the pressure level in the chamber cavity, the charge collected from the sample, and a strain gauge attached in close proximity of the reference electrode. A schematic presentation of the set-up used is shown in Figure **3.14**.

Due to the higher deformation levels in this set-up with respect to the original one, a new probe configuration had to be used to reduce tip traveling effects on the top of the sample. Tip traveling causes scratching of the top electrode, reduction of the electrode area during measurement and shorting. To increase the flexibility and the vertical motion range of the modified probe, a bent copper sheet was used as an elbow connection between the probe arm and probe tip. The probe tip used was a 5 mil tungsten wire welded to nickel-S shank probe tip (American Probe & Technologies Inc., Milipitas,

CA), that allowed to follow the wider spatial movement the sample with the probe tip. A schematic drawing of the probe is shown in Figure 3.15.

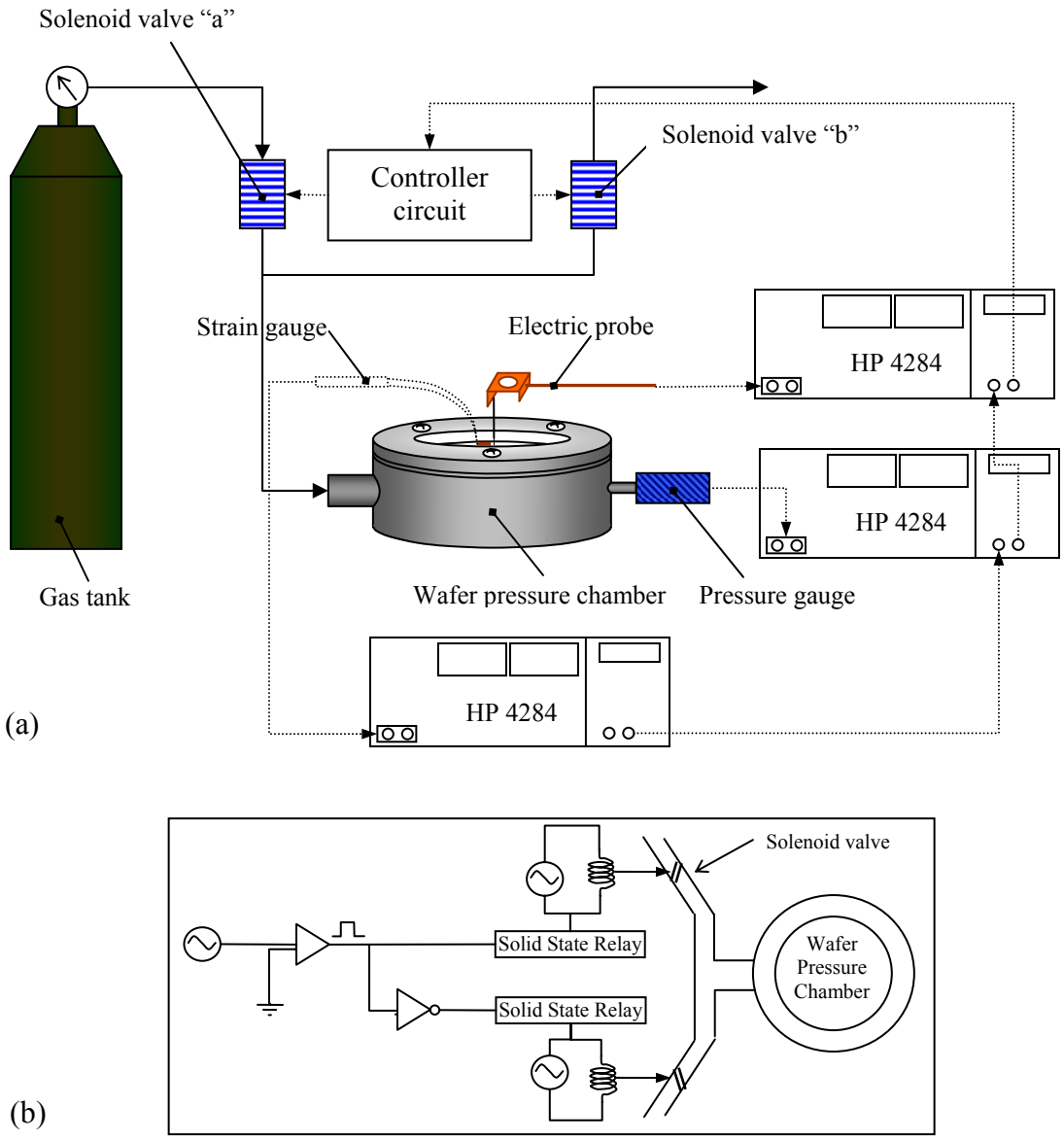

Figure 3.14: Schematic representation of (a) the experimental set-up used for the nonlinear direct piezoelectric e_{31} effect and (b) the controller circuit (courtesy of Paul Moses, MRI, PSU) to actuate the solenoids. The gas flow lines are indicated by solid lines and the electrical connections by dotted lines. The output signal of the three lock-in amplifiers is synchronized.

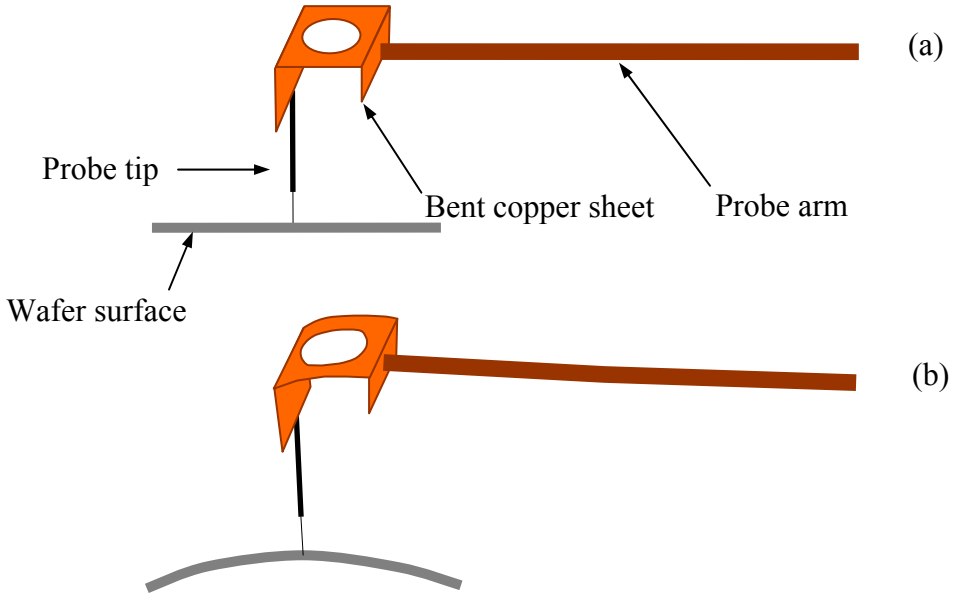

Figure **3.15**: Schematic representation of the probe used for the charge measurements in the modified e_{31} set-up. (a) Initial contact of the probe with wafer and (b) continuous contact of the probe tip with the bent sample. Note in case (b) the curvature of the copper sheet and the bending of the tip.

Chapter 4

Preparation and Characterization of {111} and {100} Oriented PYbN-PT Thin Films

This chapter describes the work on the optimization of the process parameters for the deposition of the PYbN-PT films. The amount of excess lead source, pyrolysis and crystallization temperatures and finally the heating rates used for the crystallization step were varied in order to increase the perovskite content and the {100} or {111} orientation. The characterization of highly {100} and {111} oriented PYbN-PT films is then discussed, in terms of morphology, dielectric and piezoelectric properties.

4.1 Orientation Control and Processing Parameters

0.5PYbN-0.5PT thin films with {111} and {100} preferential orientation were fabricated with the procedures specified in sections **3.1** and **3.2**. The processing conditions had to be optimized to reduce the presence of second phases and increase the

orientation of the films. It has been reported for other perovskite ferroelectric thin films that the {111} Pt fiber textured bottom electrode, if allowed to dominate the nucleation, would yield {111} orientation. [163] Particular attention therefore has been given to obtain parameters that would increase the {100} orientation of the films.

Many different factors can contribute to the phase purity of the thin films, their crystallographic orientation and degree of crystallization. Table 4-1 gives a list of some of the most important factors:

Table 4-1: List of factors influencing degree of crystallization, crystallographic orientation and phase purity in CSD derived thin films.

1. Solution chemistry	2. Substrate	3. Heat treatment
• excess lead content; • hydrolysis degree; • aging of the solution; • precursor species size; • precursor viscosity; • solution homogeneity;	• lattice parameters match between substrate and film; • stress levels on the film at the T_C;	• pyrolysis temperature; • heating rate; • annealing / crystallization temperature; • hold time at the crystallization temperature; • crystallization ambient (reducing or oxidizing atmosphere).
[181]	[182] [183] [184]	[185] [186] [187] [188] [189]

Although it has been shown in the literature that specific substrates, in particular single crystals with appropriate crystallographic orientation can be used to tailor specific crystallographic orientations in the film [190][191][192][193], in this work, particular attention has been given to factors 1 and 3. In fact, Si wafers are the most widely used substrates for MEMS. Furthermore, a crystallographic orientation achieved only by means of heat treatment and solution chemistry, allows use of different substrates, which could broaden the fields of use.

4.1.1 Solution Chemistry: Excess Lead Content

As mentioned in the previous chapter, the PYbN-PT solution was extremely sensitive to humidity. Therefore, the degree of hydrolysis was reduced to a minimum by performing all preparation steps under a flow of dry argon gas. The final solution was kept in sealed containers in humidity controlled boxes. The film deposition was performed as soon as possible after the preparation of the solution. The degree of homogeneity of the solution was increased by long mixing times at high temperatures.

In order to influence the phase formation, the degree of crystallinity, and grain size, variations in the amount of excess Pb in the solution were considered. As mentioned in section 3.1, due to the high volatility of lead oxides [160][161][162], the lead acetate used in batching the sol-gel precursor was in excess of the stoichiometrically required

amounts. Reports in the literature indicate that high volatility of lead can create locally depleted zones, especially near the surface in Pb-based oxide thin films. [184][194] The result of local deficiency is often formation of a parasitic pyrochlore phase that degrades the electrical and electromechanical properties.

Positive effects of excess Pb in PZT films have been reported to be [195]:

- higher permittivity;
- less space charge;
- better resistance against repeating fatigue cycles.

On the other hand, addition of excess Pb in PZT films can also result in negative effects such as creation of second phase (i.e. PbO) which can result in lower permittivity and higher loss values.

In this work, three different amounts of excess Pb were used in batching the precursor solution. It was found that excess Pb amounts of 20 mol% or higher increased the relative amounts of perovskite to pyrochlore phase (see Figure 4.1). On the other hand, films produced with ~30 mol% excess Pb showed reduced dielectric permittivity and increased loss values that suggest the presence of PbO in the films, although this could not be confirmed by X-Ray diffraction. The reduced dielectric properties of the film could also be due to a layer of lower permittivity pyrochlore phase. Im and Choo [154] reported that Pb deficiency as well as its excess can increase formation of pyrochlore phase at the expense of perovskite PYbN-PT. No experimental evidence by X-Ray diffraction could be found to support that conclusion in this work.

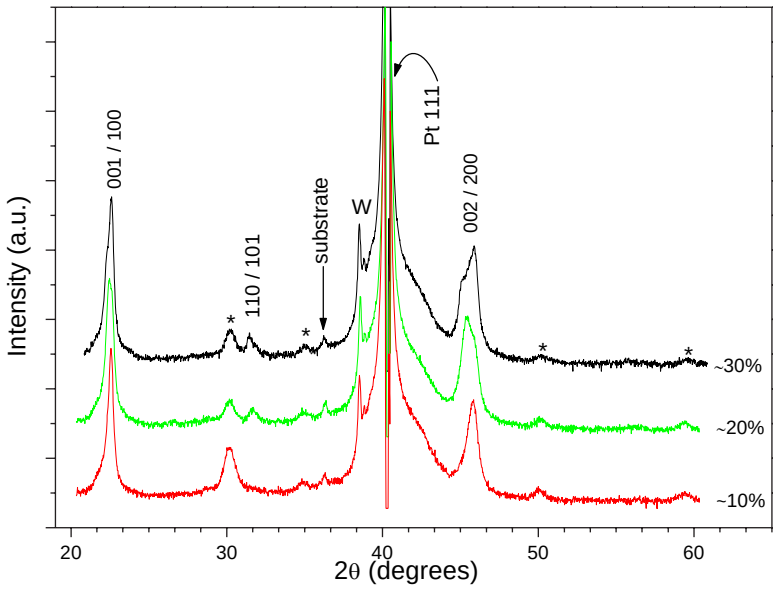

Figure **4.1**: Effect of amount of excess lead in the precursor solution on the phase development of PYbN-PT films and their crystallographic orientation. * denotes peaks due to pyrochlore phase. W represents peak due to tungsten contamination from the filament in the X-Ray tube.

The Pb excess content in the precursor solution was limited to 20-25 mol% in all the following work. The narrow window of excess Pb tolerated in the solution are in agreement with the narrow Pb target power reported for the PYbN-PT films sputter deposited by Im et al. [**154**]. It was also found (see Figure **4.2**) that slightly higher amounts of excess Pb (~25%) increased the relative amount of {100} crystallographically oriented grains in the films.

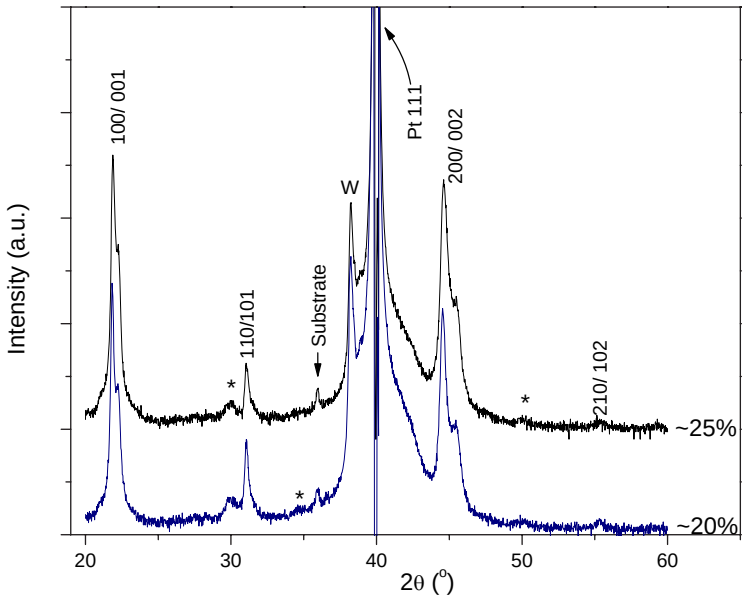

Figure **4.2**: Effect of amount of excess lead in the precursor solution on the relative {100} crystallographic orientation of the films. * denotes peaks due to a pyrochlore phase. W represents peaks due to tungsten contamination from the filament in the X-Ray tube.

4.1.2 Heat Treatment

As mentioned in section **3.2**, each layer of PYbN-PT thin film deposited by sol-gel spin coating was treated to a single pyrolysis step before being crystallized by RTA treatment. The sol-gel spin coating, followed by pyrolysis and crystallization was performed up to 10 times to obtain the required thickness. The film quality and morphology depended on the temperatures used for the processing steps (both pyrolysis and crystallization) and the ramp rate to the crystallization temperature. The influence of these factors is discussed in the following sections. It was found that the quality of the

films showed no dependence on the O_2 content in the atmosphere used for the crystallization step, for P_{O2} values higher than those of room air.

4.1.2.1 Pyrolysis Temperature

As mentioned earlier in section 3.2, as-deposited films were subjected to a single pyrolysis step. The pyrolysis step has been associated with development of medium-range order in sol-gel coating. [163] It has been reported for similar perovskite systems that the degree of nano-scale heterogeneity observed after the initial heat treatment decreased with higher heat treatment temperatures (from 300°C to 450°C). [196] Furthermore, during the pyrolysis step the solvent is removed, accompanied also by partial or complete removal of the organic components in the film. [163] For ferroelectric perovskite thin films, the reported pyrolysis temperatures range is between ~300° to 450°C. [163]

Figure 4.3 shows the effects of pyrolysis temperature on phase formation. Films were pyrolized at 325ºC, 400ºC or 450ºC, followed by crystallization at 700 ºC. The film pyrolized at 325 ºC was poorly crystallized. Pyrolysis at 400ºC increased the relative amount of perovskite to secondary phase, relative to the film pyrolized at 450 ºC. It is possible that pyrolysis at 325ºC did not completely eliminate the organics, and therefore created a more reducing atmosphere during crystallization, leading to poor oxidation of the films. But as reported earlier, no particular dependence of the phase creation on the

increased oxygen levels during crystallization step was noticed. Alternatively, a higher degree of nano-scale homogeneity created during the pyrolysis might be responsible for the higher degree of perovskite crystallization achieved with the ~ 400ºC pyrolysis.

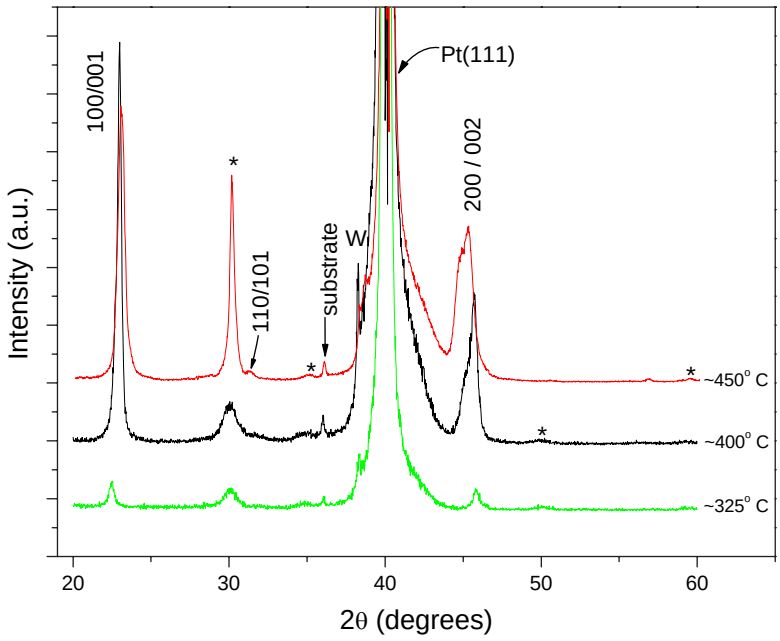

Figure **4.3**: X-Ray diffraction pattern of PYbN-PT samples pyrolized at 325ºC, 400ºC and 450 ºC. All samples were then crystallized at 700ºC. * denotes peaks corresponding to the pyrochlore phase. W represents peaks due to tungsten contamination from the filament in the X-Ray tube.

Pyrolysis at ~ 450ºC increased the amount of pyrochlore phase with respect to perovskite. Bornand et al. [**149**] reported that the nucleation energies for perovskite and pyrochlore phases are similar in pulsed laser deposited PYbN-PT films, and that lower temperatures favor the pyrochlore phase. X-ray data for a sample pyrolyzed at 450ºC before and after crystallization are shown in Figure **4.4**. It was found that pyrolysis at

450ºC nucleated the pyrochlore phase. Subsequent heat treatment at 700ºC leads to partial conversion to the perovskite phase but also to significant growth of the pyrochlore phase already present. This suggests that phase purity is enhanced if pyrochlore nucleation is avoided during pyrolysis.

In the subsequent work, all films were pyrolized at ~400ºC for two minutes before crystallization was performed.

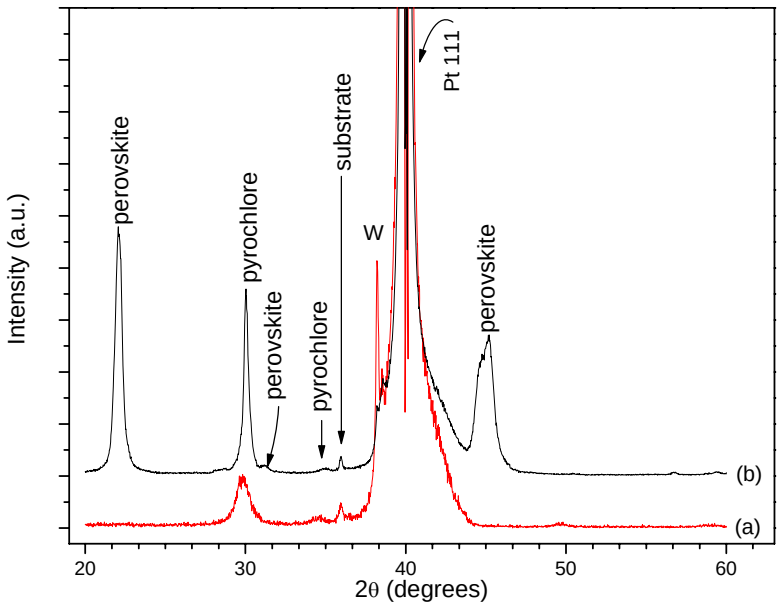

Figure **4.4**: Phase development in PYbN-PT films pyrolized at 450°C, (a) after the pyrolysis step and (b) after the crystallization step at 700°C.

4.1.2.2. Crystallization Temperature

Figure 4.5 shows the X-Ray diffraction pattern of films crystallized at various temperatures. The first perovskite PYbN-PT peaks appeared around 550ºC, while temperatures lower than 500ºC yielded only the pyrochlore phase. Increasing crystallization temperature increased the relative amount of the perovskite phase to pyrochlore for temperatures up to ~700 ºC. Further increase in the crystallization temperature decreased the relative amount of perovskite phase. This could be due to higher Pb volatilization rates at higher temperatures, which would favor formation of the pyrochlore phase, as was reported by Yoshimura et al. [152] for pulsed laser deposited (PLD) PYbN-PT films.

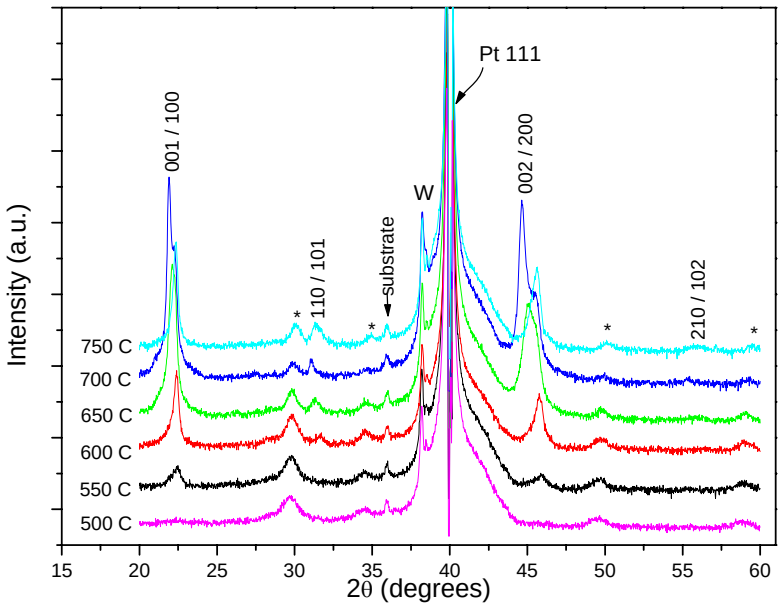

Figure 4.5: X-Ray diffraction data for PYbN-PT films (excess lead ~25%) crystallized at temperatures between 500º and 750ºC. * denotes second phase peaks. W represents peaks due to tungsten contamination from the filament in the X-Ray tube. It can be seen that the onset of crystallization of the perovskite phase is at temperatures close to 550ºC.

4.1.2.3. Heating Rate

The heating rate can also influence the orientation of the films. Crystallization can be initiated at temperatures below the annealing temperature itself. [163] This can lead to multiple nucleation and growth processes associated with different nucleation mechanisms. [163] [197]

As can be seen in Figure 4.6, for films deposited on platinized silicon wafers, increasing heating rates increased the {111} crystallographic orientation of the films. This suggests that heterogeneous nucleation from the bottom electrode is favored with higher heating rates.

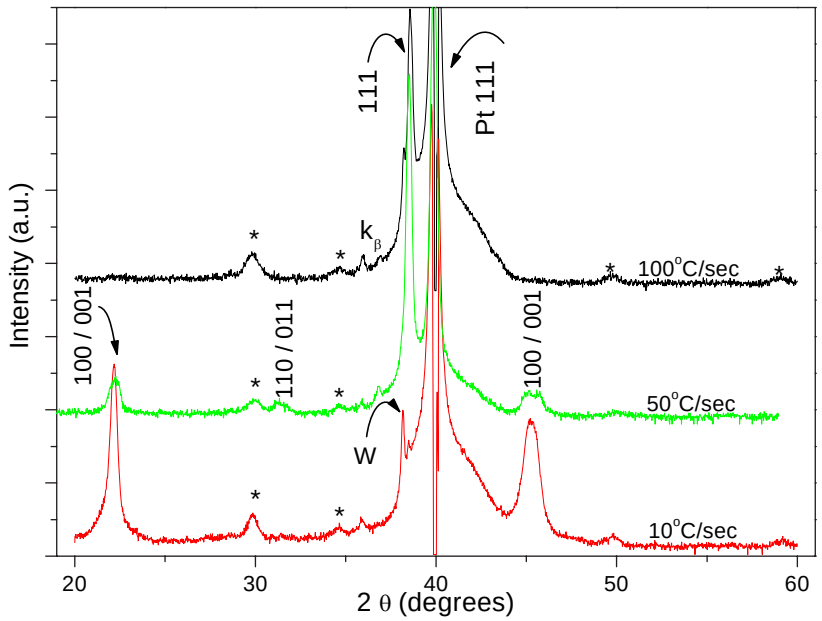

Figure 4.6: Influence of the heating rate on the film orientation. The films were deposited on (111) platinized Si wafers and crystallized at 700°C. Pyrolysis at ~ 400ºC was performed before the crystallization step. * denotes second phase peaks.

The heterogeneous nucleation was confirmed by deposition of films on wafers with a {100} oriented $PbTiO_3$ seed layer (Figure **4.7**), where heating rates of ~100ºC/sec yielded once more a prevalence of {100} crystallographic orientation in the PYbN-PT thin films.

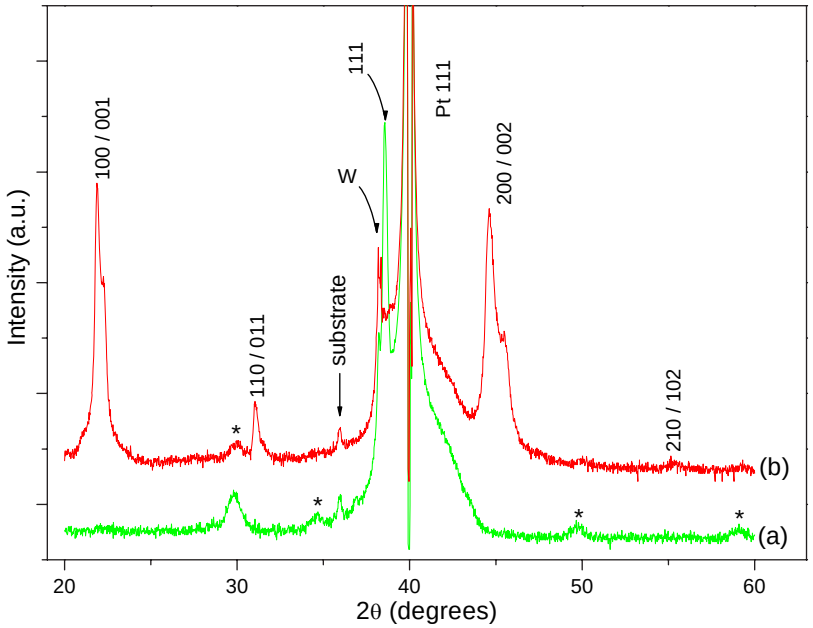

Figure **4.7**: X-ray diffraction patterns for PYbN-PT films crystallized at 700°C after pyrolysis at 400°C. The films were crystallized with ramp rates (~100°C/sec) yielding preferential (a) {111} orientation for films deposited on Pt (111) and (b) {100} orientation for films deposited on {100} lead titanate.

4.2 Highly {100} and {111} Oriented PYbN-PT Thin Films

Highly {111} and {100} oriented films of PYbN-PT were characterized to determine the degree of orientation, the presence of second phase, surface roughness and grain size. X-ray diffraction and AFM were used as the primary characterization tools here.

Figure 4.8 shows the X-Ray diffraction patterns from highly oriented thin films obtained with the procedure described in the previous paragraphs. The degree of orientation of the films was calculated by the Lotgering Factor [198] as in Equation 4.1:

$$Degree\ of\ orientation = f = \frac{\sum I_{(HKL),film} / \sum I_{hkl,film} - \sum I_{HKL,ceramic} / \sum I_{hkl,ceramic}}{1 - \sum I_{HKL,ceramic} / \sum I_{hkl,ceramic}} \qquad \textbf{4.1}$$

where $\sum I_{HKL}$ is the summation of the intensity of the peaks associated with the specific {HKL} orientation and $\sum I_{hkl}$ is the summation of the intensities of all the peaks. Peak intensities from a randomly oriented bulk ceramic were used to normalize the data from the films

On average, the {100} oriented films had Lotgering factors ≥83%, while the {111} oriented films had a degree of orientation that exceeded 95%. In both cases, the texture was out-of-plane only. Films of either orientation showed the presence of small amounts of a pyrochlore second phase.

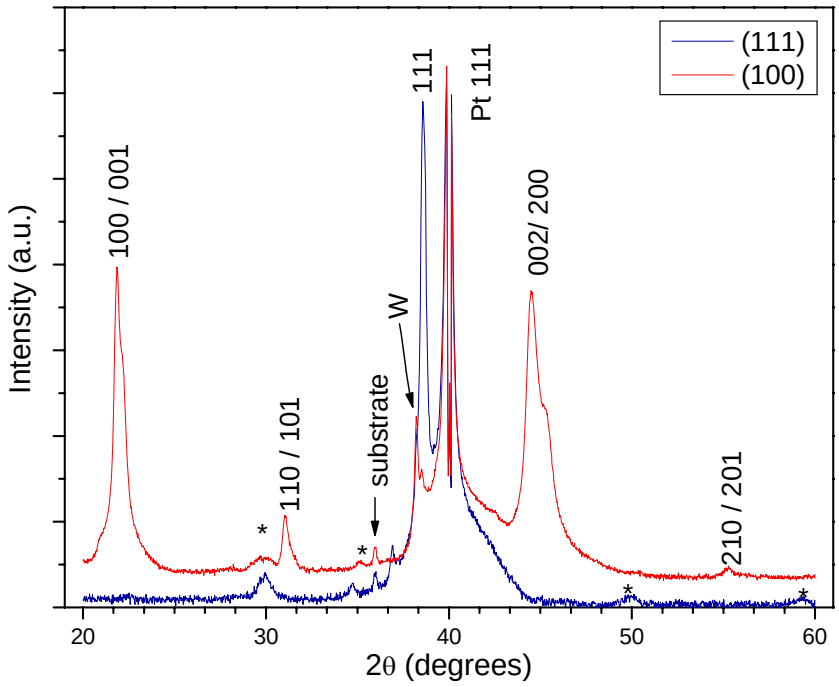

Figure **4.8**: X-Ray diffraction of highly {100} and {111} oriented PYbN-PT thin films.

A major concern for ferroelectric perovskite thin films containing a pyrochlore phase is the dilution of the dielectric properties of the thin film. In particular, a low dielectric permittivity pyrochlore phase, electrically in series with the perovskite layer, can lead to major reductions of the total capacitance, C_{total}, as in Equation **4.2**,where $C_{perovskite}$ and $C_{pyrochlore}$ are the capacitance of the perovskite and pyrochlore phase, respectively.

$$\frac{1}{C_{total}} = \frac{1}{C_{perovskite}} + \frac{1}{C_{pyrochlore}} \approx \frac{1}{C_{pyrochlore}} \quad \text{if} \quad C_{pyrochlore} << C_{perovskite} \qquad \textbf{4.2}$$

In order to quantify the presence of a surface pyrochlore phase, grazing angle X-Ray diffraction of the films was performed (see Figure 4.9a). The intensity of the pyrochlore peak increased with increasing grazing angle, and therefore with the depth of the sample since large incidence angles lead to greater penetration of the X-ray beams. This suggested that the pyrochlore phase is not segregated on the top layer of the films, but has nucleated nearer the substrate. The increasing incident angle seemed also to be accompanied by an increase in the 2θ values for the peak, as seen in Figure 4.9b. This might be due to an increase in the spacing of the crystallographic planes with increasing thickness of the films, caused by a possible relaxation of the strains associated with the constraint to the substrate.

The degree of orientation (i.e. the relative intensity of the {100} peaks in the case illustrated) seemed also to increase with increasing incident angles. This indicates that the preferential orientation of the film was somehow lost with increasing thickness of the film. Throughout this study the thickness of the films, where not otherwise specified, was ~0.6μm for both of the film orientations in order to reduce the effects of mis-orientation of the final layers.

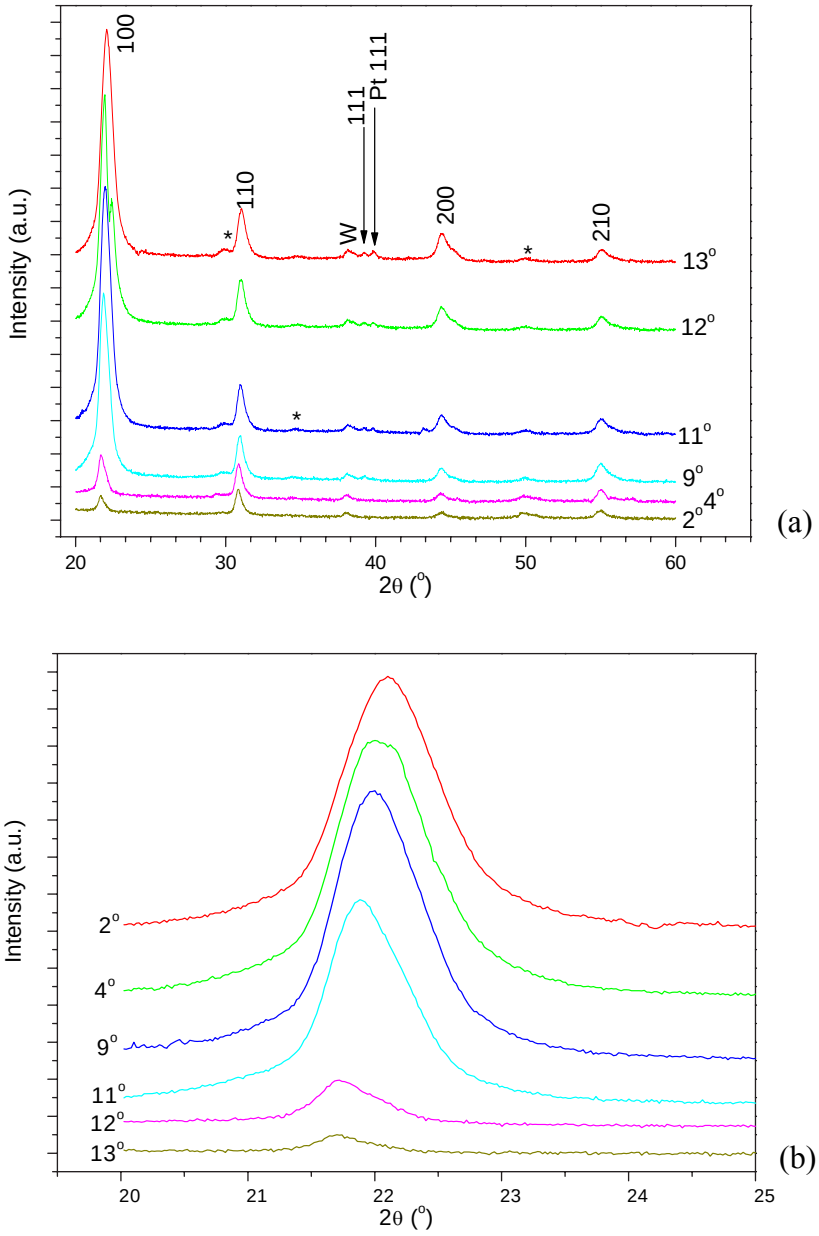

Figure **4.9**: (a) Grazing angle X-Ray diffraction patterns for a {100} oriented, 0.67µm thick PYbN-PT film, (b) {100} peaks. "W" denotes the peak due to the tungsten-filament, * the peaks due to the secondary phase (pyrochlore).

The study of the surface morphology of the films by SEM proved extremely challenging due to the small features of the films. Figure **4.10** shows the surface structure of a {100} (Figure **4.10**a) and a {111} (Figure **4.10**b) oriented film. As can be seen, the surface morphology of the {111} oriented films couldn't be well resolved, indicating probably a very fine grain structure. The {100} films seemed to show a three modal distribution of grain size: the bigger grains' diameter is around 500-600nm in diameter, medium sized grains have diameters around 200 nm and the smaller grains range around 50nm in diameter. The bigger grains could possibly be due to the continuous growth through multiple depositions of grains nucleated on the bottom. The smaller grains could be due to nuclei created on the surface. The bigger grains size was comparable to the total thickness of the films.

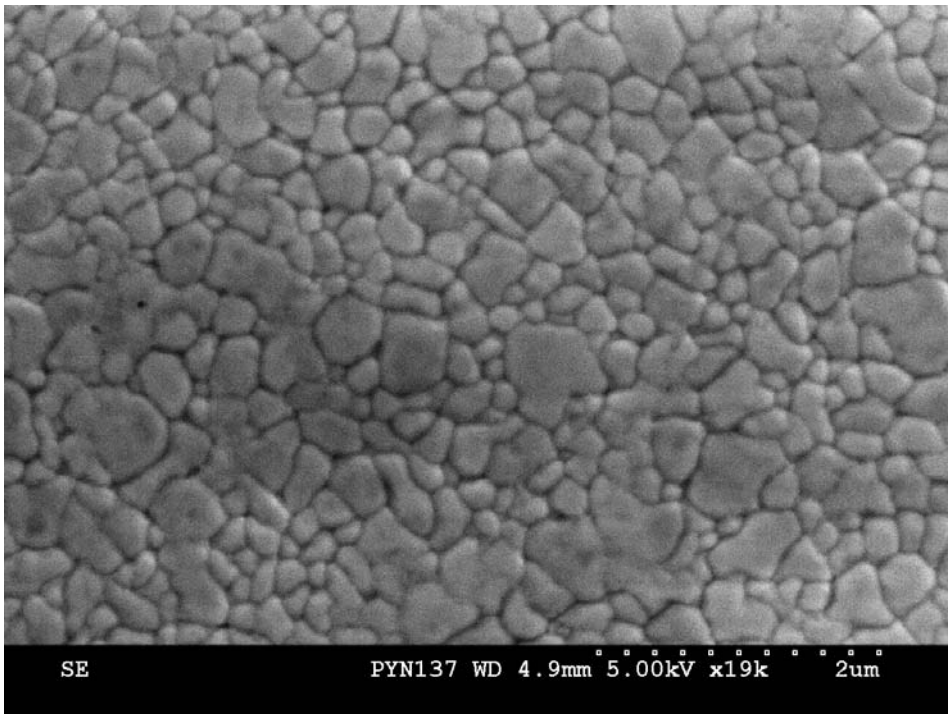

(a)

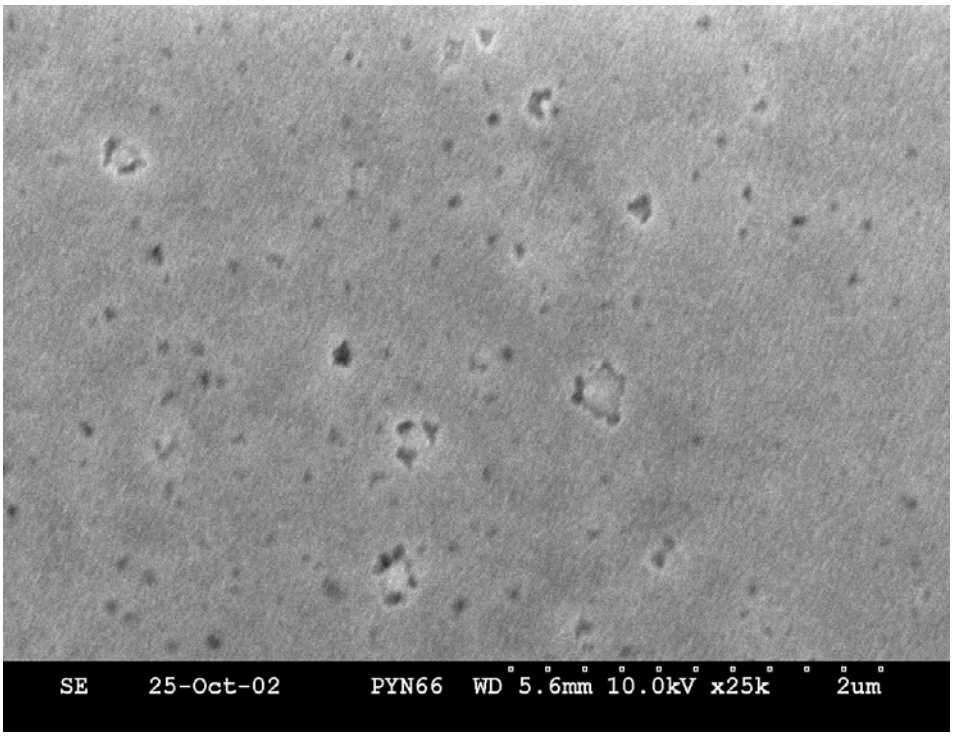

(b)

Figure **4.10**: SEM example of (a) {100} oriented and (b) {111} oriented PYbN-PT films. Because of the difficulties in focusing on the very small features of the {111} oriented film, a particular region close to the edge of the sample was used that offered defect features (darker contrast).

Figure 4.11 shows a cross-section of a {100} oriented thin film. The columnar configuration of the grains is visible in the image. No distinct separation between grains created in consecutive depositions could be observed, which suggests high density films.

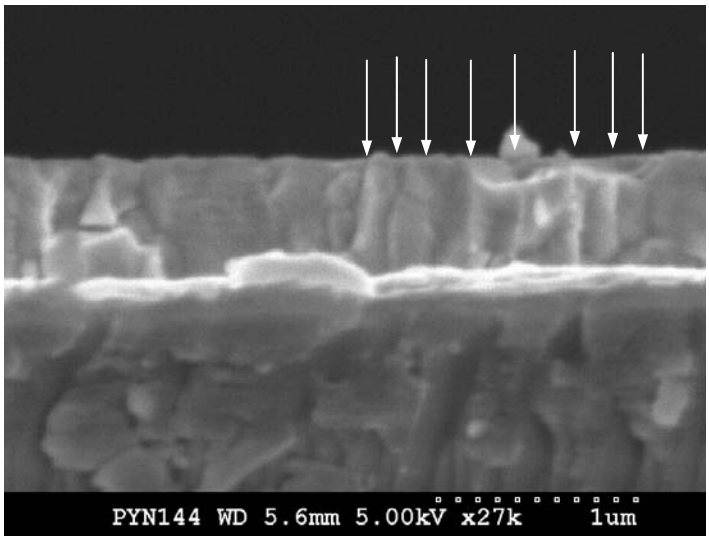

Figure **4.11**: Cross-section of a {100} oriented PYbN-PT thin film. The columnar structure of the film is particularly visible on the right side of the image.

Atomic Force Microscopy was employed to confirm the surface morphology of the films. The results can be seen in Figure 4.12. The results are summarized in Table 4-2. The {100}-oriented films showed a bimodal grain size distribution which compared relatively well to the results obtained by SEM, although the average grain size was slightly smaller in the measurements made by AFM.

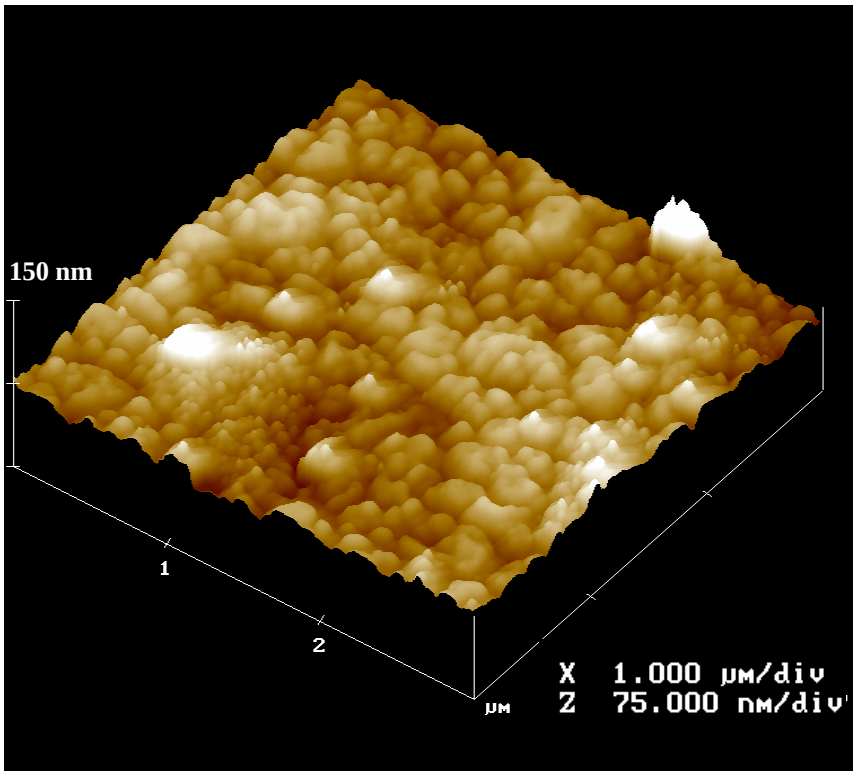

(a)

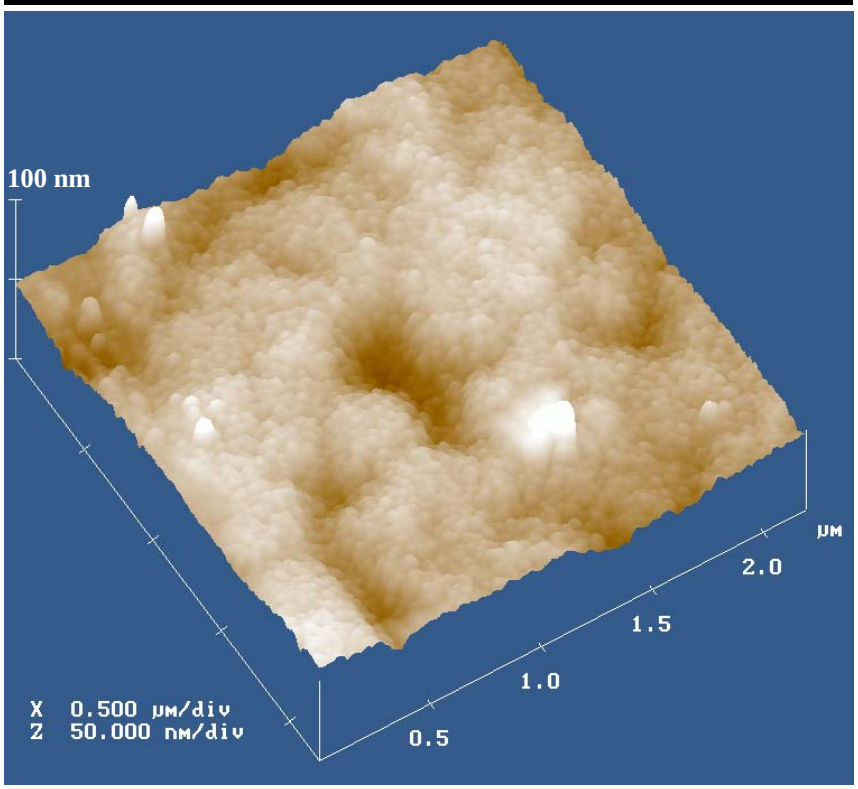

(b)

Figure **4.12**: Surface morphology of (a) {100}- and (b) {111}-oriented PYbN-PT films.

The bimodal grain size distribution of {100} oriented films may be associated with the loss of {100} orientation with increasing thickness of the films. The smaller grains could therefore be random oriented grains not nucleated on the pre-existing {100} oriented grains. The possibility of the smaller grains being grains of pyrochlore phase couldn't be completely ruled out. Although Grazing Angle X-Ray Diffraction indicated little to no pyrochlore phase close to the surface, the resolution of the measurements is limited to approximately 3-4vol%, and therefore surface amounts smaller than that wouldn't be detected.

Table 4-2: Summary of orientation and microstructure of PYbN-PT films.

Orientation	**(111)**	**(100)**
Degree of orientation (%)*	>95	>83
Roughness, Rms (nm)	5	16
Grain size (nm)	30-45	50-60 & 200-300

* Degree of orientation is defined by Equation 4.1

An XPS depth profile of the samples showed that each film consisted of alternating layers that were enriched in Yb and Nb and depleted in Ti, followed by the reverse (Figure 4.13). There appeared to be five enriched layers of each (10 total layers, corresponding to 10 deposition and crystallization steps). The first layer showed enrichment in Ti and a small increase in Pb levels. Similar results have been reported for {100} oriented thin films of MPB PZT. [199] In case of PZT films, opposite oscillating concentration gradients of Ti and Zr was attributed to the fact that the Ti rich compounds

had a lower activation energy for nucleation.[200] This could be the case also for the PYbN-PT films, where the first crystallized layer is Ti-enriched. It should also be noted that finite amounts of Ti in the Pt layer, and Pt in the first layers of the PYbN-PT films were observed, indicating some amount of diffusion of these species in the specified layers.

Although, Pb concentration showed little variation with depth, measurable amounts of Pb were also observed at the Pt-Ti interface, indicating a diffusion of Pb through the Pt layer. It is not clear whether this is due to a finite amount of porosity of the Pt or instability of the Pt layer under the processing conditions for the films (see section 3.4) or simply an artifact associated with a finite amount of knock-in during the XPS depth profile.

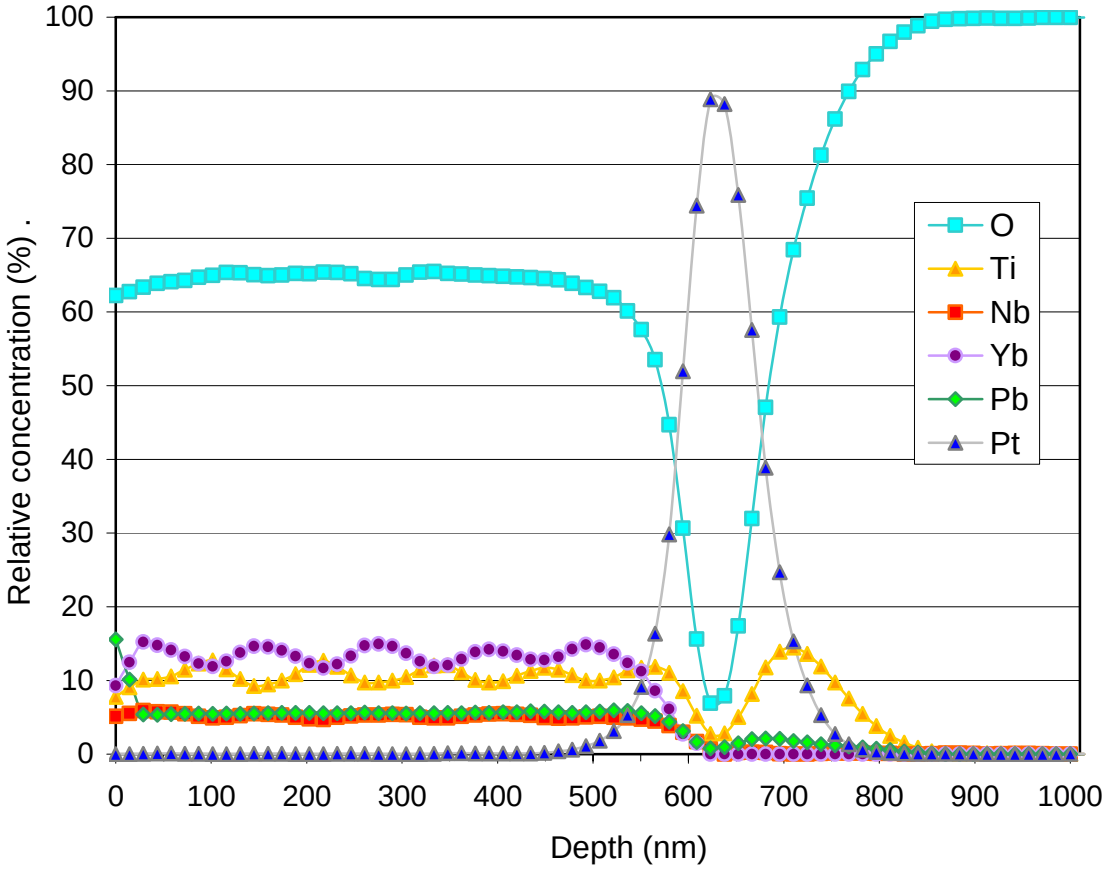

Figure **4.13**: Chemical depth profile of a {100} oriented PYbN-PT thin film (~0.55µm thick). Data courtesy of Jeff Shallenberger, MCL, PSU.

4.3 Electrical Characterization

Electrical characterization of the PYbN-PT samples included measurements of the dielectric permittivity and loss as a function of frequency and temperature, polarization-electric field hysteresis loops and tunability.

As mentioned earlier in **3.4**, due to the difficulties in etching of the films, the thickness of the films was measured via SEM observations. The 5% nominal error associated with this measurement was the highest source of error for all the dielectric properties calculations. Where not otherwise specified, the values reported in this thesis are subject to 5% error.

The as-deposited {100} oriented films showed higher permittivity than {111} oriented ones over the frequency range of 100 Hz to 100 kHz as seen in Figure **4.14**. The loss values were comparable for the two orientations of the films. The dielectric permittivity of the {100}-oriented films was higher than the values reported for epitaxial {100} thin films of 0.5PYbN-0.5PT deposited on $SrTiO_3$ substrates. [**152**] This can be due to the imperfect orientation of the films presented in this work. The dielectric permittivity of the {111} oriented films was slightly higher than the values reported for the epitaxial {111} thin films of 0.5PYbN-0.5PT deposited on $SrTiO_3$ substrates. [**152**] This can be in part due to the presence of small amounts of pyrochlore. The loss tangent for both the orientations in this work is smaller than those of the reported epitaxial films. This might be due to the lower leakage characteristic of the interface between the film and the metallic bottom electrodes used in this work relative to the interface characteristic of the conductive oxide bottom electrodes used for the epitaxial films. [**201**]. The slight increase in the loss values at higher frequencies is due to the experimental set-up. The aging rates for the dielectric properties of the poled films was $<1\frac{\%}{decade}$ and $<3\frac{\%}{decade}$ for the {100} and {111} oriented films, respectively.

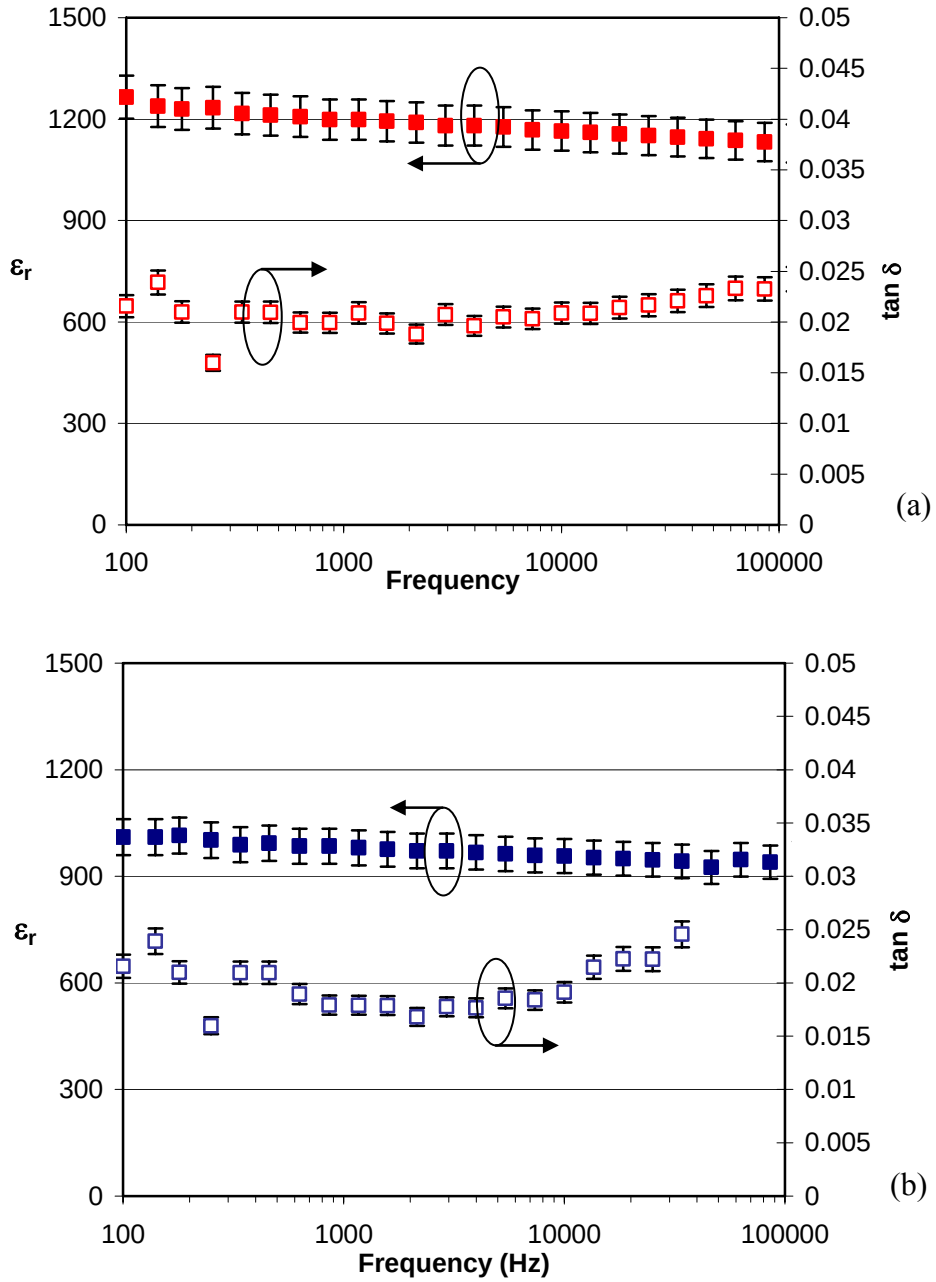

Figure **4.14**: Frequency dispersion of dielectric permittivity and loss tangent for the (a) {100} and (b) {111}-oriented PYbN-PT films.

The high field properties of the films are reported in Figure 4.15, and the characteristic values are summarized in Table 4-3:

Table 4-3: Characteristic high field values for oriented PYbN-PT films.

Orientation	P_r ($\mu C/cm^2$)	E_C (kV/cm)
{100}	23.7	59.7
{111}	30.5	78.7

The {100} films showed P_r and E_C values slightly higher than those reported by Zhou et al.[156] (~22$\mu C/cm^2$ and 55kV/cm, respectively), while the {111} oriented films had P_r values similar to those reported by Zhang et al. [155] and higher E_C values (~69kV/cm).

The ratio between the remanent polarizations for {100} and {111} oriented films is around 0.78, while the theoretical crystallographic relation between the polarization vectors for these two orientations in a rhombohedral crystal (as in Figure 2.4) predicts a factor of 0.86. This discrepancy is likely to be due in part to the imperfect orientation of the films. Incomplete orientation could result in a higher remanent polarization in {100} oriented and lower remanent polarization in {111} oriented films, with respect to ideally oriented films. It should be also noted that the chemical composition of the films is very close to the morphotropic phase boundary and therefore finite amounts of tetragonal oriented grains could be present. In tetragonal perovskites, the {100} poled films would show a higher component of polarization along the [001] axis than {111} oriented films.

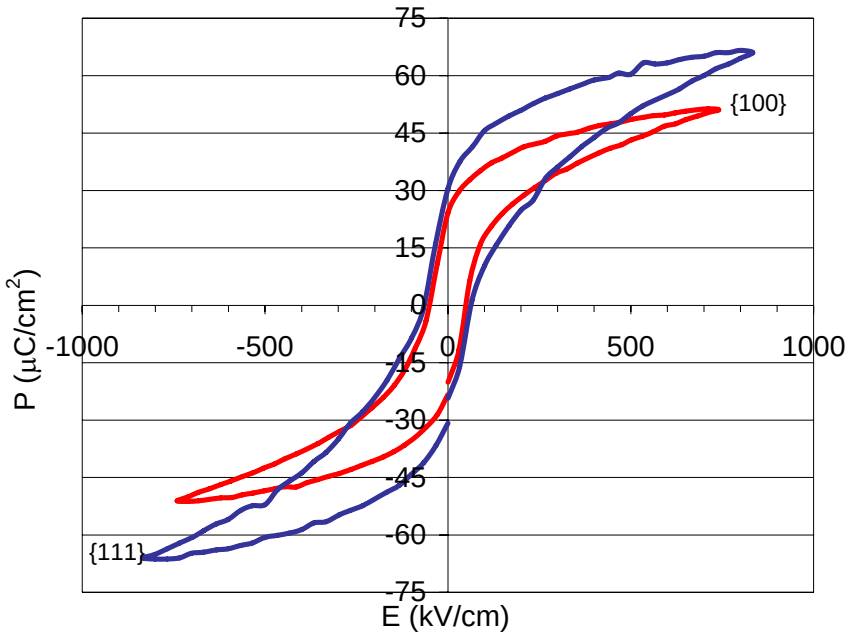

Figure **4.15**: Polarization-Electric field hysteresis loops for {100} and {111} oriented PYbN-PT thin films.

The ferroelectric character of the films was also confirmed by PFM. The films were "written" at +/-10V and then read at 3V. As can be seen in Figure **4.16**b the films could be switched locally. The in-plane component of polarization didn't indicate any preferential orientation, while the out of plane response indicated positive internal bias. The average polarization direction in the as-deposited sample has a non-zero upward out-of-plane component.

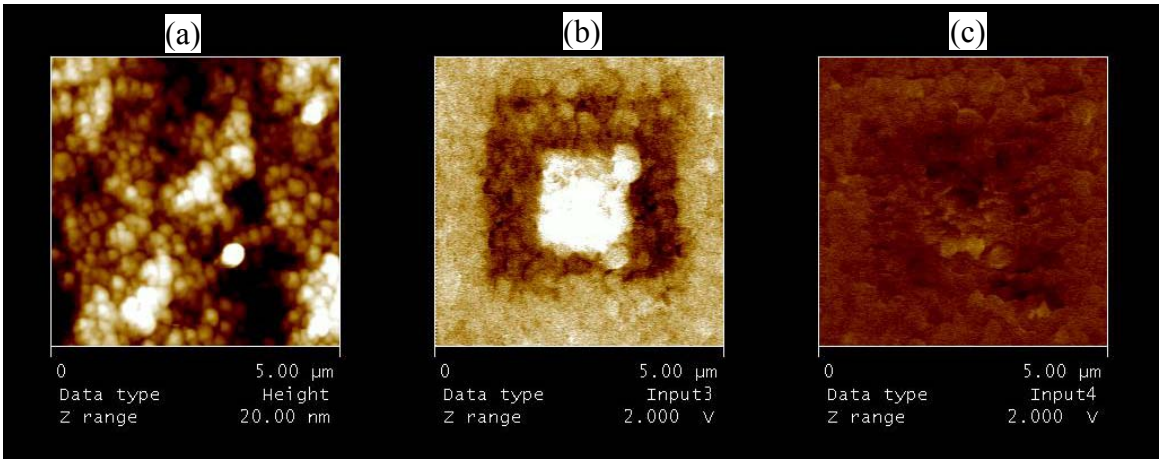

Figure **4.16**: The Piezoelectric Force Microscopy response of a {100} oriented film. (a) morphology of the film, (b) out of plane response of the tip and (c) in plane response. Picture (b) shows a darker square written with +10V. The smaller bright square was written with a subsequent run at -10V. The outer borders had an intermediate contrast, indicating partial out of plane polarization. This intermediate contrast is closer to the contrast originated by poling the sample at -10V (on the bottom electrode).

In some cases it was possible to observe a "coordinated" response in features bigger than the surface morphology as observed in the simple AFM mode (see Figure **4.17**a and b). In Figure **4.17**b arrows show multiple grains that have opposite contrast with respect to the average surrounding grains. These darker spots possibly represent volumes of the material where the polarization direction was not switched during the second writing step.

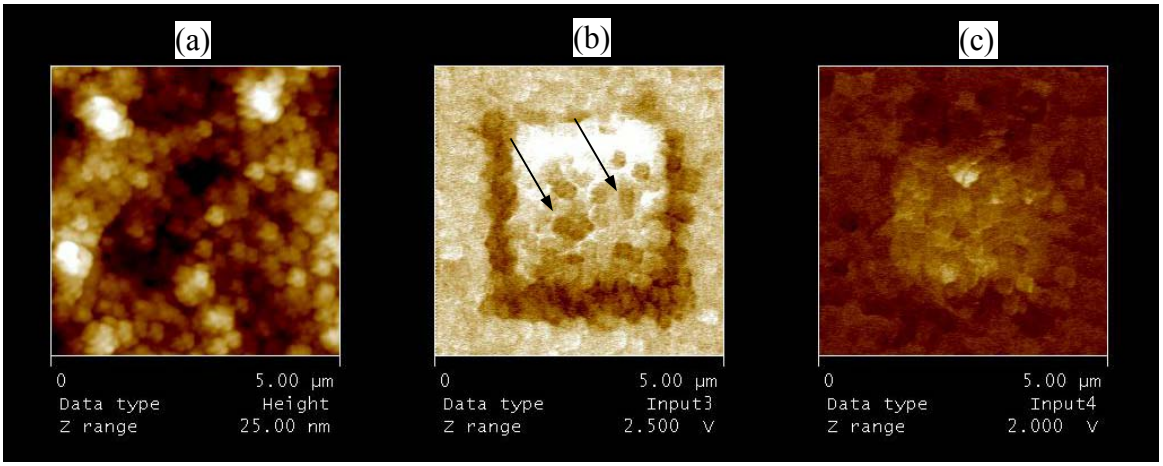

Figure **4.17**: The Piezoelectric Force Microscopy response of a {100} oriented film. (a) morphology of the film, (b) out of plane response of the tip and (c) in plane response. Arrows show features in piezo-response bigger than the grain-size as by (a). These correspond to volumes of the material that have not completely switched polarization during the second writing step at -10V. Notice that the futures indicated by the arrows with similar darker contrast are much bigger than single grains as indicated in picture (a)

The temperature dependence of the permittivity (Figure **4.18**) showed a maximum at temperatures around 365-380ºC, comparable to literature reports for bulk single crystal and ceramics, and thin films of similar composition [**124**][**136**][**149**][**153**]. A smaller shoulder at ~140-160ºC may correspond to the rhombohedral to tetragonal phase transition.[**202**] The ferroelectric/paraelectric behavior of the films, in terms of frequency dependence of the dielectric permittivity as a function of temperature, could not be well resolved at temperatures beyond the transition temperature, probably due to finite amounts of space charge. The dielectric loss (Figure **4.19**) decreased monotonically until temperatures around 250ºC. At higher temperatures, the loss tangent showed a rapid increase, which although in part justified by the phase transition, is probably due in part also to the increased conductivity levels in the films.

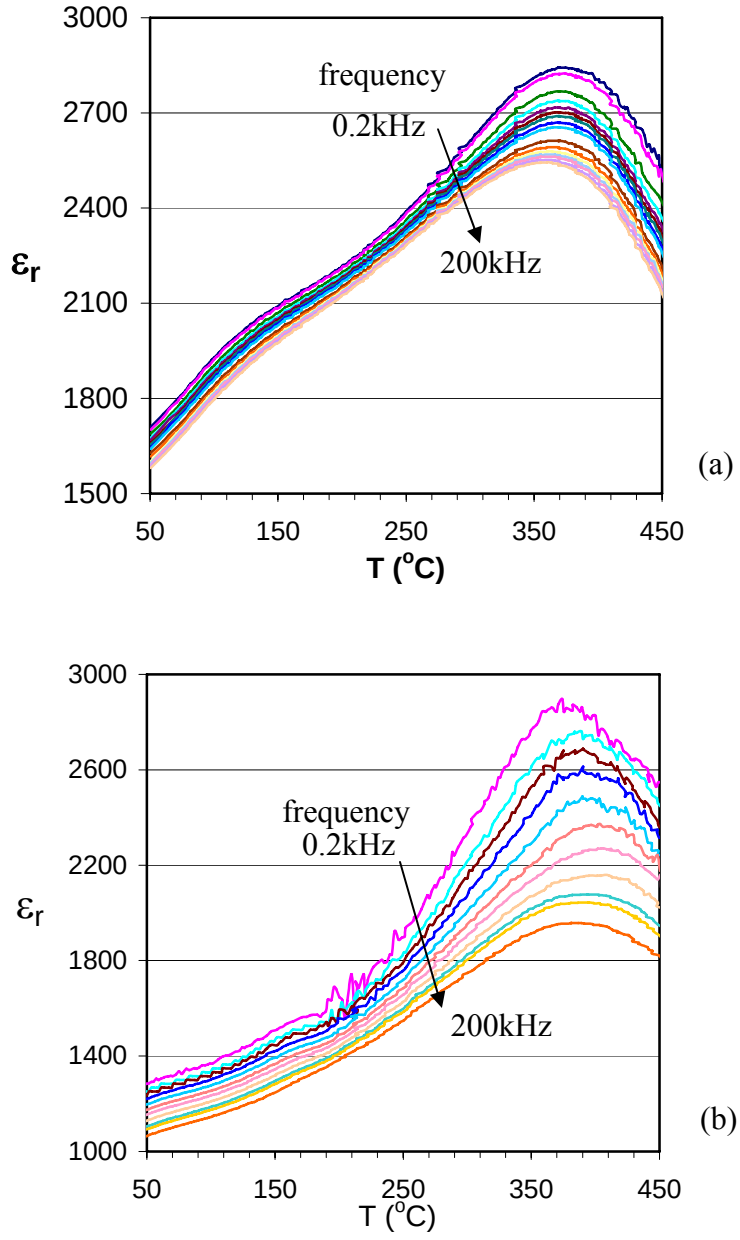

Figure **4.18**: Temperature dependence of permittivity for (a) {100} and (b) {111} oriented, unpoled PYbN-PT films. The reported curves correspond to frequencies between 200Hz and 200kHz.

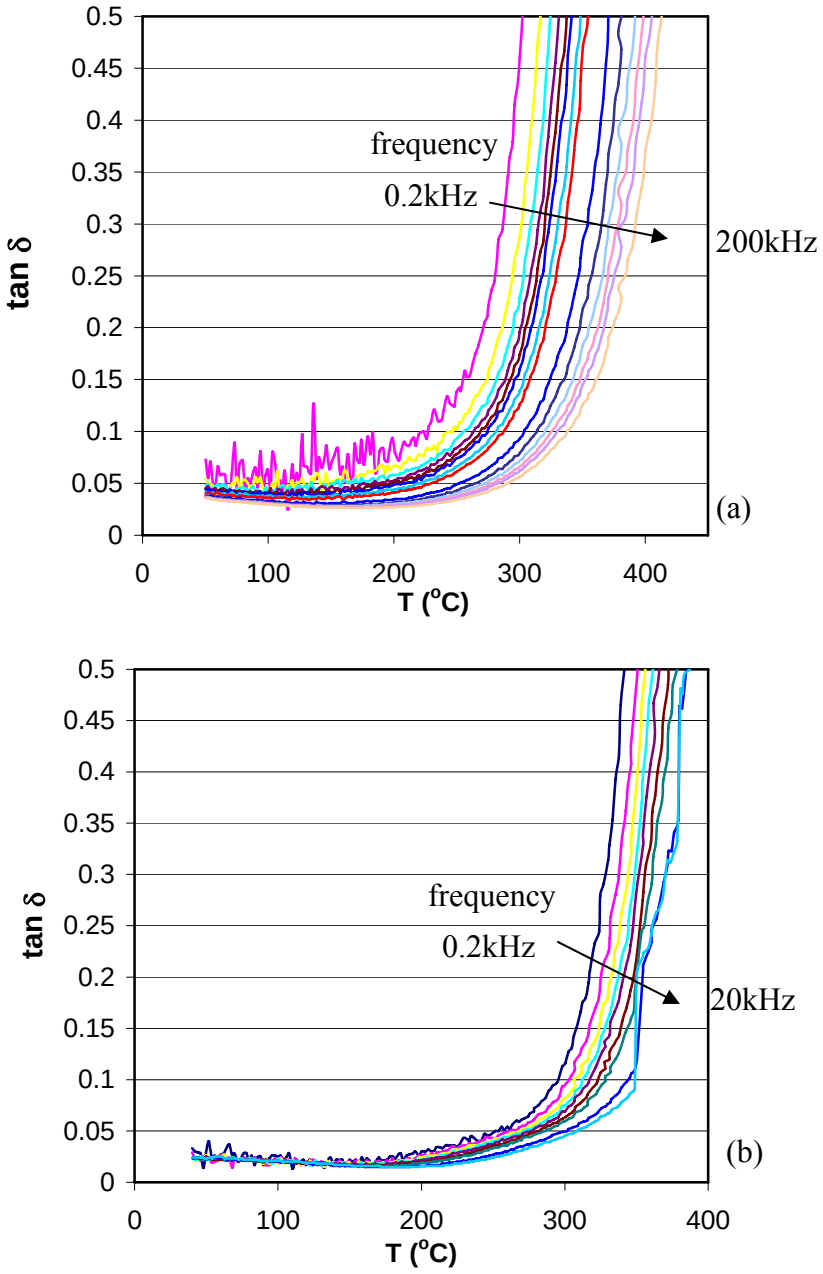

Figure **4.19**: Temperature dependence of dielectric loss for {100} oriented (a) and {111} oriented (b) PYbN-PT films. The reported curves correspond to frequencies between 200Hz and 200kHz (a) and 200Hz to 20kHz (b) respectively.

The tunability of the films was calculated using Equation **4.3:**

$$Tunability = \frac{\varepsilon_r(0) - \varepsilon_r(E)}{\varepsilon_r(E)} \times 100 \qquad \textbf{4.3}$$

where $\varepsilon_r(0)$ and $\varepsilon_r(E)$ are the dielectric permittivity of the films at zero field and under applied bias field, respectively (see Figure **4.20**). The {100} and {111} oriented PYbN-PT films had a tunability of ~77% and ~69%, respectively.

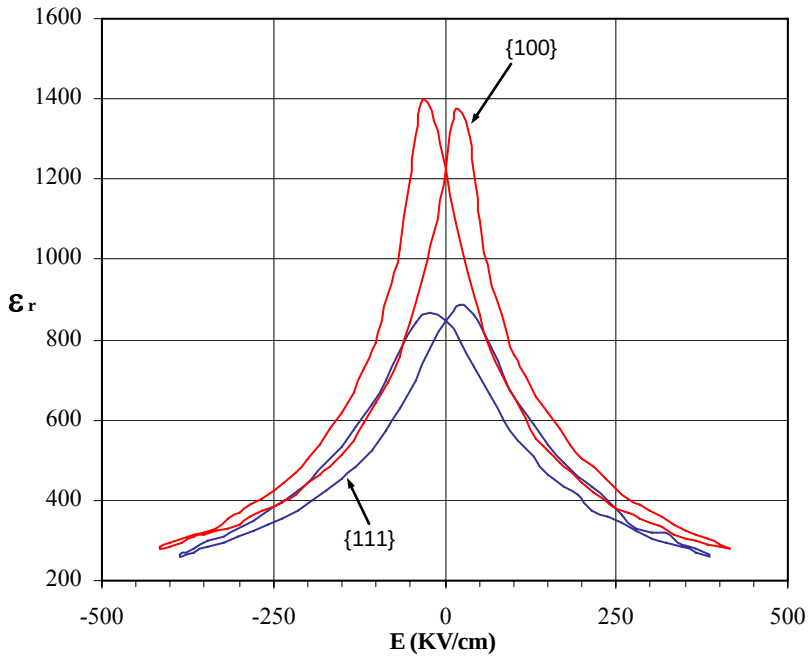

Figure **4.20**: Variation of the dielectric permittivity with applied bias fields.

Some of the {100} oriented films exhibited a slight asymmetry in the shape of the C-V curves that was probably due to the presence of internal fields (see Figure **4.21**).

The calculated amount of the internal field was relatively limited, being <5% of the coercive field and positive in sign. This is in agreement with the results of PFM characterization.

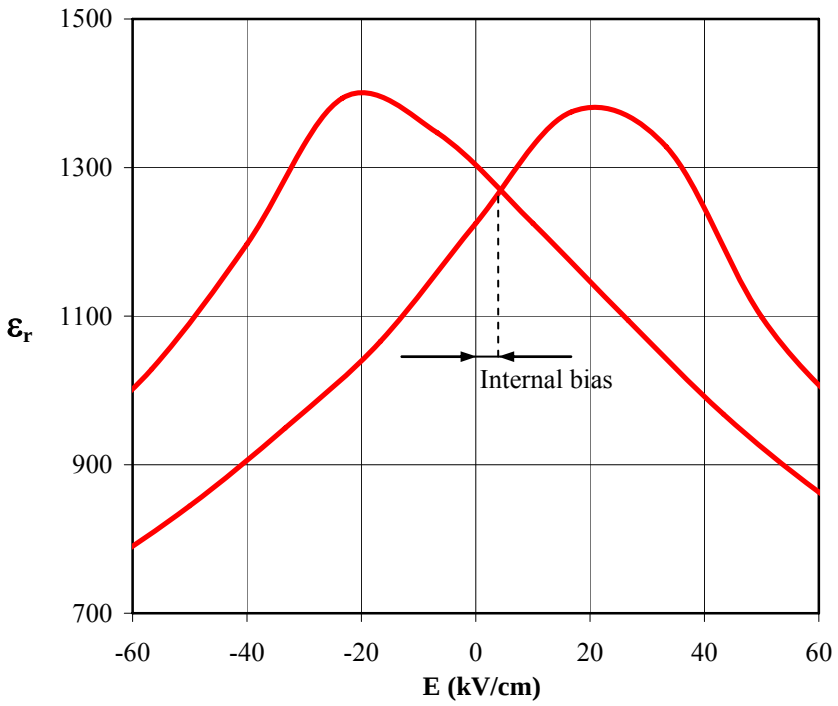

Figure **4.21**: Detail of the field dependence of the dielectric permittivity in a {100} oriented PYbN-PT thin film, showing asymmetry in the shape of the curves.

4.4 Piezoelectric Properties

The as deposited films of either preferential orientation had close to zero piezoelectric response, due to the nearly random orientation of the polarization vectors in the films. To increase the degree of alignment of the polarization vectors, the films were poled before the piezoelectric measurements. Figure 4.22 shows the effects of different poling times and fields on the final piezoelectric values of a {111} oriented PYbN-PT thin film.

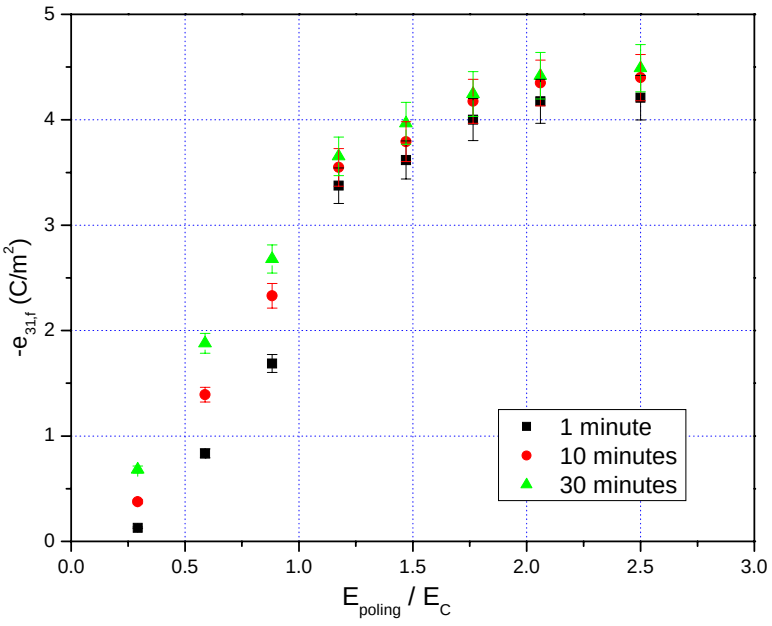

Figure 4.22: Piezoelectric properties of a {111} oriented PYbN-PT film as a function of poling time and field (expressed as ratios of the coercive field E_C).

The absolute $e_{31,f}$ values increased with increasing poling time and field, saturating for fields twice their coercive field or higher. At these fields, poling times of ten minutes or higher offer relatively similar values of $e_{31,f}$.

The effects of poling the top electrode with positive or negative sign are shown in Figure **4.23**. The piezoelectric response of the {111} oriented films showed negligible variation with poling sign. The {100} oriented films, on the other hand showed a slight increase in the absolute $e_{31,f}$ values for poling with the top electrode connected to the positive voltage supply. This can be attributed to the presence of the internal fields in the {100} oriented films, as verified by the tunability results and PFM measurements, both of which indicated the presence of an internal bias positive in sign. Poling in the opposite direction (top electrode negative) can therefore result in a less stable domain configuration and a less effective alignment of the domains, resulting in a lower piezoelectric response of the film. The absolute values of the piezoelectric coefficients were lower than the values reported in literature for highly oriented PYbN-PT deposited via sol-gel (~ -13C/m^2) [**155**] [**156**] or via pulsed laser deposition (~ -14C/m^2) [**152**]. This might be due in part to the lower degree of orientation in this work and in part to the lower thickness of these films (the reported sol-gel deposited films were ~0.7μm, while the pulsed laser deposited films were ~1.0μm thick).

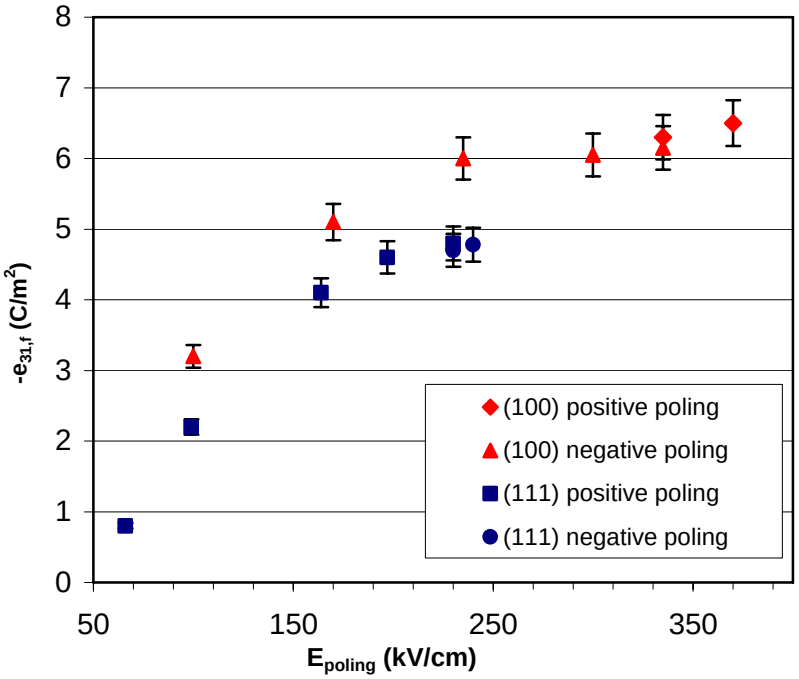

Figure **4.23**: Piezoelectric response of the {100} and {111} oriented PYbN-PT thin films as a function of poling field. The films were poled for 30 minutes.

The piezoelectric properties of the films could be further increased by poling the films at higher temperature. Figure **4.24** shows the effects of poling at higher temperatures on the piezoelectric behaviors of the {100} oriented films. The samples were poled at twice their coercive fields for ten minutes at the indicated temperature and field cooled consequently. Poling at ~150°C yields the highest piezoelectric response in the films with $-e_{31,f} \sim 11\frac{C}{m^2}$. Note that poling at still higher temperatures reduced the actual piezoelectric response of the material. This might be due to the rhombohedral to tetragonal crystallographic phase transformation $T_{R\to T}$ that, as seen in section **4.3**, is

observed at ~140-160°C. Poling at temperatures higher than $T_{R\rightarrow T}$ can induce a tetragonal phase that is stabilized to room temperature, thus reducing the final response of the film.

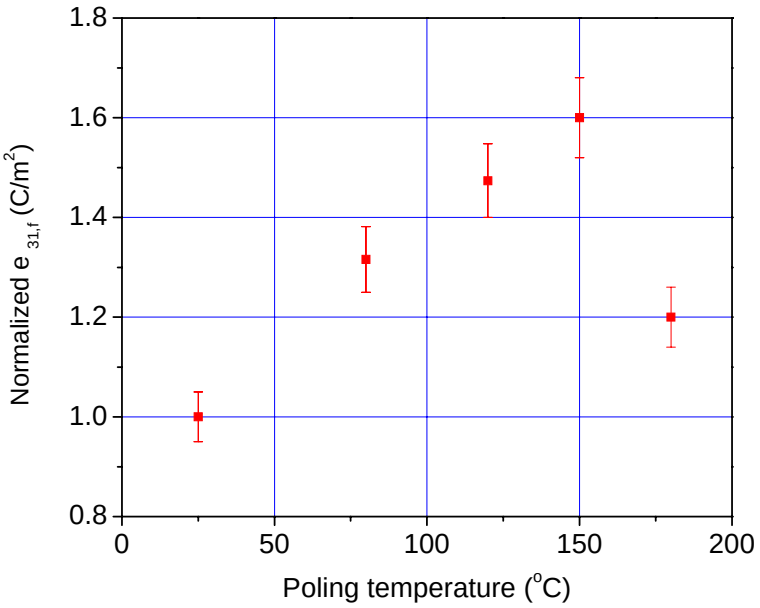

Figure **4.24**: Influence of the poling temperature on the final piezoelectric properties of the {100} oriented PYbN-PT films. The films were field cooled after hot poling.

Chapter 5

Dielectric Nonlinearity

This chapter discusses the nonlinear dielectric behavior of the {100} and {111} oriented PYbN-PT films. The field amplitude dependence of the real and imaginary part of the dielectric permittivity is quantified using Rayleigh analysis. The frequency dependence of the nonlinearities, the effects of external electric and strain bias fields, and the change in the dielectric nonlinear behavior of the films with temperature are also discussed.

The samples used in this chapter, if not otherwise specified, were characterized at 1kHz and poled at room temperature, at twice their coercive field values for 20 minutes before the nonlinear measurements. The aging rate for the dielectric properties was <1 *%/decade* and <3 *%/decade* for the {100} and {111} oriented films, respectively. After poling, the permittivity dropped by about 10% of the initial value. For those films with internal bias present, the nonlinear measurements were performed under a reverse bias field so that the net field should be approximately zero.

5.1 Orientation Dependence of the Dielectric Nonlinearity

The AC electric field dependence of the dielectric properties for {100} and {111} oriented films at 1kHz is shown in Figure 5.1. In films of both orientations, the dielectric permittivity was initially constant with increasing driving field amplitude. After reaching a threshold voltage, a zone where the dielectric permittivity increased almost linearly with the applied field value occurred, and was followed by a third zone where the behavior was sub-linear. Finally the permittivity reached a plateau at field values close to the coercive field strength. The subsequent sub-linear zone probably corresponds to the onset of the depoling and switching of the domains and so a reduced number of interfaces with strong pinning.

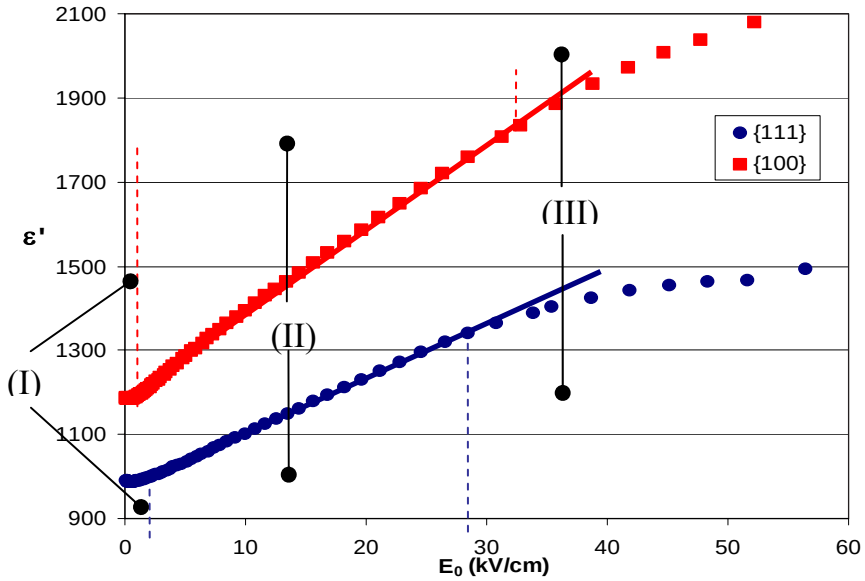

Figure 5.1: The field dependence of the real dielectric permittivity for {111} and {100} oriented films at 1kHz. (I) is the Low Field Region. (II) is the Rayleigh region and (III) is the High Field Region.

The nonlinear behavior of the films were independent of the substrate (NOVA or EPFL) or top electrode material (Pt or Cr-Au) used, suggesting that the differences were characteristic of the PYbN-PT's microstructure and crystallographic orientation. The linear region of Figure 5.1 was fit to Rayleigh behavior. The reasonableness of the approach can be seen in Figure 5.2, where the Rayleigh parameters obtained were used to predict the Polarization-Electric field hysteresis loops.

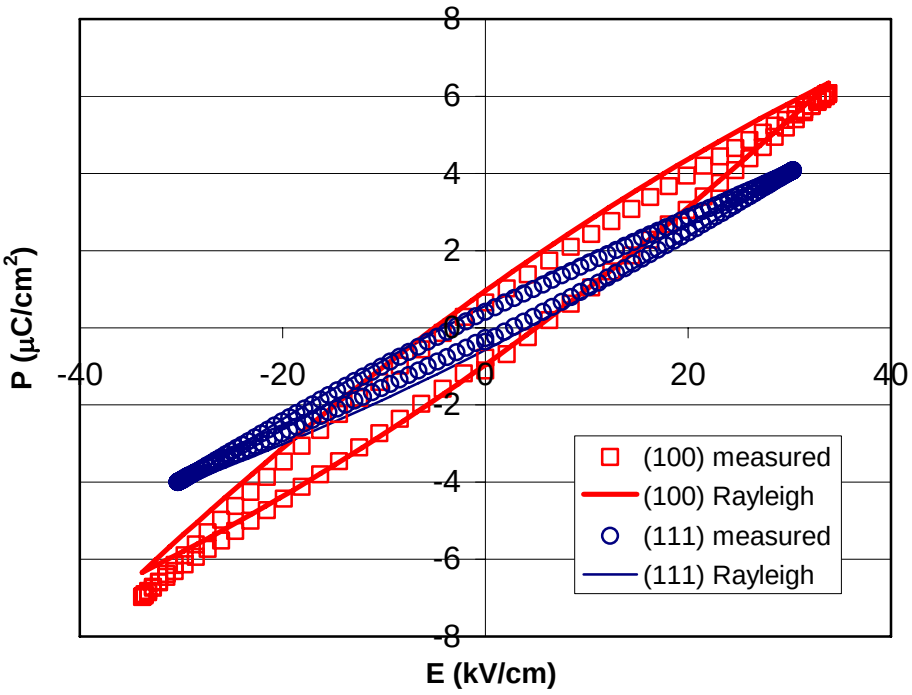

Figure 5.2: The adherence to Rayleigh Law was verified by comparing experimental hysteresis curves and predicted curves obtained by inserting the Rayleigh parameters in Equation 2.27. The measurements were performed at 100Hz.

In Figure 5.2 the experimental hysteresis loops have been mathematically re-centered at zero-field to reduce the effect of imprint. The modeled behavior is very close to the experimental data for both orientations. Note also that the Rayleigh predicted curves are wider than the experimental hysteresis curves. This indicates some amount of nonlinearity that isn't accompanied by hysteresis in the films. Non-hysteretic nonlinearities is typically observed in harder piezoelectrics as reported by Morozov et al. [203]

Four main differences in the nonlinear behavior of the real part of the dielectric constant of the {111} and {100} oriented films were observed:

a) while a threshold field ≈2.2kV/cm is clearly evident in the {111} oriented films, in the {100} oriented films the onset of nonlinearity is not higher than ≈1.0kV/cm;

b) {100} oriented films conform to the Rayleigh law type behavior of the relative dielectric constant for higher values of applied ac fields than the {111} oriented films, mirroring a higher field required for the onset of depoling in the {100} films or a random distribution for motion energies of the interfaces up to higher energy values;

c) the Rayleigh coefficient, α', is ~40% higher in the {100} oriented films than in {111} oriented ones, (19.5±0.4 cm/kV and 14.1±0.1 cm/kV respectively);

d) the ratio of the irreversible to the reversible Rayleigh coefficient is higher in the {100} oriented films, $\left(\frac{\alpha'}{\varepsilon'_{init}}\right)_{(100)} \approx 0.017\frac{cm}{kV}$, than in the {111}

oriented ones where $\left(\frac{\alpha'}{\varepsilon'_{init}}\right)_{(111)} \approx 0.014\frac{cm}{kV}$. It is important to notice that the error on these ratios is in the fourth decimal place, so that the difference between these values is statistically significant.

All these points indicate a higher extrinsic contribution to the dielectric properties in the {100} oriented films with respect to the {111} oriented ones. In particular, they point to either a higher mobility of the interfaces or a larger number of mobile interfaces being present in the {100} films.

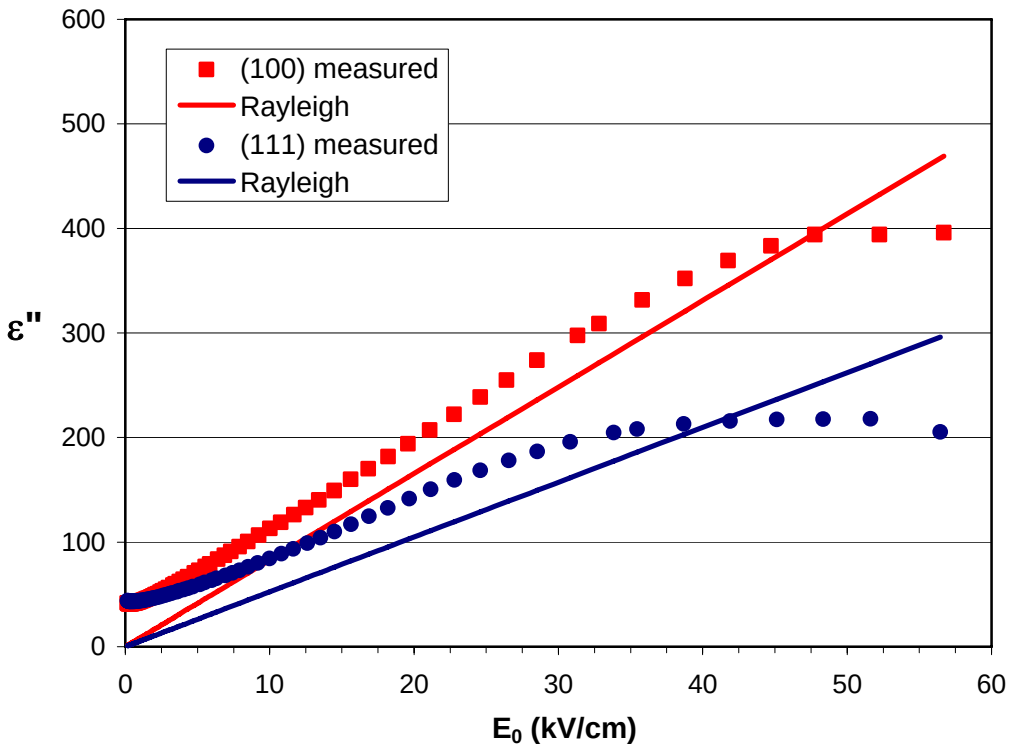

Figure 5.3: The field dependence of the imaginary part of the dielectric permittivity for (111) and (100) oriented films at 1kHz.

Figure 5.3 shows the response of the imaginary component of ε^* as a function of the applied field. According to the Rayleigh Law, the field dependence of ε'' is directly proportional to E_0 with a constant coefficient of $\frac{4}{3\pi}\alpha'$ and no offset. However, the measured ε'' follows the Rayleigh predictions only partially. Although the ratio of α'' to α' is equal to the Rayleigh estimated $\frac{4}{3\pi}$, the field dependence of the imaginary part of the dielectric constant also includes a constant ε''_{init}. This offset could be due to the presence of field independent loss mechanisms in the samples (for example conductivity, hopping displacement of the point defects or reversible domain wall displacements as suggested by Damjanovic [16]). Eitel [97] has recently shown for Bismuth Scandate-Lead Titanate (BS-PT) systems that the loss offset is not present for rhombohedral compositions, while large offsets between measured and calculated imaginary components are observed for tetragonal compositions, suggesting a dependence of the offset on the crystal structure. In the PYbN-PT films, a higher value of ε''_{init} has been observed in the {111} oriented films with respect to the {100} oriented ones. This might be due to slightly different conductivity levels in the films, but further studies are required to understand the real origin of the offset.

The polar directions for the tetragonal and rhombohedral phases are respectively along the <001> and <111> directions.[11] [001]-poled rhombohedral PMN-PT and PZN-

[11] In this work the compositions have been targeted on the rhombohedral side of the MPB. As mentioned in section 4.3, a non-zero amount of PYbN-PT has tetragonal phase. As observed by comparison of the remanent polarization values, the amount of tetragonal phase is much smaller than the amount of

PT single crystals have been reported to have a twinned polydomain state, while [111]-poled ones have single domain structures (especially under bias) or regular macrodomains. [204][205][206] Kholkin et al.[206] have shown recently that [001]-poled single crystals of PZN-4.5%PT have a higher concentration of domain walls than [111] samples, and that the micron-sized domains actually consist of much finer irregular domain structures with sizes down to 20nm (with an average of ~65nm, this being the upper limit due to the resolution limits of the instrument used). They also reported that no nano-domains were observed in [111]-poled crystals. The different domain sizes along different crystallographic orientations were attributed to the relaxor nature of the material. Recent work by Wada et al.[207] has showed that the engineered domain structure is not exclusive of the relaxor family of materials, but indeed can be obtained by poling along a non-polar axis for a proper ferroelectric such as $BaTiO_3$ too. Wada and Tsurumi [204] had previously reported a single domain configuration for the tetragonal single crystal of $BaTiO_3$ when poled along the $[001]_c$ axis, while poling along the $[111]_c$ axis yields a multi-domain structure with domain size ~200-300μm. The multi-domain structure showed an enhancement of the piezoelectric response of the crystal. Based on the idea of the engineered domain structure, the authors then created a much finer domain structure (domain sizes between ~5.5-40μm) by poling the tetragonal $BaTiO_3$ along the $[111]_c$ axis at temperatures close to T_C. The obtained domain structure was then stable at room temperature without applied eternal field. The authors showed an enhancement of the piezoelectric properties of the crystal with decreasing domain size. The higher

rhombohedral phase, therefore the following discussion in this chapter and followings refer to the rhombohedral phase.

concentration of domain walls therefore seems to be attainable in both proper and relaxor ferroelectric for poling along a non-polar axis.

It is possible that some vestige of this different microstructure created in the domains by poling along polar and non-polar axes is present in the PYbN-PT films. This higher concentration of interfaces in (100) oriented films would explain both the lower threshold fields and the higher limit for the Rayleigh zone with the presence of a higher number of mobile domain walls. In thin films, the concentration of mobile interfaces could also be affected by the constraints associated with the substrate, the smaller grain size and a higher concentration of defects.[98][208]

For example, the different microstructures and grain size of the films, could contribute to the difference in the behavior of the two orientations. Damjanovic and Demartin[15][104] reported a much weaker dependence of the piezoelectric coefficient on the amplitude of the ac applied pressure for fine-grained (grain size≈0.8μm) $BaTiO_3$ ceramics when compared to coarse-grained ones (grain size≈1-5μm) due to high internal stress. In their experiments, for coarse grain ceramics, the piezoelectric coefficient d_{33} increased linearly with the applied pressure, whereas the fine-grained ceramics had a sublinear dependence. This response was attributed to the higher force constant for vibrating domain walls in thinner domains.[209] In fact, it has been observed that the non-180˚ domain size decreases with decreasing grain size, thus increasing the density of the domain walls in fine-grained materials.[210] Additionally, Arlt has shown that a critical grain size exists, below which the grains don't contain enough elastic energy to foster creation of twinned non-180° domain walls. This critical grain size for $BaTiO_3$ was shown to be ~ 40nm.[73] Kholkin et al. also reported on the effects of the grain size on

the effective piezoelectric coefficients of 0.9PMN-0.1PT thin films.[211] Weak piezoelectric activity was associated with the small grains, whereas the larger grains exhibit strong piezoelectric activity. The difference was attributed to the possible grain size dependence of the polar clusters, similar to the grain size dependence of the domain size in ferroelectric materials[12]. The grain size range of the {111} oriented films in this work is around 30-40 nm, close to the critical grain size reported for $BaTiO_3$ ceramics, and therefore maybe a smaller concentration of non-180° domain walls. In this work, the grain size of the {100} films is almost an order of magnitude higher than for the {111} films. Therefore, there could be either a lower concentration or mobility of domain walls in {111} films relative to the {100} oriented ones.

There are also reports that indicate the presence of clusters of grains in perovskite ferroelectrics with continuous domain walls across grain boundaries. This would require the motion of the domain walls to be coordinated across multiple grains.[212] It seems therefore reasonable to suppose that the concentration of the grain boundaries will directly influence the motion of the domain walls.[213] The {111} oriented films with a higher concentration of grain boundaries, would therefore show a lower mobility of the domain walls.

At $E_0 = 20$kV/cm, the fraction of the total relative dielectric permittivity, ε_r which is due to the irreversible extrinsic contributions is around 25% in the {100} oriented

---

[12] It has to be also noted that the PMN-PT films used in that work were not phase pure and the smaller grains could have been secondary phase (pyrochlore), "masking" the piezoelectric effect of the underlying bigger, ferroelectric grains. The authors presented no report on any compositional variation between the bigger and smaller grain either. A different ratio of PMN:PT in the different grains could also have led to different piezoelectric coefficients of those grains.

PYbN-PT films and around 21% in the {111} oriented ones. At 30kV/cm, the irreversible contribution in the {100} oriented films contributes 34% of the total dielectric response of the film. It has been shown previously that tetragonal PZT(45/55) films about one micron thick, at E_0 = 20kV/cm owe 15 to 20% of the dielectric properties to irreversible components[17][214], while PMN-PT films of similar thickness and MPB composition owe 30 to 38% of their dielectrics properties at E_0 = 20kV/cm to the irreversible contributions (for further details see Chapter 7).

5.2 Frequency Dependence of the Dielectric Nonlinearities

As mentioned earlier, the dielectric nonlinear properties of the PYbN-PT thin films are frequency dependent (Figure 5.4 a and b) while the Rayleigh law is time-independent. As can be seen in Figure 5.5, the experimental dependence of the real part of the reversible and irreversible Rayleigh coefficients can be fitted with a logarithmic frequency dependence, as in Equation 5.1

$$A(\omega) = a_0 + a \ln\left(\frac{1}{\omega}\right) \qquad \textbf{5.1}$$

where ω is equal to $2\pi f$ and A can be the reversible or irreversible dielectric constant and a_0 and a are different fitting parameters for each case.

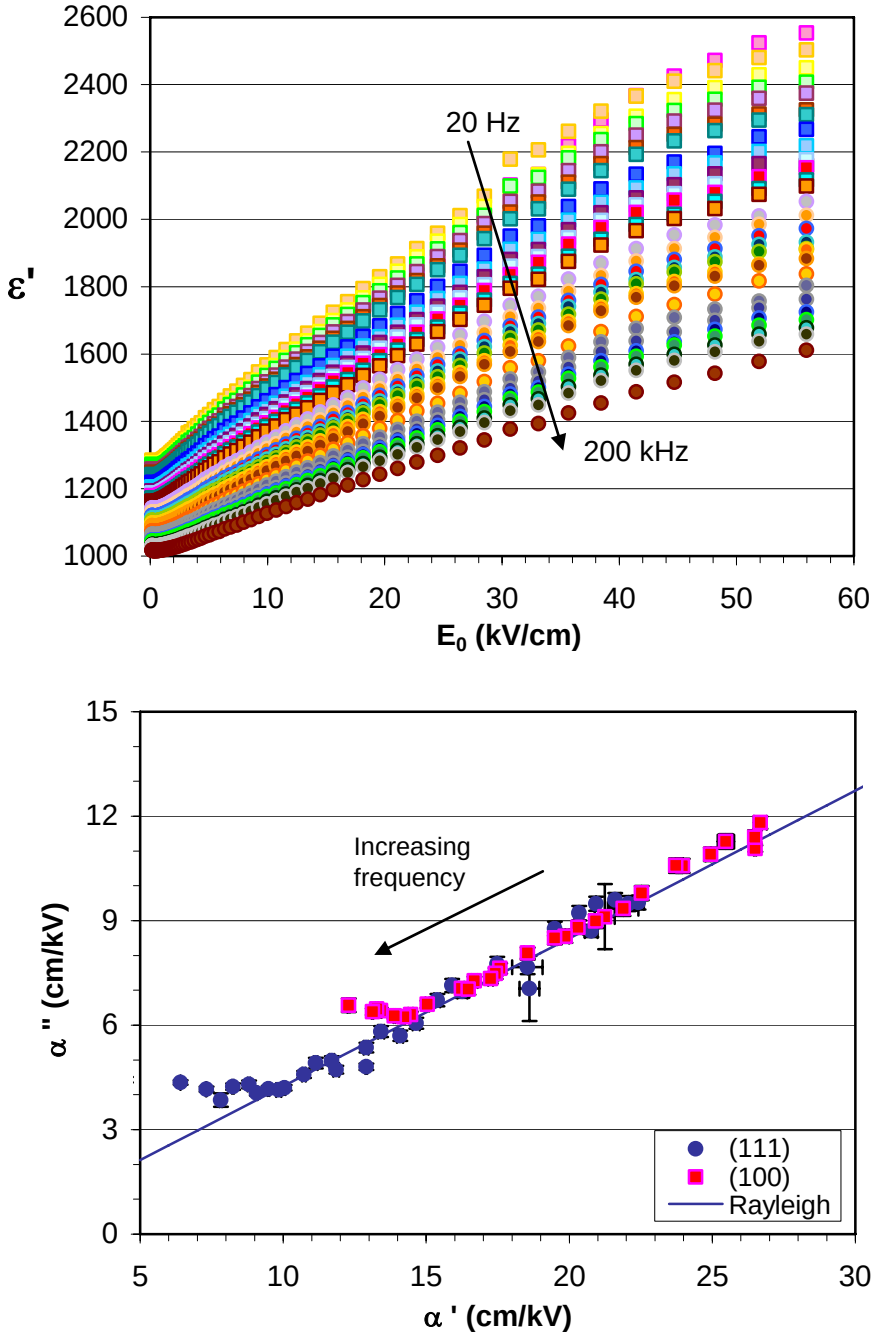

Figure **5.4**: (a) Frequency dependence of the nonlinear behavior of a {100} oriented thin film. (b) Adherence to the Rayleigh Law was verified for frequencies between 20Hz and 200kHz. From 20Hz to 50kHz very good adherence to the Rayleigh Law was observed. At higher frequencies, increasing instrumental errors reduce the accuracy of the measurements.

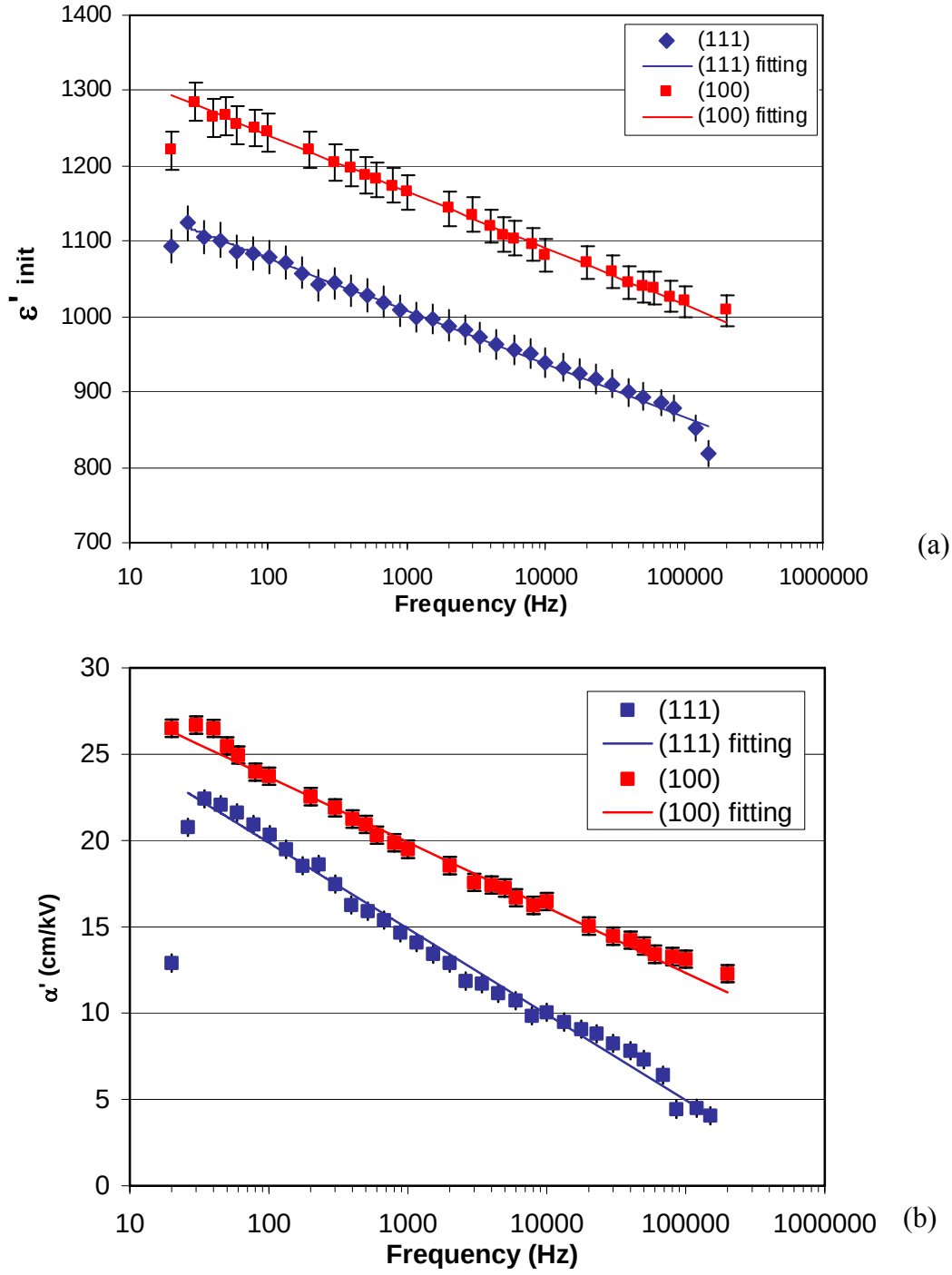

Figure 5.5: Logarithmic dependence of the reversible (a) and irreversible (b) Rayleigh parameters on frequency.

$$\varepsilon'_{init(111)}(\omega) = 1264 + 29\ln\left(\frac{1}{\omega}\right) \qquad \alpha'_{(111)}(\omega) = 33.8 + 2.16\ln\left(\frac{1}{\omega}\right) \qquad \textbf{5.2}$$

$$\varepsilon'_{init(100)}(\omega) = 1452 + 33\ln\left(\frac{1}{\omega}\right) \qquad \alpha'_{(100)}(\omega) = 34.2 + 1.64\ln\left(\frac{1}{\omega}\right) \qquad \textbf{5.3}$$

The logarithmic dependence of the susceptibility on the frequency ω of the applied field was first theoretically demonstrated by Nattermann et al. [**215**] for ferromagnetic systems and it was attributed to domain wall or interface pinning phenomena. As pointed out by different authors [**214**][**216**][**217**][**218**][**219**], the same should also be valid for mechanisms of domain wall pinning in non-magnetic, physically equivalent systems, such as ferroelectrics.

Remarkably, even though the frequency dependence of the reversible Rayleigh parameter is higher in {100} oriented films than in {111} oriented ones, the same trend is not observed for the irreversible Rayleigh parameter. In fact, the a parameter for $\alpha'_{(111)}$ is ~50% higher than the a parameter for $\alpha'_{(100)}$. Ozgul [**132**] has shown recently that for single crystals of PZN-4.5PT, the frequency dependence of the dielectric polarization is less pronounced along the [001] direction than along the [111] direction. The author suggested the narrower time constant distribution for relaxation along [111] to be the origin of this anisotropy. In general, the (100) poled crystals exhibited faster polarization kinetics than the (111) poled ones.

A similar approach could be used to explain the anisotropic frequency response of the irreversible Rayleigh parameters in PYbN-PT films. The weaker dependence of

$\alpha'_{(100)}$ on frequency can be seen as another aspect of the higher mobility of the domain walls in these films with respect to the {111} oriented ones. The higher concentration of domain walls in these films could also produce a faster response to the applied field if statistically the higher concentration of domain walls translates also to the presence of a larger number of mobile domain walls.

The Rayleigh law can be modified to incorporate the frequency dependence of the reversible and irreversible parameters in the following forms:

$$\varepsilon'_r(\omega, E_0) = \varepsilon'_{init}(\omega) + \alpha'(\omega) \cdot E_0 \qquad \textbf{5.4}$$

$$\varepsilon'_r(\omega, E_0) = \varepsilon'(E_0) + \varepsilon'_0(E_0) \cdot \ln\left(\frac{1}{\omega}\right) \qquad \textbf{5.5}$$

Equation **5.4** and **5.5** are equivalent. In this work, the modified Rayleigh law used is in the form of Equation **5.4**. This modified Rayleigh law is able to predict relatively well the dielectric properties of PYbN-PT films at intermediate AC fields and frequencies as can be seen in Figure **5.6**. This model should be very useful to predict the behavior of film based devices under high applied fields.

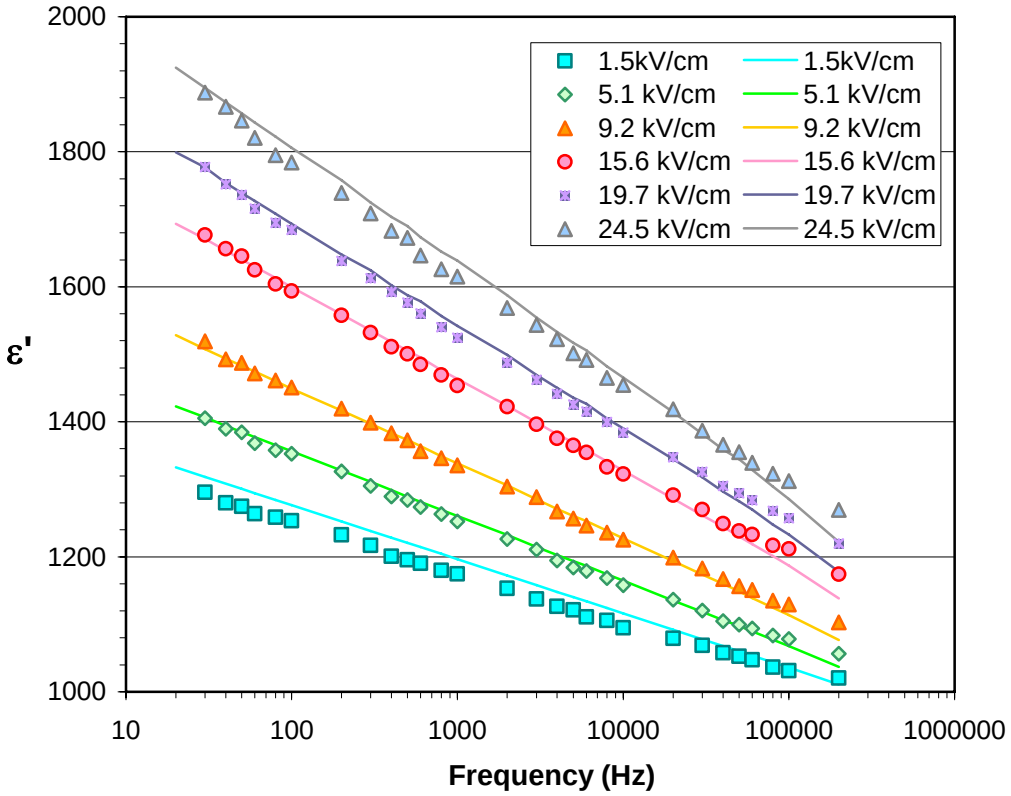

Figure **5.6**: Comparison of the experimental data with a modified Rayleigh Law fit for the PYbN-PT films over an intermediate field and frequency range. The example shown refers to a {100} oriented PYbN-PT thin film.

5.3 Effects of External Electric and Elastic Bias on the Dielectric Nonlinearities

Although numerous reports have described the effects of the static elastic and electric fields on the low field properties of the ferroelectrics,[**220**][**221**][**222**] few have paid full attention to the effects of these on the high field nonlinear properties [**223**][**224**]

and to the author's best knowledge none has studied these effects in thin film ferroelectrics. In many cases the processing steps necessary to the production of a ferroelectric thin film based device create internal stresses.[225][226] This is in part due to the high crystallization temperatures used and the thermal expansion mismatch between the different layers.[227] In addition, some devices require application of an external dc electric field in the working regime, which can also influence the dielectric and piezoelectric behavior of the ferroelectric interfaces. In the following sections the influence of dc electric fields and biaxial strains on the {100} and {111} oriented PYbN-PT are discussed.

5.3.1 Effects of External Electric Bias on the Dielectric Nonlinearities

The effects of application of external positive and negative bias on the dielectric nonlinear properties were studied. As can be seen in Figure 5.7, the nonlinear behavior of the ferroelectric films depends on the applied external bias field. With increasing external positive bias field, the threshold field for the onset of nonlinear behavior increased. This extends the Rayleigh region, while lowering the field dependence in the Rayleigh region. The extension of the Rayleigh region to much higher values is not unexpected as the application of an applied bias should stabilize the domain structure, retarding the onset of depoling and switching.

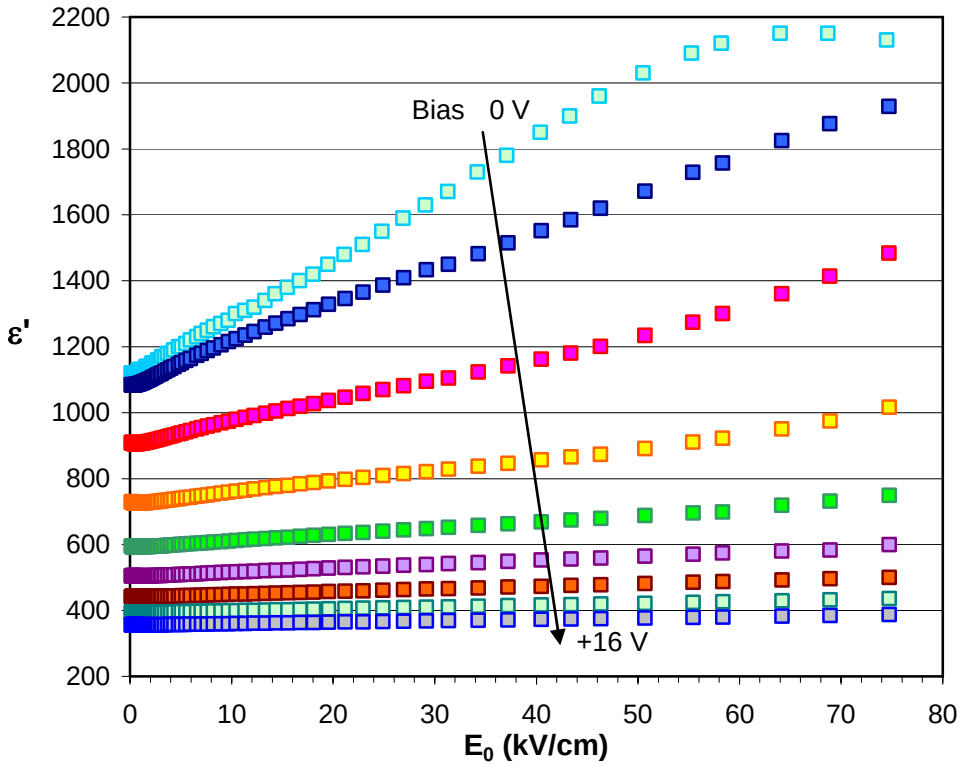

Figure 5.7: Modification of the dielectric nonlinear behavior of a {100} oriented, ~0.6μm thick PYbN-PT film, upon application of superimposed positive electric bias fields (data is in 2V increments).

The reduced Rayleigh coefficients can be explained by the fact that an applied external bias, in the same direction of the poling, can lead to stabilization of the domain configuration created by poling. This effect can be imagined as an increased depth of the potential energy wells in the energy profile for the motion of the interfaces or equivalently as an increase in the barrier height for their motion from one potential well to the next.

Figure 5.8 (a) and (b) show the bias field dependence of the Rayleigh parameters and Figure 5.9 shows the bias field dependence of the ratio of the irreversible to

reversible Rayleigh parameter. The samples have been poled with top electrode positive before study of nonlinear behavior with application of either positive or negative bias field. It can be seen that the bias field dependence can be well fitted with an exponential decay as in Equation **5.6**:

$$B(E) = b_0 + b\exp(cE_{bias}) \qquad \textbf{5.6}$$

where E_{bias} is the applied bias field, B can be either of the Rayleigh parameters or their ratio and b_0, b and c are the fitting parameters for each case. The fitting parameters for {100} oriented PYbN-PT films are summarized in Table **5-1**.

Table **5-1**: Exponential decay parameters, as defined in Equation **5.6**, for external bias dependence of Rayleigh parameters in {100} oriented PYbN-PT films.

B	b_0	b	$c\left(\frac{cm}{kV}\right)$	Bias sign[13]
ε'_{init}	345±18	973±40	-0.0094±0.0006	Positive
	350±18	1156±40	0.0101±0.0003	Negative
α' (cm/kV)	0.53±0.10	18.9±0.2	-0.0238±0.0006	Positive
	0.23±0.16	19.3±0.2	0.0193±0.0006	Negative
$\alpha'/\varepsilon'_{init}$ (cm/kV)	0.0014±0.0002	0.0152±0.0008	-0.0217±0.001	Positive
	0.0015±0.0002	0.0150±0.0008	0.0197±0.0008	Negative

[13] Defined as the sign of the source lead connected to the top electrode.

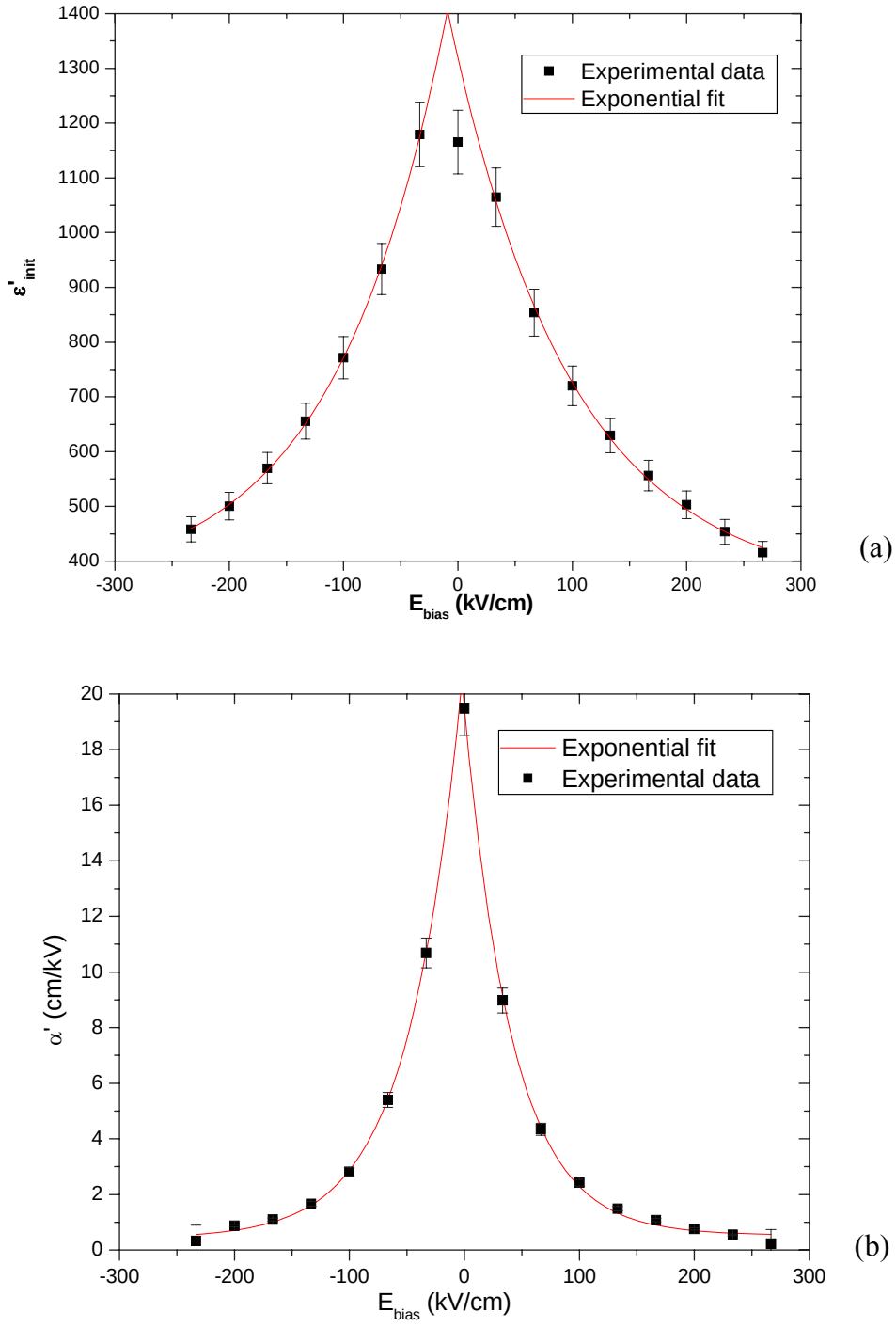

Figure **5.8**: Effects of positive and negative bias fields on the reversible (a) and irreversible (b) Rayleigh coefficients in {100} oriented PYbN-PT thin films.

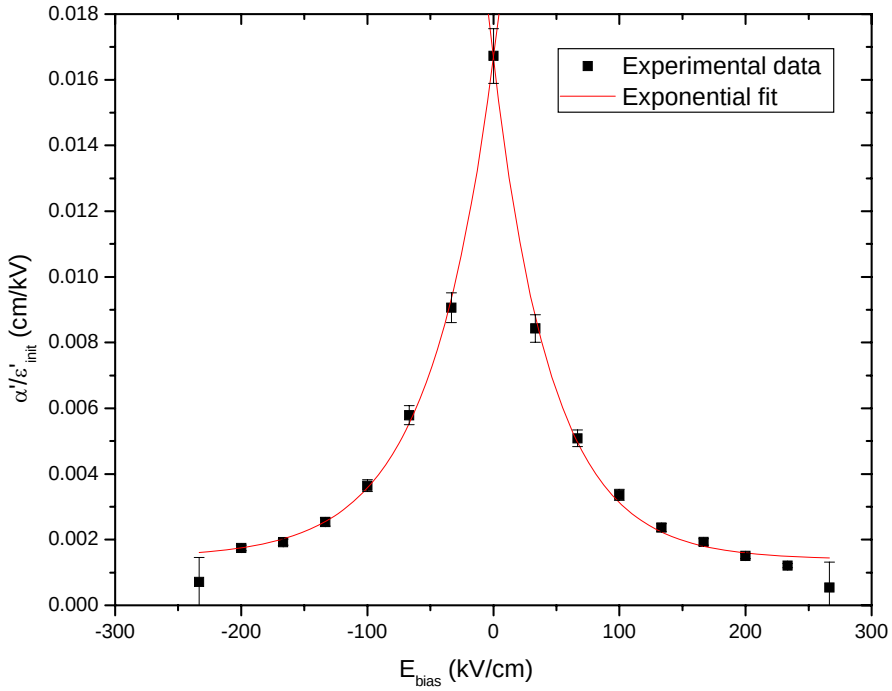

Figure **5.9**: Bias field dependence of the ratio of the irreversible to reversible Rayleigh parameters for {100} oriented PYbN-PT thin films.

It should be noted that the phenomenological theory, based on the Landau-Devonshire theory, predicts for ferroelectric materials a dependence of the intrinsic dielectric permittivity on the amplitude of the bias field described by Equation **5.7** [**1**][**228**]:

$$\varepsilon = \frac{1}{-\xi T + 3(\psi E_{bias})^{2/3}} \qquad \textbf{5.7}$$

where T is the temperature at which the measurements are performed and ξ and ψ are two constants of the material, related to the free energy, non-linear dielectric coefficients of the material and the Curie temperature. Equation **5.7** is valid for a ferroelectric

material, but does not include the domain wall motion contribution to the dielectric permittivity. In fact use of the above mentioned equation to fit the Rayleigh parameters yields $R^2 \approx 0.95$ while the use of the exponential decay Equation **5.6** yields $R^2 \geq 0.96$, with an average $R^2 \approx 0.996$. The inadequacy of the phenomenological model based only on the intrinsic polarization change in a ferroelectric has been also reported by Ang et al. [**93**]. The authors showed for PZT thin films that the phenomenological theory offered a relatively good fit at cryogenic temperatures. With increasing temperatures, the phenomenological model begins to be less and less accurate, untill at room temperature, it can account for less than 50% of the experimental dielectric constant observed at intermediate fields. Ang et al. suggested also a "reorientational polar cluster" model that could describe the extrinsic contributions. [**94**] The comprehensive expression suggested by the authors proved to be mathematically complex and valid only at small polarization values ($\leq 5\mu C/cm^2$), which is not a valid hypothesis for the present work. Therefore, in this work, a separate mathematical expression was sought and to this end, the exponential decay was found to express the best fit to the experimental data points. It has also to be noted that the use of Equation **5.7** proved to be satisfactory for the bias field dependence of the Rayleigh parameters and their ratio at high bias fields ($E_{bias} \geq 100\ kv/cm$), yielding $R^2 \approx 0.99$. The improved fitting of the experimental data with the phenomenological approach in this range is probably due to the stabilization of the domain structure with increasing bias fields.

Figure **5.10** shows the dependence of the Rayleigh parameters on external bias field for a {111} oriented PYbN-PT film. Figure **5.11** shows the bias field dependence of

the ratio of the irreversible to reversible Rayleigh parameter. The fitting parameters (as in Equation **5.6**) for {111} oriented PYbN-PT films are summarized in Table **5-2**.

Table **5-2**: Exponential decay parameters, as defined in Equation **5.6**, for external bias dependence of Rayleigh parameters in {111} oriented PYbN-PT films.

B	b_0	b	c	Bias sign
ε'_{init}	190±38	828±35	-0.0065±0.0007	Positive
	166±40	854±37	0.0062±0.0007	Negative
α' (cm/kV)	0.11±0.02	14.2±0.3	-0.0149±0.0007	Positive
	0.16±0.02	13.6±0.1	0.0148±0.0001	Negative
$\alpha'/\varepsilon'_{init}$ (cm/kV)	0.0008±0.0001	0.013±0.001	-0.0131±0.0003	Positive
	0.0006±0.0001	0.013±0.001	0.0119±0.0003	Negative

It can be seen that in both the {100} and the {111} oriented films, applied negative bias leads to higher reversible and irreversible parameters than application of positive bias values. This is translated into a slight difference in the fitting parameters values of the exponential curves. The asymmetric behavior can be due to the presence of the internal fields in the samples. Because the observed internal fields were usually positive in sign, application of positive bias field would lead to further stabilization of the domain structure created in poling. In contrast, application of a negative bias field would destabilize the domain structure of the films, increasing the domain wall mobility in the films.

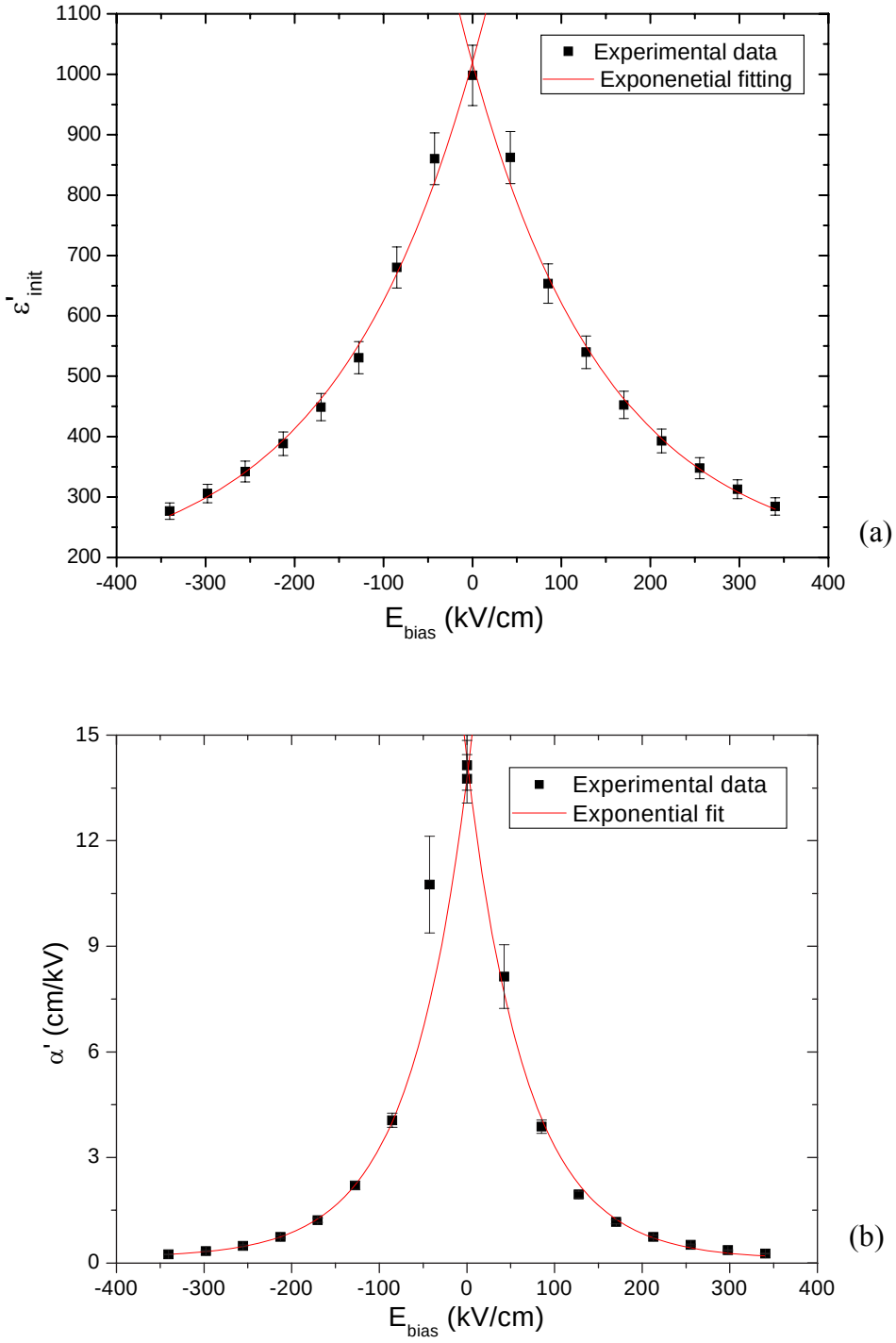

Figure **5.10**: Effects of positive and negative bias fields on the (a) reversible and (b) irreversible Rayleigh parameters in {111} oriented PYbN-PT thin films.

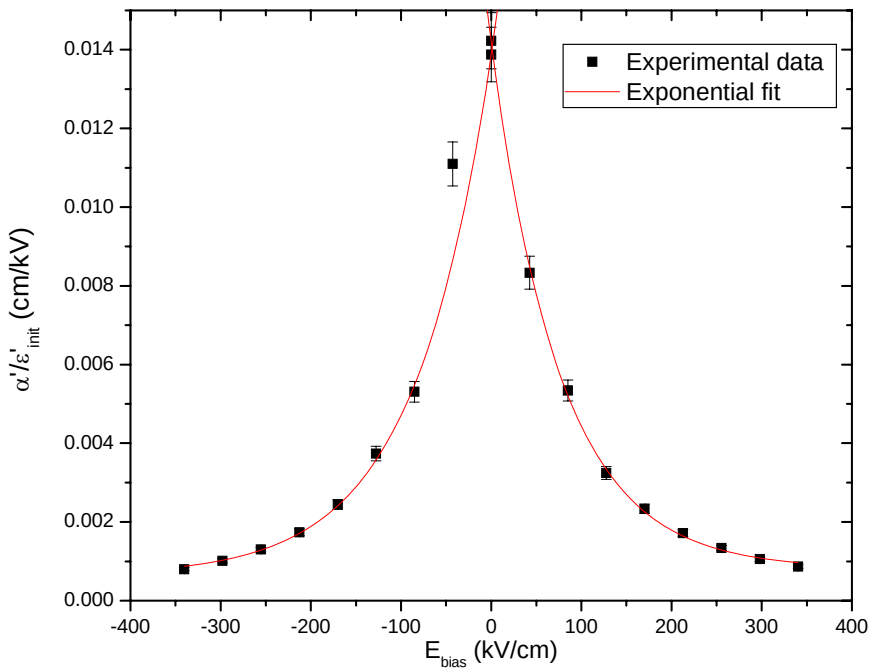

Figure **5.11**: Effects of positive and negative bias fields on the ratio of the irreversible to reversible Rayleigh coefficients in a {111} oriented PYbN-PT thin film.

The offset values b_0 for α' and $\alpha'/\varepsilon'_{init}$ of the {111} oriented films were approximately half the values of the {100} oriented films. As mentioned earlier, application of a bias field induces a stabilization of the domain structure, and therefore a reduction of the extrinsic contributions to the dielectric nonlinearities. Higher offset values indicate consequently a higher contribution of the mobile interfaces even at higher applied bias fields. The {100} oriented PYbN-PT films exhibited also higher absolute values for the c coefficients, indicating a faster decay of the extrinsic contributions with applied bias fields.

Both of the above observations seem to indicate a wider distribution of the mobile domain walls in terms of the potential energies necessary for their motion. This has been schematically shown in Figure **5.12**[14]. A wider distribution of the energies necessary for the motion of the domain walls translates into a more gradual decrease of the number of the mobile domain walls with increasing bias fields. Conversely, a narrower distribution of the domain walls pinning energies, leads to an initial slow decrease in the number of the mobile interfaces, followed by a sudden drop in their number and thereafter a very limited number of "active" domain walls contributing to the dielectric nonlinearities at the highest bias fields. The wider the distribution of the domain wall pinning energies, the higher the "incremental" number (decreasing) of the mobile interfaces stabilized at lower fields and the higher the "incremental" number (decreasing) of the mobile interfaces still available at higher bias fields. Therefore, both the initial slope of the exponential decay curve of the Rayleigh parameters and the offset values of them will be higher for the samples with a wider distribution of the domain wall energies. The {100} oriented PYbN-PT films should therefore have a wider distribution of the potential energies for the motion of the domain walls than the {111} oriented films. This observation is in agreement with the previous observations in terms of the frequency dependence of the Rayleigh parameters reported in section **5.2**.

---

[14] Note that the idea of hysteretically mobile interface distribution affecting the properties of the material has been already developed mathematically by Preisach. For a comprehensive study of the subject in ferromagnetic materials refer to reference [**229**].

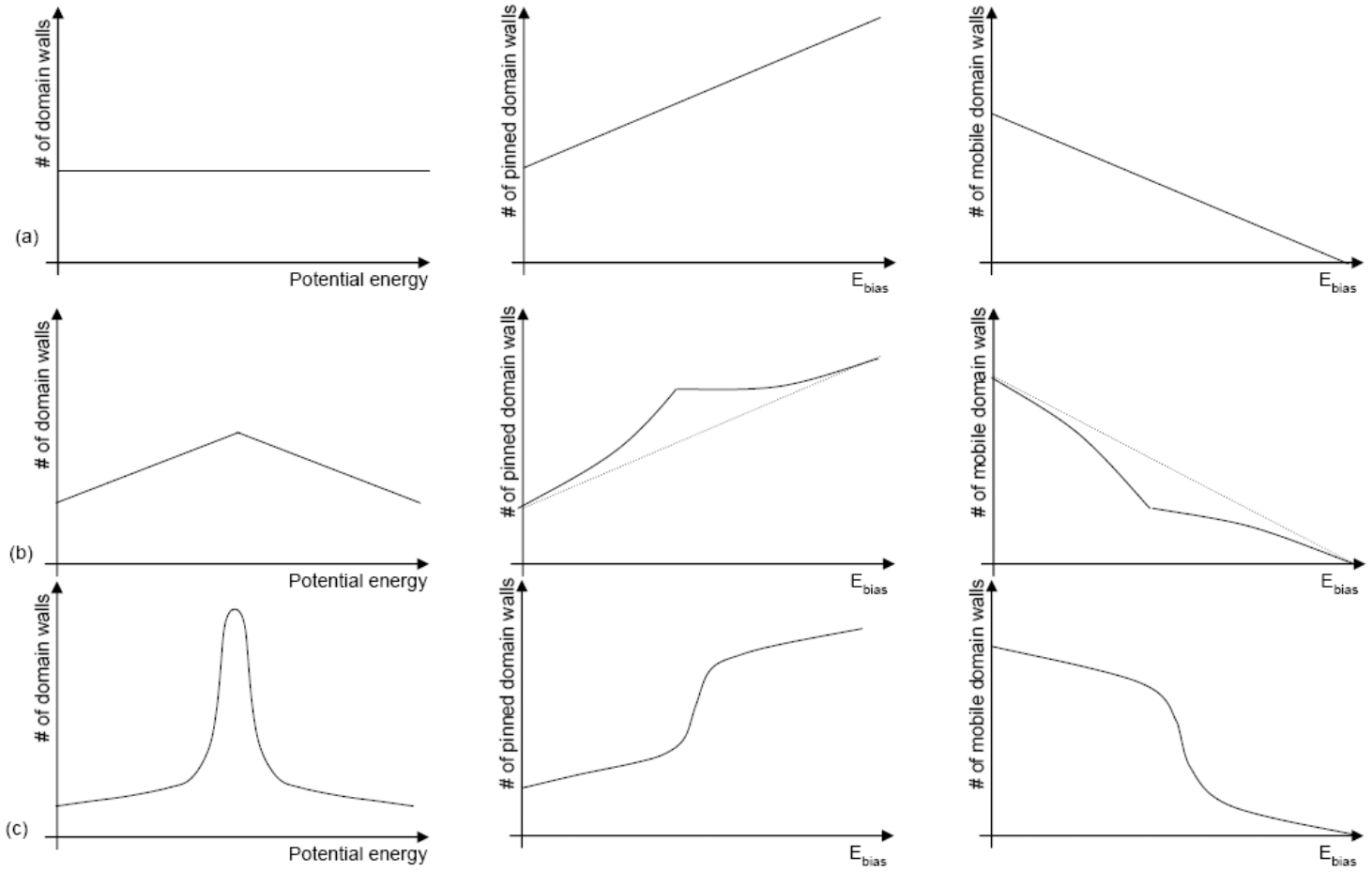

Figure **5.12**: Schematic presentation of the influence of the potential energy distribution for the motion of the domain walls on the number of the contributing domain walls to the dielectric properties of the ferroelectric material at different bias fields. (a) uniform distribution of domain wall potential energies; (b) a wide but not uniform distribution of potential energies for motion of domain walls and (c) a very narrow distribution of potential energies for domain wall motion.

5.3.2 Effects of External Biaxial Tensile Stress on the Dielectric Nonlinearities

The mechanical stress dependence of the nonlinear behavior of the films is reported in Figure 5.13 and 5.14.[15] Because the elastic properties of the films are unknown, the horizontal axis is given as the measured strain.[16] In fact, to calculate the applied stress to the film based on the strain level, knowledge of Young modulus and Poisson coefficients of the films are required. In {100} oriented films, both the reversible and the irreversible Rayleigh parameters show an initial increase upon application of the biaxial tensile stress, followed by a weak maximum and an asymptotic decrease. With the unloading cycle, ε'_{init} and α' recover to values similar to the original unstressed values. The initial increase might indicate a small depinning of the domain walls, with subsequent clamping of the domains state at higher strains.

In terms of magnitude, application of a positive pressure (e.g. a tensile stress in the film) had a relatively small effect on either the reversible or the irreversible Rayleigh coefficients for either orientation of the PYbN-PT films. The largest relative change of the values of the Rayleigh coefficients was less than 4% in the {100} oriented films. This small magnitude of the variation of the dielectric properties is consistent, for the {100} oriented films, with the crystallographic orientation of the sample. In fact, considering the

---

[15] Note that the parameters have been normalized to the values measured in the free films.

[16] The same levels of strain in a similar PZT on Si wafer stack resulted in applied stresses of ~100MPa. These are comparable with residual stress values calculated for sol-gel PZT thin films deposited on platinized silicon wafers.[230][231]

available polarization directions in a rhombohedral crystal with {100} orientation (see Figure 2.4) application of a biaxial stress parallel to {001} should not reorient the polarization vectors. Biaxial stresses parallel to {001} could yield major variation of the dielectric properties, if the stress values are high enough to create a phase transformation from rhombohedral to tetragonal perovskite or to cause ferroelastic switching of existing tetragonal material. In this work, the property changes due to the applied tensile mechanical stress were not strong enough to indicate any such contribution. The modest response of the dielectric nonlinearities to applied biaxial stress thus suggests that the domain structures cannot be modified by applied tensile stresses of the magnitude used here.

In the case of {111} oriented films, due to the crystallographic orientation of the crystal, the polarization vector could, in principle, be ferroelastically switched by application of biaxial stress (i.e. non-180° domain wall motion). The negligible variation of the Rayleigh parameters in the case of the {111} oriented films, therefore indicates that the contribution of the non-180° domain walls and the phase boundary motion to the dielectric nonlinear properties of these films at room temperature is negligible.

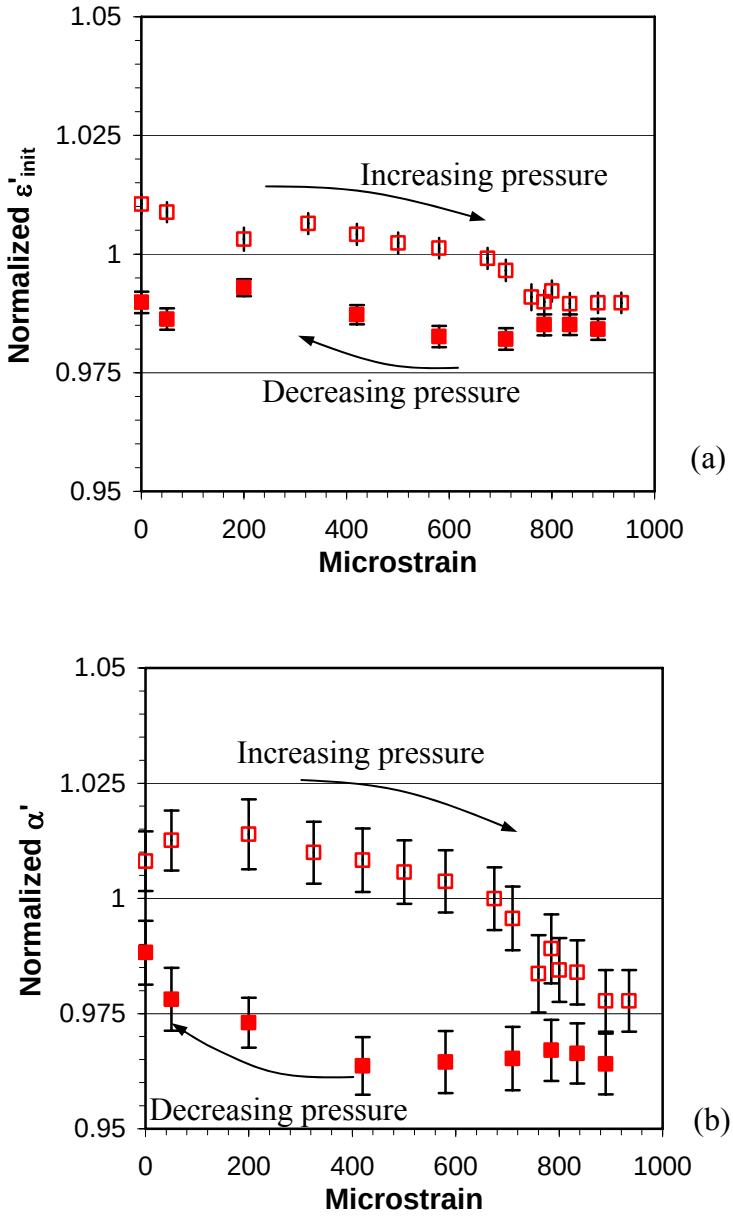

Figure **5.13**: Biaxial strain dependence of the (a) reversible and (b) irreversible Rayleigh parameters in {100} oriented PYbN-PT thin films. The arrows indicate the order in which the measurements were done. The parameters have been normalized to the values measured in the free films.

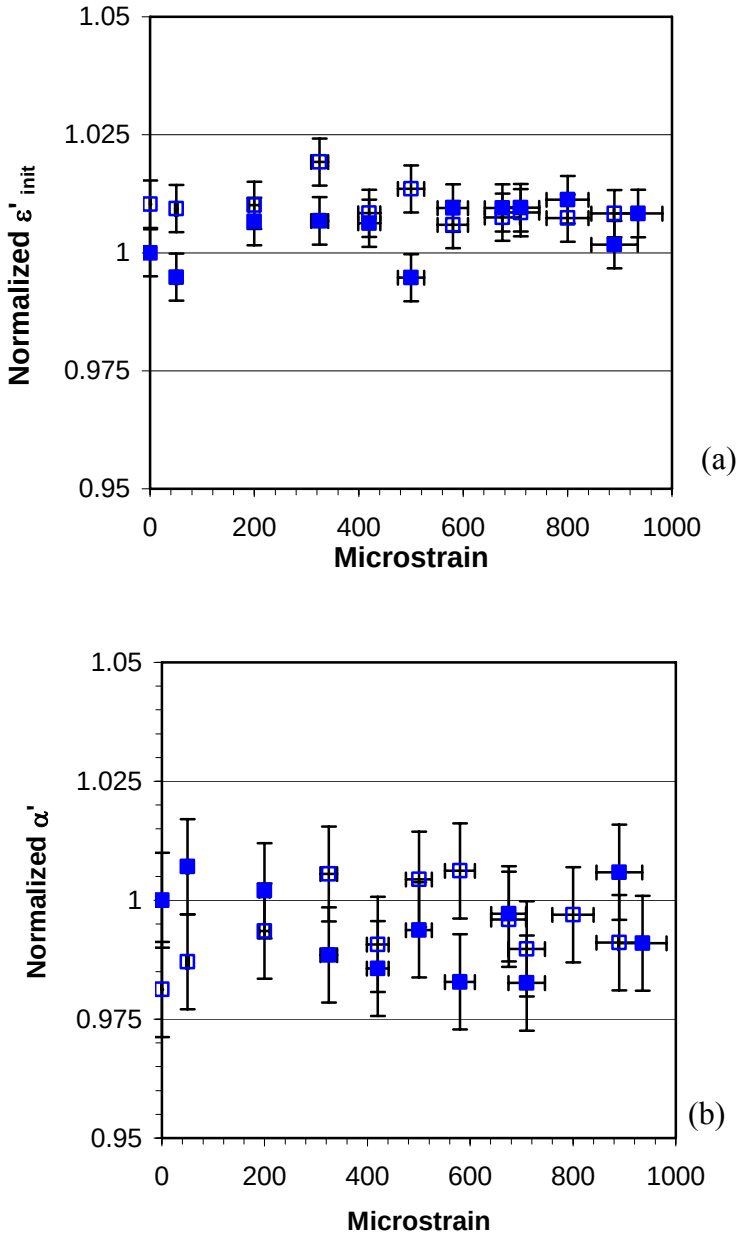

Figure **5.14**: Biaxial strain dependence of the (a) reversible and (b) irreversible Rayleigh parameters in {111} oriented PYbN-PT thin films. The outlined squares were measured on increasing pressure and the filled squares were measured on decreasing pressure. The parameters have been normalized to the values measured in the free films.

5.4 Temperature Dependence of the Dielectric Nonlinearities

The temperature dependence of the dielectric nonlinearities was also characterized. In fact, the extrinsic contributions are mainly due to domain wall motion and this process is thermally activated. It is important therefore toward the goal of quantification of extrinsic contributions to study the temperature dependence of the Rayleigh parameters. The dielectric nonlinear measurements were performed from cryogenic temperatures up to T_C .

The temperature dependent measurements were performed without poling the samples and at 1kHz. This is because both the poling and the aging behavior of the films depend on the temperature at which they are performed. Therefore the nonlinear measurements could be affected by different poling quality or aging rates at different temperatures. [156] The Rayleigh behavior of the dielectric permittivity of the *unpoled* PYbN-PT oriented thin films at around room temperature can be written as Equation 5.8:

$$\varepsilon'_{(100)} = 1212 + 19.8E_0 \text{ and } \varepsilon'_{(111)} = 874 + 16.8E_0 \qquad \textbf{5.8}$$

Therefore, the ratio of the irreversible to reversible Rayleigh parameters is (Equation 5.9):

$$\left(\frac{\alpha'}{\varepsilon'_{init}}\right)_{(100)} = 0.016\,\frac{cm}{kV} \text{ and } \left(\frac{\alpha'}{\varepsilon'_{init}}\right)_{(111)} = 0.019\,\frac{cm}{kV} \qquad \textbf{5.9}$$

Although the Rayleigh parameters are higher for the *unpoled* {100} oriented PYbN-PT thin films with respect to *unpoled* {111} oriented ones, the ratio of the

irreversible to reversible Rayleigh parameter is higher in the {111} oriented films. For the *poled* films, this ratio is higher in the {100} films with respect to the {111} oriented ones. The higher Rayleigh parameters and ratio in the *poled* {100} oriented films compared to the *poled* {111} oriented ones, and therefore the higher concentration of mobile domain walls in the former is a result of the poling process and not an inherent property of the samples due to the different grain size in the two different orientation of the films.

5.4.1 High Temperature Dielectric Nonlinearities

As can be seen in Figure 5.15 the dielectric nonlinearities also depend on the temperature at which the dielectric properties are measured. As a reminder the T_C values for these films were ~380°C. The onset for the high field region reduces with increasing temperatures, which is illustrated in Figure 5.16. This is not unexpected considering that the switching of domains or polarization reversal is facilitated at higher temperatures. [1][232] The final effect is that of decreasing the width of the Rayleigh region.

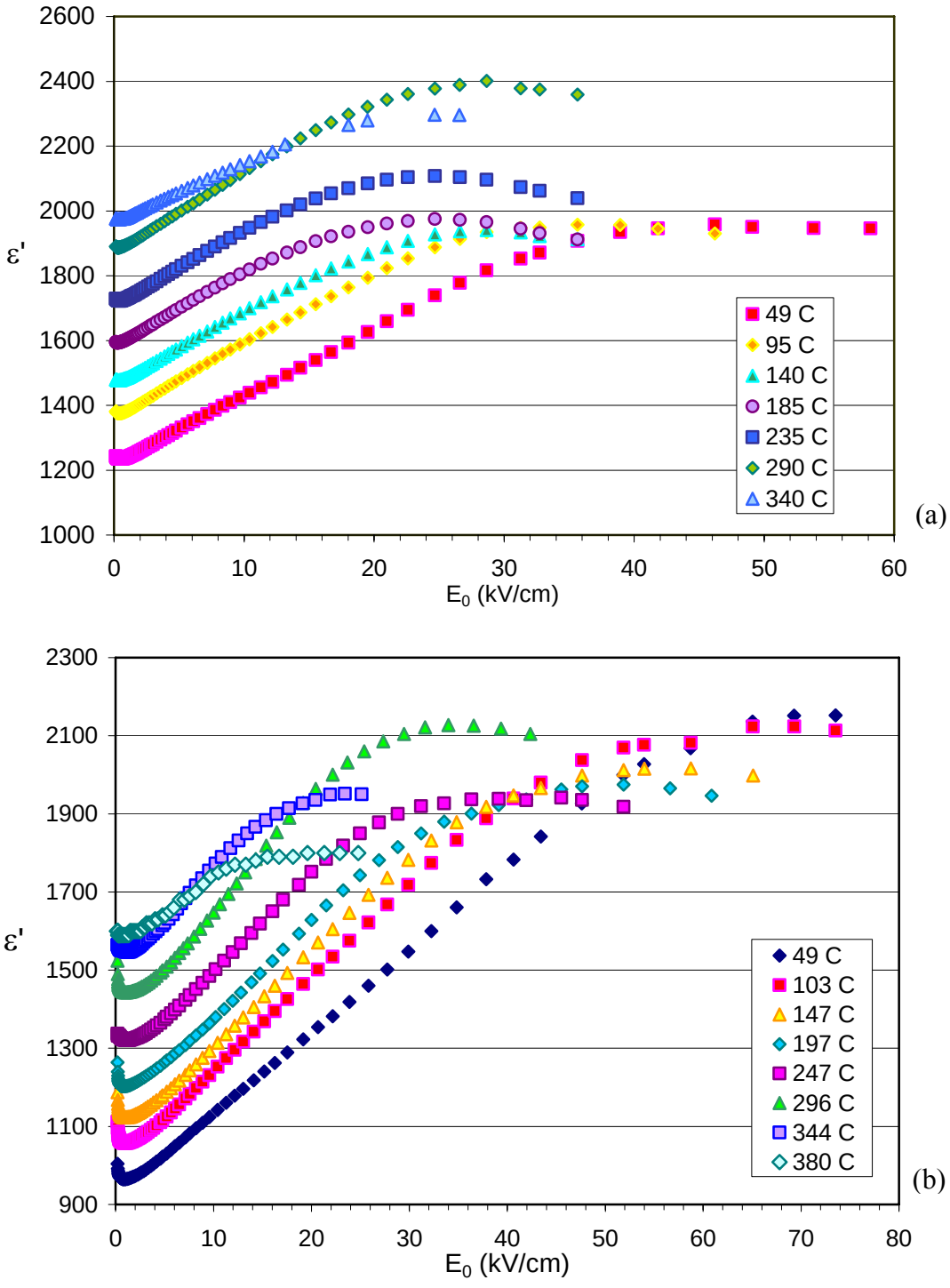

Figure **5.15**: Temperature dependence of dielectric nonlinearity in (a) {100}, and (b) {111}oriented PYbN-PT films.

The temperature dependence of the reversible and irreversible Rayleigh coefficients for the PYbN-PT films is shown in Figure 5.17. The reversible Rayleigh parameter increased almost linearly for both the {100} and {111} oriented films up to temperatures close to the Curie temperature. The irreversible Rayleigh parameter increased for both the film orientations in a similar fashion for temperatures up to ~250°C: an initial relatively rapid increase of the α' values was followed by a plateau between 100 and 250°C. At still higher temperatures, the irreversible Rayleigh parameter of the {111} oriented films increased rapidly, reaching values almost double those at room temperature, while the {100} oriented films showed a relatively small increase in α', before it decays at temperatures around 360°C.

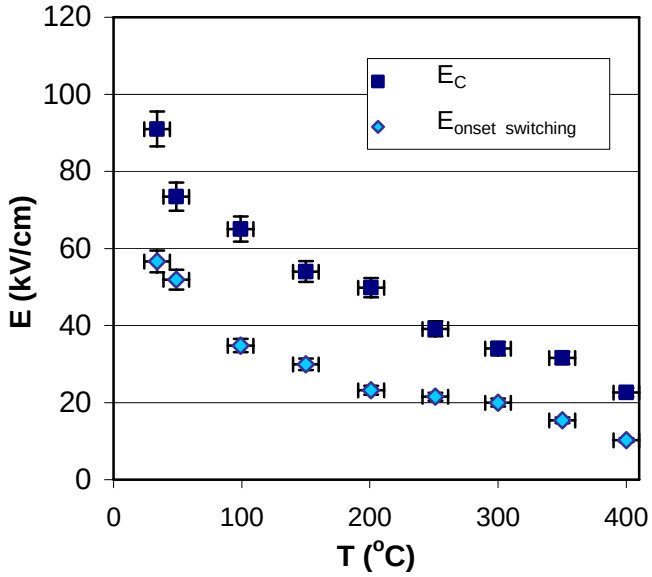

Figure 5.16: Temperature dependence of the high field region onset for a {111} oriented PYbN-PT film at 1kHz.

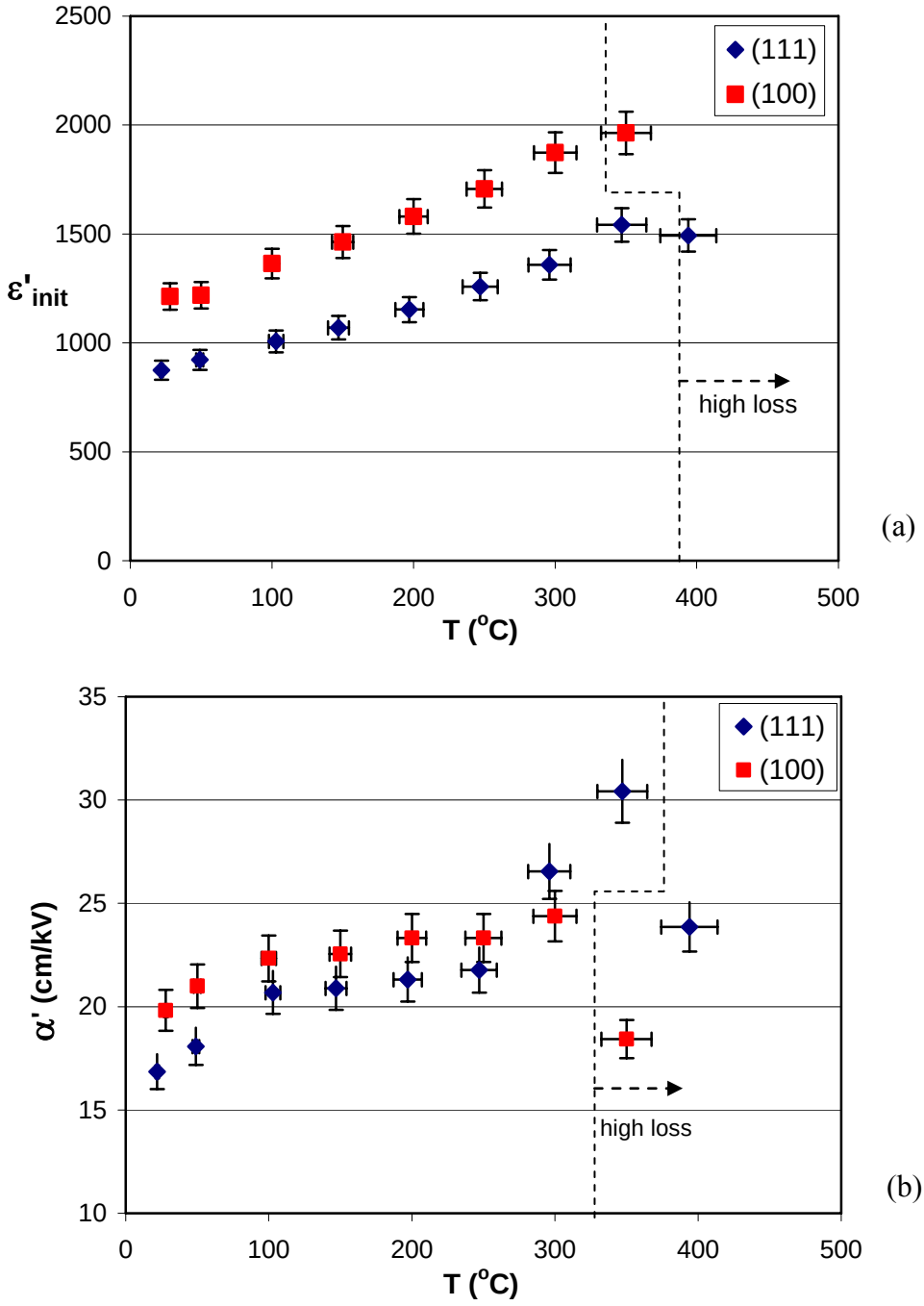

Figure **5.17**: Temperature dependence of the (a) reversible and (b) irreversible Rayleigh coefficients in {100} and {111} oriented PYbN-PT at 1kHz.

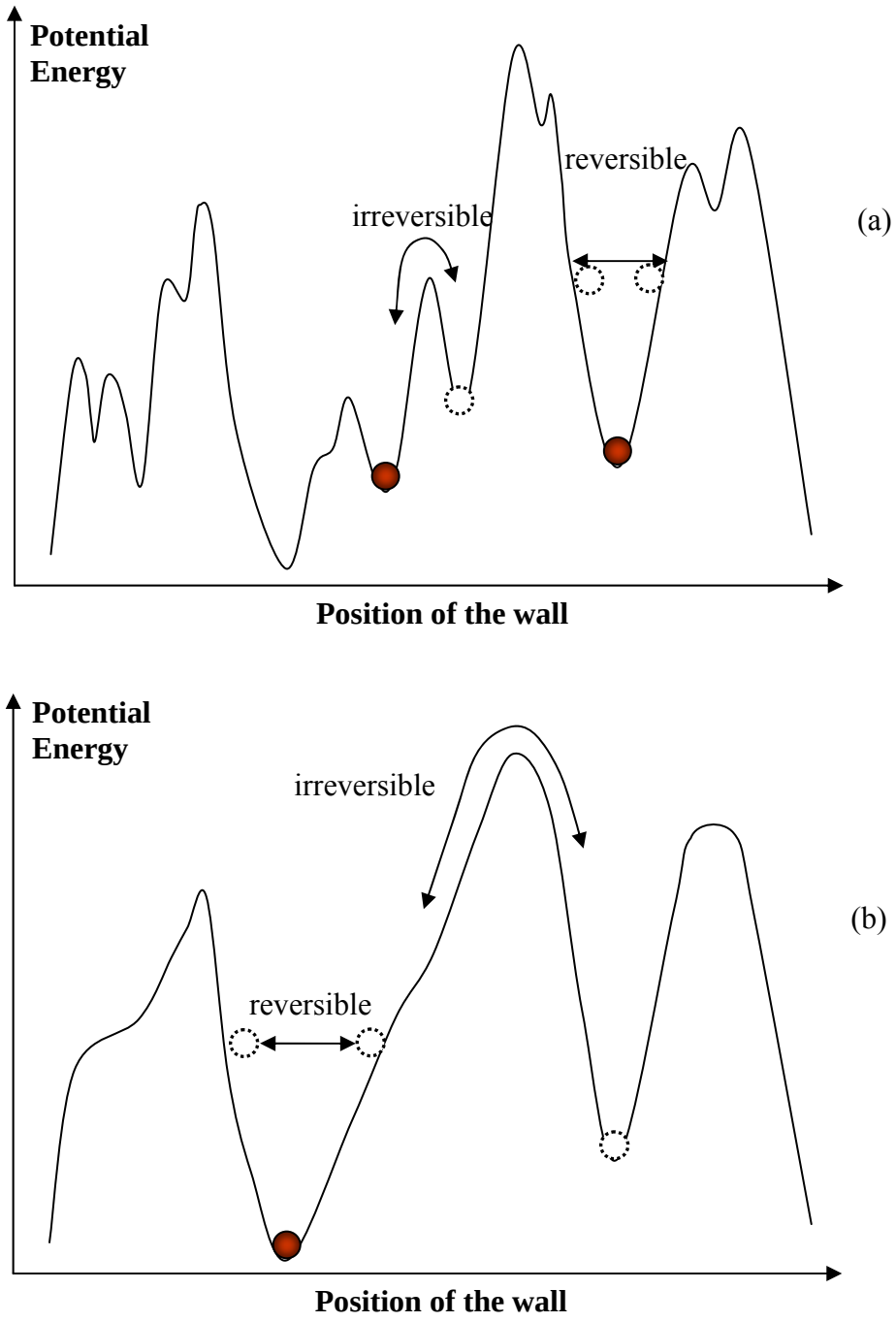

Figure **5.18**: Schematic comparison of the potential energy profile at (a) room temperature and (b) higher temperatures.

The increase in the reversible Rayleigh parameter with temperature is expected both due to the intrinsic increase in the dielectric permittivity of the material near T_C, and the increase in domain wall motion (along with all other thermally activated processes) This is illustrated schematically in Figure 5.18. At higher temperatures, the increased thermal energy makes shallow potential wells inefficient as pinning points for a domain wall. As a result the energy profile is effectively smoothened. This enables larger amplitude, more reversible, domain wall motion. The smoother energy profile should therefore result in a reduction of the irreversible to reversible Rayleigh parameter ratio. This is confirmed in Figure 5.19.

The further increase in the reversible and irreversible Rayleigh parameters of {111} oriented films at temperatures around 300-350°C is very probably due to the nearing of the phase transformation. Failure to observe an increase in the Rayleigh parameters of the {100} oriented films might be due to the much higher loss levels observed in this orientation of the PYbN-PN thin films at similar temperatures.

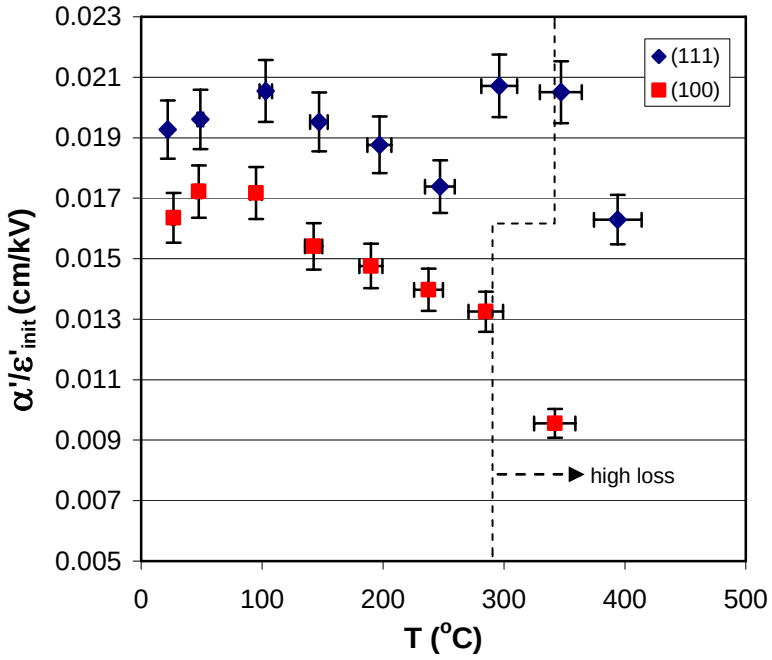

Figure **5.19**: Temperature dependence of the ratio of the irreversible to reversible Rayleigh parameters in {100} and {111} oriented PYbN-PT thin films at 1kHz.

Similarly the initial change in the slope of the irreversible Rayleigh parameter vs. temperature at around 100-110°C could be due to the crystallographic phase transformation (rhombohedral to tetragonal) of the material. This corresponds also to a relative maximum in the irreversible to reversible Rayleigh parameters ratio at approximately the same temperatures. The change in the increase rate of α' values for temperatures >100-110°C can be then interpreted as a change in either the concentration of the mobile domain walls or their mobility. It should be observed that the rhombohedral to tetragonal phase transformation temperature, $T_{R\to T}$, as observed in the Rayleigh parameters is lower by 10-50°C respect to the value observed in the dielectric

permittivity peaks characterized at low fields (see Figure **4.18**). It is reasonable to consider that the motion of the phase boundaries might become important at temperatures closer to $T_{R\to T}$, increasing the irreversible contributions to α'. Phase boundary motion could be become active at high fields, and therefore "assist" the rhombohedral to tetragonal phase transformation, resulting in a decreased $T_{R\to T}$ compared to the simple thermally assisted transformation. Similar results have been reported for 0.7PMN-0.3PT thin films: the low field transition temperature of the films was reported to be lowered by 30-40°C when measured at higher field [**233**]. The DC field dependence of the structural phase transitions has been also reported by Fesenko et al. [**234**] in lead zirconate crystals, who suggested a modification of the phase diagram as a function of field and temperature. Application of the same idea to the MPB curvature in PYbN-PT phase diagram is represented schematically in Figure **5.20**.

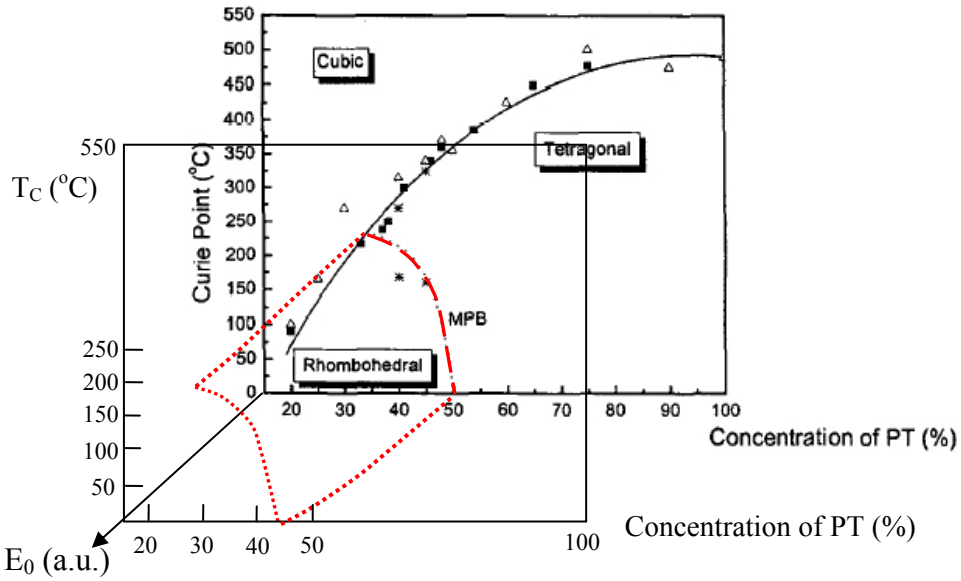

Figure **5.20**: Schematic representation of the ac field dependence of the MPB curvature in the PYbN-PT system. The change of curvature is exaggerated for clarity.

It is also expected that the extrinsic nonlinearity should disappear at temperatures higher than T_C due to the loss of domain structure in the paraelectric phase. This could not be confirmed in the PYbN-PT films due to the strong increases in the loss values of the films at temperatures higher than ~300°C (as seen in section **4.3**). At temperatures around 340°C for the {100} oriented films and ~380°C for the {111} oriented ones (see Figure **5.15**), the nonlinear curves began to flatten out, resulting in a reduction of the Rayleigh parameters. This flattening of the nonlinear curves could be due to the steep increase in the loss values of the films at higher temperatures instead of the reduction of the domain walls concentration. To check this, the temperature dependence of the dielectric nonlinearity was studied in a PMN-PT sample with lower loss values at

temperatures close to T_C. As shown in section 7.2 for the PMN-PT films, even when the loss values are kept $\leq 5\%$ over the same temperature range, the dielectric nonlinear curves flattened out at temperature higher than T_C, indicating a reduction of the extrinsic contribution to the dielectric constant due to the elimination of the ferroelectric phase.

5.4.2 Low Temperature Dielectric Nonlinearities

As can be seen in Figure 5.21, both the reversible and irreversible Rayleigh parameters decreased at decreasing temperatures. A steeper decrease was observed in the irreversible Rayleigh parameters of the {111} oriented films than the {100} oriented ones. At temperatures ~ -250°C, a sudden drop in the Rayleigh parameters of the {100} oriented films was observed, while for the {111} oriented films no sudden change in the Rayleigh values was observed, although the values seemed to stabilize at temperatures around -250°C and lower.

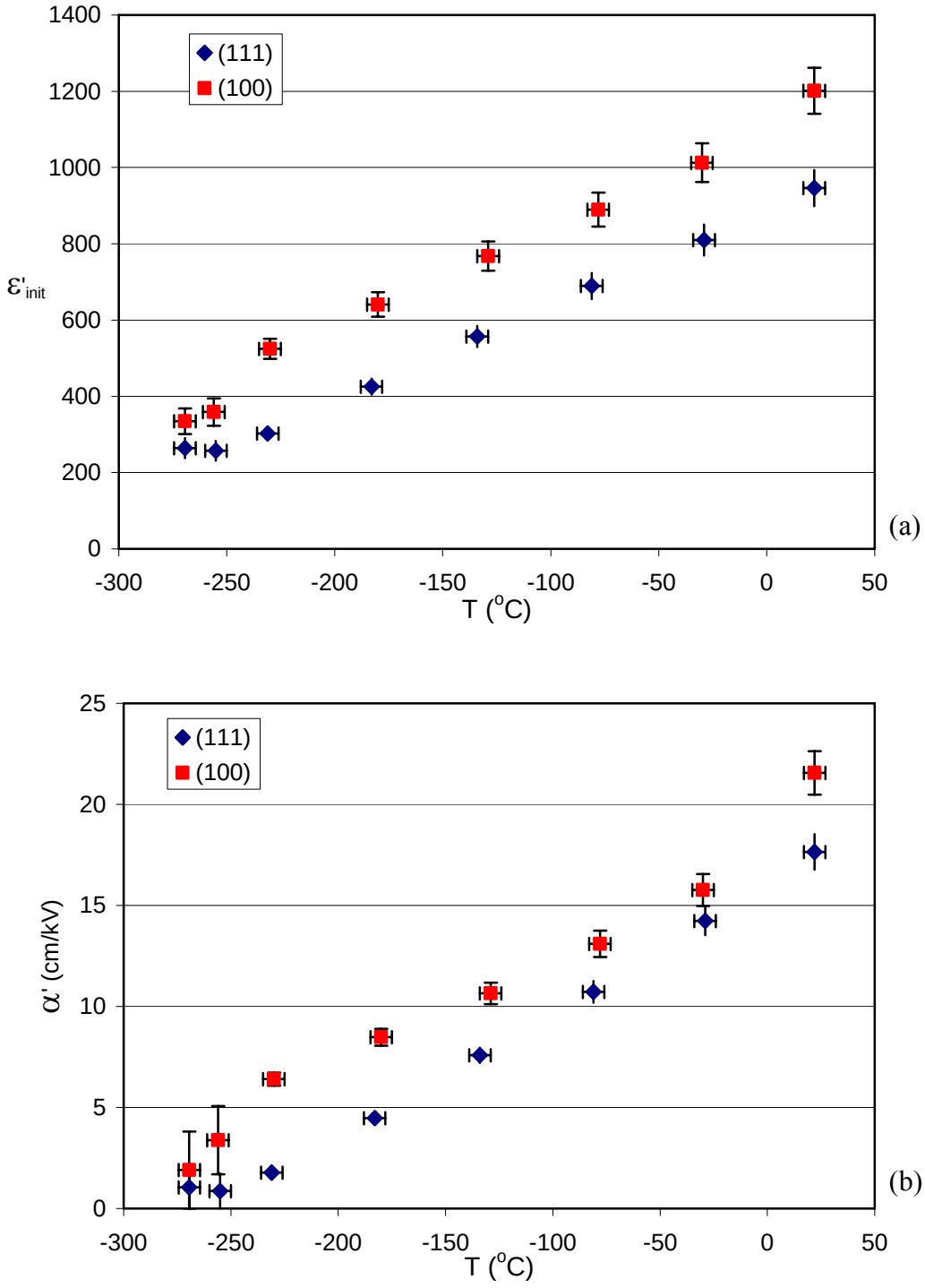

Figure **5.21**: Reversible (a) and irreversible (b) Rayleigh parameters of {100} and {111} oriented PYbN-PT thin films as a function of temperature.

The zero-field dielectric permittivity (reversible Rayleigh parameter) decreases at decreasing temperatures both due to the reduction of the intrinsic dielectric permittivity and due to the reduction of the reversible motion of the domain walls. Reports in the literature indicate that the domain walls have lower mobility with decreasing temperature. [235] The reduced mobility of the domain walls translates into a reduction of both the reversible and the irreversible Rayleigh parameters.

At temperatures ~ -240/-260°K a change in the slope of both the Rayleigh parameters curves was noticed. In the case of the {100} oriented films, a sudden drop of the Rayleigh parameters, and in the case of the {111} oriented films, a stabilization of the Rayleigh parameters could be seen. An anomalous change in the low field dielectric properties of these films at approximately the same temperatures (see Figure 5.22) suggests that the change in the Rayleigh parameters could be due not only to a change in the mobility of the domain walls, but also to an instrumental "change of range" problem. A closer analysis of the data in Figure 5.22 shows that the drop in the dielectric permittivity values at low characterization field corresponds to a different capacitance range for {111} and {100} oriented films and therefore the change in the Rayleigh parameters is more probably due to a change in the mobility of the domain walls at the very low temperatures rather than a measurement range change of the LCR-meter.

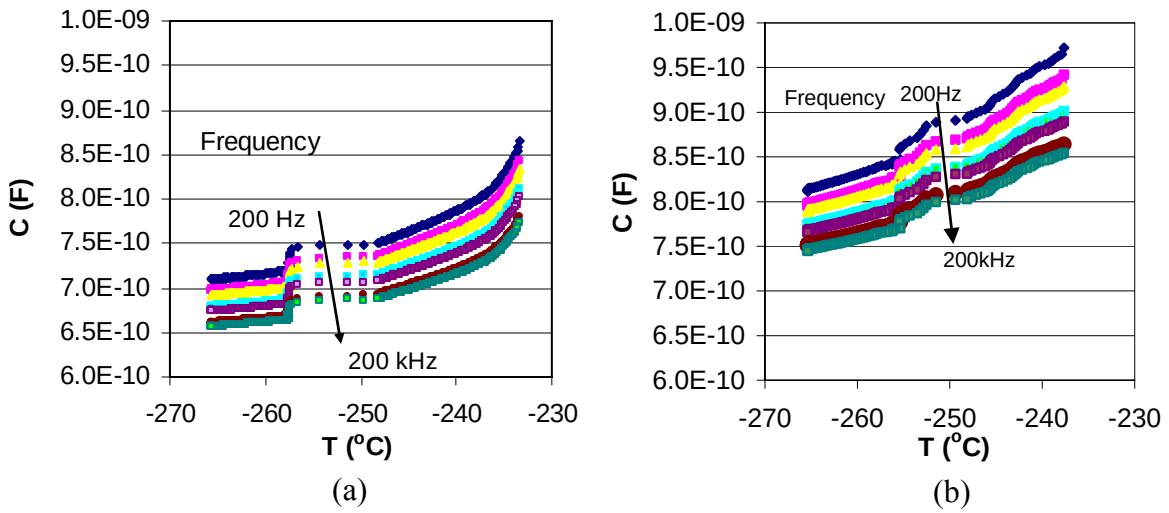

Figure 5.22: Very low temperature dependence of the dielectric constant in (a) {111} and (b) {100} oriented PYbN-PT thin films measured at $E_0<E_{th}$.

Figure 5.23 shows the decrease in the irreversible to reversible Rayleigh parameter ratio with decreasing temperatures for unpoled films. Although at higher temperatures the values were higher for the {111} oriented films, at temperatures close to ~ -140°C a cross-over in the behavior was observed. For temperatures lower than this the {100} oriented films exhibited a higher ratio of the irreversible to reversible Rayleigh parameters. It should also be noted that in both film orientations a change in the slope of the curves could be observed with decreasing temperatures. The temperature at which this discontinuity was observed, $T_{x\to R}$, was ~ -180°C for the {111} oriented thin films and ~ -250°C for the {100} oriented films. The origin of this change could be due to a change in the mobility of the domain walls.

In the low field temperature dependence of the dielectric loss for the same films (see Figures 5.23b and 5.23c), a local maximum was observed in a temperature range

slightly higher than the indicated temperatures. One possibility is that the maximum corresponds to a phase transition of the material from rhombohedral to a different phase. In other perovskite PT-solid solution ferroelectric systems, the presence of a monoclinic or orthorhombic phase close to the MPB has been reported. [**116**][**236**][**237**][**238**][**239**] [**240**] Alternatively, literature reports indicate possible intersection of octahedral tilting transition with the MPB at lower temperatures in other perovskites.[**241**][**242**]

The temperature at which the maximum in the low field loss tangent at 1kHz occurred didn't differ, within experimental error from $T_{x\to R}$ for the {111} oriented films, but it was by approximately 50-60°C higher than $T_{x\to R}$ for the {100} oriented films. The lowering of this transformation in the high field values is very similar to what observed for the $T_{R\to T}$ (section **5.4.1**). The lowering of this transition temperature in high field measurements with respect to the low field measurements observed only in the {100} oriented films might be due to the higher degree of mobility of the domain walls in the {100} orientation of the PYbN-PT films with respect to the {111} oriented ones.

The higher mobility of the domain walls at intermediate fields would allow a decrease of the free energy of the system that otherwise should be accommodated by the transition. A higher mobility of the domain walls will therefore translate into a larger decrease of the transition temperature. This is in fact the case with the {100} oriented films that showed a higher domain mobility respect to the {111} oriented films.

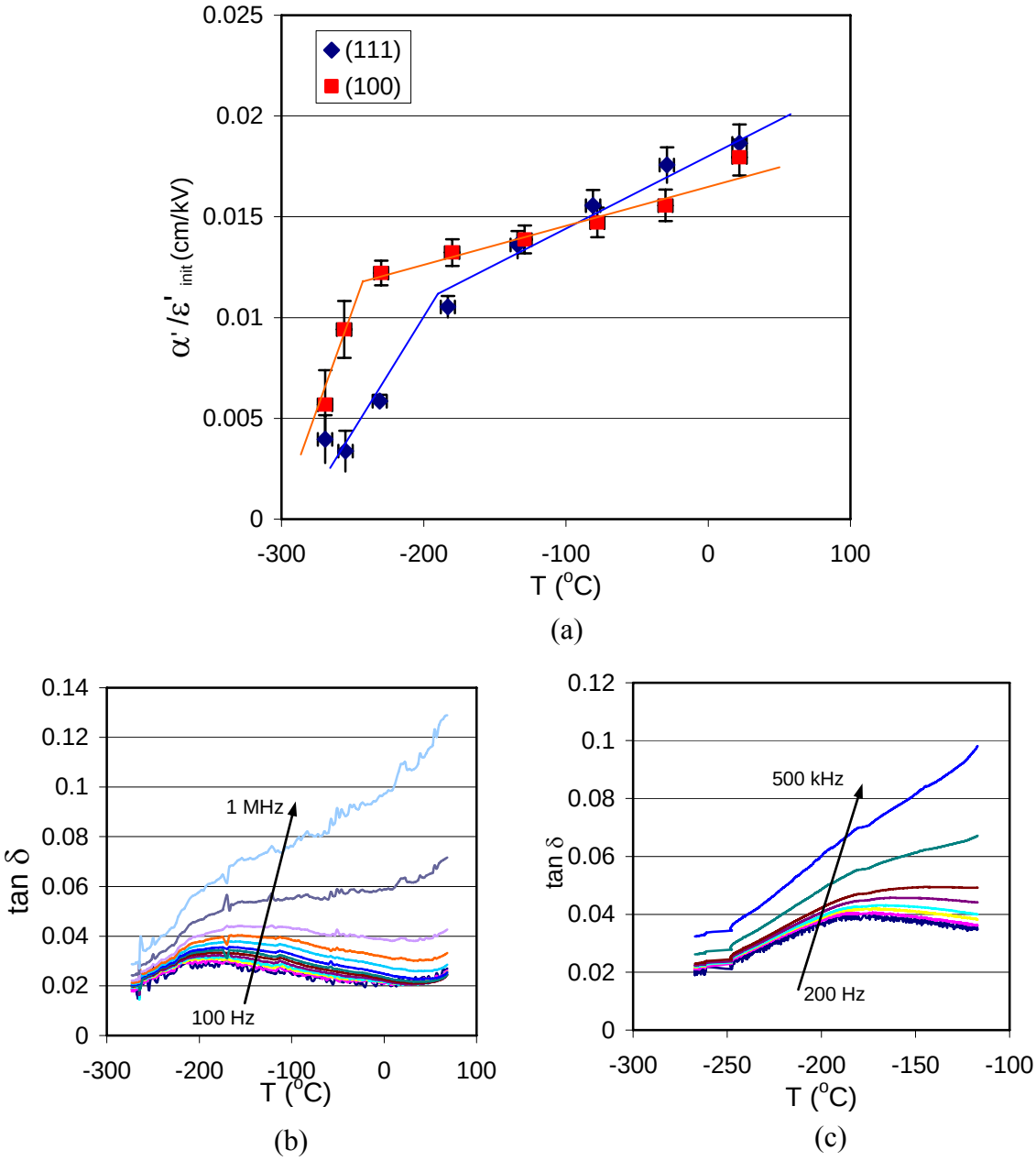

Figure **5.23**: (a) Temperature dependence of the irreversible to reversible Rayleigh parameters ratio at 1kHz and low field ($E < E_{th}$), low temperature variation of the loss tangent for the (b) {111) and (c) {100} oriented PYbN-PT thin films for different frequencies. The solid lines in (a) are guides to indicate the change of the slope in the curves

5.4.3 Overall Temperature Dependence of the Dielectric Nonlinearities

The results from the two previous sections are summarized in Figure 5.24: the temperature dependence of the Rayleigh parameters of the {111} and {100} oriented PYbN-PT films is shown from cryogenic temperatures to the Curie temperature.

It can be seen that in both the film orientations, the reversible Rayleigh parameter increased almost linearly from cryogenic temperatures to T_C. The irreversible Rayleigh parameter also increased with temperature, although for both the {111} and the {100} oriented films, at temperatures ~110°C and higher, the increase of α' with temperature was much slower. The ratio of irreversible to reversible Rayleigh parameters could be inferred to be close to zero cm/kV at temperatures close to zero degree Kelvin. At increasing temperatures up to ~110°C, this ratio increased, probably due to a higher number of thermally depinned domain walls. At still higher temperatures, the Rayleigh ratio decreased. This could be due to a different concentration of the mobile domain walls or a higher reversibility of the motion of the domain walls with respect to the lower temperatures.

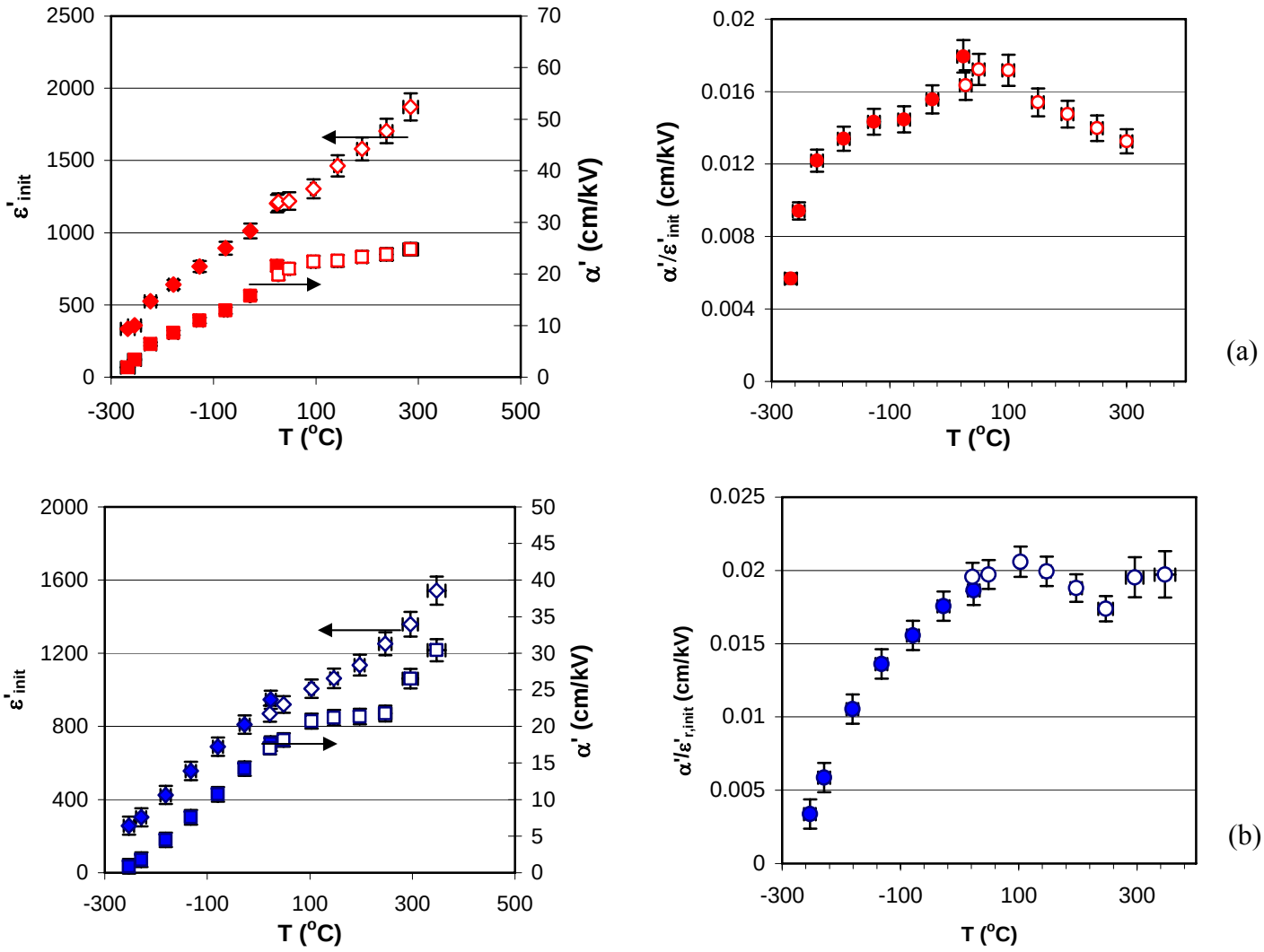

Figure **5.24**: Temperature dependence of the Rayleigh parameters in (a) {100} and (b) {100} oriented PYbN-PT films at 1kHz. Note that the data possibly contaminated by very high loss ($\geq 15\%$) were removed.

It should be noted here that aging a ferroelectric at different temperatures should also influence the temperature dependence of its Rayleigh parameters. In fact aging at a different temperature can possibly influence the domain structure of the material. This was tentatively confirmed for a {111} oriented PYbN-PT thin film, aged for an hour at ~250°C. The Rayeligh parameters of the film were measured on cooling to room temperature at intervals of ~50°C (see Figure **5.25** and **5.26**).

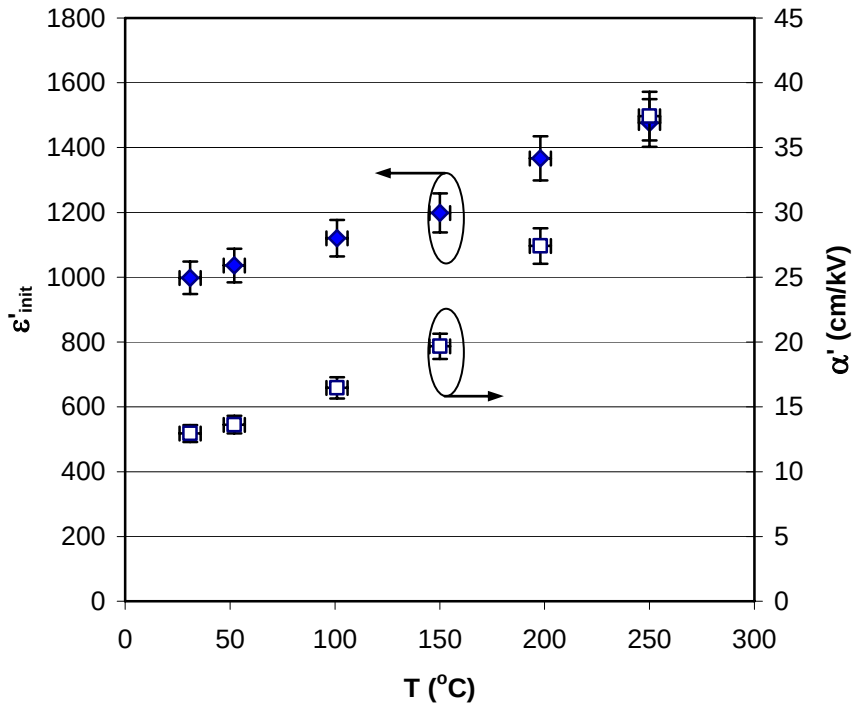

Figure **5.25**: Temperature dependence of Rayleigh parameters for a {111} oriented PYbN-PT film on cooling. The film has been allowed to age at ~250°C for an hour before the measurements.

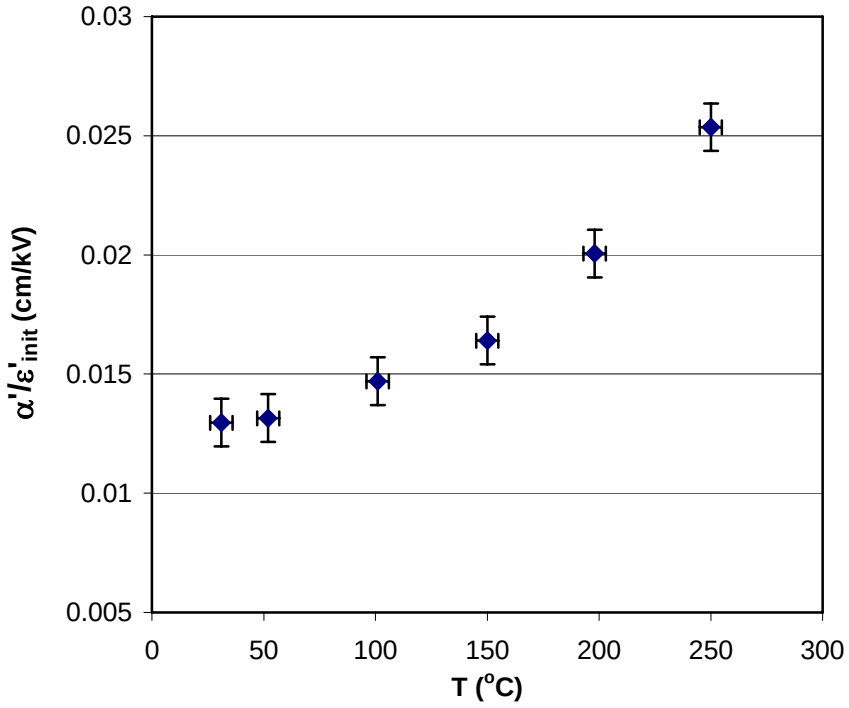

Figure **5.26**: Temperature dependence of the irreversible to reversible Rayleigh parameters ratio for a {111} oriented PYbN-PT film on cooling. The film has been allowed to age at ~250°C for an hour before the measurements.

Intriguingly, in the sample aged at ~250°C and measured on cooling the Rayleigh parameters and their ratio increase continuously with temperature. A change in the slope of both curves was observed at ~100°C that possibly corresponds to the rhombohedral to tetragonal phase transformation, similarly to what observed for the temperature dependence of the Rayleigh parameters ratio on heating from room temperature.

5.5 Conclusions

The Rayleigh relations have been applied to study the nonlinear dielectric response of PYbN-PT thin films on the rhombohedral side of the MPB with {111} and {100} preferential orientation. The *unpoled* PYbN-PT thin films showed higher irreversible to reversible Rayleigh parameters ratios in {111} oriented films with respect to the {100} oriented ones at room temperatures (and higher temperatures). It was also found that the *poled* {100} oriented films have a higher irreversible contribution to their dielectric properties than the *poled* {111} oriented films. The results suggest a higher mobility and/or a higher concentration of the mobile interfaces (domain walls, phase boundaries) in the *poled* films with {100} preferential orientation than in the {111} oriented films. This difference could be due to the effect of poling along a non-polar axis of the material, which in single crystals has been reported to yield a higher concentration of domain walls. Additionally, the effects of different microstructures of the two orientations of the films may contribute to differences in the dielectric nonlinear behavior of the films. The smaller grain size of the {111} oriented PYbN-PT films could be accompanied by a smaller domain size and lower mobility of the domain walls due to the stiffer elastic force constant for vibrating domain walls in thinner domains.

A modified Rayleigh Law has been proposed for the frequency and field dependence of the dielectric nonlinearities. The modification of the Rayleigh Law is based on the logarithmic dependence of the Rayleigh parameters on frequency. The proposed relations show a good prediction of the dielectric constant of the PYbN-PT thin

films for fields up to half the coercive field and frequencies over three orders of magnitude (20 Hz to 50 kHz).

The study of the dielectric nonlinearities under applied bias showed higher extrinsic contributions under negative bias with respect to positive applied bias. This was attributed to the destabilization of the poled domain structure under an opposing bias field.

The dielectric Rayleigh parameters showed small variation under applied biaxial tensile strains. This suggested reduced/negligible contribution of non-180° domain wall and phase boundary motion to the dielectric nonlinearity in {111} and {100} oriented PYbN-PT thin films.

A crossover in the temperature dependence of the Rayleigh parameters ratios for the two orientations of the films was observed at lower temperatures (~-140°C) in the unpoled films. The fact that at lower temperatures, where the mobility of the domain walls is reduced, the {100} oriented films showed larger extrinsic contribution to the dielectric permittivity might be attributed to the different grain size of the films. It is also worth noting that at ~5°K, where the domain wall contribution should be frozen, the ratio of the irreversible to reversible Rayleigh parameters for both of the PYbN-PT thin films' orientations is similar within experimental error.

The temperature dependence of dielectric nonlinearity showed a steady, almost linear, increase of the reversible Rayleigh parameters with temperature (from ~-268°C to ~350°C), while the irreversible Rayleigh parameters increased from low temperature, reaching a relative maximum at temperatures ~310°C. The change of ratio of the

irreversible to reversible Rayleigh parameters with temperature seemed to mimic the phase transition of the material as measured by the dielectric permittivity and loss at low field. It was found that the high field characterization reduced the transition temperature with respect to the low field characterization. The reason for the difference in transition temperatures, as found from low and high field dielectric characterizations, was attributed to field assisted transitions, leading therefore to the stabilization of the higher temperature phase to lower temperatures.

A possible phase transition was also observed at ~-190°C in both the {111} and {100} oriented films as seen in a (frequency dispersive) local maxima in the dielectric loss with temperature. The origin of the peak in the loss values could be attributed to either a crystallographic phase transition from rhombohedral to monoclinic or orthorhombic phase or a low temperature rhombohedral phase with tilting of the oxygen octahedral. Further studies are required to clarify the origin of the phenomena.

Chapter 6

Piezoelectric Nonlinearity

This chapter discusses the piezoelectric nonlinearities of the {111} and {100} oriented 0.5PYbN-0.5PT films. A brief introduction on the stability of the piezoelectric response is given before discussion in terms of the Rayleigh analysis of the ac amplitude field dependence of the effective piezoelectric coefficient $d_{33,f}$. The frequency dependence of the piezoelectric nonlinearity is then presented.

The piezoelectric and dielectric nonlinearity in the {100} oriented films are compared and the differences are explained in terms of a phenomenological "dynamic poling" mechanism. The higher harmonic response of the dielectric displacement and strain are reported as a function of the ac field amplitude. It is concluded that there are circumstances under which 180° domain wall motion can contribute to the piezoelectric response.

6.1 Piezoelectric Response and Signal Stability

The $e_{31,f}$ values of the PYbN-PT were reported in section **4.4**. This chapter will analyze the piezoelectric response of the films as measured by PFM and double beam interferometer. Figure **6.1** shows the piezo-response of an unpoled {100} oriented PYbN-PT film at different AC signal levels. Measurements were made using a ~6kHz oscillating signal over a slowly swept dc bias. The curves showed a pronounced asymmetry in their shape that can be due to the internal fields present in the films. The piezoelectric hysteresis became better defined with increasing the AC electrical field amplitude. The asymmetry of the curves was reduced, probably due to the randomization of the internal fields due to the repeated cycling through the hysteresis loop. The increase in the $d_{33,f}$ coefficients with the magnitude of the ac signal level suggests that the PYbN-PT thin films show a nonlinear piezoelectric behavior.

Figure **6.1**b reports the effects of poling the sample of Figure **6.1**a at ~80kV/cm for 30 minutes. After poling, the amplitude of the piezoelectric response increases only at near zero field values, while it decreases at higher fields. The saturated values of d_{33} are ~14% smaller in the poled sample with respect to the unpoled sample. This might indicate a reduction of the extrinsic contributions to the piezoelectric response after poling.

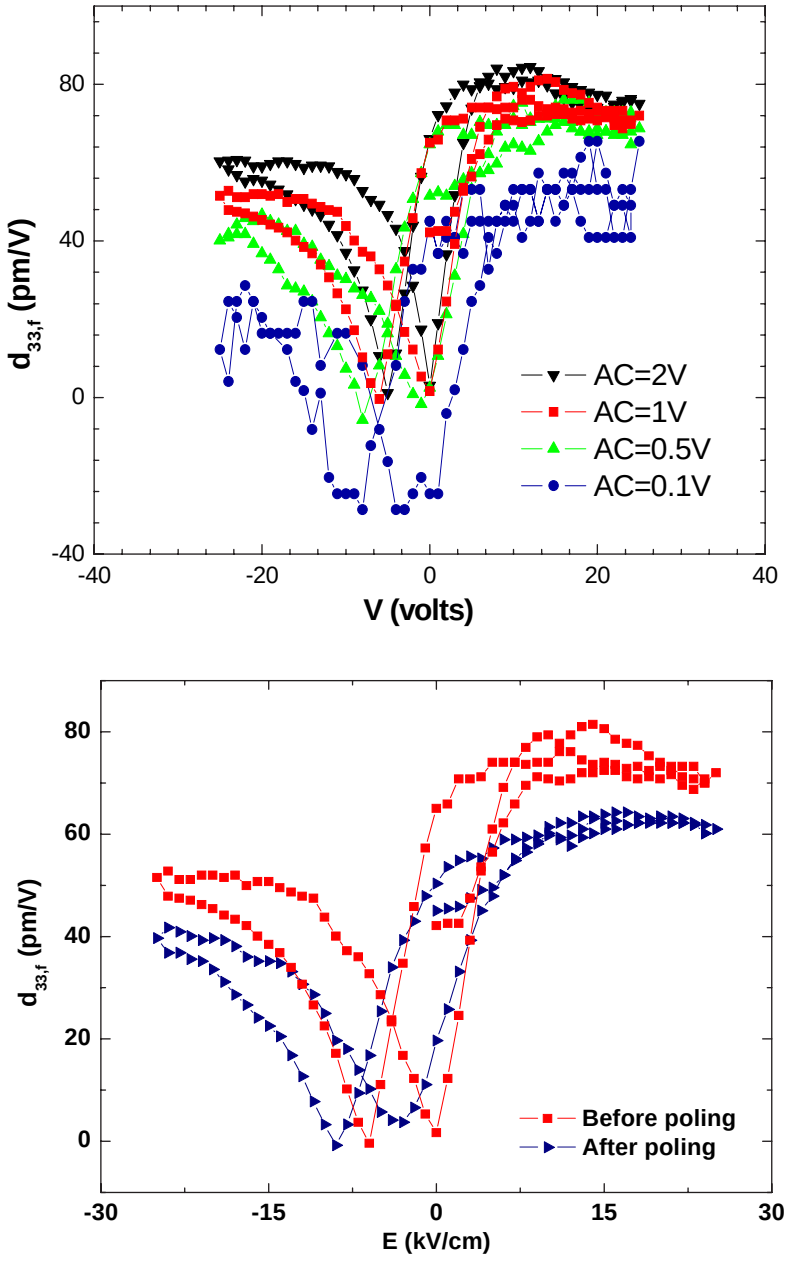

Figure **6.1**: Piezoelectric response of (a) an unpoled, {100} oriented PYbN-PT films as measured by PFM with different AC signal amplitudes. (b) Comparison of unpoled and poled (at ~80kV/cm for 30 minutes) piezoelectric response of the same sample as in (a). The Ac signal used in (b) was 1V for both the poled and unpoled sample. The PYbN-PT films were approximately 0.6 μm thick. Measurements courtesy of Jun Ouyang, University of Maryland.

The double beam interferometer measurements confirmed that the piezoelectric response of the PYbN-PT films was unstable (that is, very rapid aging was observed) even after poling for long times (~30 minutes), although under the same conditions, the dielectric response was very stable. This is shown schematically in Figure **6.2** for a poled {111} oriented PYbN-PT film. The measurements were performed starting at zero bias and then the bias level was increased in the following measurements.

With no applied bias, the dielectric response followed a Rayleigh-like behavior with the capacitance linearly increasing with increasing ac fields. The piezoelectric response under the same conditions increases slightly but doesn't show a well-defined linear regime. This would suggest that the domain structure is not particularly stable, so that modest ac fields changed the domain configuration. Indeed, sometimes when the zero field response was measured after a measurement under bias, the measured $d_{33,f}$ actually *decreased* with increasing ac field amplitude due to rapid aging. To avoid complications associated with aging, most interferometry measurements were made under dc bias. Application of a positive bias field during the measurements increased the piezoelectric response of the sample, inducing a Rayleigh-like behavior with linear increase of d_{33} with the field amplitude. Under applied bias, similarly to what reported in section Figure **5.8**, the dielectric response was reduced, although it maintained the linear increase with the field amplitude.

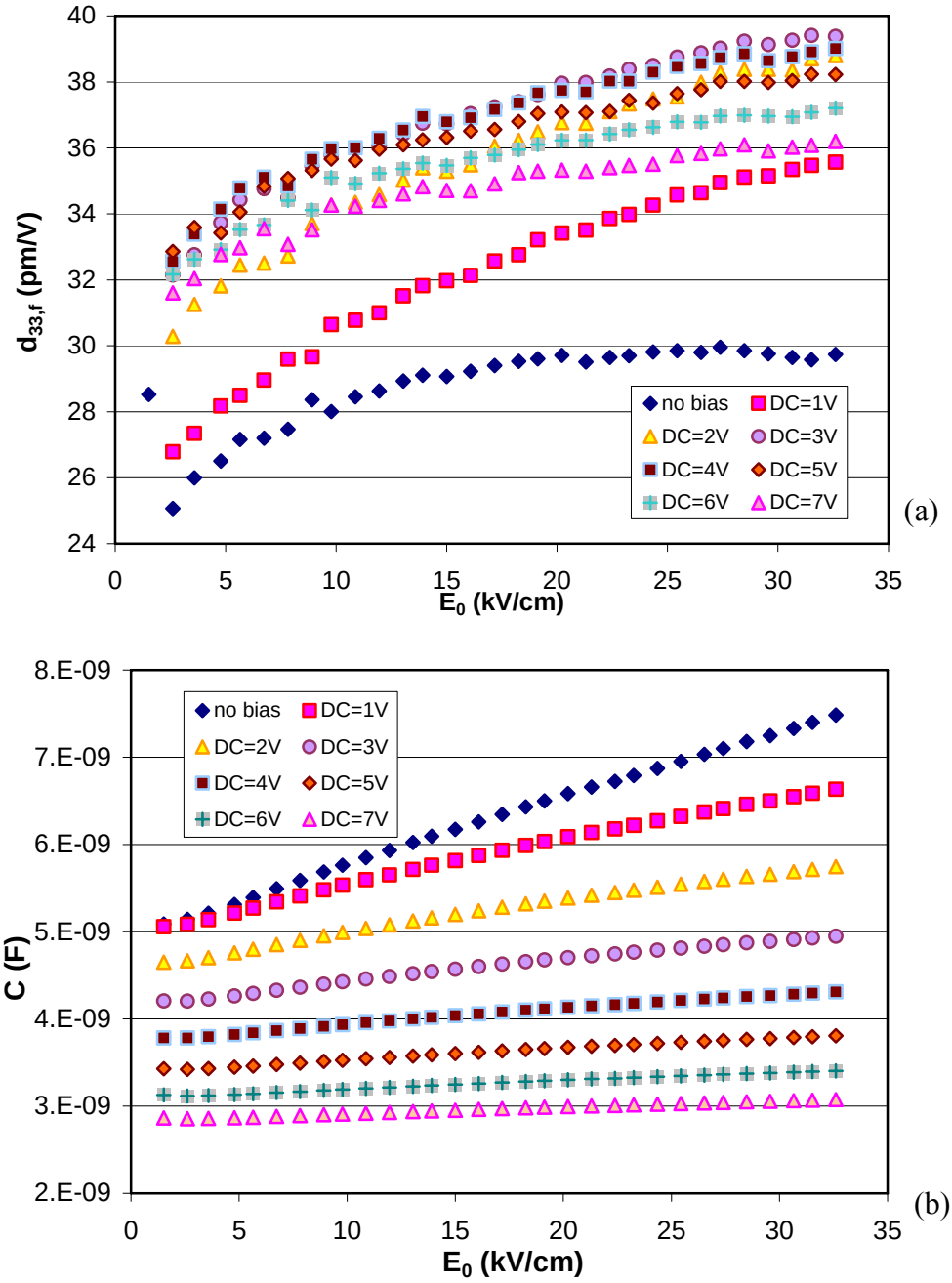

Figure **6.2**: Comparison of the (a) piezoelectric and (b) dielectric response of a poled {111} PYbN-PT sample with different levels of applied bias measured at 1kHz. The films were 0.46µm thick.

The improvement in the piezoelectric properties of the films increased with applied bias up to 4V (≈ 65 kV/cm). Higher DC bias values reduced the nonlinear behavior of the films (lower α') and the piezoelectric response ($d_{33,f}$) as would be expected since the dc bias decreases the polarizability.[1] In order to stabilize the domain configuration of the films, the piezoelectric measurements in this chapter, unless otherwise specified, were performed under an applied bias of ~4V. Higher biases also led to problems with resistance degradation after hours at field.

As mentioned in section 3.9.1, not all the frequencies in the instrumental range of the double beam interferometer (20Hz to 20kHz) gave reliable results for the piezoelectric analysis. A frequency sweep of the piezoelectric response is shown for reference in Figure 6.3. The frequencies corresponding to various resonances of the sample, or the fixturing were avoided, as well as higher frequencies at which the phase angle deviated more than ~10° from zero. Many of the piezoelectric measurements were made at 5kHz, considering the closeness of a couple of the smaller resonance peaks.

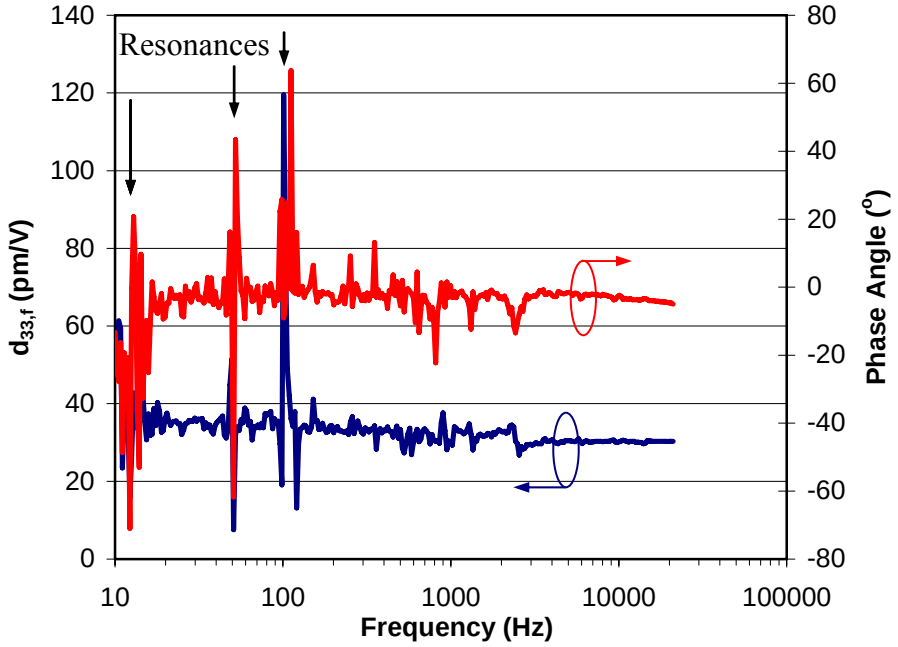

Figure **6.3**: Frequency scan of the piezoelectric coefficient and the phase angle of a {100} oriented PYbN-PT sample measured at zero bias and at low ac field. Some resonances are marked.

6.2 Orientation Dependence of the Piezoelectric Nonlinearity

The AC field dependence of $d_{33,f}$ of {100} and {111} oriented PYbN-PT films is shown in Figure **6.4**. Both film orientations exhibited an initial region where the piezoelectric coefficient was nearly independent of the probing field amplitude, followed by a Rayleigh region, where d_{33} increased almost linearly with the applied field.

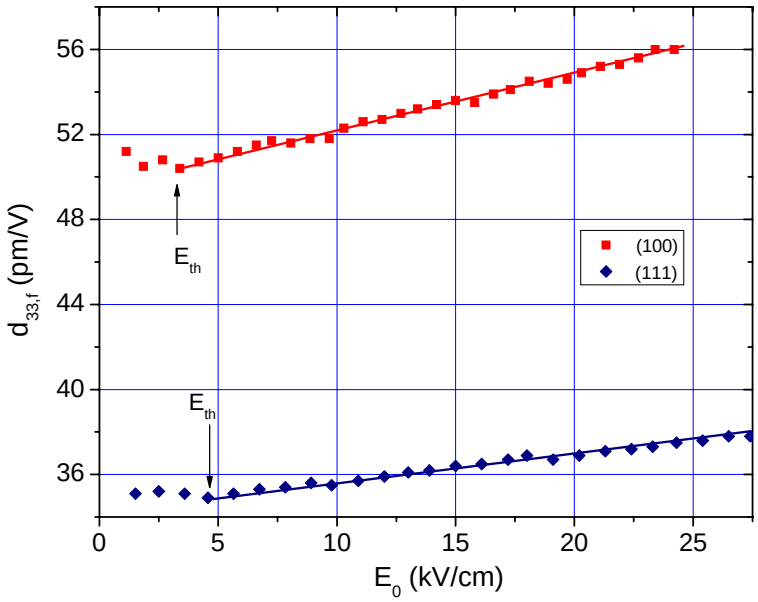

Figure **6.4**: AC field amplitude dependence of the effective piezoelectric coefficient for {111} and {100} oriented PYbN-PT thin films at 5kHz, under ~6.5 kV/cm bias field. The threshold field E_{th} for onset of piezoelectric nonlinearity is indicted by arrows for each orientation. The solid lines are used for eye guides to show the Rayleigh region.

The piezoelectric response of the films, even under these "optimized" conditions was still quite modest. The modest values for the piezoelectric coefficients are probably a function both of clamping by the substrate and of measuring under dc bias. [**168**][**243**][**244**] As for the orientation dependence, similar to the dielectric results, the threshold field for the onset of the piezoelectric nonlinearity was slightly smaller for the {100} oriented films than for the {111} oriented PYbN-PT films, suggesting a higher mobility of the interfaces in the formers. At 5 kHz and ~65 kV/cm bias field, the Rayleigh fitting of the curves yield:

$$d_{33,f(100)}\left(\frac{pm}{V}\right) = 49.6 + 0.26E_0 \text{ and } d_{33,f(111)}\left(\frac{pm}{V}\right) = 34.5 + 0.12E_0 \quad \textbf{6.1}$$

$$\left(\frac{\alpha'}{d_{33,init}}\right)_{(100)} = 0.0053\,\frac{cm}{kV} \text{ and } \left(\frac{\alpha'}{d_{33,init}}\right)_{(111)} = 0.0036\,\frac{cm}{kV} \quad \textbf{6.2}$$

Note that throughout this section, the piezoelectric coefficients are expressed in $\left(\frac{pm}{V}\right)$ and fields in $\left(\frac{kV}{cm}\right)$.

A comparison of the Rayleigh parameters and their ratios, yielded similar results to the dielectric nonlinearities: the {100} oriented PYbN-PT films had higher reversible and irreversible Rayleigh parameters and higher ratio of the irreversible to reversible Rayleigh parameters than {111} films. Therefore, there is a higher concentration of mobile interfaces that contribute to the piezoelectric properties of the {100} oriented PYbN-PT films with respect to the {111} oriented ones. This is surprising and quite counter-intuitive in view of the fact that for {001} rhombohedral perovskites, the four ferroelastic domain states are ideally energetically equivalent with respect to the field applied along [001] pseudo-cubic axis, so that there should be no driving force for wall motion due to applied electric fields.[245] In fact, while non-180˚ domain walls are both ferroelastically and ferroelectrically active, 180˚ domain walls are only ferroelectrically active. Thus, while both types of domain walls contribute to the dielectric response, 180° domain walls can typically be discounted as a contributor to the piezoelectric response at low fields. [2][3][15][99][246] Based on these theoretical considerations and the crystallographic orientations of the films, the {111} oriented films (with ferroelastically

non-equivalent domain states) should show higher extrinsic contributions and therefore nonlinear piezoelectric response. But as mentioned earlier, ferroelastic domain wall motion is very reduced in thin films. In section **6.3** a different origin for the observed piezoelectric nonlinearity in the thin films will be proposed.

The piezoelectric nonlinearity was observed to be frequency dependent[17]. The frequency dependence of the reversible and irreversible Rayleigh parameters is reported in Figure **6.5**. It can be seen that the Rayleigh parameters followed an approximately logarithmic decrease with frequency (as in Equation **6.3**), where C is either the reversible or irreversible piezoelectric Rayleigh parameter, ω is the radial frequency and c_0 and c are the two fitting parameters. The values of these fitting parameters are reported in Table **6-1**.

$$C = c_0 + c\ln\left(\frac{1}{\omega}\right) \qquad \textbf{6.3}$$

Although the data points with phase angle differing from ~180° have been removed for this analysis, some noise in the measured piezoelectric response could be still observed. This resulted in difficulties in comparison of the frequency dependence coefficients of the piezoelectric Rayleigh parameters for the two orientations of the films. For comparison, the logarithmic dependence of the dielectric Rayleigh parameters in a

[17] Note that the frequency dependence of the piezoelectric nonlinearity indicates an extrinsic origin of the phenomenon. Electrostriction, for example, could explain in part the field dependence of the piezoelectric response, but it can't explain the frequency dependence of this response. The electrostrictive effect is in fact an intrinsic response of the material. A detailed discussion of the extrinsic contribution to the piezoelectric nonlinearity in the PYbN-PT films is presented in section 6.3.

{100} oriented PYbN-PT film, poled and measured under the same conditions as films in Figure 6.5 are shown in Figure 6.6.

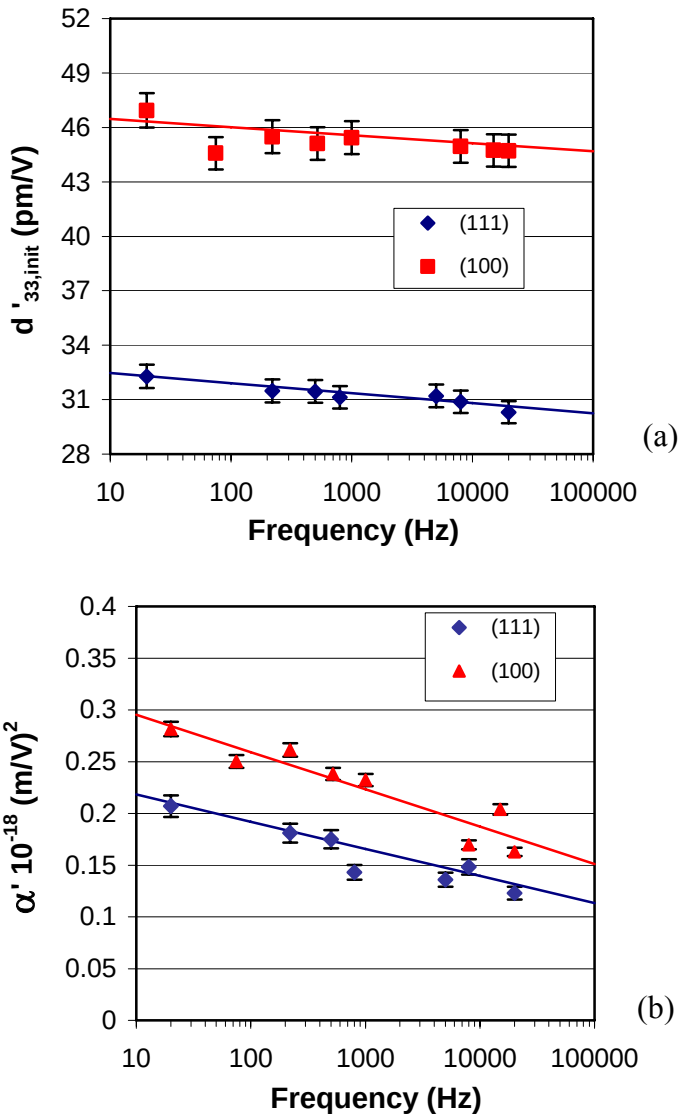

Figure 6.5: Frequency dependence of the (a) reversible and (b) irreversible piezoelectric Rayleigh parameters in {100} and {111} oriented PYbN-PT thin films, poled at twice the coercive field for 30 minutes, and measured under ~50kV/cm bias. The solid points represent the experimental data, while the lines represent the fitting curves based on Equation 6.3. The ac field range used for the Rayleigh analysis was approximately between 5 and 25 kV/cm.

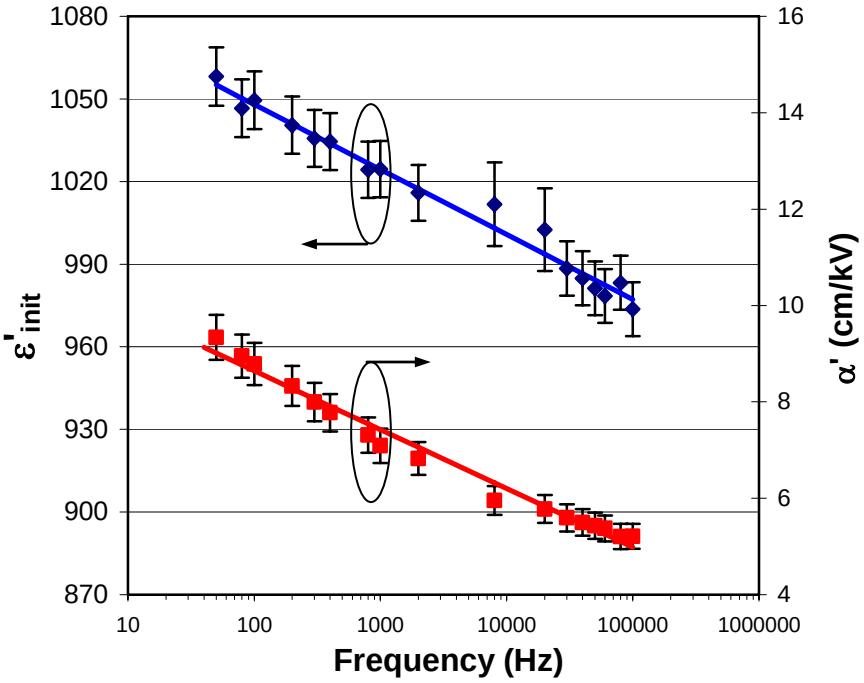

Figure **6.6**: Frequency dependence of the reversible and irreversible dielectric Rayleigh parameters in {100} oriented PYbN-PT thin films, poled at twice the coercive field for 30 minutes, and measured under ~50kV/cm bias. The solid points represent the experimental data, while the lines represent the fitting curves based on Equation **6.3**.

Table 6-1: Frequency dependence of the piezoelectric Rayleigh parameters for films poled at twice their coercive field for 30 minutes and measured under ~50kV/cm bias.

		c_0	c
$d'_{33,init}\left(\frac{pm}{V}\right)$	(111)	$33.4 \pm 0.3\left(\frac{pm}{V}\right)$	$-0.24 \pm 0.04\left(\frac{pm \cdot rad}{V}\right)$
	(100)	$46.9 \pm 0.8\left(\frac{pm}{V}\right)$	$-0.19 \pm 0.09\left(\frac{pm \cdot rad}{V}\right)$
$\alpha'\left(10^{-9}\frac{m}{V}\right)^2$	(111)	$0.24 \pm 0.18\left(10^{-9}\frac{m}{V}\right)^2$	$-0.12 \pm 0.02\left(10^{-9}\frac{m}{V}\right)^2 \cdot (rad)$
	(100)	$0.36 \pm 0.22\left(10^{-9}\frac{m}{V}\right)^2$	$-0.15 \pm 0.04\left(10^{-9}\frac{m}{V}\right)^2 \cdot (rad)$

Both of the Rayleigh parameters were higher in {100} oriented films than in {111} films in the studied frequency range. The static field value c_0 was higher for both the Rayleigh parameters in {100} oriented films respect to the {111} oriented PYbN-PT films. The values of the frequency coefficient for both of the orientations of the films were within experimental error of each other (both for the reversible and the irreversible Rayleigh parameters).

The reversible and irreversible Rayleigh parameters were then used to predict the hysteretic behavior of strain against applied field. The results are presented in Figure 6.7 and show a poor fit of the curves derived from the Rayleigh parameters to the experimental curves. This is almost certainly due, at least in part, to shifts in the phase angle caused by the approach to a resonance in the interferometer/sample system. The phase angle is generally much more sensitive an indication of the onset of a mechanical resonance than is the amplitude.

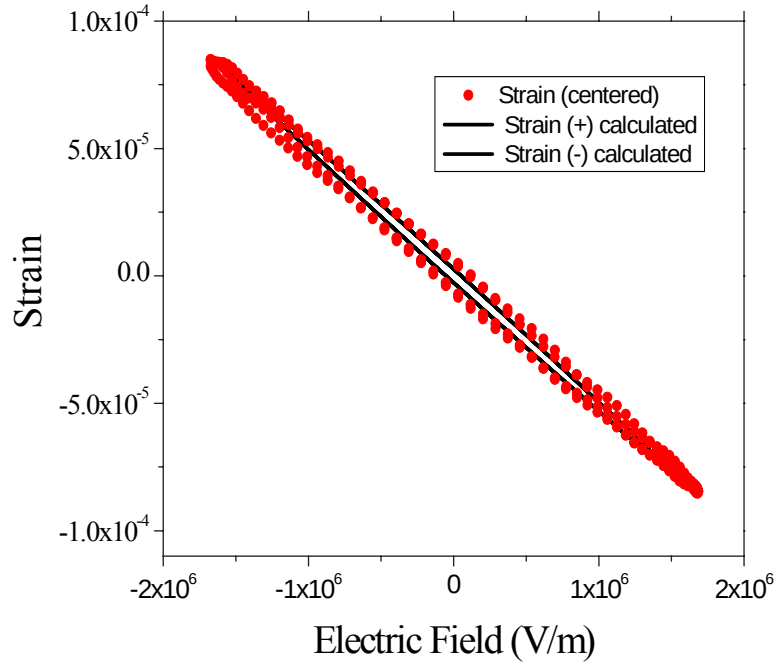

(a)

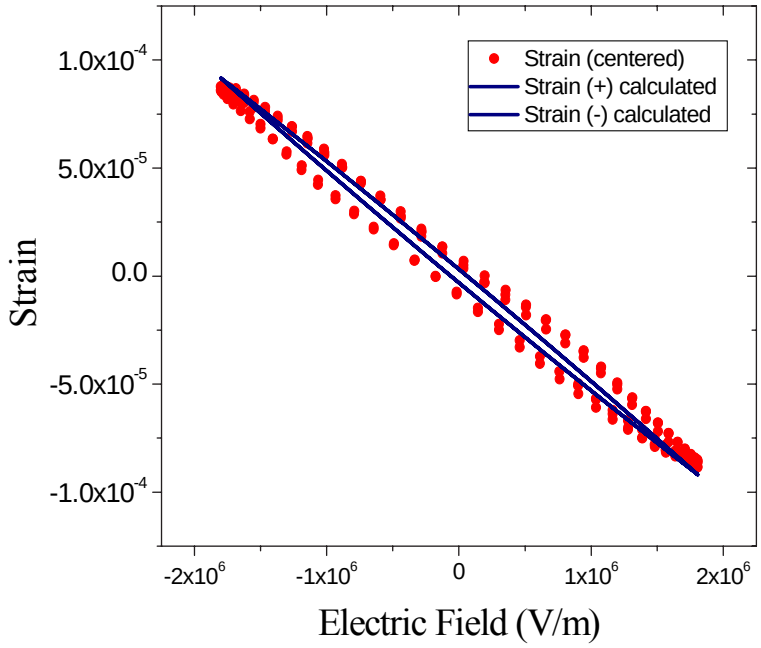

(b)

Figure **6.7**: Experimental strain-electric field hysteresis curves vs. the curves obtained using the piezoelectric Rayleigh parameters for a {100} oriented sample under ~65kV/cm bias field, at (a) 14kHz and (b) 4kHz.

6.3 Dynamic Poling Model

It can be seen in Figure 6.8 that the measured first harmonic of both the dielectric and piezoelectric response follow a linear Rayleigh-like behavior.[18] However, the piezoelectric nonlinearity under bias is one order of magnitude smaller than the dielectric nonlinearity at zero bias. This is evident both from a comparison of the irreversible Rayleigh coefficients (see Equation 6.4) and from the ratio of the irreversible to the reversible Rayleigh coefficients.

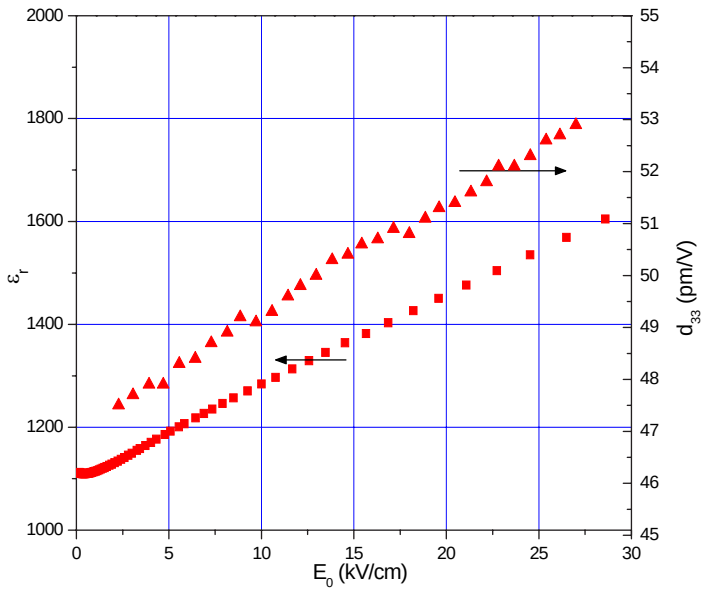

Figure 6.8: First harmonic, ac field dependence of the dielectric and piezoelectric response of {100} oriented PYbN-PT 50/50 films at 5 kHz. The samples were poled at 180kV/cm for 30 minutes. The piezoelectric measurements were performed under ~50kV/cm applied bias.

$$\varepsilon_r = 1108.3 + 17.5E_0\left(\frac{cm}{kV}\right) \quad \text{and} \quad \left(\frac{\alpha_\varepsilon}{\varepsilon_{init}}\right) = 0.015\left(\frac{cm}{kV}\right)$$
$$d_{33} = 47.4 + 0.28E_0\left(\frac{pm}{V}\right) \qquad \left(\frac{\alpha_d}{d_{init}}\right) = 0.0059\left(\frac{cm}{kV}\right) \qquad \textbf{6.4}^{19}$$

The measured difference between the dielectric and piezoelectric nonlinearity is not surprising in light of the fact that dielectric nonlinearity is due to both 180° and non-180° domain wall motion, while piezoelectric nonlinearity is typically attributed to non-180° domain wall motion only. In addition, the piezoelectric response was measured under bias, which would be expected to reduce the nonlinearities.[**244**] A comparison of the dielectric and piezoelectric nonlinearities was performed under the same bias conditions. The results are shown in Figure **6.9** and the Rayleigh parameters are reported in Equation **6.5**. Also, as shown earlier in section **6.2**, Figures **6.5** and **6.6**, the Rayleigh parameters for both dielectric and piezoelectric nonlinearities follow a logarithmic decay with frequency.

$$\varepsilon_r = 1026 + 5.95E_0\left(\frac{cm}{kV}\right) \quad \text{and} \quad d_{33} = 47.4 + 0.28E_0\left(\frac{pm}{V}\right) \qquad \textbf{6.5}$$
$$\left(\frac{\alpha_\varepsilon}{\varepsilon_{init}}\right) = 0.0058 \pm 0.0002\left(\frac{cm}{kV}\right) \text{ and } \left(\frac{\alpha_d}{d_{init}}\right) = 0.0059 \pm 0.0004\left(\frac{cm}{kV}\right)$$

---

[18] Note that through this section, the irreversible Rayleigh coefficients have subscripts to distinguish piezoelectric irreversible Rayleigh coefficient (α_d) from the dielectric one (α_ε).

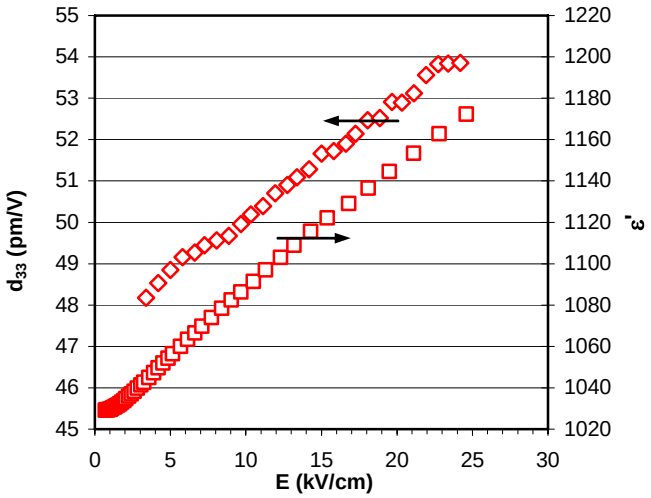

Figure **6.9**: First harmonic, ac field dependence of the dielectric and piezoelectric response of {100} oriented PYbN-PT 50/50 films at 5 kHz. The samples were poled at 180kV/cm for 30 minutes. Both measurements were performed under ~50kV/cm applied bias.

The extrinsic contributions to the piezoelectric and dielectric properties are of the same order of magnitude, considering that the ratios of the irreversible to reversible Rayleigh parameters are within experimental error of each other. Non-180° domain wall motion, usually considered the principal contributor to the piezoelectric nonlinearities, is typically very heavily clamped in thin films. [**6**][**88**][**98**][**246**][**247**] As mentioned in section **5.3.2**, measurements on these films showed negligible changes in the *dielectric* Rayleigh coefficients when additional biaxial tensile stresses were imposed. This suggests that even if the morphotropic phase boundary had shifted from the bulk value, or

[19] All electric fields are expressed in $\left(\frac{kV}{cm}\right)$.

that there was tetragonal material present due to composition fluctuations in the films, so that there was tetragonally distorted ferroelectric phase present, there is still little evidence for non-180° domain wall motion.

What is more surprising here is that the piezoelectric response shows *any* Rayleigh region. For {001} rhombohedral perovskite films, the four ferroelastic domain states are ideally energetically equivalent with respect to the field applied along [001] pseudo-cubic axis so that there should be no driving force for wall motion due to applied electric fields.[**245**]

In light of this, other means by which 180° domain wall motion could be responsible for the field dependence of the *piezoelectric* coefficient were sought. Figure **6.10** shows a schematic of the response of a hypothetical poled ferroelectric crystal made of 2 domains with one 180˚ domain wall. The sample is excited by an applied sinusoidal electric voltage, higher than the threshold voltage for the onset of nonlinear effects. It is presumed that the domain wall can be moved nearly reversibly by the alternating field.

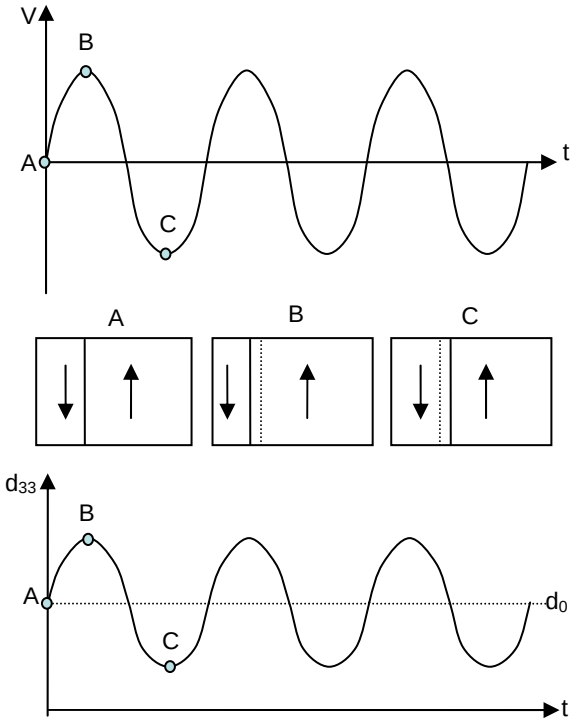

Figure **6.10**: Schematic piezoelectric response, dij, of a poled ferroelectric crystal made of 2 domains with one 180˚ domain wall, excited by a sinusoidal ac voltage, V higher than the threshold voltage for onset of nonlinearity, E_{th} .

At time *A* (zero field applied), the sample has a remanent polarization (P_r) in the up direction and the piezoelectric response of the material is given by d_0. At point *B*, the application of a field parallel to P_r increases the volume of the domain with this polarization direction. Therefore, at time B , there is a larger volume of the material with the upward polarization. Consequently, the piezoelectric response of the material increases above d_0. If this domain state is not stable, the opposite effect happens at time C : the antiparallel field shrinks the first domain, and therefore the piezoelectric response of the material is lower at time *C* than at time *A*. The application of a sinusoidal

field, $E = E_0 \sin(\omega t)$ therefore creates a piezoelectric response that is also oscillating in time. The reversible Rayleigh coefficient d_{init} can then be written as another sinusoidal function of time: $d_{init} = d_0[1 + \beta \sin(\omega t)]$ where β is a scaling factor. Any irreversibility in the domain wall motion is then incorporated into α_d. Consequently, the field dependence of the strain can be written as in Equation **6.6**:

$$x(E) = \{d_0[1 + \beta \cdot \sin(\omega t)] + \alpha_d \cdot E_0\} \cdot E_0 \cdot \sin(\omega t) \pm \frac{\alpha_d}{2}(E_0^2 - E_0^2 \cdot \sin^2(\omega t)) \qquad \textbf{6.6}$$

The Fourier expansion of Equation **6.6** leads to Equation **6.7**:

$$x(E) = \beta d_0 E_0 + (d_0 + \alpha_d E_0) E_0 \sin(\omega t) + \frac{4\alpha_d E_0^2}{3\pi}\cos(\omega t) + \\ -\frac{\beta d_0 E_0}{2}\cos(2\omega t) + \frac{4\alpha_d E_0^2}{15\pi}\cos(3\omega t) - \frac{4\alpha_d E_0^2}{105\pi}\cos(5\omega t) + \cdots \qquad \textbf{6.7}$$

The time dependent d_{init} consequently creates a static term and a second order harmonic, while for all the higher harmonics only the odd order ones remain.

A further step can be taken in this approximation if the application of a sinusoidal voltage creates a piezoelectric response that is not only time dependent but also dependent on the maximum applied voltage. In fact, it is logical to think that a higher E_0 would move the domain wall further and therefore, increase the oscillation in d_{init}. This is schematically illustrated in Figure **6.11** , where the full lines represent the new case for higher maximum voltage applied; the dotted lines show the initial domain configuration and the dashed lines represent the case of a smaller sinusoidal voltage. To describe this, the reversible Rayleigh coefficient is modified to include both the time and

field dependence $d_{init} = d_0\left[1 + (\beta + \beta' E_0)\sin(\omega t)\right]$. Then the strain function is written as in Equation **6.8** :

$$x(E) = \beta d_0 E_0 + \beta' d_0 E_0^2 + (d_0 + \alpha_d E_0)E_0 \sin(\omega t) + \frac{4\alpha_d E_0^2}{3\pi}\cos(\omega t) + \\ -\frac{\beta d_0 E_0 + \beta' d_0 E_0^2}{2}\cos(2\omega t) + \frac{4\alpha_d E_0^2}{15\pi}\cos(3\omega t) - \frac{4\alpha_d E_0^2}{105\pi}\cos(5\omega t) + \cdots \qquad \textbf{6.8}$$

The variation in d_{init} changes the second harmonic: it now includes a linear and a square field dependent term.

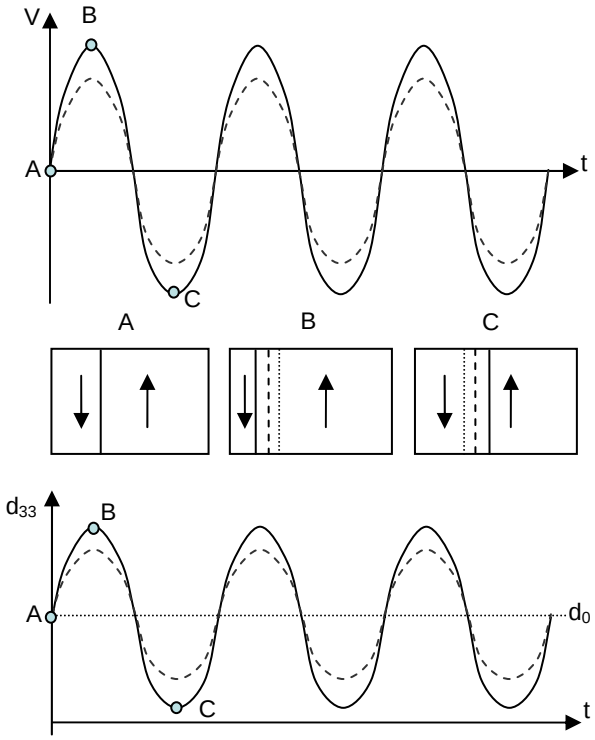

Figure **6.11**: The piezoelectric response of the same crystal as in Figure **6.10** under a higher amplitude excitation voltage. The full lines represent the new voltage and the dashed ones the lower voltage.

There are several points to note about this extension to the role of nearly reversible domain wall motion to Rayleigh behavior. First, this affects only properties which rely on a remanent polarization, such as the piezoelectric response. Thus, the dielectric constant should not show a second harmonic response due to this mechanism. Secondly, the motion of any type of phase boundary or domain wall motion could contribute to the amplitude dependence of d_{init}. Therefore, it is possible to develop an amplitude dependent d_{ij} coefficient (with associated hysteresis[20]) even if *only* 180° domain wall motion is present. Therefore, both the dielectric nonlinearities and the piezoelectric nonlinearities in {100} oriented PYbN-PT thin films are believed to be due to the reversible and irreversible motion of 180° domain walls. The common origin of the dielectric and piezoelectric nonlinearities is seen in the frequency dependence of the Rayleigh parameters. Figure **6.12** shows the normalized Rayleigh parameters to 40Hz. The reversible Rayleigh parameters decay with similar trends, likewise, the decay in the irreversible Rayleigh parameters are also comparable for the dielectric and piezoelectric responses.

[20] Note that the terms in Equation 6.8 associated with hysteresis are only the ones including the irreversible Rayleigh coefficient (α') and therefore, the second order harmonic doesn't contribute to the hysteresis, while all the other harmonics (due to the irreversible motion of 180° domain walls) contribute to hysteresis.

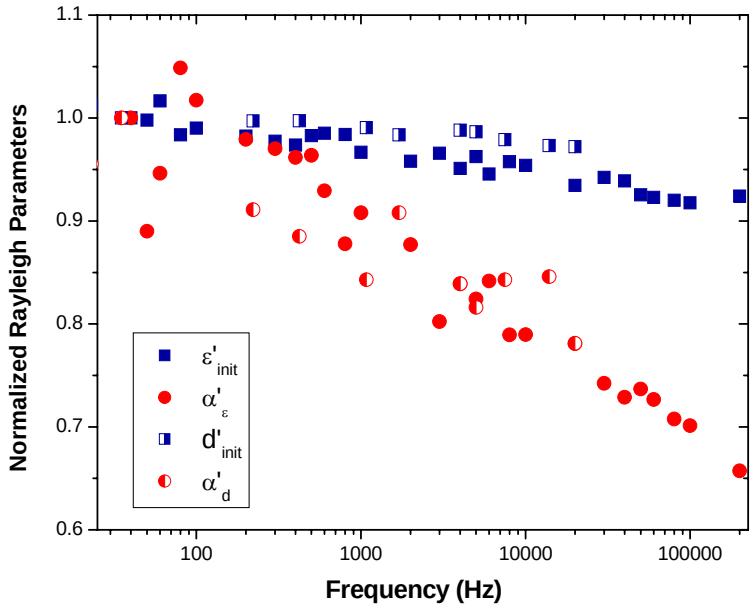

Figure **6.12**: Normalization of the dielectric and piezoelectric Rayleigh parameters to values at 40Hz for measurements performed on {100} oriented PYbN-PT thin films under ~60 kV/cm.

Another method used to ascertain whether the motion of 180° domain walls could, in fact, be responsible for the observed field dependence was the higher order harmonics of the dielectric and piezoelectric responses. In this case, to avoid complications associated with the effect of a dc bias field, the sample was poled, aged, and then measured without any applied bias. The dielectric and piezoelectric measurements were made at the same frequency and field range to simplify comparisons. As can be seen in Figure **6.13** the first harmonic strain increased almost linearly with the amplitude of the ac electric field: thus, $\alpha_d E_0 < d_0$. The small value for $\alpha_d E_0$ is

reasonable since α_d is large when the mobility of the ferroelastic walls is high.[**110**] For these films, the ferroelastic wall mobility is low.

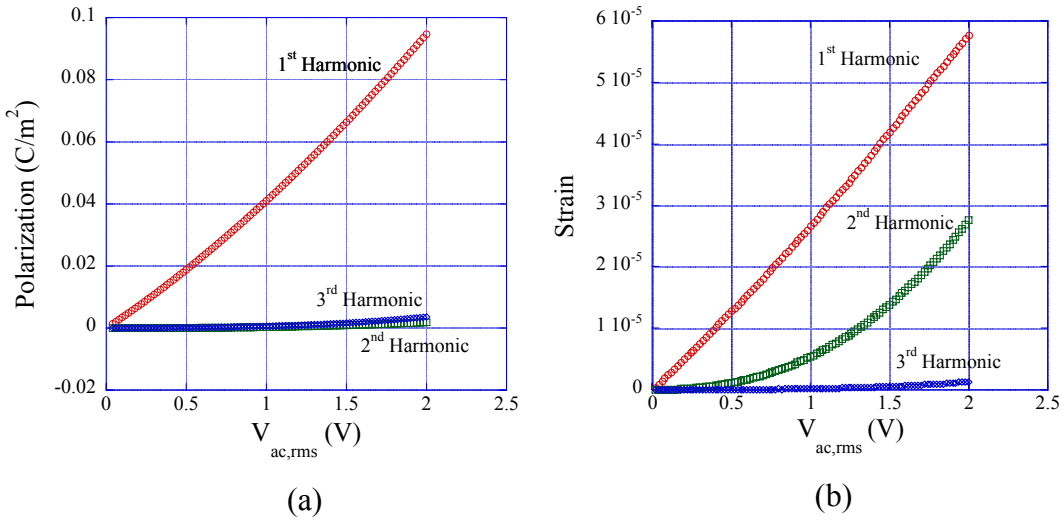

Figure **6.13**: Field dependence of the harmonic response in the (a) polarization and (b) strain of {100} oriented PYbN-PT 50/50 films. The samples were poled at 150kV/cm for 30 minutes and then allowed to age for 5 hours before the measurements were performed. The data were collected at 5kHz.

The polarization response shows a strong first harmonic, a much smaller third harmonic, and a negligible second harmonic. In contrast, the piezoelectric response has a relatively high second harmonic and a much smaller third order harmonic. The second harmonic in the displacement cannot be fit with the linear dependence suggested in Equation **6.7** , but is very well fit by the quadratic form suggested in Equation **6.8** , with an R^2 value of 0.999. The fit gives $\frac{\beta d_0}{2}$ as negative and $\frac{\beta' d_0}{2}$ as positive. When the

data are fit without the linear term, $\frac{\beta' d_0}{2}$ is positive, and the R^2 value is 0.991 (see Figure **6.14**.

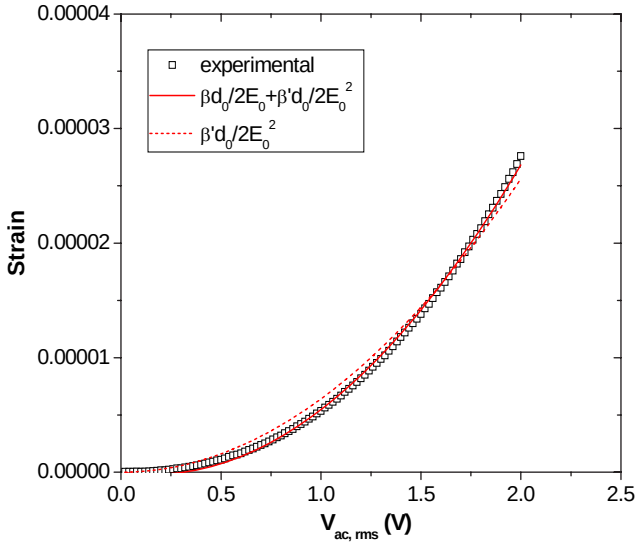

Figure **6.14**: Field dependence of strain's second harmonic (full squares), fitted with Equation **6.8**, with (full line) and without (dashed line) the linear term.

This is consistent with the predictions of Equation **6.8**, suggesting that the amplitude dependence of the piezoelectric coefficient is associated with the electric field driving a poling/depoling process. The result is Rayleigh-like behavior of the piezoelectric coefficient that will exist even in the case where only 180° domain wall motion is present. The positive sign of the β' coefficient is consistent with the "dynamic poling" model proposed: the piezoelectric response (d_{init}) increases with increasing electric field in the direction parallel to the poling direction and decreases with increasing fields antiparallel to the poling direction of the sample. The actual increase in the value of

d_{init} in the Rayleigh region due to the dynamic poling (calculated using the calculated β' and d_0) is reported in Figure **6.15** and is equal to ~60% at ~30kV/cm.

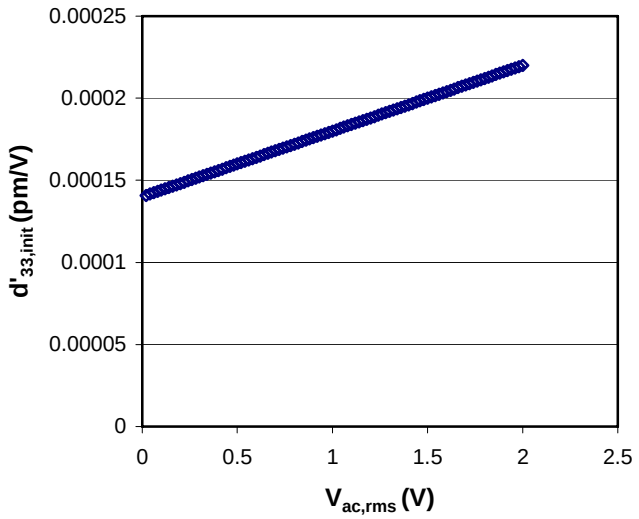

Figure **6.15**: A plot of the actual increase in the piezoelectric parameter, $d_{33,init}$, due to the dynamic poling model at 5kHz.

In principle, the second harmonic in the strain response could also be electrostrictive in origin, as in Equation **6.9** :

$$x = \varepsilon_0^2 \varepsilon_r^2 Q (E_0 \sin(\omega t))^2 = \varepsilon_0^2 \varepsilon_r^2 Q E_0^2 (1 - \cos(2\omega t)) \qquad \textbf{6.9}$$

However, several observations suggest that electrostriction does not dominate the second harmonic strain response in this work. First, the electrostrictive strain was estimated using the electrostrictive constants and intrinsic dielectric permittivity of MPB lead zirconate titanate ceramics [**248**] and thin films [**246**] (unfortunately, the relevant

property coefficients aren't available for PYbN-PT, but the two systems are analogous in many ways). The measured 2nd order harmonic of strain is a factor of 3 to 10 larger than the calculated electrostrictive response, depending on which value for the intrinsic permittivity is chosen. In addition, as seen in Figure **6.16** , the second harmonic in the strain response *decreased* with increasing frequency. The amount of decrease measured from 200 Hz to 5 kHz was approximately 7 %. The second harmonic amplitude also decreased somewhat when the sample was poled at 80°C and field cooled in an attempt to stabilize the domain configuration (see Figure **6.17**), rather than being poled at room temperature. Such behavior is consistent with the observed frequency dependence and poling dependence of domain wall motion [**15**], and inconsistent with a pure electrostrictive response. These results suggest that although the electrostrictive effect contributes to the second harmonic, nearly reversible motion of ferroelectric domain walls also contributes.

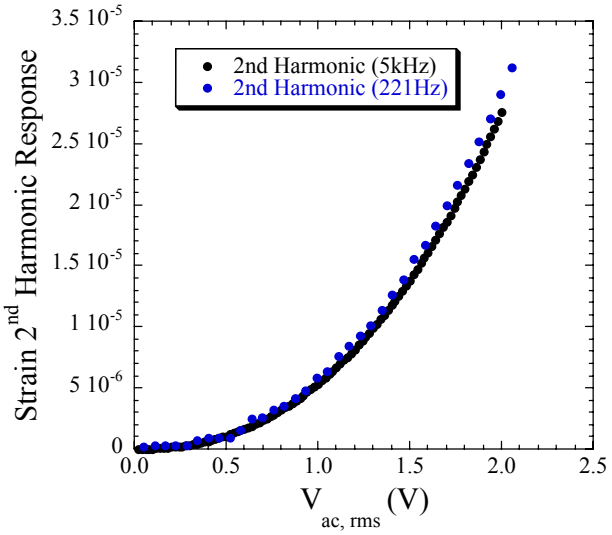

Figure **6.16**: AC field dependence of second harmonic of strain response for two different frequencies of applied ac field.

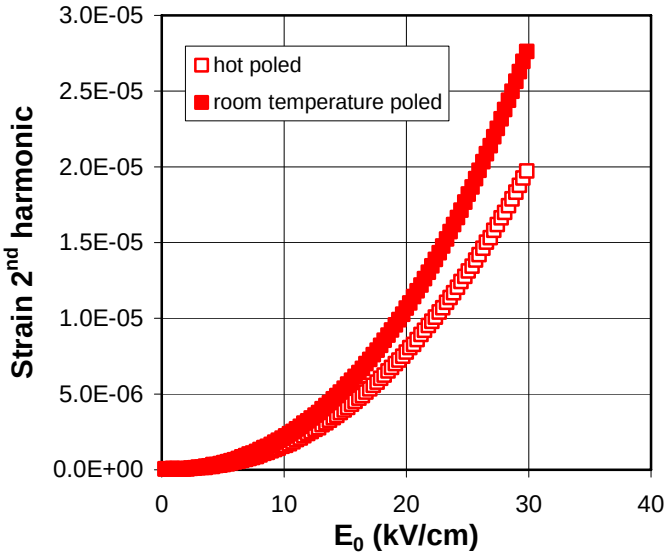

Figure **6.17**: Change in the strain 2nd harmonic response amplitude due to the poling conditions (room temperature poling or poling at 80°C) at 5kHz

As can be seen in Figure 6.18 the phases of the higher harmonics are also consistent with the predictions in Equation 6.8. As expected, the phase angle of the first harmonic is very close to zero; the piezoelectric response is nearly in phase with the applied voltage. The second harmonic's phase angle is around 90º in advance of the probing signal. As $\sin(\omega t + \frac{\pi}{2}) = -\cos(\omega t)$, this 90º phase advance is also consistent with Equation 6.8. The slight deviation from 90º could be due to other loss mechanisms present in the films. The third harmonic's phase angle differs from the Rayleigh predictions. This is due in part to instrumental limitations on detection of phase angles of very small signals. In fact the amplitude of the 3rd order harmonic of strain is at least an order of magnitude smaller than the amplitude of the 1st and 2nd order harmonics. Another reason for deviation of the 3rd harmonic's phase angle from –90° is the presence of any additional nonlinear reversible motion of domain walls in a symmetric potential. Such displacement of domain walls contributes only to the in-phase response of odd harmonics but not to its out-of-phase component and does not contribute to even harmonics.[249] The phase angle of the third harmonic thus becomes different from –90° predicted by Equations 6.7 and 6.8. For simplicity, such effects, which contribute only to the in-phase component of the odd harmonics, are not taken into account in Equations 2.35, 6.7 and 6.8.

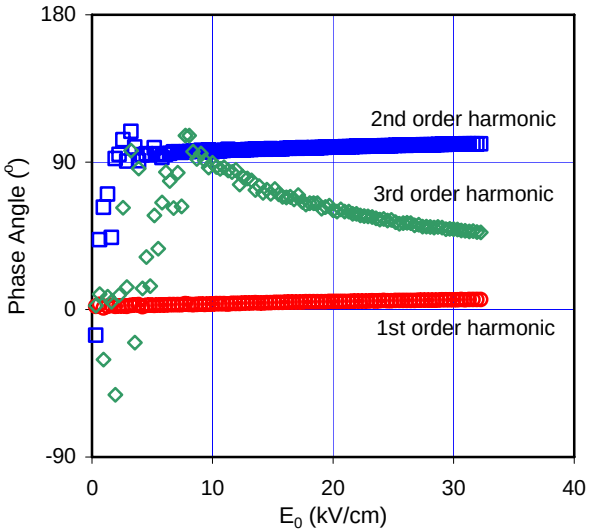

Figure **6.18**: Field dependence of the phase angles for the harmonics of the displacement response for {100} oriented PYbN-PT 50/50 film of Figure **6.13**. The sample was poled at 150kV/cm for 30 minutes and then allowed to age for 5 hours before the measurements were performed. The data were measured at 5kHz.

It is worthwhile thinking about the types of materials for which this contribution to Rayleigh behavior is important. First, since it hinges on the large scale, largely reversible motion of domain walls (or phase boundaries), it would be most likely to be important in samples with tilted polarization – electric field hysteresis loops. A strong slope at the top of the hysteresis loop suggests that the domain state is not stable, and that P_r can be modulated even in cases where the dc bias field exceeds the peak to peak oscillation of the probing signal. Therefore the more stable the polarization state the smaller the 2nd harmonic should be. Eventually, the situation should collapse to normal Rayleigh behavior, as has been observed in piezoelectric ceramics.[**250**] Secondly, it is likely in cases where the domain state is more stable and non-180° domain wall motion is present that the strong 1st and 3rd harmonic contributions to the piezoelectric constant will

overwhelm the contribution from the 180° domain walls, so that this becomes a minor contributor.

6.4 Piezoelectric Nonlinearities as a Function of AC Strain

As shown in the previous section, 180° domain wall motion can contribute to the piezoelectric nonlinearity under increasing ac field amplitudes. It is important to note, though, that 180° domain walls should not be driven elastically. Thus, if indeed 180° domain wall motion is the cause of the observed piezoelectric nonlinearity and the second order harmonic of strain response *as a function of ac electric field*, the piezoelectric coefficient *as a function of increasing strain levels* should follow the "basic" Rayleigh behavior with only odd order harmonics present. Therefore nonlinear piezoelectric measurements were performed as a function of increasing biaxial strain levels. The set-up used for these measurements was described in section **3.13** and the results for a {100} oriented PYbN-PT thin film at 1Hz are reported in Figure **6.19**.

As can be seen in Figure **6.19**, the film showed no significant increase of the piezoelectric coefficient with the applied strain for the amplitudes used here. This was in part expected due to the crystallographic orientation of the film: in a {100} oriented crystal with a rhombohedral perovskite structure, application of a biaxial stress parallel to {001} should not reorient the polarization vectors. Furthermore, as shown in section

5.3.2, under applied biaxial tension levels up to thousands of microstrain the ferroelastic non-180° domain wall motion is not activated in the PYbN-PT thin films and therefore can't contribute to the piezoelectric properties of these films. Similarly, no evidence of phase boundary motion contribution to the dielectric properties was found under the same strain levels (see section 5.3.2). The apparent decrease of the piezoelectric coefficient at higher strain values is probably due both to aging and to a continuous scratching of the top electrode by the micro-probe which leads to a reduction of the effective area of the top electrode and therefore an apparent reduction of the measured charge per unit area.

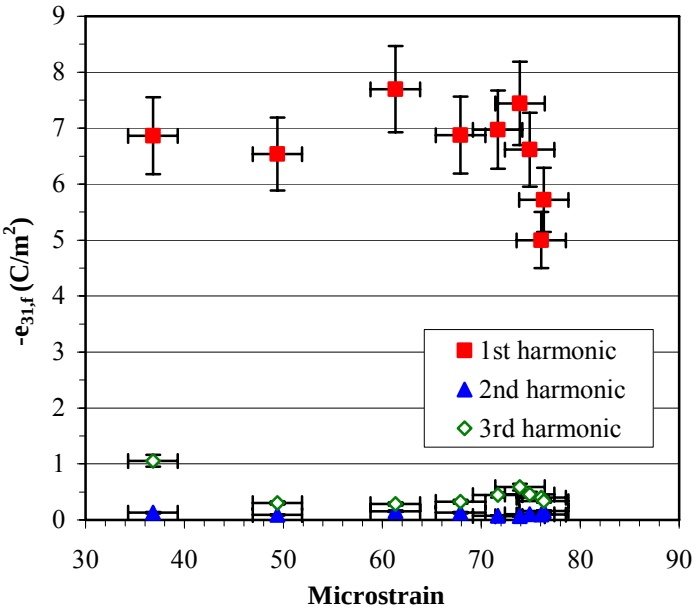

Figure 6.19: Piezoelectric response ($e_{31,f}$) of a {100} oriented PYbN-PT film measured at 1Hz under increasing strain levels. The film was poled at twice the coercive field for 20 minutes before the measurements.

It is also interesting to notice that over the whole studied range of biaxial strain, the amplitude of the second harmonic is one order of magnitude smaller than the third harmonic response. This is in agreement with normal Rayleigh behavior for a piezoelectric. That is, reversible and irreversible motion of hysteretic interfaces across a random and uniform distribution of "pinning" energy profiles should generate only odd order harmonics of the nonlinear response. The observation of a Rayleigh behavior in $d_{33,f}$ along with a strong second harmonic in the strain response for electric field drive, coupled with the lack of the amplitude dependence for a strain excitation is consistent with the dynamic poling model.

6.5 Conclusions

The piezoelectric nonlinear behavior of the PYbN-PY was studied in the Rayleigh analysis frame. The {100} oriented films showed higher Rayleigh parameters and higher irreversible to reversible Rayleigh parameter ratio with respect to the {111} oriented films. The results confirm the outcome of the dielectric nonlinearities: the {100} oriented films showed a higher concentration of mobile interfaces than the {111} oriented films. The piezoelectric Rayleigh parameters were also shown to follow an approximately logarithmic dependence on frequency, similarly to the dielectric Rayleigh parameters.

The origin of the nonlinear piezoelectric behavior in the {100} oriented PYbN-PT films was discussed. It was shown that there are circumstances under which the strain – ac electric field amplitude nonlinearity can be due to largely reversible motion of 180° domain walls. The proposed underlying mechanism was the dynamic poling of the material by the external ac field. One distinguishing feature of this type of nonlinearity is a large second harmonic component in the strain response to an applied ac electric field. If this process is irreversible it will also result in the field dependence of the piezoelectric coefficient that is customarily measured from the first harmonic strain response.

The piezoelectric $e_{31,f}$ response of the films was also studied as a function of ac biaxial stress. The $e_{31,f}$ response didn't show any significant increase over the studied strain range, indicating insignificant contributions from non-180° domain wall and phase boundary motion to this piezoelectric coefficient. Furthermore, the amount of the second harmonic response was much smaller than the first and third harmonic of the piezoelectric response as predicted by normal Rayleigh Law for piezoelectric materials. Therefore, the comparison of the $d_{33,f}$ nonlinearity as a function of ac electric field drive with the $e_{31,f}$ response as a function of increasing strain levels confirmed the dynamic poling origin of the observed linear dependence of $d_{33,f}$ on applied field and the presence of the second harmonic of strain in ac electric field driven experiments.

Chapter 7

Nonlinearities in Other Ferroelectric Films

This chapter will present the dielectric nonlinear results from other ferroelectric systems, in particular PZT and PMN-PT films over a range of compositions, crystallographic orientations and thicknesses. The transition temperature and temperature dependence of the dielectric nonlinear behavior for these systems are also reported and the Rayleigh parameters are compared to the values obtained for the PYbN-PT thin films. This is extremely relevant for a quantitative "classification" of "hard" and "soft"-ness of the ferroelectric materials. Denominations like "soft" and "hard" have been historically used in the literature to distinguish the properties of doped PZT samples, with different levels of pinning of the domain walls.

7.1 PZT Thin Films

The MPB $PbZr_{0.58}Ti_{0.42}O_3$ (PZT) thin films were deposited on platinized Si wafers using sol-gel processing. The details for the precursor preparation and deposition of the films are described in reference [251]. Two different orientations (preferential {100} and {111}) of the films were used for the dielectric nonlinear measurements: the X-Ray diffraction data for these films is reported in Figure 7.1 . The thickness of both films was approximately ~0.9μm, and T_C between ~360 and 380 °C.

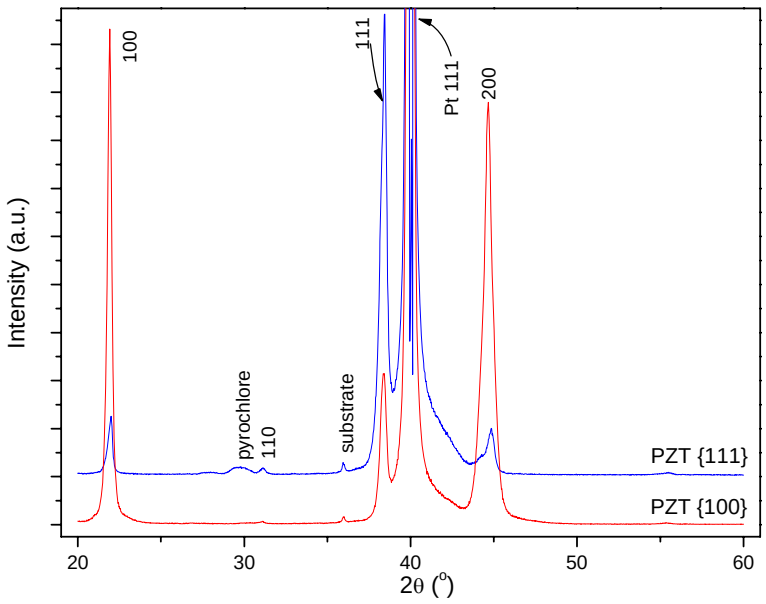

Figure 7.1: X-Ray diffraction patterns for the {111} and {100} oriented PZT 58/42 thin films.

The dielectric nonlinear behavior of the films is reported in Figure 7.2. The respective Rayleigh parameters for each orientation of the PZT films are reported in Table 7-1.

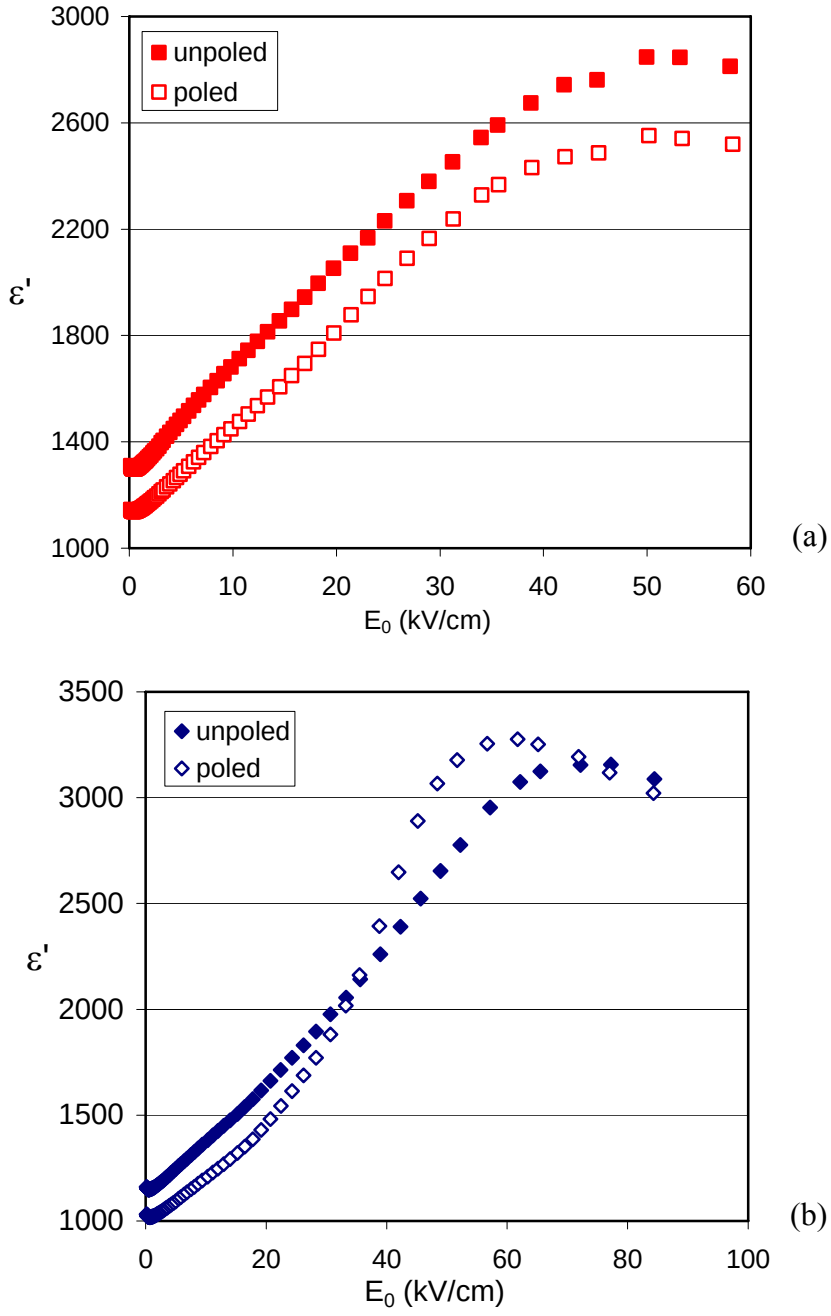

Figure 7.2: Nonlinear dielectric behavior of the (a) {100} and (b) {111} oriented PZT films before (solid squares) and after poling (open squares) measured at room temperature and 1kHz.

Table 7-1: Rayleigh parameters for the {100} and {111} oriented PZT thin films.

Film orientation		ε'_{init}	$\alpha'\left(\frac{cm}{kV}\right)$	$\frac{\alpha'}{\varepsilon'_{init}}\left(\frac{cm}{kV}\right)$
{100}	Unpoled	1288±13	38.2±0.2	0.030±0.002
	Poled*	1098±9	36.3±0.3	0.033±0.002
{111}	Unpoled	1097±10	28.2±0.3	0.026±0.001
	Poled*	980±20	22.0±2.0	0.024±0.002

* The films were poled at twice their coercive field for 30 minutes.

The irreversible Rayleigh parameter and the ratio of the irreversible to reversible Rayleigh parameters are higher in the {100} oriented films than in the {111} oriented films, indicating a higher contribution of the mobile interfaces to the nonlinear dielectric behavior in the former. This observation is in agreement with the behavior observed in the oriented PYbN-PT thin films.

It can be seen in Figure 7.2b that the {111} oriented PZT film present two linear zones, with the first linear zone for $E_0 \leq 20\,\frac{cm}{kV}$ and the second linear zone, with higher slope, for $\sim 25 \leq E_0 \leq 40\,\frac{cm}{kV}$. The peculiar behavior of the poled {111} oriented PZT films may possibly indicate some contribution of non-180° domain wall motion to the dielectric nonlinear behavior in these films. Taylor and Damjanovic [12] have reported piezoelectric nonlinearity for {111} oriented rhombohedral $Pb(Zr_{0.6}Ti_{0.4})O_3$ of approximately same thickness (~0.9 μm), attributing it to the motion of non-180° domain

walls.[21] The motion of the ferroelastic domain walls, especially at higher fields, could give an "extra" contribution to the dielectric permittivity, leading to the higher slope of the high field permittivity curve. The {100} oriented films wouldn't exhibit the same behavior because of crystallographic orientation of the crystal, where movement of a 180° or non-180° domain wall would lead to the same change in the longitudinal permittivity.

The irreversible Rayleigh parameters and the ratio of the irreversible to reversible Rayleigh parameters are much higher than the values reported for the same orientations of PYbN-PT thin films, indicating a higher contribution of the mobile interfaces to the nonlinear dielectric behavior of the PZT films. But it should be noted that the PZT have a higher perovskite phase purity than the reported PYbN-PT thin films. No pyrochlore peak was in fact detected in the PZT films with {100} preferential orientation, while the pyrochlore peak seen in the X-Ray diffraction pattern of the {111} oriented PZT film has a relative intensity to the Pt peak that is much smaller than the same relative intensity in the {111} oriented PYbN-PT thin films. The effects of the eventual presence of ~1.5% (detection limit of the XRD instrument is ~5%) pyrochlore phase in the {100}-oriented PZT film is illustrated in Figure 7.3. For the calculations, the pyrochlore phase was considered to be a linear dielectric with relative permittivity of ~200. The PZT film was considered to have the nonlinear parameters as measured for the poled {100} oriented

[21] It should also be mentioned here that the authors (Taylor and Damjanovic) did not consider the possible contribution of the 180° domain walls motion to the piezoelectric nonlinearities. The presence of the piezoelectric nonlinearities in the {100} oriented PZT films of similar composition and thickness in the same article was attributed to the small degree of mis-orientation in the films. Indeed higher harmonic measurements of the piezoelectric nonlinearities in those films showed also a significant amount of the second harmonic of strain vs. ac electric field amplitude (see Appendix B).

film of Figure 7.2a. The PZT and pyrochlore phase were considered to be capacitors in series. As it can be seen, the irreversible Rayleigh parameter decreased, accompanied by a more pronounced sub-linear behavior of the dielectric permittivity ($\alpha'_{\{100\}PZT} \approx 36.3 \frac{cm}{kV}$ while $\alpha'_{\{100\}PZT+pyrochlore} \approx 27.9 \frac{cm}{kV}$).

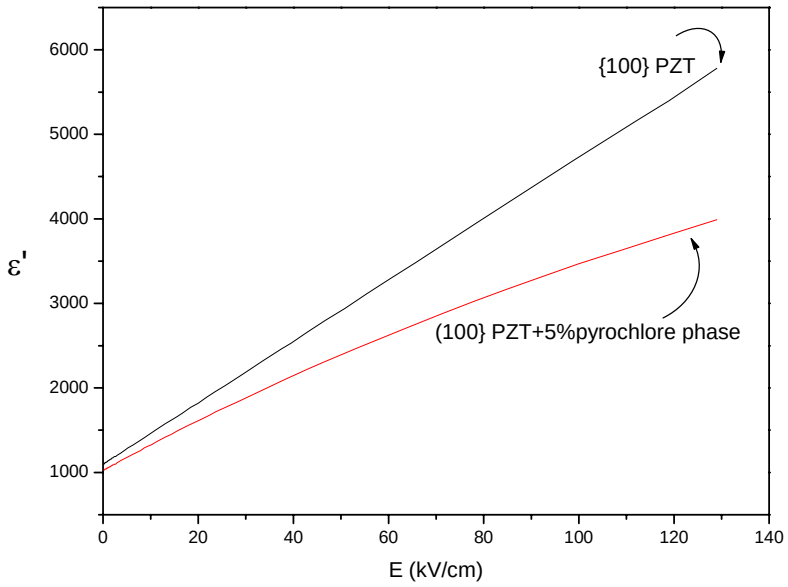

Figure 7.3: Comparison of the nonlinear dielectric behavior of a phase pure 0.6μm thick, {100} oriented PZT film and the effects of the presence of ~1.5% pyrochlore phase. The relative dielectric permittivity of the pyrochlore has been assumed to be ~200 and treated as a linear dielectric. Note also that the behavior showed for the {100} PZT is also idealized. Only the Rayleigh-like behavior is shown (no E_{th} or onset for high field behavior is modeled).

Another factor that could contribute to the difference between the Rayleigh parameters for the PZT films and the PYbN-PT films is the different thickness of the

used films. The thickness of the PZT films is approximately 30% higher than the thickness of the PYbN-PT thin films. With increasing thickness of the ferroelectric films, the substrate constraints are reduced and the non-180° domain walls can begin to contribute to the dielectric permittivity of the samples at higher field amplitudes. [252]

To verify if the PYbN-PT films were also sensitive to the thickness dependent effects, the nonlinear dielectric behavior of a ~0.4μm thick, {100} oriented PYbN-PT film was compared with those of a ~0.6μm thick film of similar orientation. The nonlinear curves are reported in Figure 7.4. The thinner films showed lower reversible and irreversible Rayleigh parameters and their ratio, as can be noted from the Rayleigh parameters of the thinner film reported in Equation 7.1. This is probably due to the reduced population of mobile domain walls that could contribute to the nonlinear dielectric permittivity.

$$\varepsilon'_{0.46\mu m, PYbN-PT\{100\}} = 1128 + 12.4E_0 \text{ and } \left(\frac{\varepsilon'_{init}}{\alpha'}\right)_{0.46\mu m, PYbN-PT\{100\}} = 0.011\,\frac{cm}{kV} \qquad \textbf{7.1}$$

A similar effect is observed by comparison of the above-mentioned {111} oriented PZT films with a similar film 0.6 microns thick, as can be seen in Figure 7.4b: both the reversible and irreversible Rayleigh parameters, and their ratio are smaller in the thinner PZT film (see Equation 7.2) than in the ~0.9 μm thick films of the same orientation. Therefore, the thickness difference between the oriented PZT and PYbN-PT films could be also a reason for the smaller value of the Rayleigh parameters in the latter. The thickness difference is especially important in view of the fact that, as mentioned earlier in the 0.9 μm thick PZT films, non-180° domain wall motion could also contribute

to the dielectric nonlinear behavior, while in the 0.6 μm thick PYbN-PT, as shown in section **5.3.2**, the contribution of the motion of non-180° domain wall is extremely reduced.

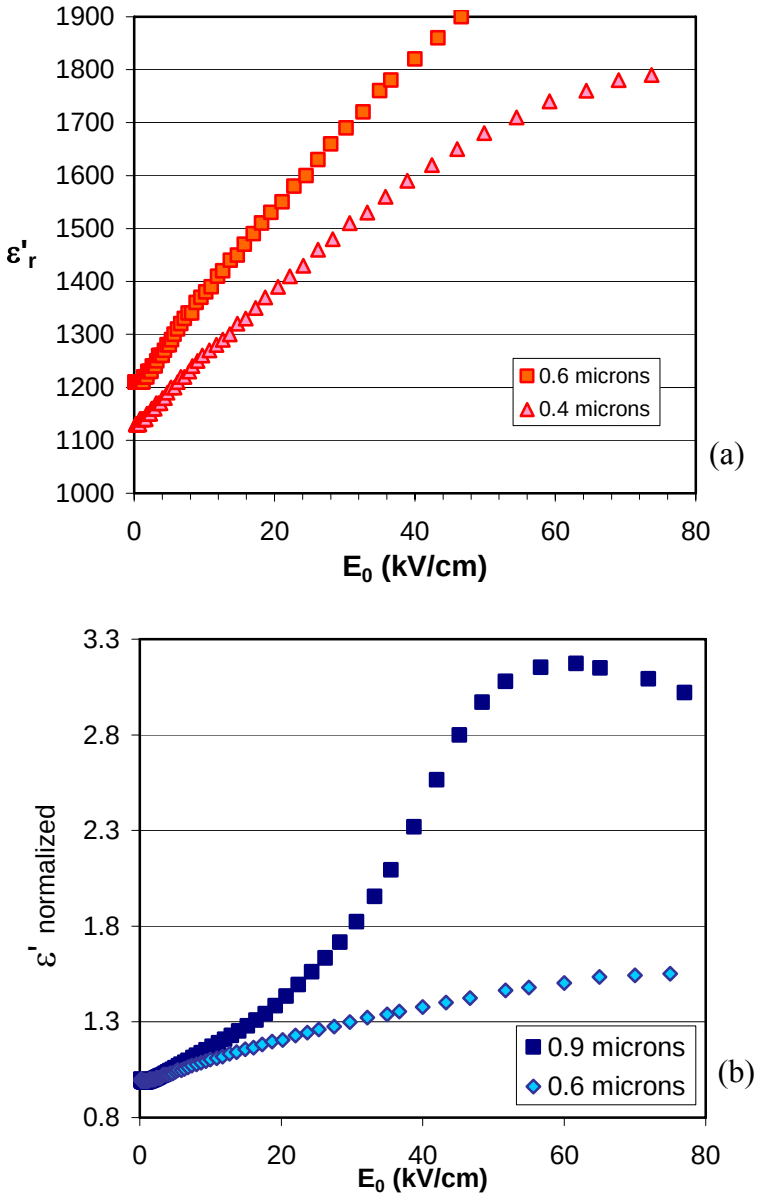

Figure **7.4**: Thickness dependence of the nonlinear dielectric behavior of (a) {100} oriented PYbN-PT thin films and (b) 0.6 and 0.9 micron thick, {111} oriented PZT film.

$$\varepsilon'_{0.6\mu m,PZT\{111\}} = 1253 + 13.8E_0 \quad \text{and} \quad \left(\frac{\varepsilon'_{init}}{\alpha'}\right)_{0.6\mu m,PZT\{111\}} = 0.011\,\frac{cm}{kV} \qquad \textbf{7.2}$$

For reference the dielectric Rayleigh parameters for various PZT thin films and ceramics, as available in literature, is reported in Table 7-2. Where available and/or pertinent, the composition and orientation of the samples are also indicated.

Table 7-2: Rayleigh parameters of PZT thin films at 1kHz. For the films denominated as (A) no data regarding thickness or orientation was given.

Composition	Sample	Orientation	ε'_{init}	$\alpha'\left(\frac{cm}{kV}\right)$	$\frac{\alpha'}{\varepsilon'_{init}}\left(\frac{cm}{kV}\right)$	Ref.
Zr:Ti=45:55	Film,1.3 μm	(111)	888	7.8	0.0088	[16]
Zr:Ti=45:55	Film,1.5 μm	(111)	1340	13	0.0097	[17[106]*
Zr:Ti=45:55	Film (A)	-	890	18	0.020	[214]*
Ferroperm PZ26 (hard)	Ceramic	-	1365	67	0.049	[61]
soft	Ceramic	-	1820	320	0.18	[223]*
Zr:Ti=58:42	Ceramic	-	530	130	0.25	[203]*
Zr:Ti=58:42 +0.2% Nb	Ceramic	-	540	305	0.56	[203]*
soft	Ceramic	-	1450	900	0.62	[3]*

*: Extrapolated data.

It can be seen from the data in Table 7-2 that the Rayleigh parameters and the ratio of the irreversible to reversible Rayleigh parameters are an excellent quantitative tool to measure the extrinsic contributions to dielectric properties of a ferroelectric. Note that the α' values increase with increasing thickness of films of same composition and orientation. Note also the order of magnitude difference between these values and the

ones reported for the ceramic materials. It's understood that the smaller average grain size of thin films than ceramics, in addition to clamping to the substrate, yields a lower concentration of mobile interfaces for the same composition of a ferroelectric material and therefore lowers extrinsic contributions to the dielectric and especially the piezoelectric properties in thin films. A comparison between the irreversible Rayleigh parameters (and the ratio of the irreversible to reversible Rayleigh parameters) shows that the values of these are one order of magnitude smaller for the hard PZT compositions with respect to the soft compositions. The films are harder than hard ceramics.

The film labeled as sample (A) has unexpectedly high irreversible and irreversible to reversible Rayleigh parameter ratio, although it comes from the same research institute as the other two PZT thin films reported in Table 7-2. The values of these parameters in sample A are in fact are much closer to the ones reported for the MPB, ~0.9 μm-thick PZT films reported earlier in this section and to the hard ceramic PZT reported in the above mentioned table. A few factors could explain this discrepancy. First, the dielectric properties and mobility of domain walls are extremely dependent on the thickness and grain size in thin films. In none of the above-mentioned literature reports, is information given on the average grain size or its distribution in the studied samples. Secondly, other reports [253][254] from the same research institution indicate a maximum in $e_{31,f}$ piezoelectric properties of the PZT thin films at compositions with Zr:Ti~ 45:55, with an indication of a shift in the morphotropic phase boundary, due to a B site Pb substitution.[255] It could be that for sample A, too, there is a shift in the MPB and

therefore there is contribution to the nonlinear dielectric properties not only from the domain wall motion but also from the motion of phase boundaries.

7.2 PMN-PT Thin Films

The $70Pb(Mg_{1/3}Nb_{2/3})O_3–30PbTiO_3$ (PMN–PT) thin films were deposited on platinized Si wafers using sol-gel processing. The details for the precursor preparation and deposition of the films are described in reference [256]. Two different orientations (preferential {100} and {111}) of the films were used for the dielectric nonlinear measurements: the X-Ray diffraction data for these films is reported in Figure 7.5. The preferential orientation in the former was better than the latter, as can be deduced by a comparison of the intensity of the principal orientation peak with the other orientations. The {100} oriented sample was ~1.0 microns thick and the {111} oriented sample's thickness was ~0.6μm. The transition temperature T_C was between ~85 and 110°C. The dielectric nonlinear behavior of the films is reported in Figure 7.6. The respective Rayleigh parameters for each orientation of the PMN-PT films are reported in Table 7-3.

Table 7-3: Rayleigh parameters for the {100} and {111} oriented PMN-PT thin films

Film orientation		ε'_{init}	$\alpha'\left(\frac{cm}{kV}\right)$	$\frac{\alpha'}{\varepsilon'_{init}}\left(\frac{cm}{kV}\right)$
{100}	Unpoled	2060±11	61.5±0.4	0.030±0.002
	Poled*	2042±8	58.2±0.4	0.029±0.002
{111}	Unpoled	1746±23	40.2±0.2	0.023±0.001
	Poled*	1625±13	32.2±0.3	0.020±0.002

* The films were poled at twice their coercive field for 30 minutes.

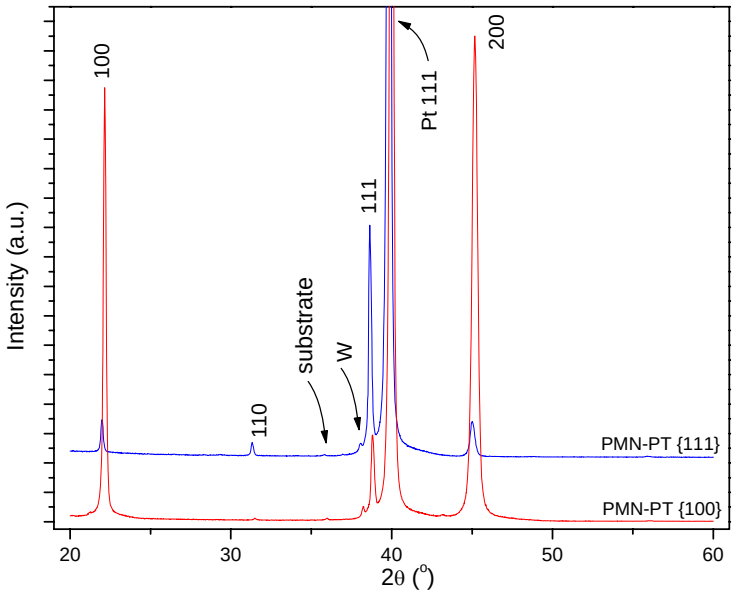

Figure 7.5: X-Ray diffraction patterns for the {111} and {100} oriented PMN-PT 70/30 thin films.

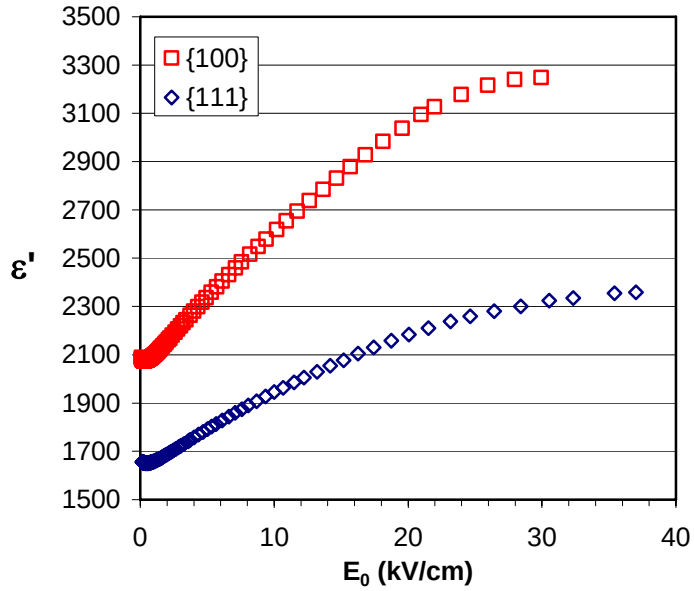

Figure **7.6**: Nonlinear dielectric behavior of {100} and {111} oriented PMN-PT 70/30 thin films.

Although the {100} oriented PMN-PT films show higher Rayleigh parameters and higher irreversible to reversible Rayleigh parameters ratio, due to the difference in the thickness of the two films, a comparison of the Rayleigh parameters between these two orientations of the films is not straightforward. In fact, a comparison of the Rayleigh parameters is more useful between the {111} oriented PMN-PT sample with the same orientation of PYbN-PT films and the thin {111} oriented PZT film. The irreversible Rayleigh parameter and the ratio of the irreversible to reversible were the highest in the PMN-PT films, followed by the PYbN-PT films and the PZT {111} oriented thin films. Considering that the order of the Rayleigh parameters corresponds to the common classification of "softness" of the ferroelectrics, therefore, PMN-PT films behave as the

softest films, followed by the PYbN-PT films and the PZT films. Indicating an intermediate behavior of PYbN-PT with respect to PZT and PMN-PT

The low transition temperature of the PMN-PT films makes them excellent candidates for verification of the temperature dependence of the Rayleigh analysis beyond the Curie temperature. The temperature dependence of the dielectric nonlinear behavior of the {100} oriented films (T_C ~110°C) is shown in Figure 7.7.

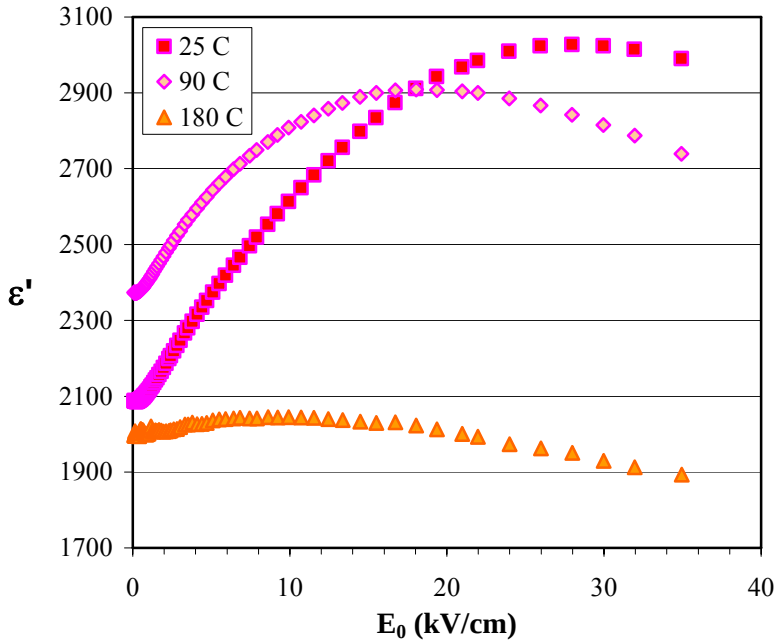

Figure 7.7: Temperature dependence of the dielectric nonlinear behavior in a 1μm thick, {100} oriented PMN-PT film at 1kHz.

For temperatures near, but lower than T_C, the Rayleigh parameters increase (see Figure 7.8). At the same time, the width of the Rayleigh region decreased, due to the reduction of the high field region onset. This is similar to observations in the PYbN-PT

films as discussed in section **5.4.1**. As expected, for temperatures higher than Curie temperature, the dielectric permittivity curve flattened: the reversible Rayleigh parameter is lower than the value the film exhibited at temperatures below T_C, while the irreversible Rayleigh parameters falls to values close to zero. The fact that any field dependence at all can be still observed in the film at ~ 180°C is probably due to the fact that small volumes of the material retain their ferroelectric state till higher temperatures. This might be due to local compositional variations across the probed volume of material.

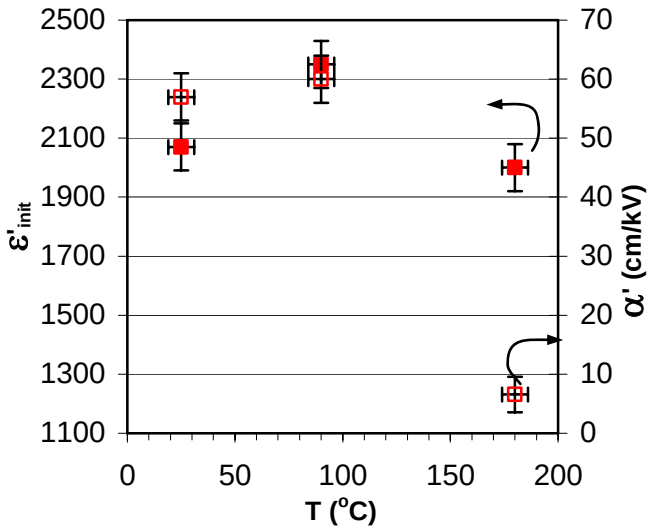

Figure **7.8**: Temperature dependence of the Rayleigh parameters in a 1 μm thick, {100} oriented PMN-PT film at 1kHz.

7.3 Conclusions

The dielectric nonlinear behavior of PZT and PMN-PT films was studied. The 0.6-micron thick PYbN-PT films showed Rayleigh parameters similar but slightly higher than the PZT film of similar thickness. Conversely, the Rayleigh parameters for the PYbN-PT were smaller than the values reported for the {111} oriented PMN-PT films of similar thickness.

Table 7-4 summarizes the Rayleigh parameters for the studied films, in order of increasing Rayleigh parameters. For reference, a $PbTiO_3$ (260 nm thick, preferential {100} orientation, grain size in the range of 100-500 nm) thin film's dielectric nonlinear properties are also reported. Considering the widely accepted reference to PZT in terms of "hard" and "soft" as a measure of mobility of the domain walls in the material, the extrinsic contribution to the dielectric and piezoelectric properties should be higher in softer materials. The concept can be therefore extended to all other ferroelectric materials. The data reported in this chapter (see Table 7-4) seemed to validate the fact that the irreversible Rayleigh parameter and the ratio of the irreversible to reversible Rayleigh parameter can constitute a valid parameter to quantify the "softness" or "harness" of the ferroelectric materials in various forms.

It was also showed for the PMN-PT films that nonlinear behavior of the material "dies" at temperatures higher than T_C, leading to flattened nonlinear permittivity curves. This is due to the fact that at temperatures higher than T_C, only smaller volumes of the material (probably due to local compositional variations) maintain the ferroelectric state and therefore domain walls, whose motion could contribute to the field dependent

dielectric permittivity. The more paraelectric the material, the lower the concentration of domain walls becomes and the lower the nonlinear behavior and the Rayleigh parameters of the material.

Table 7-4: Rayleigh parameters for the dielectric properties of poled (at twice the coercive field for 30 minutes) ferroelectric thin films, measured at 1kHz and room temperature.

Material	**Thickness (μm)**	**Orientation**	ε'_{init}	$\alpha'\left(\frac{cm}{kV}\right)$	$\frac{\alpha'}{\varepsilon'_{init}}\left(\frac{cm}{kV}\right)$
$PbTiO_3$ [257]	0.26	{100}and {111}	340±20	3.25±0.5	0.0096±0.002
PYbN-PT	0.46[22]	{100}	1128±12	12.4±0.2	0.011±0.0004
PZT	0.6	{111}	1253±10	13.8±0.1	0.011±0.0004
PYbN-PT	0.6	{111}	1036±20	14.1±0.1	0.014±0.0005
PYbN-PT	0.6	{100}	1165±15	19.5±0.4	0.017±0.0007
PMN-PT	0.6	{111}	1625±13	32.2±0.3	0.020±0.002
PZT	0.9	{111}	980±20	22.0±2.0	0.024±0.002
PMN-PT	1.0	{100}	2042±8	58.2±0.4	0.029±0.002
PZT	0.9	{100}	1098±9	36.3±0.3	0.033±0.002

[22] Note that the reduced thickness of the films could also increase the effects of the pyrochlore phase, if this indeed nucleates at the bottom electrode, resulting into artificially lower Rayleigh parameters for these films.

Chapter 8

Conclusions and Recommendations for Future Work

This chapter will briefly summarize the major findings in this thesis. Based on the experimental observations, guidelines for future works will be recommended.

8.1 Preparation and Characterization of {111} and {100} Oriented PYbN-PT Thin Films

The high Curie temperature of PYbN-PT in combination with the high piezoelectric and dielectric properties, make it a candidate for application in MEMS sensors and actuators and capacitive components. The highest properties have been reported along the <100> crystallographic direction of crystals with compositions on the rhombohedral of the MPB. In this work, using a CSD method, {111} and {100} oriented $0.5Pb(Yb_{1/2}Nb_{1/2/})O_3$-$0.5PbTiO_3$ were obtained. X-Ray studies showed a high degree of

orientation (>~83%) of the perovskite phase and the presence of minor amounts of second phase (pyrochlore). The grain size distribution of the films was bimodal (~200-300nm and ~50-60nm) for the {100} oriented films, while the {111} oriented films showed much smaller grains (~30-45nm).

The dielectric permittivities of the films were ~1200 and ~1000 at 1kHz, respectively for the {100} and {111} oriented films, comparable to the values reported for epitaxial films of the same composition and orientation [**153**]. The dielectric loss values were lower than ~3% over the frequency range of 100Hz to 100kHz for both film orientations. The transition temperature T_C of the films was ~385°C as measured by the temperature dependence of permittivity. A smaller peak in the dielectric permittivity at ~140-160°C was also observed that could correspond to the rhombohedral to tetragonal phase transformation ($T_{R\to T}$). The $e_{31,f}$ coefficients for films poled at room temperature were ~ -6.5C/m^2 and ~ -4.8C/m^2 for the {100} and {111} oriented PYbN-PT films respectively. Hot poling at ~150°C accompanied by field cooling resulted in $-e_{31,f}$ values as high as ~11C/m^2 for {100} oriented films.

8.2 Dielectric Nonlinearity

The Rayleigh relations were applied to the dielectric nonlinear behavior of the oriented PYbN-PT thin films. It was found that both the Rayleigh coefficients and the

ratio of the irreversible to reversible Rayleigh parameters are higher in the {100} oriented films with respect to the {111} oriented PYbN-PT films. This was attributed to a higher concentration of mobile interfaces (domain walls or phase boundaries) in the {100} oriented films.

A logarithmic dependence of the Rayleigh parameters on frequency was observed. The irreversible Rayleigh parameter was less frequency dependent in the {100} oriented films than in the {111} films, confirming a higher concentration of mobile interfaces or a higher mobility of the available interfaces. A modified Rayleigh Law with a logarithmic dependence on frequency successfully predicts the dielectric permittivity of the films for fields up to half the coercive field and frequencies from 20 Hz to 50 kHz.

The study of the nonlinear behavior under applied biaxial stress showed that the 180° domain walls are the major contributors to the dielectric nonlinearity in the PYbN-PT films, while phase boundaries and non-180° domain walls motion is very limited under the experimental conditions used. The bias field dependence of the dielectric nonlinearities followed an exponential decay law, which differs from the power law dependence predicted using phenomenological theory. The difference was attributed to the extrinsic (domain wall motion) contribution to the dielectric permittivity at higher field amplitudes.

The temperature dependence of the irreversible Rayleigh parameter mimicked, in part, the behavior of the low field dielectric permittivity dependence on temperature. The peaks in the irreversible to reversible Rayleigh parameters ratio vs. temperature were observed at temperatures lower than the temperatures reported for the same transitions at

low fields. This was explained in terms of a modified phase diagram where application of higher electric fields reduced the onset for the phase transformations.

8.3 Piezoelectric Nonlinearity

The piezoelectric nonlinear behavior of the PYbN-PT was studied in the Rayleigh analysis frame. The {100} oriented films showed higher Rayleigh parameters and a higher irreversible to reversible Rayleigh parameter ratio than {111} oriented films. The results confirmed the outcome of the dielectric nonlinearities: the {100} oriented films showed a higher concentration of mobile interfaces than the {111} oriented films. The piezoelectric Rayleigh parameters were also shown to follow an approximately logarithmic dependence on frequency, similarly to the dielectric Rayleigh parameters.

The origin of the nonlinear piezoelectric behavior in the {100} oriented PYbN-PT films was discussed. It was shown that there are circumstances under which the strain – ac electric field amplitude nonlinearity can be due to largely reversible motion of 180° domain walls. The proposed underlying mechanism was the dynamic poling of the material by the external ac field. One distinguishing feature of this type of nonlinearity is a large second harmonic component in the strain response to an applied ac electric field. If this process is irreversible, it will also result in the field dependence of the piezoelectric coefficient that is customarily measured from the first harmonic strain response.

The piezoelectric $e_{31,f}$ response of the films was also studied as a function of ac biaxial stress. The $e_{31,f}$ response didn't show any relevant increase over the studied strain

range, indicating insignificant contribution from non-180° domain wall and phase boundary motion to this piezoelectric coefficient. Furthermore, the amount of the second harmonic response was much smaller than the first and third harmonic of the piezoelectric response as predicted by normal Rayleigh Law for piezoelectric materials. Therefore, the comparison of the $d_{33,f}$ nonlinearity as a function of *ac electric field* drive with the $e_{31,f}$ response as a function of *increasing strain levels* confirmed the dynamic poling origin of the observed linear dependence of $d_{33,f}$ on applied field and the presence of the second harmonic of strain in ac electric field driven experiments.

8.4 Nonlinearities in Other Ferroelectric Systems

The dielectric nonlinear behavior of PZT and PMN were studied and compared to the results obtained for the PYbN-PT films. The PYbN-PT films showed Rayleigh parameters similar to, but slightly higher than rhombohedral MPB PZT films of similar thickness, indicating a higher contribution of domain walls motion to the dielectric nonlinear behavior of the PYbN-PT films. The PYbN-PT films showed lower Rayleigh parameters than PMN-PT films of same thickness with compositions on the rhombohedral side of the morphotropic phase boundary, indicating a higher extrinsic contribution to the dielectric properties in the PMN-PT films.

Rayleigh parameters were also compared for PZT and PYbN-PT films of different thicknesses. It was shown that the Rayleigh parameters decreased with decreasing thickness of the films. This was attributed to a reduction in the population of the mobile domain walls in the thinner films. For film thicknesses close to one micron and higher, the activation of the ferroelastic (non-180°) domain walls could also be the source of an additional contribution to the nonlinear properties of the films.

Data from literature reports on PZT were also used to compare the Rayleigh parameters in thin films of different thicknesses and ceramics (both soft and hard). The data confirmed the "hard" behavior of PZT thin films with much reduced domain wall contribution to the dielectric nonlinearities. It was also seen that the Rayleigh parameters increased with increasing thickness of the films and then increased, in order, in hard PZT ceramics and soft PZT ceramics. Based on all the above observation, use of the Rayleigh parameters for quantification of domain wall motion contribution to the dielectric properties of ferroelectrics at sub-switching fields was proposed.

The temperature dependence of the dielectric nonlinear behavior of PMN-PT films was also studied. The experiments confirmed the disappearance of the Rayleigh behavior, and in general dielectric nonlinearity, at temperatures higher than the ferroelectric transition temperature.

8.5 Recommendations for Future Work

This work is a step in the quantification of the extrinsic contributions at sub-switching fields for the dielectric and piezoelectric nonlinearity in thin films. This section presents recommendations for further studies that could confirm or further the theories proposed in this thesis.

8.5.1 Domain Wall Concentration Dependence on Poling Directions

A comparison of the dielectric and piezoelectric Rayleigh parameters in the {100} and {111} oriented PYbN-PT thin films in this work suggested a higher concentration of mobile domain walls in the poled {100}-oriented rhombohedral MPB films. The origin of this result was proposed to be the poling process along a non-polar axis. Although the different morphology of the films could have also influenced the domain wall motion, the fact that in the unpoled films the Rayleigh parameters were higher in the {111} oriented films seemed to confirm the higher importance of the poling direction compared to the morphology of the films.

To confirm the results, the dielectric nonlinearity should be studied with the microstructural factor eliminated. Two different approaches could be used to confirm these results:

1. A study of the dielectric nonlinear behavior of {111} and {100} oriented films in a system where the polarization is directed along <100> rather than <111>.
2. A study of the dielectric nonlinearities along different crystallographic directions in materials with similar morphology.

The first approach is appropriate for sol-gel deposited films where control of the orientation separately from the morphology has proved to be extremely difficult. On the other hand, on the tetragonal side of the morphotropic phase boundary, the polarization direction lies along the [001] crystallographic axis and therefore, the tetragonal {100}-oriented films would be poled along a polar axis, while the {111}-oriented films would be poled along the non-polar axis. If the concentration of the domain walls is actually increased in perovskites poled along a non-polar axis, then tetragonal {111} oriented films should show higher Rayleigh parameters than {100} oriented ones.

Epitaxial films offer the higher advantage of studying the properties of oriented films independently from the microstructure. {111} and {100} oriented PYbN-PT rhombohedral MPB can be [151][152][153] deposited on (111) and (100) $SrTiO_3$ substrates by pulsed laser deposition for thicknesses up to 1 micron. Furthermore, the reported phase purity of the epitaxial films was higher than that in the sol-gel films on Pt-coated Si.

Experiments on bulk single crystals would have the advantage of eliminating both morphology and any effects due to the substrate. In fact, deposition conditions of the different films could lead to different levels of internal bias [258][259], residual biaxial stress [174][260] and shifts in transition temperatures [261][262]. All these factors could

influence the motion of the ferroelectric domain walls present in the system. Therefore, studying the nonlinear behavior of a specific chemistry in a bulk single crystal would eliminate all the above-mentioned external factors.

The single crystal results should also be valid for other systems, such as single crystal of PMN-PT and PZN-PT. These systems have been studied extensively and the production of high quality single crystals of rhombohedral MPB compositions is further advanced than PYbN-PT single crystals.

8.5.2 High Extrinsic Contributions in Low T_C Systems

Many perovskite relaxor-ferroelectric solid solutions have been reported to have very high piezoelectric response along the [001] direction on the rhombohedral side of the MPB.[4][5] As mentioned in section 2.7.1, the high piezoelectric and dielectric response at the MPB in many of these systems are accompanied by low T_C and $T_{R\rightarrow T}$ transition temperatures, which greatly reduces the usability of these materials in industrial applications.[4][5]

Previous literature reports by Roberts et al. [264] indicated an increase of the Rayleigh parameters, for $0.5(PbNi_{1/3}Nb_{2/3})O_3$-$Pb(Zr_{0.16}Ti_{0.34})O_3$ (PNN-PZT) samples poled at 25°C, for increasing temperatures up to $T_{R\rightarrow T}$. The authors argued that the extrinsic contributions increased because of the increased domain wall mobility at higher

temperatures. The preliminary results of this thesis seem to agree with this hypothesis. It would be therefore advisable to compile Rayleigh coefficients on the nonlinear behavior of the different ferroelectric compositions as a function of temperature and normalize these as a function of their transition temperatures. The normalization of the Rayleigh parameters with respect to the transition temperature would allow a better comparison tool for the evaluation of the extrinsic contributions to the dielectric and piezoelectric properties of ferroelectric materials at sub-switching fields. It would then be quite intriguing to compare the Rayleigh parameters of normal ferroelectrics to relaxor-ferroelectrics solid solutions. The normalization of the properties to similar $T_C - T$ or $T_{R \to T} - T$ values could possibly indicate if the relaxor-ferroelectric solid solutions show consistently higher extrinsic contributions to their dielectric and piezoelectric properties.

It was already pointed out in this thesis that many difficulties arise in the nonlinear measurements of the ferroelectric thin films at higher temperatures, due to the increased loss values, possibly as a result of the combined effects of high field and high temperature. High quality thin films with very loss values are therefore required for these measurements. Alternatively, it is possible to measure the nonlinear behavior of the relaxor-ferroelectric systems at low and cryogenic temperatures, so that they are comparable to the room temperature nonlinear measurements in normal ferroelectric systems such as PZT or $BaTiO_3$ in terms of $T_C - T$ and $T_{R \to T} - T$. PMN-PT and PZN-PT would be two ideal candidate systems for this work because of their well established processing routes both for thin film and bulk single crystals. [**265**] PZT single crystals have historically been problematic to process and therefore a comparison of the

temperature dependent nonlinearities in the different chemistry systems in *thin film form* seems to be more promising. It should be mentioned that the deposition conditions of the different films could lead to different levels of internal bias [258] [259] , residual biaxial stresses [174] [260] and shifts in transition temperatures [261] [262]. These effects could be ideally reduced with opportune modifications of the experimental set-up, such as measurements performed under external bias fields and choice of substrates with reduced thermal expansion coefficient mismatch between the substrate and the films.

8.5.3 Dynamic Poling Model

As mentioned earlier in this thesis, the proposed dynamic model should be valid in any ferroelectric system with reduced contribution of the non-180° domain wall motion, with relatively unrestricted, largely reversible motion of 180° domain walls. Good candidates for the experimental verification of this model are therefore those ferroelectric systems were only 180° domain walls are allowed either due to the crystal symmetry of the material or because of the specific domain configuration created by domain engineering. Two such examples are $LiNbO_3$ and triglycine sulphate.

Lithium niobate's space group is *R3c* at room temperature and ferroelectric domains with antiparallel polarization are readily induced in the crystals as shown by various literature reports [263][266]. Figure 8.1 shows the polarization reversal at atomic

level in a lithium niobate crystal by application of an external electric field after reference [267]. Because only 180° domain walls are allowed in the system, any *linear* ac field amplitude dependence of piezoelectric coefficient would be due to the dynamic poling. The hypothesis could be confirmed by measuring the higher order harmonics of the strain response. A recent report by Cain et al. [268] showed increasing piezoelectric loss levels with increasing ac signal amplitude in hard and soft PZT ceramics and lithium niobate. The results were unexpected for the lithium niobate system and therefore the authors concluded that the losses might be due to a problem with the experimental set-up. In view of the dynamic poling model proposed here, the losses could still be due to the 180° degree domain wall motion and therefore a "real" response of the material.

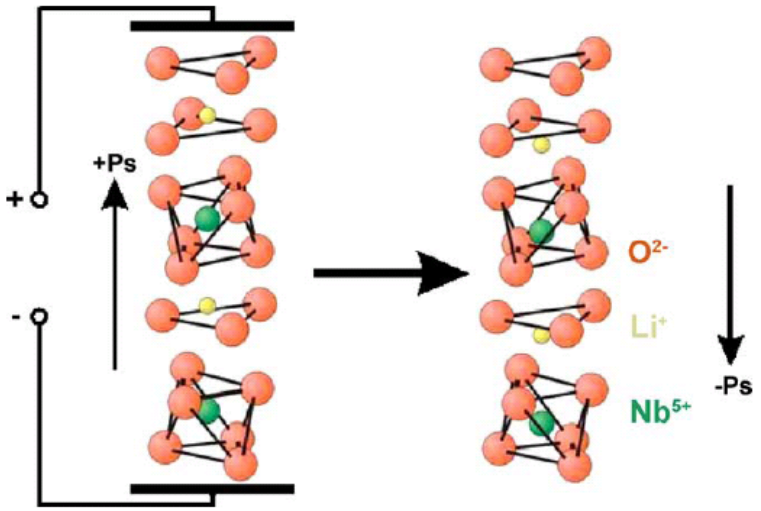

Figure **8.1**: The two polarization direction directions in $LiNbO_3$. By application of an external electric field, the Li^+ and Nb^{5+} ions can be shifted to the opposite lattice positions: the direction of spontaneous polarization is inverted. It is assumed that O^{2-} anions are motionless in this regard and only cations move relative to the O^{2-} anions.[267]

References

1. M.E. Lines and A.M. Glass, *Principles and Applications of Ferroelectrics and Related Materials*, Oxford University Press, New York, (1977)

2. Q.M. Zhang, H. Wang, N. Kim and L.E. Cross, "Direct evaluation of domain-wall and intrinsic contributions to the dielectric and piezoelectric response and their temperature dependence on lead zirconate-titanate ceramics," *J. Appl. Phys.*, **75**, 454, (1994)

3. S. Li, W. Cao and L.E. Cross, "The extrinsic nature of nonlinear behavior observed in lead zirconate titanate ferroelectric ceramic," *J. Appl. Phys.*, **69**, 7219, (1991)

4. S.-E. Park and T. R. Shrout, "Ultrahigh strain and piezoelectric behavior in relaxor based ferroelectric single crystals," *J. Appl. Phys.*, **82**, 1804, (1997)

5. S. E. Park and T. R. Shrout, "Relaxor based ferroelectric single crystals for electro-mechanical actuators," *J. Mater. Res. Innov.*, **1**, 20, (1997)

6. T.M. Shaw, S. Trolier-McKinstry and P. McIntyre, "Properties of ferroelectric films at small dimensions," *Annual Rev. Mat. Sci.*, **30**, 263, (2000)

7. V.D. Kugel and L.E. Cross, “Behavior of soft piezoelectric ceramics under high sinusoidal electric fields,” *J. Appl. Phys.*, **84**, 2815 (1997)

8. D.A. Hall, “Nonlinearity in piezoelectric ceramics,” *J. Mater. Sci*., **36**, 4575, (2001)

9. Lord Rayleigh, “Notes on electricity and magnetism: on the behavior of iron and steel under the operation of magnetic forces,” *Phil. Mag.*, **23**, 225, (1887)

10. L. Néel, “Theorie des Lois D'aimantation de Lord Rayleigh. 1re Partie: Les Deplacements d'une Paroi Isolee,” *Cahier de Physique*; **12**, 1, (1942)

11. L. Néel, "Theorie des Lois D'aimantation de Lord Rayleigh. 2e Partie: Multiples Domaines et Champ Coercitif,” *Cahier de Physique*, **13**, 18, (1943)

12. D.V. Taylor and D. Damjanovic, “Piezoelectric properties of rhombohedral Pb(Zr, Ti)O_3 thin films with (100), (111), and "random" crystallographic orientation,” *Appl. Phys. Lett*., **76**, 1615, (2000)

13. M. Demartin and D. Damjanovic, “Dependence of the direct piezoelectric effect in coarse and fine grain barium titanate ceramics on dynamic and static pressure,” *Appl. Phys. Lett.*, **68**, 3046, (1996)

14. D. Damjanovic and M. Demartin, “The Rayleigh law in piezoelectric ceramics,” *J. Phys. D: Appl. Phys.*, **29**, 2057, (1996)

15. D. Damjanovic, "Stress and frequency dependence of the direct piezoelectric effect in ferroelectric ceramics," *J. Appl. Phys.,* **82**, 1788, (1997)

16. D.V. Taylor and D. Damjanovic, "Evidence of domain wall contribution to the dielectric permittivity in PZT thin films at sub-switching fields," *J. Appl. Phys.,* **82**, 1973, (1997)

17. D. Damjanovic and D.V. Taylor, "Contributions to the nonlinear dielectric and piezoelectric response of ferroelectric thin films and ceramics," *Ferroelectrics,* **221**, 137, (1999)

18. D.A. Hall and P.J. Stevenson, "High field dielectric behavior of ferroelectric ceramics," *Ferroelectrics*, **228**, 139, (1999)

19. D.A. Hall and P.J. Stevenson, *Proc. 4th UK Transducers and Transducers Materials*, Canterbury, (1998)

20. D. A. Hall and M. M. Ben-Omran, "Ageing of high field dielectric properties in BaTiO3-based piezoceramics," *J. Phys.: Condensed Matter* **10**, 9129, (1998)

21. D.A. Hall, "Ferroelectric Hysteresis Measurement & Analysis," in *Minutes of the NPL CAM7 IAG Meeting*, NPL, 18th March 1998

22. D.A. Hall, M.M. Ben-Omran and P.J. Stevenson, "Field and temperature dependence of dielectric properties in $BaTiO_3$-based piezoceramics," *J. Phys.: Condensed Matter,* **10**, 461, (1998)

23. J.F. Nye, *Physical Properties of Crystals: Their Representation by Tensors and Matrices*, Clarendon Press, Oxford, (1957)

24. W.G. Cady, *Piezoelectricity*, First Edition, Third impression, New York, (1946)

25. S.M. Pilgrim, "Electrostrictive ceramics for low-frequency active transducers," *IEEE Trans. Ultras. Ferro. Freq. Control*, **47**, 861, (2000)

26. F. Jona and G. Shirane, *Ferroelectric Crystals,* Dover Publications, New York, (1993)

27. J. Kuwata, K. Uchino and S. Nomura, "Phase transitions in the $Pb(Zn_{1/3}Nb_{2/3})O_3$-$PbTiO_3$ system," *Ferroelectrics*, **37**, 579, (1981)

28. S.-E. Park and T.R. Shrout, "Characteristics of relaxor-based piezoelectric single crystals for ultrasonic transducers," *IEEE Trans. Ultras. Ferro. Freq. Control*, **44**, 1140, (1997)

29. An American National Standard IEEE Standard Definitions of Terms Associated with Ferroelectric and Related Materials, *IEEE Trans. Ultras. Ferro. Freq. Control,* **50**, 1, (2003)

30. R. C. Buchanan, ed., *Ceramic Materials for Electronics - Processing, Properties and Applications*, Marcel Dekker, New York, (1986)

31. L. M. Levinson, ed., *Electronic Ceramics - Properties, Devices and Applications*, Marcel Dekker, New York, (1987)

32. H. J. Hagemann, D. Hennings and R. Wernicke, "Ceramic multilayer capacitors," *Philips Tech. Rev.*, **41**, 89 (1983/84)

33. J. H. Adair, D. A. Anderson, G. O. Dayton, and T. R. Shrout, *J. Matl. Ed.*, **9**, 71 (1987)

34. W. Jillek and W.K.C. Yung, "Embedded components in printed circuit boards: A processing technology review," *Int. J. Adv. Manuf. Technol*., **25**: 350, (2005)

35. L. Dellmann, G.-A. Racine and N.F. de Rooij, "Micromachined piezoelectric Elastic Force Motor (EFM)," *IEEE Proc. Micro Electro Mechanical Systems (MEMS)*, 52, (2000)

36. Y. Ito, K. Kushida, K. Sugawara and H. Takeuchi, "100-MHz ultrasonic transducer array using ZnO thin films," *IEEE Trans. Ultras. Ferro. Freq. Control*, **42**, 316, (1995)

37. J. Mueller, E.H. Yang, A. Green, V. White, I. Chakraborty and R. Reinicke, "Design and fabrication of MEMS-based micropropulsion devices at JPL," *Proc. SPIE,* **4558**, 57, (2001)

38. J.W. Judy, D.L. Polla and W.P. Robbins, "A linear piezoelectric stepper motor with submicrometer step size and centimeter travel range," *IEEE Trans. Ultras. Ferro. Freq. Control*, **37**, 428, (1990)

39. W.P. Robbins, "Ferroelectric-based microactuators," *Integ. Ferro.*, **11**, 179, (1995)

40. P. Muralt, M. Kohli, T. Maeder, A. Kholkin, K. Brooks, N. Setter and R. Luthier, "Fabrication and characterization of PZT thin-film vibrators for micromotors," *Sensors and Actuators A*, **48**, 157, (1995)

41. Y. Nemirovsky, A. Nemirovsky, P. Muralt and N. Setter, "Design of a novel thin-film piezoelectric accelerometer," *Sensors and Actuators A*, **56**, 239, (1996)

42. H.S. Kim, J.H. Kim, S. Zurn and D.L. Polla, "Fabrication process of PZT piezoelectric cantilever unimorphs using surface micromachining," *IEEE Int. Symp. Appl. Ferro. '96*, (1996)

43. J.J. Bernstein, S.L. Finberg, K. Houston, L.C. Niles, H.D. Chen, L.E. Cross, K.K. Li and K. Udayakumar, "Micromachined high frequency ferroelectric sonar transducers," *IEEE Trans. Ultars. Ferro. Freq. Control,* **44**, 960, (1997)

44. D.L. Polla and L.F. Francis, "Ferroelectric thin films in micro-electromechanical systems applications," *Mater. Res. Soc. Bulletin*, **21**, 59, (1997)

45. L.P. Wang, K. Deng, L. Zou, R. Wolf, R.. Davis and S. Trolier-McKinstry, "Microelectromechanical systems (MEMS) accelerometers using lead zirconate titanate thick films," *IEEE Electron Device Lett.*, **23**, 182, (2002)

46. E. Hong, S.V. Krishnaswamy, T.T. Braggins, C.B. Freidhoff and S. Trolier-McKinstry, "Fabrication of micromachined piezoelectric diaphragm pumps actuated by interdigitated transducer electrodes," *Mater. Res. Soc. Symp. Proc.*, **741**, 111, (2002)

47. J. F. Scott, L. Kammerdiner, M. Paris, S. Traynor, V. Ottenbacher, A. Shawabkeh, and W. F. Oliver, "Switching kinetics of lead zirconate titanate submicron thin-film memories," *J. Appl. Phys.*, **64**, 787 (1988)

48. J. F. Scott, C. A. Araujo, H. B. Meadows, L. D. McMillan and A. Shawabkeh, "Radiation effects on ferroelectric thin-film memories: Retention failure mechanisms," *J. Appl. Phys.*, **66**, 1444 (1989)

49. M. Suzuki, "Review on future ferroelectric nonvolatile memory: FeRAM-from the point of view of epitaxial oxide thin films," *J. Ceram. Soc. Japan*, **103**, 1099, (1995)

50. S. Narayan, V. Joshi, L. McMillan and C. Paz De Araujo, "Sub-100 nm SBT films for low voltage and high density FeRAM applications," *Integr. Ferroelectrics*, **25**, 169, (1999)

51. R. Bruchhaus, T. Ozaki, U. Ellerkmann, J. Lian, Y. Kumura, H. Kanaya, M. Yabuki, T. Tsuchya, A. Hilliger, U. Egger, K. Tomioka, B.K. Moon, H. Itokawa, H. Zhuang, K. Natori, G. Beitel, S. Sugimoto, K. Yamakawa, I. Kunishima and N. Nagel, "Novel chain stack capacitor for 32Mb FeRAM and beyond," *Mater. Res. Soc. Symp. Proc.,* **748**, 3, (2003)

52. R. Zambrano, "Applications and issues for ferroelectric NVMs," *Mat. Sci. Semicond. Process.*, **5**, 305, (2003)

53. M.A. Todd, P.P. Donohue, R. Watton, D.J. Williams, C.J. Anthony and M.G. Blamire, "High performance ferroelectric and magnetoresistive materials for next-generation thermal detector arrays," *Proc. SPIE*, **4795**, 88, (2002)

54. R.W. Whatmore, "Pyroelectric arrays: ceramics and thin films**,"** *J. Electroceram.*, **13**, 139, (2004)

55. M.H. Lee, R. Guo and A.S. Bhalla, "Pyroelectric sensors," *J. Electroceram.*, **2**, 229, (1998)

56. M. Kohli, C. Wuethrich, K. Brooks, B. Willing, M. Forster, P. Muralt, N. Setter, P. Ryser, "Pyroelectric thin-film sensor array," *Sensors & Actuators A*, **60**, 174, (1997)

57. R. A. Steinberg, T. G. Giallorenzi and R. G. Priest, "Polarization-insensitive integrated-optical switches: a new electrode design," *Appl. Opt.*, **16**, 2166, (1977)

58. P. Tang, D.J. Towner, A.L. Meier and B.W. Wessels, "Low-voltage, polarization-insensitive, electro-optic modulator based on a polydomain barium titanate thin film," *Appl. Phys. Lett.*, **85**, 4615, (2004)

59. I.P. Kaminow, "Optical waveguide modulators," *Trans. IEEE Trans. Microw. Theory Tech.*, **23**, 57, (1975)

60. C.B. Sharpe and C.G. Brockus, "Method for measuring dielectric constant of ferroelectric ceramics at S-band frequencies," *J. Am. Ceram. Soc.*, **43**, 302, (1954)

61. O. Lohse, D. Bolten, M. Grossman, R. Waser, W. Hartner and G. Schindler, "Relaxation mechanisms in ferroelectric thin film capacitors for FeRAM application," *Ferroelectric Thin Films VI Symp. Mater. Res. Soc.*, 267, (1998)

62. U. Botter, *Europ. Symp. Polar Oxides: Properties, Characterization and Imaging*, 1 (2003)

63. B. Jaffe, W.R. Cooke Jr. and H. Jaffe, *Piezoelectric Ceramics*, Academic Press Limited, London, (1971)

64. U. Böttger, "Dielectric Properties of Polar Oxides" *Polar Oxides: Properties, Characterization and Imaging*, Capri 1, (2003)

65. H. F. Kay and P. Vousden, "Symmetry changes in barium titanate at low temperatures and their relation to its ferroelectric properties," *Phil. Mag.*, **40**, 1019, (1949)

66. L.E. Cross, *Ferroelectric Ceramics*, edited by N. Setter and E. Colla, Birkhauser, Basel, Switzerland, (1993)

67. E.I. Bondarenko, V. Y. Topolov and A.V. Turik, "The role of 90 degrees domain wall displacements in forming physical properties of perovskite ferroelectric ceramics," *Ferro. Lett. Sect.*, **13**, 13, (1991)

68. T. Mitsui and J. Furuichi, "Domain Structure of Rochelle Salt and KH_2PO_4," *Phys. Rev.*, **90**, 193, (1953)

69. G. Arlt and S. Sasko, "Domain configuration and equilibrium size of domains in $BaTiO_3$ ceramics," *J. Appl. Phys.*, **51**, 4956, (1980)

70. G. Arlt, "The influence of microstructure on the properties of ferroelectric ceramics," *Ferroelectrics*, **104**, 217, (1990)

71. C. Kittel, "Theory of structure of ferromagnetic domains in films and small particles," *Phys. Rev.*, **70**, 965, (1946)

72. W. Zhong, *Physics of Ferroelectrics*, Scientific Press, Beijing, China, (1996)

73. G. Arlt, "Twinning in ferroelectric and ferroelastic ceramics: stress relief" *J. Mater. Sci.*, **25**, 2655, (1990)

74. G. Arlt, D. Hennings and D. de With, "Dielectric properties of fine-grained barium titanate ceramics," *J. Appl. Phys.*, **58**, 1619, (1985)

75. N. Kim, "Grain size effect on the dielectric and piezoelectric properties in compositions which are near the morphotropic phase boundary of lead zirconate-titanate based ceramics," *Doctoral Thesis Dissertation*, The Pennsylvania State University, (1994)

76. L.D. Madsen, E.M. Griswold and L. Weaver, "Domain structures in $Pb(Zr,Ti)O_3$ and $PbTiO_3$ thin films," *J. Mater. Res.*, **12**, 2612, (1997)

77. J. Fousek and V. Janovec, "Orientation of domain walls in twinned ferroelectric crystals," *J. Appl. Phys.*, **40**, 135, (1969)

78. Y.L. Li, S.Y. Hu and L.Q. Chen, "Ferroelectric domain morphologies of (001) $PbZr_{1-x}Ti_xO_3$ epitaxial thin films," *J. Appl. Phys.*, **97**, 034112, (2005)

79. B. Lewis, "Energy loss processes in ferroelectric ceramics," *Proc. Phys. Soc. (London)*, **73**, 17, (1958)

80. R. Herbiet, U. Robels, H. Dederichs and G. Arlt, "Domain wall and volume contributions to material properties of PZT ceramics," *Ferroelectrics*, **98**, 107, (1989)

81. A.Von Hippel, "Ferroelectricity, Domain Structure, and Phase Transitions of Barium Titanate," *Rev. Mod. Phys.*, **22**, 221, (1950)

82. Y.M. Poplavko, V.G. Tsykalov and V.I. Molchanov, "Microwave dielectric dispersion of the ferroelectric and paraelectric phases of barium titanate," *Sov. Phys. –Solid State,* **10**, 2708, (1969)

83. A.V. Turik and N.B. Shevchenko, "Dielectric spectrum of $BaTiO_3$ single crystals," *Phys. Stat. Sol.*, **95**, 585, (1979)

84. O. Kersten, M. Hofmann and G. Schmidt, "Dielectric dispersion of Mn doped ceramics," *Ferrolectrics Letters*, **6**, 75, (1992)

85. U. Bottger and G. Arlt, "Dielectric microwave dispersion in PZT ceramics," *Ferroelectrics*, **127**, 95, (1992)

86. G. Arlt, U. Bottger and S. Witte, "Dielectric dispersion of ferroelectric ceramics and single crystals at microwave frequencies," *Ann. Physik*, **3**, 578, (1994)

87. Yu.M. Poplavko and V.G. Tsykalov, "Study of antiferroelectric materials millimeter wavelenght," *Sov. Phys. Solid State*, **9**, 2600, (1968)

88. F. Xu, S. Trolier-McKinstry, W. Ren, B. Xu, Z.L. Xie and K.J. Hemker, "Domain wall motion and its contribution to the dielectric and piezoelectric properties of lead zirconate titanate films," *J. Appl. Phys.*, **89**, 1336, (2001)

89. Z.Q. Zhuang, M.J. Haun, S.J. Jang and L.E. Cross, "Composition and temperature dependence of the dielectric, piezoelectric and elastic properties of pure PZT ceramics," *IEEE Trans. Ultras. Ferro. Freq. Control*, **36**, 413, (1989)

90. S. Sherrit, R.B. Stimpson, H.D. Wiederick and B.K. Mukherjee, "Stress and temperature dependence of the direct piezoelectric charge coefficient in lead zirconate titanate ceramics," *Proc. SPIE*, **3321**, 74, (1996)

91. G. Arlt, "Domain contributions to piezoelectricity in ceramics," *IEEE Trans. Ultras. Ferro. Freq. Control*, **2**, 733, (1990)

92. X.L. Zhang, Z.X. Chen, L.E. Cross and W.A. Schulze, "Dielectric and piezoelectric properties of modified lead titanate zirconate ceramics from 4.2 to 300K," *J. Mater. Sci.*, **18**, 968, (1983)

93. C. Ang and Z. Yu, "Dielectric behavior of $PbZr_{0.52}Ti_{0.48}O_3$ thin films: Intrinsic and extrinsic dielectric responses," *Appl. Phys. Lett.*, **85**, 3821, (2004)

94. C. Ang and Z. Yu, "DC electric-field dependence of the dielectric constant in polar dielectrics: multipolarization mechanism model," *Phys. Rev. B*, **69**, 174109, (2004)

95. R. Herbiet, H. Tenbrock and G. Arlt, "The aging behaviour of the complex material parameters epsilon, d and s in ferroelectric PZT ceramics," *Ferroelectrics*, **74**, 37, (1987)

96. G. Arlt, H. Dederichs and R. Herbiet, "90 degrees -domain wall relaxation in tetragonally distorted ferroelectric ceramics," *Ferroelectrics*, **76**, 319, (1987)

97. R. E. Eitel, "Novel piezoelectric ceramics: development of high temperature, high performance piezoelectrics on the basis of structure," *Doctoral Thesis Dissertation,* Penn State University, (2003)

98. A. L. Kholkin, "Non-linear piezoelectric response in lead zirconate-titanate (PZT) films," Ferroelectrics, 238, 235, (2000)

99. Q.M. Zhang, W.Y. Pan, S.J. Jang and L.E. Cross, "Domain wall excitations and their contributions to the weak-signal response of doped lead zirconate titanate ceramics," *J. Appl. Phys.*, **64,** 6445, (1988)

100. H.J. Hagemann, "Loss mechanisms and domain stabilisation in doped $BaTiO_3$," *J. Phys. C: Solid State Phys,* **11**, 3333, (1978)

101. D.A. Hall, "Rayleigh behaviour and the threshold field in ferroelectric ceramics," *Ferroelectrics*, **223**, 319, (1999)

102. H. Kronmüller, "Suprastriction in superconductors," *Z. Angew. Physik,* **30**, 9, (1970)

103. O. Boser, "Statistical theory of hysteresis in ferroelectric materials," *J. Appl. Phys.*, **62**, 1344, (1987)

104. D. Damjanovic and M. Demartin, "Contribution of the irreversible displacement of domain walls to the piezoelectric effect in barium titanate and lead zirconate titanate ceramics," *J. Phys.: Condens. Matter,* **9**, 4943, (1997)

105. V. Perrin, M. Troccaz and P. Gonnard, "Non linear behavior of the permittivity and of the piezoelectric strain constant under high electric field drive," *J. Electroceram.*, **4**, 189, (2000)

106. D.V. Taylor and D. Damjanovic, "Domain wall pinning contribution to the nonlinear dielectric permittivity in Pb(Zr, Ti)O_3 thin films," *Appl. Phys. Lett.,* **73**, 2045, (1998)

107. U. Robels, C. Zadon and G. Arlt, "Linearization of dielectric nonlinearity by internal bias fields," *Ferroelectrics* **133**, 163, (1992)

108. V. Mueller and H. Beige, "Nonlinearity of soft PZT piezoceramic for shear and torsional actuator applications," *Proc. Int. Symp. Appl. Ferroelecr. '98,* 459, (1998)

109. V. Mueller and Q.M. Zhang, "Nonlinearity and scaling behavior in donor-doped lead zirconate titanate piezoceramic," *Appl. Phys. Lett.,* **72** , 2692, (1998)

110. D. Damjanovic, M. Demartin, H. S. Shulman, M. Testorf and N. Setter, "Instabilities in the piezoelectric properties of ferroelectric ceramics," *Sensors and Actuators A*, **53**, 353, (1996)

111. V. Muller and H. Beige, "Nonlinearity of soft PZT piezoceramic for shear and torsional actuator applications," *Proc. Int. Symp. Appl. Ferro. '98*, 459, (1998)

112. H.J. Hagemann, "Loss mechanisms and domain stabilisation in doped $BaTiO_3$," *J. Phys. C: Solid State Phys.*, **11**, 3333, (1978)

113. O. Boser and D.N. Besher, *Characterization of Defects in Materials,* edited by R.W. Siegel, R Sinclair, and J.R. Weertman, Materials Research Society, Pittsburg, **82**

114. B. Wul and I. M. Goldman, "Dielectric constants of titanates of metals of the second group," *C. R. Acad. Sci. U.R.S.S.,* **46**, 177, (1945)

115. D. A. Berlincourt, C. Cmolik and H. Jaffe, "Piezoelectric properties of polycrystalline lead titanate zirconate compositions," *IRE Proc.,* **2**, 220, (1960)

116. B. Noheda, J. A. Gonzalo, L. E. Cross, R. Guo, S.-E. Park, D. E. Cox and G.

117. A.L. Kholkin, Ch. Wűtchrich, D.V. Taylor and N. Setter, "Interferometric measurements of electric field-induced displacements in piezoelectric thin films," *Rev. Sci. Instr.*, **67**, 1935, (1996)

118. B. Noheda, D.E. Cox, G. Shirane, R. Guo, B. Jones and L.E. Cross, "Stability of the monoclinic phase in the ferroelectric perovskite $PbZr_{1-x}Ti_xO_3$," *Phys. Rev. B*, **63**, 014103, (2000)

119. M. J. Haun, E. Furman, S. J. Jang, H. A. McKinstry, Z. Q. Zhuang, T. R. Halemane and L. E. Cross, "Thermodynamic theory of $PbTiO_3$," *Ferroelectrics*, **99**, 13, (1989)

120. S.W. Choi, T.R. Shrout, S.J. Jang and A.S. Bhalla, "Morphotropic phase boundary in $Pb(Mg_{1/3}Nb_{2/3})O_3PbTiO_3$ system," *Ferroelectrics*, **100**, 29, (1989)

121. S. Nomura, T. Takahashi and y. Yokomizo, "Ferroelectric properties in the system $Pb(Zn_{1/3}Nb_{2/3})O_3$-$PbTiO_3$," *J. Phys. Soc. Jpn.,* **27**, 262, (1969)

122. Y. Yamashita, "Piezoelectric properties of niobium-doped $[Pb(Sc_{1/2}Nb_{1/2})_{1-x}Ti_x]O_3$ ceramics material near the morphotropic phase boundary," *Jpn. J. Appl. Phys.*, **33**, 4652, (1994)

123. J. F. Wang, J. R. Giniewicz, and A. S. Bhalla, "Soft piezoelectric (1-x) $Pb(Sc_{1/2}Ta_{1/2})O_3$ ceramics with high coupling factors and low QM**,"** *Ferroelectr. Lett.,* **16**, 113, (1993)

124. T. Yamamoto and S. Ohashi, "Dielectric and piezoelectric properties of $Pb(Yb_{1/2}Nb_{1/2})O_3$-$PbTiO_3$ solid solution system," *Jpn. J. Appl. Phys.*, 34, 5349, (1995)

125. C. Duran, S. Trolier-McKinstry and G.L. Messing, "Processing and electrical properties of 0.5Pb($Yb_{1/2}Nb_{1/2}$)O_3-0.5$PbTiO_3$ ceramics," *J. Electroceramics*, **10**, 47, (2003)

126. T. Shrout, *Z*.P. Chang, N. Kim, and S. Markgraf, "Dielectric behavior of single crystals near the (1-x) Pb($Mg_{1/3}Nb_{2/3}$)O_3-(x) $PbTiO_3$ morphotropic phase boundary," *Ferroelectr. Lett*., **12**, 63, (1990)

127. J. Wolak, B. Hilczer, C. Caranoni, P. Lampin and C. Boulesteix, "Dielectric studies of PSNT single crystals," *Ferroelectrics*, **158**, 399, (1994)

128. Y. Yamashita, "Pb(B'/B")0_3-$PbTiO_3$ Materials," *The 7th US-Japan Study Seminar on Dielectric and Piezoelectric Ceramics,* Tsukuba, 181, (1995)

129. T. Kobayashi, S. Shimanuki, S. Saitoh and Y. Yamashita, "Improved growth of large lead zinc niobate titanate piezoelectric single crystals for medical ultrasonic transducers," *Jpn. J. Appl. Phys.,* **36**, 6035, (1997)

130. S. Zhang, P. W. Rehrig, C. Randall and T. R. Shrout, "Crystal growth and electrical properties of Pb($Yb_{1/2}Nb_{1/2}$)O_3-$PbTiO_3$ perovskite single crystals," *J. Crystal Growth*, **234**, 415, (2002)

131. S.-E. Park and T. R. Shrout, "Ultrahigh strain and piezoelectric behavior in relaxor based ferroelectric single crystals," *J. Appl. Phys.*, **82**, 1804, (1997)

132. M. Ozgul, "Polarization switching and fatigue anisotropy in relaxor-lead titanate ferroelectric single crystals," *Doctoral Thesis Dissertation,* Penn State University, (2003)

133. S. Wada and T. Tsurumi, "Enhanced piezoelectricity of barium titanate single crystals with engineered domain configuration," *Brit. Ceram. Trans.*, **103**, 93, (2004)

134. W. Kleemann, J. Dec, Th. Woike and R. Pankrath, "Relaxor Ferroelectrics - -from Random Field Models to Domain State Physics" in *Polar Oxides: Properties, Characterization and Imaging*, Capri 1, (2003)

135. R. C. Turner, P. A. Fuierer, R. E. Newnham and T. R. Shrout, "Materials for high temperature acoustic and vibration sensors: a review," *Appl. Acoustic*, **41**, 299, (1994)

136. H. Lim, H. J. Kim and W. K. Choo, "X-ray and dielectric studies of the phase transitions in $Pb(Yb_{1/2}Nb_{1/2})O_3$-$PbTiO_3$ ceramics," *Jpn. J. Appl. Phys.*, **34,** 5449, (1995)

137 G.A. Smolenskii, A.I. Agranovskaia, S.N. Povov and V.A. Isupov, *Sov. Phys. Tech. Phys.*, **3**, 1981, (1958)

138 V.S. Filip'ev, M.F. Kuprianov and E.G. Fesenko, *Sov. Phys. Cryst.*, **8**, 630, (1964)

139 M.F. Kupriyanov and E.G. Fesenko, *Bull. Acad. Sci. USSR Phys. Rev.*, **29**, 930, (1965)

140. V.A. Isopov and N.N. Krainik, *Sov. Phys. Solid State*, **6**, 2975, (1965)

141. W.K. Choo, H.J. Kim, J.H. Yang, H. Lim, J.Y. Lee, J.R. Kwon and C.H. Chun, "Crystal structure and B-site ordering in antiferroelectric $Pb(Mg_{1/2}W_{1/2})O_3$, $Pb(Co_{1/2}W_{1/2})O_3$ and $Pb(Yb_{1/2}Nb_{1/2})O_3$," *Jpn. J. Appl. Phys.*, **32**, 4249, (1993)

142. J.R. Kwon and W.K. Choo, "Dielectric and X-ray diffraction studies in highly ordered complex perovskite $Pb(Yb_{½}Nb_{½})O_3$," *J. Phys.: Condens. Matter*, **13**, 2147

143. G. Shirane, S. Hoshino, and K.J. Suzuki, "Crystal structure of lead titanate and of lead-barium titanate," *Phys. Soc. Japan*, **6**, 453, (1950)

144. G. Shirane, S. Hoshino, and K.J. Suzuki, "X-ray study of the phase transition in lead titanate," *Phys. Rev.*, **80**, 1105, (1950)

145. S. Ikegami, I. Ueda and T. Nagata, "Electromechanical properties of $PbTiO_3$ ceramics containing La and Mn," *J. Acoustic. Soc. Amer.*, **50**,1060, (1971)

146. D. Damjanovic, T. R. Gururaja and L. E. Cross, "Anisotropy in piezoelectric properties of modified lead titanate ceramics," *Amer. Ceram. Soc. Bulletin*, **66**, 699, (1987)

147. C. Duran, S. Trolier-McKinstry and G. Messing, "Processing and electrical properties of $Pb(Yb_{1/2}Nb_{1/2})$-$PbTiO_3$ ceramics at the morphotropic phase boundary," *IEEE Int. Symp. Appl. Ferro.* 2000, 409, (2000)

148. S. Zhang, S. Rhee, C.A. Randall and T.R. Shrout, "Shear-mode piezoelectric properties of $Pb(Yb_{1/2}Nb_{1/2})O_3$-$PbTiO_3$ single crystals," *Jpn. J. Appl. Phys.*, **41**, 722, (2002)

149. V. Bornand and S. Trolier-McKinstry, "Structural and electrical characterization of heteroepitaxial $Pb[Yb_{1/2}Nb_{1/2}]O_3$-$PbTiO_3$ thin films," *J. Appl. Phys.*, **87**, 3958, (2000)

150. V. Bornand, S. Trolier-McKinstry, K. Takemura and C.A. Randall, "Orientation dependence of fatigue behavior in relaxor ferroelectric-$PbTiO_3$ thin films," *J. Appl. Phys.*, **87**, 3965, (2000)

151. V. Bornand and S. Trolier-McKinstry, "Phase development in pulsed laser deposited $Pb[Yb_{1/2}Nb_{1/2}]O_3$-$PbTiO_3$ thin films," *Thin Solid Films*, **370**, 70, (2000)

152. T. Yoshimura and S. Trolier-McKinstry, "Growth and piezoelectric properties of $Pb(Yb_{1/2}Nb_{1/2})O_3$-$PbTiO_3$ epitaxial films," *J. Appl. Phys.,* **92**, 3979, (2002)

153. T. Yoshimura and S. Trolier-McKinstry, "Transverse piezoelectric properties of epitaxial $Pb(Yb_{1/2}Nb_{1/2})O_3$-$PbTiO_3$ (50/50) films," *J. Cryst. Growth*, **229** , 445, (2001)

154. K.V. Im and W.K. Choo, "The perovskite phase formation of $0.4b(Yb_{1/2}Nb_{1/2})O_3$-$0.6PbTiO_3$ thin films prepared on Pt/Ti electrode by reactive magnetron sputtering," *J. Eur. Cer. Soc.,* **21**, 1551, (2001)

155. Q.Q. Zhang, Q. Zhou and S. Trolier-McKinstry, "Structure and piezoelectric properties of sol-gel-derived 0.5 $Pb[Yb_{1/2}Nb_{1/2}]O_3$-0.5 $PbTiO_3$ thin films," *Appl. Phys. Lett*, **80**, 3370, (2002)

156. Q. Zhou, Q.Q. Zhang and S. Trolier-McKinstry, "Structure and piezoelectric properties of sol-gel-derived 0.5 $Pb[Yb_{1/2}Nb_{1/2}]O_3$-0.5 $PbTiO_3$ thin films," *J. Appl. Phys.*, **94**, 3397, (2003)

157. S. Zhang, L. Lebrun, S. Rhee, C.A. Randall, T.R. Shrout, "Dielectric and piezoelectric properties as a function of temperature for $Pb(Yb_{1/2}Nb_{1/2})O_3$-$PbTiO_3$ single crystals," *IEEE Int. Symp. Appl. Ferro.* '04, 455, (2002)

158. K.R. Udayakumar, J. Chen, V. Kumar, S.B. Krupanidhi and L.E. Cross, "Fabrication and characterization of PMN-PT thin films," *IEEE Int. Symp. Appl. Ferro. '92*, 744, (1992)

159. F. Chu, F. Xu, J. Shepard, Jr., and S. Trolier-McKinstry, "Thickness dependence of the electrical properties of sol-gel derived lead zirconate titanate thin films with (111) and (100) texture," *Mater. Res. Soc. Symp. Proc.*, **493**, 409, (1995)

160. H.C. Wang and W.A. Schulze, "Role of excess magnesium oxide or lead oxide in determining the microstructure and properties of lead magnesium niobate," *J. Am. Ceram. Soc.*, **73**, 825, (1990)

161. M. Villegas, J.F. Fernández, C. Moure and P. Durán, "Preparation, microstructural development and dielectric properties of $Pb(Mg_{1/3}Nb_{2/3})O_3$-$Pb(Ti_xZr_{1-x})O_3$ multilayer ceramic capacitors," *J. Mater. Sci.,* **29**, 4999, (1994)

162. S.M. Gupta and A.R. Kulkarni, "Role of excess PbO on the microstructure and dielectric properties of lead magnesium niobate," *J. Mater. Res.*, **10**, 953, (1995)

163. R.W. Schwartz, "Chemical Solution Deposition of Perovskite Thin Films," *Chem. Mater.,* **9**, 2325, (1997)

164. S. Hiboux and P. Muralt, "Mixed titania-lead oxide seed layers for PZT growth on Pt(111): a study on nucleation, texture and properties," *J. Eur. Electroceramic Soc.*, **24**, 1593, (2004)

165. S. Hiboux, P. Muralt, and N. Setter, "Orientation and composition dependence of piezoelectric-dielectric properties of sputtered $Pb(Zr_x,Ti_{1-x})O_3$ thin films," *Mater. Res. Soc. Symp. Proc.*, **596**, 499, (2002)

166. C. F. Knollenberg, "Sputter deposition of piezoelectric lead zirconate titanate thin films for use as sensors and actuators in MEMS," *Master's Thesis Dissertation,* University of California, Berkeley (2000)

167. P. Muralt, "Piezoelectric thin films for MEMS," *Integr. Ferroelectrics*, **17**, 297, (1997)

168. K. Lefki and G.J.M. Dormans, "Measurement of piezoelectric coefficients of ferroelectric thin films," *J. Appl. Phys.*, **76**, 1764, (1994)

169. S. Trolier-McKinstry and P. Muralt, "Thin film piezoelectrics for MEMS," *J. Electroceram.*, **12**, 7, (2004)

170. W. Y. Pan and L.E. Cross, "A sensitive double beam laser interferometer for studying high-frequency piezoelectric and electrostrictive strains," *Rev. Sci. Instrum.,* **60**, 2701, (1989)

171. A.L. Kholkin, A.K. Tagantsev, K.G. Brooks, D.V. Taylor and N. Setter, "Piezoelectric characterization of Pb(Zr, Ti)O_3 thin films by interferometric technique," *IEEE Int. Symp. Appl. Ferr.'96*, 351, (1996)

172. J. F. Shepard, Jr., P. J. Moses, and S. Trolier-McKinstry, "Wafer flexure technique for the determination of the transverse piezoelectric coefficient (d_{31}) of PZT thin films," *Sensor & Actuators A*, **71**, 133, (1988)

173. J.P. Maria, J.F. Shepard Jr., S. Trolier-McKinstry, T.R. Watkins and A.E. Payzant, "Characterization of the piezoelectric properties of $Pb_{0.98}$ $Ba_{0.02}(Mg_{1/3}Nb_{2/3})O_3$- $PbTiO_3$ epitaxial thin films," *Int. J. Appl. Ceram. Tech.*, **2**, 51, (2005)

174. J.F. Shepard Jr., "The investigation of biaxial stress effects and the transverse piezoelectric (d_{31}) characterization of lead zirconate titanate thin films," *Doctoral Thesis Dissertation*, The Pennsylvania State University, (1998)

175. A. Gruverman, O. Auciello, R. Ramesh and H. Tokumoto, "Scanning force microscopy of domain structure in ferroelectric thin films: imaging and control," *Nanotech.*, **8**, A38, (1997)

176. S.V. Kalinin and D.A. Bonnell, "Contrast mechanism maps for piezoresponse force microscopy," *J. Mat. Res.*, **17**, 936, (2002)

177. A. Roelofs, U. Bottger, R. Waser, F. Schlaphof, S. Trogisch and L.M. Eng, "Differentiating 180 ° and 90 ° switching of ferroelectric domains with three-dimensional piezoresponse force microscopy," *Appl. Phys. Lett.*, **77**, 3444, (2000)

178. L. M. Eng, M. Abplanalp, and P. Günter, "Ferroelectric domain switching in tri-glycine sulphate and barium-titanate bulk single crystals by scanning force microscopy," *Appl. Phys. A: Mater. Sci. Process.,* **66**, S679, (1998)

179. A. L. Gruverman, O. Auciello, and H. Tokumoto, "Nanoscale investigation of fatigue effects in Pb(Zr,Ti)O_3 films," *Appl. Phys. Lett.*, **69**, 319, (1996)

180. A. Gruverman, H. Tokumoto, A. S. Prakash, S. Aggarwal, B. Yang, M. Wuttig, R. Ramesh, T. Venkatesan, and O. Auciello, "Nanoscale imaging of domain dynamics and retention in ferroelectric thin films," *Appl. Phys. Lett.*, **71**, 3492, (1997)

181. C.J. Brinker, ""Ultramicroporous" silica-based supported inorganic membranes," *J. Membr. Sci.*, **77**, 165, (1993)

182. F.F. Lange, "Chemical solution routes to single-crystal thin films," *Science*, **273**, 903, (1996)

183. A. Seifert, F.F. Lange and J.S. Speck, "Epitaxial growth of $PbTiO_3$ thin films on (001) $SrTiO_3$ from solution precursors," *J. Mater. Res.*, **10**, 680, (1995)

184. R.M. Waser, "Microstructure of ceramic thin films," *Curr. Opinion Solid. Stat. Mater. Sci.,* **1**, 706, (1996)

185. S.Y. Chen and I.W. Chen, "Texture development, microstructure evolution, and crystallization of chemically derived PZT thin films," *J. Amer. Ceram. Soc.*, **81**, 97 (1998)

186. M. Klee, R. Eusemann, R.Waser, W. Brand and H. van Hal, "Processing and electrical properties of Pb $(Zr_xTi_{1-x})O_3$ (x = 0.2-0.75) films. Comparison of metallo-organic decomposition and sol-gel processes," *J. Appl. Phys.*, **72**, 1566, (1997)

187. S.Y. Chen and I.W. Chen, "Temperature-time texture transition of $Pb(Zr_{1-x}Ti_x)O_3$ thin films: I, role of Pb-rich intermediate phases," *J. Amer. Ceram. Soc.*, **77**, 2332 (1994)

188. S.Y. Chen and I.W. Chen, "Temperature-time texture transition of $Pb(Zr_{1-x}Ti_x)O_3$ thin films: II, heat treatment and compositional effects," *J. Amer. Ceram. Soc.*, **77**, 2337 (1994)

189. T. Tani, Z. Xu and D.A. Payne, "Preferred orientations for sol-gel derived PLZT thin layers," *Mater. Res. Soc. Symp. Proc.*, **310**, 269, (1993)

190. V. Kumar, Y. Ohya, and Y. Takahashi, "Sol-gel processing of ferroelectric $PbTiO_3$ and $Pb(Zr_{0.5}Ti_{0.5})O_3$ thin films," *Jpn. J. Appl. Phys.*, **37**, 4477, (1998)

191. Y. Xu, C.H. Cheng, Y. Lou and J. MacKenzie, "Epitaxial ferroelectric thin films prepared by the sol-gel technique," *Ferroelectrics,* **195**, 283, (1997)

192. L. Pintilie, I. Boerasu, M.J.M. Gomes and M. Pereira, "Properties of $Pb(Zr_{0.92}Ti_{0.08})O_3$ thin films deposited by sol-gel," *Thin Solid Films*, **458**, 114, (2004)

193. R.R. Neurgaonkar, I.S. Santha, J.R. Oliver, J.G. Nelson, J.T. Cheung, P.E.D. Morgan and K.R. Udayakumar, "Grain oriented ferroelectric PZT thin films on lattice-matched substrates," *Mater. Res. Bulletin*, **28**, 719, (1993)

194. M.J. Lefevre, J.S. Speck, R.W. Schwartz, D. Dimos and S.J. Lockwood, "Microstructural development in sol-gel derived lead zirconate titanate thin films: The role of precursor stoichiometry and processing environment," *J. Mater. Res.,* **11**, 2076, (1996)

195. J. K. Yang, W. S. Kim, and H.H. Park, "Effect of excess Pb content on the crystallization and electrical properties in sol-gel derived Pb $(Zr_{0.4}Ti_{0.6})O_3$ thin films," *Thin Solid Films,* **739**, 377-378, (2000)

196. C.D.E. Lakeman, Z. Xu and D.A. Payne, "On the evolution of structure and composition in sol-gel-derived lead zirconate titanate thin layers," *J. Mater. Res.*, **10**, 2042, (1995)

197. A.P. Wilkinson, J.S. Speck, A.K. Cheetham, S. Natarajan and J.M. Thomas, "In situ x-ray diffraction study of crystallization kinetics in $PbZr_{1-x}Ti_xO3$, (PZT, x = 0.0, 0.55, 1.0)," *Chem. Mater.*, **6**, 750, (1994)

198. F. K. Lotgering, "Topotactical reactions with ferromagnetic oxides having hexagonal crystal structures, I," *J. Inorg. Nucl. Chem*. **9,** 113, (1959)

199. N. Ledermann, P. Muralt, J. Baborowski, S. Gentil, K. Mukati, M. Cantoni, A. Seifert and N. Setter, "{1 0 0}-textured, piezoelectric $Pb(Zr_x, Ti_{1-x})O_3$ thin films for MEMS: Integration, deposition and properties," *Sensors and Actuators A*, **105**, 162, (2003)

200. C.H. Peng and S.B. Desu, "Lead titanate thin films prepared by metalorganic chemical vapor deposition (MOCVD) on sapphire, Pt, and RuO_x substrates," *Mater. Res. Soc. Symp. Proc.*, **335**, 93, (1992)

201 B. Nagaraj, S. Aggrawal and R. Ramesh, "Influence of contact electrodes in leakage characteristics of ferroelectric thin films," *J. Appl. Phys.*, **90**, 375, (2001)

202. S. Zhang, C.A. Randall and T.R. Shrout, "Characterization of high Curie temperature piezocrystals in doped $Pb(Yb_{1/2}Nb_{1/2})O_3$-$PbTiO_3$ system," *Ceram. Trans.*, **150**, 149, (2004)

203. M. Morozov, D. Damjanovic and N. Setter, "The nonlinearity and subswitching hysteresis in hard and soft PZT," *J. Eur. Ceram. Soc.*, **25**, 2483, (2005)

204. S. Wada, S. Suzuki, T. Noma, T. Suzuki, M. Osada, M. Kakihana, S.-E. Park, L.E. Cross and T.R. Shrout, "Enhanced Piezoelectric Property of Barium Titanate Single Crystals with Engineered Domain Configurations," *Jpn. J. Appl. Phys.*, **38**, 5505, (1999)

205. X.Y. Zhao, J. Wang, K.H. Chew, W.L.H. Chan, C.L. Choy and H.S. Luo, "Room-temperature nonlinear dielectric constants and dielectric tunability in poled $Pb(Mg_{1/3}Nb_{2/3})O_3$-$PbTiO_3$ single crystals," *Chin. Phys. Lett.*, **20**, 1131, (2003)

206. I.K. Bdikin, V.V. Shvartsman and A.L. Kholkin, "Nanoscale domains and local piezoelectric hysteresis in $Pb(Zn_{1/3}Nb_{2/3})O_3$-4.5%$PbTiO_3$ single crystals," *Appl. Phys. Lett.*, **83**, 4232, (2003)

207. S. Wada, K. Yako, H. Kakemoto, T. Tsurumi and T. Kiguchi, "Enhanced piezoelectric properties of barium titanate single crystals with different engineered-domain sizes," *J. Appl. Phys.*, **98**, 014109, (2005)

208. S. Trolier-McKinstry, P. Aungkavattana, F. Chu, J.L. Lacey, J.P. Maria, J.F. Shepard Jr., T. Su and F. Xu, "The impact of domains on the dielectric and electromechanical properties of ferroelectric thin films," *Proc. Mater. Res. Soc. Symp.*, **493**, 59, (1998)

209. G. Arlt, and N.A. Pertsev, "Force constant and effective mass of 90 degrees domain walls in ferroelectric ceramics," *J. Appl. Phys.*, **70**, 2283, (1991)

210. W. Cao and C. Randall, "Grain size and domain size relations in bulk ceramic ferroelectric materials," *J. Phys. Chem. Solids*, **57**, 1499, (1996)

211. V.V. Shvatsman, A.Yu. Emelyanov, A. L. Kholkin and A. Safari, "Local hysteresis and grain size effect in $Pb(Mg_{1/3}Nb_{2/3})O_3$-$PbTiO_3$ thin films," *Appl. Phys. Lett.*, **81**, 117, (2002)

212. N. Kim, "Intrinsic and extrinsic size effects in fine-grained morphotropic-phase-boundary lead zirconate titanate ceramics," *Doctoral Thesis Dissertation,* Penn State University, 1994

213. C.A. Randall, N. Kim, J.P. Kucera, W. Cao and T.R. Shrout, "Intrinsic and extrinsic size effects in fine-grained morphotropic-phase-boundary lead zirconate titanate ceramics," *J. Amer. Ceram. Soc.*, **81**, 677, (1998)

214. D. Damjanovic, S.S.N. Bharadwaja and N. Setter, "Toward a unified description of nonlinearity and frequency dispersion of piezoelectric and dielectric responses in $Pb(Zr,Ti)O_3$," *Mat. Sci. Eng. B*, **120**, 170, (2005)

215. T. Nattermann, Y. Shapir and I. Vilfan, "Interface pinning and dynamics in random systems," *Phys. Rev. B*, **42**, 8577, (1990)

216. W. Kleemann, J. De, S. Miga, T. Woike and R. Pankrath, "Non-Debye domain-wall-induced dielectric response in $Sr_{0.61-x}Ce_xBa_{0.39}Nb_2O_6$," *Phys. Rev. B*, **65**, 220101, (2002)

217. V. Mueller, Y. Shchur, H. Beige, A. Fuith and S. Stepanov, "Non-Debye domain wall response in KH_2PO_4," *Europhys. Lett.*, **57**, 107, (2002)

218. V. Mueller, Y. Shchur and H. Beige, "Logarithmic domain-wall dispersion," *Ferroelectrics*, **269**, 201, (2002)

219. Y. Park, "Low-frequency-dispersion of $Pb(Fe_{1/2}Nb_{1/2})O_3$ single crystal in the region of its paraelectric ferroelectric phase transition," *Solid State Comm.*, **113**, 379, (2000)

220 W.R. Buessem, L.E. Cross and A.K. Goswami, "Phenomenological theory of high permittivity in fine-grained barium titanate," *J. Am. Ceram. Soc.*,**49**, 33 (1966)

221. W.R. Buessem, L.E. Cross and A.K. Goswami, "Effect of two-dimensional pressure on permittivity of fineand coarse-grained barium titanate," *J. Am. Ceram. Soc.*,**49**, 36 (1966)

222. J.F. Shepard Jr., S. Trolier-McKinstry, M.A. Hendrickson and R. Zeto, "Properties of PZT thin films as a function of in-plane biaxial stress," *Proc. Intl. Symp. Appl. Ferro. '96,* 161, (1996)

223. H.H.A. Krueger, "Stress sensitivity of piezoelectric ceramics -- 1," *J. Acoust. Soc. Am.* **42**, 636 (1967)

224. V. Perrin, M. Troccaz and P. Gonnard, "Non linear behavior of the permittivity and of the piezoelectric strain constant under high electric field drive," *J. Electroceram.*, **4**, 189, (2000)

225. K. Maruyama, M. Tsukada, O. Matsuura, M. Kurasawa, H. Yamawaki, M. Kondo, K. Kurihara, Y. Horii and T. Eshita, "Highly-oriented crystallinity of ferroelectric layers for reliable FRAM capacitors," *Electrochem. Soc. Proc.*, **4**, 206, (2004)

226. Z.G. Ban and S.P. Alpay, "Dependence of the pyroelectric response on internal stresses in ferroelectric thin films," *J. Appl. Phys.*, **82**, 3499, (2003)

227. R. Bruchhaus, D. Pitzer, R. Primig, M. Schreiter and W. Wersing, "PZT thin films grown by multi-target sputtering: analysis of thin film stress," *Integ. Ferroelectrics*, **21**, 461, (1998)

228. K.M. Johnson, "Variation of dielectric constant with voltage in ferroelectrics and its application to parametric devices," *J. Appl. Phys.*, **33**, 2826, (1962)

229. G. Bertotti, "Hysteresis in magnetism : for physicists, materials scientists, and engineers," Academic Press, New York (1998)

230. B.A. Tuttle, J.A. Voigt, T.J. Garino, D.C. Goodnow, R.W. Shwartz, D.L. Lamppa, T.J. Headly and M.O. Eatough, "Chemically prepared Pb(Zr,Ti)O_3 thin films: the effects of orientation and stress," *Proc. Intl. Symp. Appl. Ferro. '92*, **8**, 344, (1992)

231. G.A.C. Spierings, G.J.M. Dormans, W.G.J. Moors, M.J.E. Ulenaers and P.K. Larsen, " Stresses in Pt/Pb(Zr,Ti)O_3/Pt thin films stacks for integrated capacitors," *J. Appl. Phys.*, **78**, 1926, (1995)

232. S.-M. Nam, Y.-B. Kil, S. Wada and T. Tsurumi, "Domain switching kinetics of lead zirconate titanate thin films," *Jap. J. Appl. Phys.*, **42**, L1519, (2003)

233. A. Laha, S.B. Krupanidhi, "Effect of electric field on dielectric response of PMN-PT thin films," *Mat. Sci. Eng. B*, **113**, 190, (2004)

234. O.E. Fesenko, R.V. Kolesova and Yu.G. Sindeyev, "The structural phase transitions in lead zirconate in super-high electric fields," *Ferroelectrics*, **20**, 177, (1978)

235. Z.Q. Zhuang, M.J. Haun, S.J. Jang and L.E. Cross, "Low temperature dielectric, piezoelectric and elastic properties of pure (undoped) PZT ceramics.," *IEEE Int. Symp. Appl. Ferr. '86*, 394, (1986)

236. B. Noheda, D. E. Cox, G. Shirane, J. A. Gonzalo, L. E. Cross, and S.-E.Park, "Monoclinic ferroelectric phase in the $Pb(Zr_{1-x}Ti_x)O_3$ solid solution," *Appl. Phys. Lett.*, **74**, 2059, (1999)

237. Y. Lu, D.-Y. Jeong, Z.-Y. Cheng, Q.M. Zhang, H.S. Luo, Z.Y. Yin and D. Viehland "Phase transitional behavior and piezoelectric properties of the orthorhombic phase of $Pb(Mg_{1/3}Nb_{2/3})O_3$-$PbTiO_3$ single crystals," *Appl. Phys. Lett.,* **78**, 3109, (2001)

238. Y. Guo, H. Luo, T. He, H. Xu and Z. Yin, "Domain configuration and ferroelectric related properties of the $(110)_{cub}$ cuts of relaxor-based Pb(Mg1/3Nb2/3)O3-PbTiO3 single crystals," *Jpn. J. Appl. Phys.*, **41**, 1, (2000)

239. K. Fujishiro, R. Vlokh, Y. Uesu, Y. Yamada, J.-M. Kiat, B. Dkhil and Y. Yamashita, "Optical observation of heterophase and domain structures in relaxor ferroelectrics $Pb(Zn_{1/3}Nb_{2/3})O_3$/9% $PbTiO_3$," *Jpn. J. Appl. Phys.*, **37**, 5246, (1998)

240. M.K. Durbin, J.C. Hicks, S.-E. Park and T.R. Shrout, "X-ray diffraction and phenomenological studies of the engineered monoclinic crystal domains in single crystal relaxor ferroelectrics," *J. Appl. Phys.*, **87**, 8159, (2000)

241. E.R. Eitel, S.J. Zhang, T.R. Shrout, C.A. Randall and I. Levin, "Phase diagram of the perovskite system (1-x)$BiScO_3$-x$PbTiO_3$," *J. Appl. Phys.*, **96**, 2828, (2004)

242. H. Zheng, I.M. Reaney, W.E. Lee, H. Thomas and N. Jones, "Effects of octahedral tilting on the piezoelectric properties of strontium/barium/niobium-doped soft lead zirconate titanate ceramics," *J. Amer. Ceram. Soc.*, **85**, 2337, (2002)

243. A.J. Masys, W. Ren, G. Yang and B.K. Mukherjee, "Piezoelectric strain in lead zirconate titante ceramics as a function of electric field, frequency, and dc bias," *J. Appl. Phys*., **94**, 1155, (2003)

244. S.F. Liu, W. Ren, B.K. Mukherjee, S.J. Zhang and T.R. Shrout, "DC bias dependence of piezoelectric properties of [111] oriented $Pb(Zn_{1/3}Nb_{2/3})O_3$-$PbTiO_3$ single crystals," *IEEE Intl. Symp. Appl. Ferr. '02*, **13**, 427, (2002)

245. J.K. Lee, J.Y. Yi, K.S. Hong, S.E. Park and J. Millan, "Domain configuration and crystal structure of $Pb(Zn_{1/3}Nb_{2/3})O_3$-5%$PbTiO_3$ crystals as a function of the electric-field direction," *J. Appl. Phys.*, **91**, 4474, (2002)

246. D.J. Kim, J.P. Maria, A. Kingon and S.K. Streiffer, "Evaluation of intrinsic and extrinsic contributions to the piezoelectric properties of $Pb(Zr_{1-X}T_X)O_3$ thin films as a function of composition," *J. Appl. Phys.*, **93**, 5568, (2003)

247. J.F. Shepard Jr., S. Trolier-McKinstry, M.A. Hendrickson and R. Zeto, "The effects of biaxial stress on the ferroelectric characteristics of PZT thin films," *Mat. Res. Soc. Symp. Proc.*, **459**, 47, (1997)

248. M.J. Haun, "Thermodynamic theory of the lead zirconate-titanate solid solution system," *Doctoral Thesis Dissertation,* Penn State University, (1989)

249. D. Damjanovic, *Science of hysteresis*, Edited by. I. Mayergoyz and G. Bertotti, Elsevier, in print

250. Y. Saito, "Measurements of complex piezoelectric d_{33} constant in ferroelectric ceramics under high electric field driving," *Jpn. J. Appl. Phys.* **34**, 5313, (1995)

251. R.A. Wolf, "Temperature dependence of the piezoelectric response of lead zirconate titanate films for MEMS applications," *Masters Thesis Dissertation,* Penn State University, (2001)

252. F. Xu, "Longitudinal piezoelectric characterization and domain wall contributions in lead zirconate titanate thin films," *Doctoral Thesis Dissertation,* Penn State University, (1998)

253. M.A. Dubois and P. Muralt, "Measurement of the effective transverse piezoelectric coefficient $e_{31,f}$ of AlN and $Pb(Zr_x,Ti_{1-x})O_3$ thin films," *Sensors and Actuators A*, **77**, 106, (1999)

254. P. Muralt, M.A. Dubois, A. Seifert, D.V. Taylor, N. Ledermann and S. Hiboux, "In-plane piezoelectric coefficient of PZT thin films as a function of composition," *Ferroelectrics*, **224**, 235, (1999)

255. P. Muralt, S. Hiboux, C. Mueller, T. Maeder, L. Sagalowicz, T. Negami and N. Setter, "Excess lead in the perovskite lattice of PZT thin films made by in-situ reactive sputtering," *Integ. Ferroelectrics*, **36**, 53, (2001)

256. J.H. Park, F. Xu and S. Trolier-McKinstry, "Dielectric and piezoelectric properties of sol-gel derived lead magnesium niobium titanate films with different textures," *J. Appl. Phys.*, **89**, 568, (2001)

257. Z. Kighelman, D. Damjanovic, M. Cantoni and N. setter, "Properties of ferroelectric $PbTiO_3$ thin films," *J. Appl. Phys.*, **91**, 1495, (2002)

258 J. Cheng, N. Li, L.E. Cross and Z. Meng, "Self-poling effects in sol-gel derived $Pb(Zr_{1-x}Ti_x)O_3$ thin films," *Proc. Mat. Res. Soc. Symp.*, **748**, 179, (2003)

259 M.C. Glinchuk, A.N. Morozovska, "The internal electric field originating from the mismatch effect and its influence on ferroelectric thin film properties," *J. Phys.: Cond. Mat.,* **16**, 3517, (2004)

260 T.A. Berfield, N.R. Sottos, R.J. Ong and D.A. Payne, "Residual stress effects in ferroelectric thin films," *Proc. Mat. Res. Soc. Symp.*, **784**, 29, (2004)

261. G.F. Huang and S. Berger, "Combined effect of thickness and stress on ferroelectric behavior of thin $BaTiO_3$ films," *J. Appl. Phys.*, **93**, 2855, (2003)

262. N.A. Pertsev, A.G. Zembilgotov and A.K. Taganstev, "Effect of mechanical boundary conditions on phase diagrams of epitaxial ferroelectric thin films," *Phys. Rev. Lett.*, **80**, 1988, (1998)

263. T. Jach, S. Kim, V. Gopalan, S. Durbi and D. Bright, "Long-range strains and the effects of applied field at 180° ferroelectric domain walls in lithium niobate," *Phys. Rev. B*, **69**, 064113, (2004)

264 G. Roberts, D. Damjanovic and N. Setter, "Temperature dependence of piezoelectric properties for relaxor-ferrroelectric solid solutions undergoing a rhombohedral to tetragonal phase transition," *Ferroelectrics*, **224**, 97, (1999)

265. L.E. Cross, "Recent developments in piezoelectric ferroelectric materials and composites," *Smart Materials and Structures. Proceedings of the 4th European*

Conference on Smart Structures and Materials in conjunction with the 2nd International Conference on Micromechanics, Intelligent Materials and Robotics, 89, (1998)

266. B.J. Rodrigez, R. J. Nemanich, A. Kingon, and A. Gruverman, S.V. Kalinin, K. Terabe, X. Y. Liu, and K. Kitamura, "Domain growth kinetics in lithium niobate single crystals studied by piezoresponse force microscopy," *Appl. Phys. Lett.*, **86**, 012906, (2005)

267. H. Xiangke, X. Dongfeng and k. Kitamura, "Defects and domain engineering of lithium niobate crystals," *Mat. Sci. Eng. B*, **120**, 27, (2005)

268. M. Cain, M. Lodeiro, M. Stewart and M. Theobalds, "6MPIO301: losses in piezoelectric materials," in NPL Report MATCA(A), Nat. Phys. Lab., Teddington, UK, (2002)

269. E.A. Wood, "Detwinning ferroelectric crystals," *Acta Cryst.*, **4**, 353, (1951)

270. M.L. Keith and R. Roy, "Structural relations among double oxides of trivalent elements," *Am. Min.,* **39**, 1, (1954)

271. K.H. Noh, B. Yang, S.W. Lee, S.S. Lee, H.B. Kang and Y.J. Park, "Issues and reliability of high-density FeRAMs," *Jap. J. Appl. Phys., Part 1: Regular Papers and Short Notes and Review Papers*, **42**, 2096, (2003)

272. R. S. Roth, "Classification of perovskite and other ABO_3-type compounds," *J. Res. Nat. Bur. Std.*, **58**, 75, (1957)

273. H. Koike, K. Amanuma, T. Miwa, J. Yamada, and H. Toyoshima, "FeRAM retention analysis method based on memory cell read signal voltage measurement," *IEEE International Conference on Microelectronic Test Structures*, 37, (2001)

274. B.G. Demczyk, R.S. Rai and G. Thomas, "Ferroelectric domain structure of lanthanum-modified lead titanate ceramics," *J. Appl. Phys.*, **70**, 2283, (1991)

275. V. M. Goldschmidt, Geochemistry, Edited by N. F. Mott and S. E. Bullard. Clarendon Press, Oxford, (1954)

276. R.D. Shannon, "Revised effective ionic radii and systematic studies of interatomic distances in halides and chalcogenides," *Acta. Crystallogr. Sec. A*, **32**, 751, (1976).

277. C. Kittel, "Theory of structure of ferromagnetic domains in films and small particles," *Phys. Rev.*, **82**, 729, (1951)

278. C.A. Randall, "Scientific and engineering issues of the state-of-the-art and future multilayer capacitors," *J. Ceram. Soc. Jpn.*, **109**, S2, (2001)

279. H. Kishi, Y. Mizuno and H. Chazono, "Base-metal electrode-multilayer ceramic capacitors: past, present and future perspectives," *Jpn. J. Appl. Phys.*, **42**, 1, (2003)

280. Shirane, "Tetragonal-to-monoclinic phase transition in a ferroelectric perovskite: The structure of $PbZr_{0.52}Ti_{0.48}O_3$," *Phys. Rev. B*, **61**, 8687, (2000)

Appendix A

Fourier Expansions for Dynamic Poling

The Fourier series expansion for polarization as a function of the Rayleigh parameters is reported in this appendix. All the expression are based on an applied ac electric field, $E = E_0 \sin(\omega t)$, where E_0 is the maximum applied field amplitude, ω is the angular frequency and t is time. The Fourier coefficients for the higher harmonics are reported in matrix form where the nth row represents the (n-1)th harmonics coefficient (the first row is the static term, the second row is the first order harmonic, the third row is the second order harmonic and so on). The matrices *a* and *b* refer respectively to the cosine and sine components of the higher order harmonics, as shown in Equation **A.1**.

$$\begin{aligned} strain(\omega t) &= \frac{1}{\pi}\int_{-\pi}^{\pi}\left(strain(\omega t)\cos(n\omega t)\right)d\omega t + \frac{1}{\pi}\int_{-\pi}^{\pi}\left(strain(\omega t)\sin(n\omega t)\right)d(\omega t) \\ &= a.X + b.Y \end{aligned} \qquad \textbf{A.1}$$

A.1 Fundamental Rayleigh Analysis

$$strain(\omega t) = (d_{init} + \alpha E_0)E_0 \sin(\omega t) \pm \frac{\alpha}{2}\left[E_0^2 - E_0^2 \sin^2(\omega t)\right]$$

$$a = \begin{pmatrix} 0 \\ \frac{4}{3\pi}\alpha E_0 \\ 0 \\ \frac{4}{15\pi}\alpha E_0 \\ 0 \\ \frac{-4}{105\pi}\alpha E_0 \\ 0 \\ \frac{4}{315\pi}\alpha E_0 \\ 0 \\ \frac{4}{639\pi}\alpha E_0 \end{pmatrix}$$

$$X = \begin{pmatrix} 1 & \cos(\omega t) & \cos(2\omega t) & \cos(3\omega t) & \cos(4\omega t) & \cos(5\omega t) & \cos(6\omega t) & \cos(7\omega t) & \cos(8\omega t) & \cos(9\omega t) \end{pmatrix}$$

$$b = \begin{pmatrix} 0 \\ d_{init}E_0 + \alpha E_0^2 \\ 0 \\ 0 \\ 0 \\ 0 \\ 0 \\ 0 \\ 0 \\ 0 \end{pmatrix}.$$

$$Y = \begin{pmatrix} 1 & \sin(\omega t) & \sin(2\omega t) & \sin(3\omega t) & \sin(4\omega t) & \sin(5\omega t) & \sin(6\omega t) & \sin(7\omega t) & \sin(8\omega t) & \sin(9\omega t) \end{pmatrix}$$

A.2 Dynamic Poling: Frequency Dependent Response

$$d_{init} = d_0(1+\beta)\sin(\omega t)$$

$$strain(\omega t) = \left\{ d_0\left[1+\beta\cdot\sin(\omega t)\right]+\alpha\cdot E_0 \right\}\cdot E_0\cdot\sin(\omega t) \pm \frac{\alpha}{2}(E_0^2 - E_0^2\cdot\sin^2(\omega t))$$

$$a = \begin{pmatrix} \beta d_0 E_0 \\ \frac{4}{3\pi}\alpha E_0^2 \\ -\frac{1}{2}\beta d_0 E_0 \\ \frac{4}{15\pi}\alpha E_0^2 \\ 0 \\ \frac{-4}{105\pi}\alpha E_0^2 \\ 0 \\ \frac{4}{315\pi}\alpha E_0^2 \\ 0 \\ \frac{-4}{693\pi}\alpha E_0^2 \end{pmatrix}$$

$$b = \begin{pmatrix} 0 \\ d_0 E_0 + \alpha E_0^2 \\ 0 \\ 0 \\ 0 \\ 0 \\ 0 \\ 0 \\ 0 \\ 0 \end{pmatrix}$$

A.3 Dynamic Poling: Field and Frequency Dependent Response

$$d_{init} = d_0\left[1 + \left(\beta + \beta' E_0\right)\right]\sin(\omega t)$$

$$strain(\omega t) = \left\{d_0\left[1 + \left(\beta + \beta' E_0\right)\right]\sin(\omega t) + \alpha E_0\right\}E_0 \sin(\omega t) \pm \frac{\alpha}{2}\left[E_0^2 - E_0^2 \sin^2(\omega t)\right]$$

$$a = \begin{pmatrix} \beta d_0 E_0 + \beta' d_0 E_0^2 \\ \frac{4}{3\pi}\alpha E_0^2 \\ -\frac{1}{2}\beta d_0 E_0 - \frac{1}{2}\beta' d_0 E_0^2 \\ \frac{4}{15\pi}\alpha E_0^2 \\ 0 \\ \frac{-4}{105\pi}\alpha E_0^2 \\ 0 \\ \frac{4}{315\pi}\alpha E_0^2 \\ 0 \\ \frac{-4}{693\pi}\alpha E_0^2 \end{pmatrix}$$

$$b = \begin{pmatrix} 0 \\ d_0 E_0 + \alpha E_0^2 \\ 0 \\ 0 \\ 0 \\ 0 \\ 0 \\ 0 \\ 0 \\ 0 \end{pmatrix}$$

Appendix B

Piezoelectric Nonlinearities in PZT Thin Films

This appendix reports the measured piezoelectric nonlinearity in sol-gel deposited (111) oriented 1.2µm thick PZT thin films. Figure **B.1** shows the amplitude and phase angle of the strain response of the film as a function of the driving field at 3 kHz. The frequency dependence of the second order harmonic of strain is reported in Figure **B.2**.

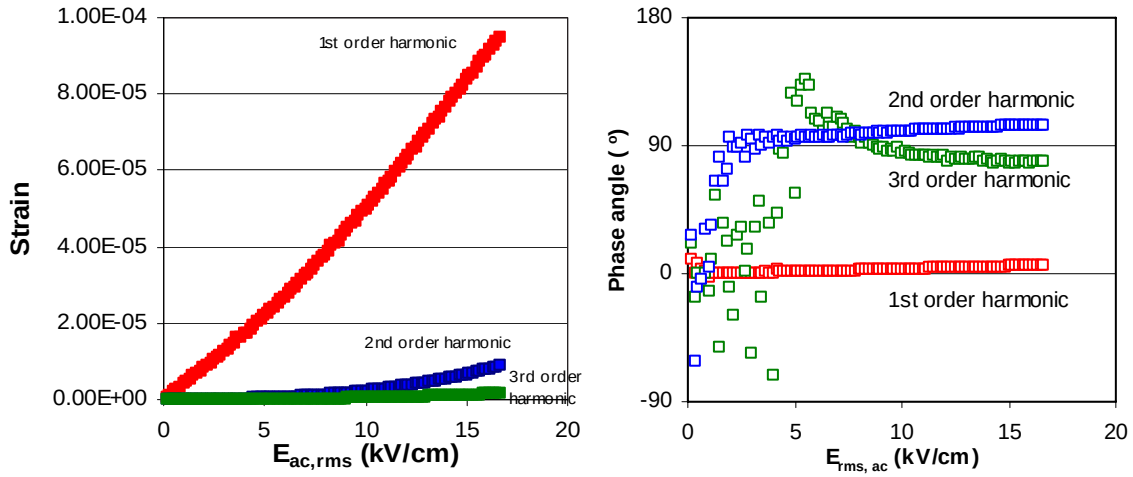

(a) (b)

Figure **B.1**: (a) Amplitude and (b) phase angle of the strain response of 1.2µm thick PZT film as a function of applied ac field, measured at 3kHz.

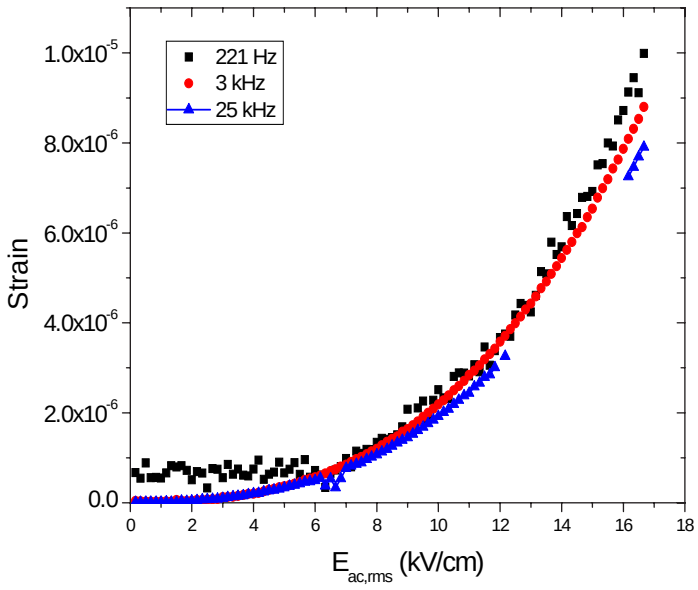

Figure **B.2**: AC field dependence of the second harmonic of strain for three different frequencies. The highly dispersed data at high field values collected at 25kH are due to loss of contact during measurement.

VITA

Nazanin Bassiri Gharb was born in London, United Kingdom on November 20th, 1977. She received her "Laurea" summa cum laude in Materials Engineering from Universita' degli Studi di Padova, Italy in July 2001. She began to work toward her doctorate degree in Materials Science and Engineering at the Pennsylvania State University in August 2001. After four years of cold Pennsylvanian weather, she decided to leave for warmer places. Miss Bassiri Gharb received her PhD in fall 2005 and left for Northern California as soon as she could.